UNIVERSIDADE DA BEIRA INTERIOR
Engenharia

Innovative Energy-efficient Wireless Sensor Network Applications and MAC Sub-layer Protocols Employing RTS/CTS with Packet Concatenation

Norberto José Gil Barroca

Tese para obtenção do Grau de Doutor em
Engenharia Electrotécnica e de Computadores
(3º ciclo de estudos)

Orientador: Prof. Doutor Fernando José da Silva Velez

Covilhã, janeiro de 2014

This thesis is dedicated to my beloved Family and my Faith

Acknowledgments

To all that believed in me.
This work was only possible due to the encouragement and support of many people, who drove me along this long journey. Among them, I would like to express my deeply gratitude to Professor Fernando José da Silva Velez, my thesis mentor. His energy, clear way of thinking, unconditional support and friendship were the key to achieve the goals during all stages of research.
I acknowledge the Ph.D. grant assigned to me by Instituto de Telecomunicações in the initial period of the research. I also would like to thank to the programmatic budget from Instituto de Telecomunicações, as it enabled to make Wireless Sensor Network hardware and software available to my research work.
I acknowledge the suggestions from Prof. Periklis Chatzimisios (Department of Informatics, Alexander TEI of Thessaloniki, Greece) in the development of the analytical models for MAC sub-layer protocols employing RTS/CTS with packet concatenation, as well as the opportunity of making a Short Time Scientific Mission in Thessaloniki, in the framework of COST IC0905 "TERRA". I also would like to thank the strong collaboration that have been established with his group, and his help in preparing a proposal on Block Acknowledgment mechanisms for WSNs, to be presented in the IEEE 802.15.4 Wireless Next Generation Standing Committee for Wireless Personal Area Networks.
I would like to thank to Prof. João Paulo Castro Gomes and Jorge Bento for the fabrication of the concrete cubes that allowed the test of the SHT15 and SHT21S sensors in the INSYSM project. I would also like to thank Prof. Nuno Borges de Carvalho, Prof. Pedro Pinho and the Ph.D Student Ricardo Gonçalves, for the collaboration within the PROENERGY-WSN project, and for making available to us the textile antennas for testing the RF energy harvesting circuits, as well as the figures related with the antenna geometry and the simulation of the radiation pattern of the proposed textile antennas presented in this thesis.
To my friends at IT-Covilhã, Luís Borges, João Ferro, João Oliveira, Orlando Cabral, Daniel Robalo, Rui Paulo, Henrique Saraiva, Paulo Gouveia and Jorge Tavares, I would like to thank all their understanding and availability, which were decisive for the conclusion of this work. Thank you for your friendship.
This work was supported by the Ph.D. FCT grant SFRH/BD/66803/2009, the European Social Fund (ESF), IT grant PEst-OE/EEI/ LA0008/2011 and IT grant PEst-OE/EEI/ LA0008/2013. I also acknowledge the support from several projects where I was involved in: Smart-Clothing, COST 2100, COST IC1004, COST IC0905, PROENERGY-WSN, PLANOPTI, INSYSM, OPPORTUNISTIC-CR and CREaTION (EXCL/EEI-TEL/0067/2012).
To my beloved wife, Sara Gomes, for her love, attention, support, friendship, encouragement and mainly for her patient along last months. At last but not least, I would like to thank my family, especially my parents, and my sister. I am very grateful for their unconditional love, care, understanding, and support, which kept me going in the hardest times.

Abstract

Nowadays, Wireless Sensor Networks (WSNs) have faced a tremendous advance both in terms of energy-efficiency as well as the number of available applications. As a consequence there are challenges that need to be tackled for the future generation of WSNs. The research work from this Ph.D. thesis has involved the actual development of innovative WSN applications contributing to different research projects. In the Smart-Clothing project contributions have been given in the development of a Wireless Body Area Network (WBAN) to monitor the foetal movements of a pregnant woman in the last four weeks of pregnancy. The creation of an automatic wireless measurement system for remotely monitoring concrete structures was an contribution for the INSYSM project. This was accomplished by using an IEEE 802.15.4 network enabling for remotely monitoring the temperature and humidity within civil engineering structures. In the framework of the PROENEGY-WSN project contributions have been given in the identification the spectrum opportunities for Radio Frequency (RF) energy harvesting through power density measurements from 350 MHz to 3 GHz. The design of the circuits to harvest RF energy and the requirements needed for creating a WBAN with electromagnetic energy harvesting and Cognitive Radio (CR) capabilities have also been addressed. A performance evaluation of the state-of-the art of the hardware WSN platforms has also been addressed. This is explained by the fact that, even by using optimized Medium Access Control (MAC) protocols, if the WSNs platforms do not allow for minimizing the energy consumption in the idle and sleeping states, energy efficiency and long network lifetime will not be achieved.
The research also involved the development of new innovative mechanisms that tries and solves overhead, one of the fundamental reasons for the IEEE 802.15.4 standard MAC inefficiency. In particular, this Ph.D. thesis proposes an IEEE 802.15.4 MAC layer performance enhancement by employing RTS/CTS combined with packet concatenation. The results have shown that the use of the RTS/CTS mechanism improves channel efficiency by decreasing the deferral time before transmitting a data packet. In addition, the Sensor Block Acknowledgment MAC (SBACK-MAC) protocol has been proposed that allows the aggregation of several acknowledgment responses in one special *Block Acknowledgment (BACK) Response* packet. Two different solutions are considered. The first one considers the SBACK-MAC protocol in the presence of *BACK Request* (concatenation) while the second one considers the SBACK-MAC in the absence of *BACK Request* (piggyback). The proposed solutions address a distributed scenario with single-destination and single-rate frame aggregation. The throughput and delay performance is mathematically derived under both ideal conditions (a channel environment with no transmission errors) and non ideal conditions (a channel environment with transmission errors). An analytical model is proposed, capable of taking into account the retransmission delays and the maximum number of backoff stages. The simulation results successfully validate our analytical model. For more than 7 TX (aggregated packets) all the MAC sub-layer protocols employing RTS/CTS with packet concatenation allows for the optimization of channel use in WSNs, $\backsim$8-48 % improvement in the maximum average throughput and minimum average delay, and decrease energy consumption.

Keywords

Wireless Sensor Networks, WSN applications, RF energy harvesting, MAC sub-layer protocols, BACK mechanism, RTS/CTS, Packet Concatenation

Resumo

Actualmente, as Redes de Sensores Sem Fios (RSSFs) estão a enfrentar novos paradigmas, tanto em termos de eficiência energética, como em número de aplicações disponíveis. Como consequência, existem novos desafios que precisam ser respondidos tendo em conta a futura geração de RSSFs. Nesta tese de doutoramento foram desenvolvidas aplicações inovadoras para RSSFs no contexto de diferentes projectos de investigação. No âmbito projecto Smart-Clothing foram dadas contribuições no desenvolvimento de uma RSSFs de Área Corporal para monitorar os movimentos fetais de uma mulher grávida nas últimas quatro semanas de gravidez. No âmbito projecto INSYSM, foi concebido um sistema de aquisição que permite monitorizar em tempo real a humidade e temperatura no período de cura de blocos de betão, utilizando RSSFs IEEE 802.15.4. No âmbito do projecto PROENEGY-WSN foram dadas contribuições na identificação das oportunidades espectrais para recolha de energia electromagnética de frequências rádio (RF) através de medições de densidade de potência entre os 350 MHz a 3 GHz do espectro radio eléctrico. Para além disso foram concebidos circuitos de recolha de energia de RF. Tendo sindo também apresentados os requisitos necessários para a criação de uma RSSFs de Área Corporal considerando recolha de energia electromagnética do meio ambiente e Rádios Cognitivos (CR). Uma avaliação do desempenho das plataformas de hardware para RSSFs baseada em critérios tais como características principais, requisitos de energia e recursos de expansibilidade, programação e comunidade foi também proposto. Mesmo usando protocolos de Controlo de Acesso ao Meio (MAC) optimizados, se as plataformas de hardware para RSSFs não permitirem minimizar o consumo de energia nos estados inactivo e adormecido, o que limita o tempo de vida da rede, a eficiência energética não será alcançada. Durante a investigação desenvolvida foram também concebidos mecanismos inovadores que permitem resolver o problema da ineficiência associada ao overhead da norma IEEE 802.15.4. Em particular, nesta tese de doutoramento propõe-se uma melhoria do desempenho da camada MAC da norma IEEE 802.15.4 usando um mecanismo de reserva de canal com pacotes RTS/CTS, combinado com concatenação de pacotes. Os resultados mostram que o uso do mecanismo de RTS/CTS melhora a eficiência do canal, diminuindo o tempo médio de transmissão de um pacote de dados. Para além disso, é também proposto o protocolo Sensor Block Acknowledgment MAC (SBACK-MAC), que permite a confirmação da entrega de um conjunto de pacotes de dados transmitidos, através da agregação de vários pacotes de resposta de entrega de dados (ACK) num único pacote, *BACK Response*, com a consequente redução de overhead causado pelos pacotes de controlo. Duas soluções considerando a agregação de pacotes são propostas. A primeira considera o protocolo SBACK-MAC contemplando a utilização do pacote de controlo *BACK Request* (concatenação) enquanto a segunda considera o SBACK-MAC sem a utilização do pacote *BACK Request* (piggyback). As soluções propostas abordam um cenário distribuído, com um ritmo de transmissão e de agregação de pacotes fixo. O desempenho em termos de débito binário e atraso é matematicamente derivado em condições ideais (sem erros de transmissão) e condições não ideais (com erros de transmissão), existindo uma melhoria entre $\backsim$8 e 48 %. Os protocolos MAC permitem também diminuir o consumo de energia dos nós sensores.

Palavras-chave

Redes de Sensores sem Fios, Aplicações para RSSFs, Recolha de Energia Electromagnética, Protocolos da Sub-camada MAC, Mecanismo de BACK, Concatenação de Pacotes.

Table of Contents

List of Figures

List of Tables

List of Acronyms

AAL	Ambient Assisted Living
ACK	Acknowledgement
ADC	Analog-to-Digital Converter
ADS	Advanced Design System
AFH	Adaptive Frequency Hopping
AP	Access Point
ASK	Amplitude Shift Keying
AWGN	Additive White Gaussian Noise
BACK	Block Acknowledgment
BER	Bit Error Rate
BI	Beacon Interval
BO	Beacon Order
BP	Backoff Period
BPSK	Band Binary Phase-Shift Keying
BSN	Beacon Sequence Number
BWSN	Building Wireless Sensor Network
CAP	Contention Access Period
CCA	Clear Channel Assessment
CFP	Contention Free Period
CMR	Centralized Management of Resources
CPU	Central Processing Unit
CR	Cognitive Radio
CRC	Cyclic Redundancy Check
CRSN	Cognitive Radio Sensor Network
CRTS/CCTS	Control-Channel-Request-To-Send/Control-Channel-Clear-To-Send
CS	Carrier Sense
CSS	Chirp Spread Spectrum
CSMA-CA	Carrier Sense Multiple Access with Collision Avoidance
CTS	Clear-To-Send

DLL	Data Link Layer
DSA	Dynamic Spectrum Access
DSN	Data Sequence Number
DQPSK	Differential Quadrature Phase-Shift Keying
DSP	Digital Signal Processing
DSSS	Direct Sequence Spread Spectrum
EC	European Commission
ED	End Device
EIRP	Effective Isotropic Radiated Power
ETSI	European Telecommunications Standards Institute
FCC	Federal Communications Commission
FCS	Frame Check Sequence
FFD	Full Function Device
FFT	Fast Fourier Transform
FHR	Foetal Heart Rate
FHSS	Frequency Hopping Spread Spectrum
FIFO	First In, First Out
GPIO	General Purpose Input/Output
GPRS	General Packet Radio Service
GTS	Guaranteed Time Slot
HiFi	High Fidelity
I2C	Inter-Integrated Circuit
IC	Integrated Circuit
IDE	Integrated Development Environment
IFS	Interframe Space
ISM	Industrial, Scientific and Medical
LIFS	Long Interframe Spacing
LoS	Line-of-Sight
LQI	Link Quality Indicator
LR-WPAN	Low-Rate Wireless Personal Area Network
LVTTL	Low-Voltage Transistor-Transistor Logic

MAC	Medium Access Control
MCU	Microcontroller Unit
MEMS	Microelectromechanical Systems
MFR	MAC Footer
MHR	MAC Header
MHWN	Multi-Hop Wireless Network
MPDU	MAC Protocol Data Unit
MSB	Most Significant Bit
MSDU	MAC Service Data Unit
MSK	Minimum Shift Keying
NAV	Network Allocation Vector
NTC	Negative Temperature Thermistor
OCV	Open Circuit Voltage
O-QPSK	Offset Quadrature Phase-Shift Keying
OTAP	Over The Air Programming
PAN	Personal Area Network
PCB	Printed Circuit Board
PDA	Personal Digital Assistant
PER	Packet Error Rate
PHR	PHY Header
PHY	Physical
PM	Piggyback Mechanism
PN	Pseudo-Random Noise
PP	Polypropylene
PPDU	PHY Protocol Data Unit
PSR	Packet Success Rate
PSDU	PHY Service Data Unit
PU	Primary User
QoS	Quality-of-Service
QPSK	Quadrature Phase-Shift Keying
RAM	Random Access Memory

RF	Radio Frequency
RFIC	Radio Frequency Integrated Circuit
RFH	Random Frequency Hopping
RSC	Radio Spectrum Committee
RSSI	Received Signal Strength Indicator
RTS	Request-To-Send
RTS/CTS	Request-To-Send/Clear-To-Send
RX	Receive
SBACK	Sensor Block Acknowledgement
SBACK-MAC	Sensor Block Acknowledgment MAC
SCWNG	Wireless Next Generation Standing Committee
SD	Superframe Duration
SDIO	Secure Digital Input Output
SDM	Sigma Delta Modulated
SDR	Software Defined Radio
SER	Symbol Error Rate
SFD	Start of Frame Delimiter
SG	Spreading Gain
SHR	Synchronisation Header
SIFS	Short Interframe Spacing
SIG	Special Interest Group
SIR	Signal-to-Interference Ratio
SNR	Signal-to-Noise Ratio
SNIR	Signal-to-Interference-plus-Noise Ratio
S-MAC	Sensor-MAC
SO	Superframe Order
SPI	Serial Peripheral Interface
SQL	Structured Query Language
SU	Secondary User
TI	Texas Instruments
UART	Universal Asynchronous Receiver/Transmitter

USB	Universal Serial Bus
UWB	Ultra-Wideband
UWPSN	Ubiquitous Wireless Power Sensor Network
WBAN	Wireless Body Area Network
WLAN	Wireless Local Area Network
WPAN	Wireless Personal Area Network
WSAN	Wireless Sensor Actuator Networks
WSN	Wireless Sensor Network
VAT	Value Added Tax

List of Symbols

A_e	Area of the antenna
$aTurnaroundTime$	RX/TX or TX/RX maximum turnaround length
$aUnitBackoffPeriod$	Backoff period length
BE	Backoff exponent
BO_c	Backoff time counter
CW	Contention window
D	Distance
D_{min}	Minimum average delay
D_{min_CCA}	Minimum delay due to CCA
$D_{min\_CCA\_RTS}$	Minimum delay due to CCA before each RTS/CTS
$D_{min\_Data\_Ret}$	Minimum delay due to packet retransmissions
$D_{min\_Data\_Ret\_RTS}$	Minimum delay due to packet retransmissions and ACK is not received
$D_{min\_RTS\_CTS}$	Minimum average delay due to the channel state and packet retransmissions
D_T	Random deferral time period
E	Electric field
E_b/N_0	SNR to noise density
E_s/N_0	Symbol to noise density
f	Frequency
f_c	Center frequency
G	Gain
I	Discharge current
$i_{\mu Pact}$	Microcontroller current on active state
$i_{\mu Psleep}$	Microcontroller current on SLEEP state
i_{rx}	Transceiver current on RX state
i_{tx}	Transceiver current on TX state
i_{sleep}	Transceiver current on SLEEP state
L_{ACK}	ACK frame length
L_{DATA}	DATA payload
L_{FL}	DATA frame length
L_{H_MAC}	MAC overhead
L_{H_PHY}	PHY length overhead
L_{SHR}	PHY SHR length
M	Codebook
N_{agg}	Number of aggregated packets
NB	Number of backoffs
$nBits$	Length of the frame
P_b	Probability of bit error
$phySymbolsPerOctet$	Symbols per octet for the current PHY
P_L	Path Loss
P_{Sleep}	Power consumption in the SLEEP state
P_s	Probability of symbol error
P_{Sleep}	Power consumption in the SLEEP state
P_r	Received power
P_{RX}	Power consumption in the receiving state

P_t	Transmitted power
P_{TX}	Power consumption in the transmitting state
Q	Capacity
Q_d	Drained capacity
Q_r	Remain capacity
R	Data rate
R_c	Chip rate
S_{max}	Maximum average throughput
S_{11}	Return loss
$S_{max\_RTS\_CTS}$	Maximum average throughput by employing RTS/CTS combined with packet concatenation
T	Battery lifetime
T_{ACK}	ACK transmission time
T_{AW}	ACK wait duration time
T_{BO}	Backoff period duration
$T_{BRequest}$	BACK Request transmission time
$T_{BResponse}$	BACK Response transmission time
T_{CCA}	CCA detection time
T_{CTS}	CTS transmission time
T_{CTS_ADDBA}	CTS ADDBA transmission time
T_{DATA}	Transmission time for DATA
t_{idle}	Time on IDLE state
T_{LIFS}	LIFS time
T_{RTS}	RTS transmission time
T_{RTS_ADDBA}	RTS ADDBA transmission time
T_{SHR}	PHY SHR duration
T_{SIFS}	SIFS time
T_{symbol}	Symbol time
T_{TA}	TX/RX or RX/TX switching time
t_{tx}	Time on TX state
t_{rx}	Time on RX state
t_{sleep}	Time on SLEEP state
$t_{\mu Pact}$	Active time microcontroller
$t_{\mu Psleep}$	Sleep time microcontroller
X_σ	Zero mean gaussian random variable
V_{in}	Input voltage
V_{out}	Output voltage
V_t	Forward conduction voltage
η_c	Conversion efficiency
η	Bandwidth efficiency
ε_r	Permittivity
λ	Wavelength

Chapter 1

Introduction

1.1 Motivation

Wireless Sensor Networks (WSNs) is one of the most exciting and important technological innovations in the field of ad-hoc wireless communications of our time. They are responsible for interconnecting several wireless sensor nodes by providing global ad-hoc communication and computational capabilities. This type of networks is capable of linking the PHY layer with the digital world by sensing, processing, and transmitting the real-world phenomena, and by converting them into a form that can be processed, stored and acted upon.
Since these types of networks are battery operated, energy harvesting can be a solution to make WSNs autonomous while enabling a widespread use of these systems in many applications where the energy storage system can consist of a supercapacitor and/or a rechargeable battery. However, one of the components with the largest power consumption in the sensor nodes is the radio transceiver, as it has a decisive influence on network lifetime. In order to achieve energy-efficiency, a MAC protocol must be chosen, to determine and change the operation mode of the radio.
Furthermore, recent advances in the field of microelectronic circuits caused an increase on the interest in the development of WSNs. Nowadays, WSNs can be deployed in many scenarios such as factory monitoring, healthcare, environment monitoring, logistics, location of persons in commercial buildings, monitoring of building structures and precision agriculture [VDMC08], [RoWR04], [ASSC02].
Some new emergent applications focus on aspects related with the management of the largest car parks. For years, traffic got all the attention: cars in motion were exciting; slow moving cars were boring. Hardly anyone talked about parking. However, in the past 10 years or so, parking has become a paramount concern among city planners and company heads. Space is limited, and yet the demand for parking places keeps increasing. Hence WSNs can be used for monitor the entrance and exit events that occur in parking structures, wirelessly transmitting the data back to a base station to process the information, and send it to a database that can be accessed remotely. Smart buildings are also a "hot topic" because about 70 % of the utility bill for the average household could be affected by the lighting and temperature-related Wireless Sensor Actuator Networks (WSAN) applications. As the utilities rates and the Value Added Tax (VAT) tends to increase over the years, by using a WSAN it is possible to diminish the impact of the increase of the price of electricity by using a energy management system responsible for controlling the cooling, heating, and lighting zones, based on real time humidity and temperature measurements.
The European Union is sensible to the importance of WSAN and the benefits of these networks with low-complexity and low-cost devices and funded or is funding several ongoing projects such as WISEBED [WISE12], COOLNESS [COOL12] and SA-WSN [SAWS11].
This thesis addresses WSN services and applications that require reliable communication between the nodes and base station. Such networks typically consist of a large number of battery operated nodes that may be deployed, in order to create a sensing, computing and communications

infrastructure, so that all the phenomena's in a specified environment can be observed and measured, Figure 1.1.

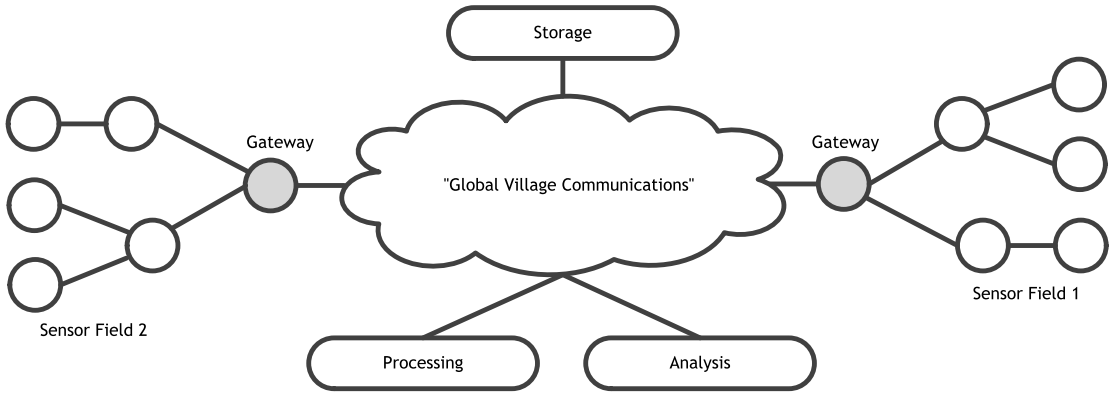

Figure 1.1: Typical topology of a WSN.

The architecture of the employed networks data rates, network size, span, power management and security protocols are all affected, if not dictated, by the communication protocols chosen for the application [WISE12]. In order to fulfill the requirements of the set of different applications, new MAC protocols and channel efficient mechanisms need to be developed in order to respond to the demands for the next generation of WSNs.

1.2 Challenges and approach

From the WSNs point of view, several research issues still need to be addressed in 2009-2013, as the current solutions are not enough optimised or are too much constrained. Although in the literature most of the proposed communication protocols improve energy efficiency to a certain extent by exploiting the collaborative nature of nodes within WSNs and its correlation characteristics, the main commonality of these protocols is the compliance to the traditional layered protocol architecture, allied to the fact they are mainly implemented in commercially available platforms that employs the IEEE 802.15.4 standard. This Ph.D. thesis establishes an evaluation criteria for the most well known WSNs platforms based on IEEE 802.15.4. Even if the MAC sub-layer protocol is designed to be energy-efficient, if the hardware platform does not allow for minimizing the energy consumption in the idle and sleeping states (which limits the network lifetime), then energy efficiency will not be achieved.

There is also an increase of the demand for new innovative WSNs applications aiming at responding to real-world situations enabling to add more value to the person's life. The current Ph.D. thesis proposes instrumentation and sensor data dissemination solutions for the foetal movement monitoring and concrete structure integrity monitoring in the context of Smart-Clothing and INSYSM projects, respectively. Furthermore, contributions are also given in the test and development of RF energy harvesting circuits for power supply a wireless sensor node by considering electromagnetic energy as the primary source.

In the WSNs domain there is a huge amount of proposals for energy-efficient MAC protocols [HXSM12]. However, these MAC protocols have not been capable of having enough success to be deployed as a real commercial application due to the lack of standardization. To design an optimized WSN MAC protocol, the following aspects must be considered [DeEA06]:

- The first one is the energy efficiency, since there are strong limitations to power supply WSN tiny devices and one of the main goals is to extend the network lifetime;

- Other important aspects are scalability and adaptability to changes. Changes in network size, node density and topology should be handled quickly and effectively for a successful adaptation. Some of the reasons behind these network property changes are limited due to node lifetime, addition of new nodes to the network and varying interference which may alter the connectivity and hence the network topology;

- Finally, Quality-of-Service (QoS) attributes, such as latency, throughput and bandwidth efficiency will also be considered, since this type of metrics is very common when we deal with multimedia applications, and specially real time applications.

Allied to the aforementioned design issues, IEEE 802.15.4 has been widely accepted as the *de facto* standard for the PHY/MAC layers of WSNs. A study conducted by IMS Research [IMSR09] have shown that over 20 million of IEEE 802.15.4 chips were sold in 2009. Therefore, in the context of this Ph.D. thesis we propose new innovative MAC sub-layer protocols that can also be considered as a future possible contribution to the standard itself.
Packet concatenation facilitates the aggregation of several consecutive packets by means of channel reservation and different types of acknowledgment and/or Network Allocation Vector (NAV) procedures. In this context, the RTS/CTS mechanism enables to reserve the channel and avoids to repeat the backoff phase for every consecutive transmitted packet, targeting to reduce overhead. In the presence of RTS/CTS two solutions are considered, one with DATA/ACK handshake and another one with no ACKs, simply relying in the establishment of the NAV.
In particular, the Sensor Block Acknowledgment MAC (SBACK-MAC) protocol allows the aggregation of several acknowledgment responses into one special packet *BACK Response* being compliant with the IEEE 802.15.4 standard. Two different solutions are addressed. The first one considers the SBACK-MAC protocol in the presence of *BACK Request* (concatenation mechanism), while the second one considers SBACK-MAC in the absence of *BACK Request* (the so-called piggyback mechanism).
The following objectives were identified as key points for research during this thesis:

- Address application-specific WSN solutions and strategies to be applied in real world applications such as: medical environments, civil engineering and utilities;

- Evaluate the IEEE 802.15.4 MAC layer performance by using the RTS/CTS combined with packet concatenation;

- Mathematical derivation of the maximum average throughput and the minimum average delay for the proposed mechanisms, either under ideal conditions (a channel environment with no transmission errors) or non ideal conditions (a channel environment with transmission errors), by varying the data payload and the number of transmitted packets. A comparison will be made with IEEE 802.15.4 in the basic access mode;

- Study of the retransmission scenarios for both IEEE 802.15.4 and SBACK-MAC, where two nodes simultaneously, identify the idle channel during Clear Channel Assessment (CCA) and start transmitting, causing data collisions;

- To disseminate the carried out research, through the publication of papers in national and international conferences and journals.

The proposed MAC protocol must be compliant with the IEEE 802.15.4 standard, since we envisaged that the proposed solutions can be integrated in the IEEE 802.15.4 standards or serve as the basis for the Wireless Next Generation Networks. Even in 2014, for IEEE 802.15.4, in the Wireless Next Generation Standing Committee (SCWNG), there is an opportunity to incorporate the proposals on SBACK-MAC protocol.

1.3 Contributions

The work presented in this thesis is part of different research European frameworks, such as the INSYSM Marie Curie IAPP [INSY13] and PLANOPTI, Marie Curie European Reintegration Grant [PLAN13], as well as cooperation in the field of Scientific and Technical Cooperation (COST) namely COST2100 [COST13a], COST IC1004 [COST13b] and COST IC0905 "TERRA" [COST13c].
Contributions have also been given on applications and MAC sub-layer protocols for WSNs, developed in the framework of the Smart-Clothing [SMAR12] portuguese project. In the framework of PROENERGY-WSN (PTDC/EEA-TEL/122681/2010) portuguese project [PROE13] contributions have also be given in radio frequency energy harvesting circuits, MAC sub-layer protocols and cognitive radio design issues for wireless body area networks.
The participation in these projects has assumed of particular importance during the research conducted in the context of this thesis. The work developed with Portuguese and other international researchers or partners has been very rewarding allowing to improve the proposed solutions as well as to gain experience in the field of telecommunications and interdisciplinary research.
The research in these applications, energy harvesting techniques, the impact of different radio transceivers in the protocol performance and on the proposal of innovative energy-efficient MAC sub-layer protocols is part of WP1 (Framework and Deployment Scenarios for Coexistence) and WP2 (MAC and Cross-layer Simulations) from Planning and Optimization for the Coexistence of Mobile and Wireless Networks Towards Long Term Evolution, PLANOPTI [PLAN13]. The work from the participation in the aforementioned projects was already disseminated through the publication or submission of papers in national and international conferences, journals and book chapters:

- Research work has been conducted in the field of instrumentation and WSN applications for real scenarios in the context of the Smart-Clothing and contributions have been given to the INSYSM IAPP project. Different sensors, data acquisition systems and dissemination solutions for wireless sensor networks, based on IEEE 802.15.4 have been proposed and tested within different applications, enabling to deliver the sensor data in real time to the end-user.

    - The main objective of the Smart Clothing for Health Monitoring and Sport Applications (Smart-Clothing) project [Sma09] was to develop an easy to wear telemedicine gear that allows for remotely monitoring a pregnant women, and count the foetus movements. The participation in this project resulted into the publication of a book chapter [BALR10], conference papers [BBVL09a], [BBVL09b] and a technical report [BBVL08];
    - The main objective of the Intelligent Systems for Structures Strengthening and Monitoring (INSYSM) project [INSY13] is to develop a WSN prototype, allowing for remotely monitoring temperature and humidity inside concrete structures. The work from this

part of the research contributed to the INSYSM IAPP by means of a journal publication [BBVM13], and a technical report [BBVM11];

- In the PROENERGY-WSN (PTDC/EEA-TEL/122681/2010) project [PROE13] contributions have be given to the investigation of the influence of the switching delay times imposed by the hardware constraints of the IEEE 802.15.4 compliant radio transceivers [BaGV13]. The radio transceivers with the shortest switching delay time can maximize the network lifetime whilst decreasing the time for switching between states (i.e., RX, TX and SLEEP).

  Contributions were also given in the identification of spectrum opportunities through power density measurements from 350 MHz to 3 GHz for RF harvesting [TBSB13]. Besides, PHY, MAC and network layer design aspects have been addressed, by considering cognitive radio (CR). The scope of the research also involved the test and development of RF energy harvesting circuits for power supply a wireless sensor node by considering electromagnetic energy as the primary source [BSGT13].

- Cognitive Radio (CR) aspects for Medical Body Area Networks (MBANs) have been addressed together with colleagues from COST IC0905 "TERRA" in [SNHN12]. Viable architectures solutions of medical body area networks, with practical CR features based no the Ultra-Wideband (UWB) radio technology are considered. PHY and MAC layer aspects also discussed, in addition to implementation aspects and challenges. Besides contributions were also be given to a book chapter, where a case study is addressed by considering CR in medical environments [SBVS14];

Also, contributions were given within the context of regular scientific meetings of the COST Action 2100 (COST2100),COST IC1004 and COST IC0905 "TERRA" as follows:

- A SMAC protocol modelling and simulation for Wireless Body Area Networks (WBAN), [BVFB10] have been investigated, were the impact of several simultaneous factors, including periodic receive/transmit and sleep cycles, the length of the transmitted packet and data rate is addressed. The use of a BACK mechanism is proposed as well account the average delay, which can be clearly reduced by means of BACK;

- Electromagnetic energy harvesting for WBANs with CR capabilities [BFBT12];

- Spectrum opportunities for electromagnetic energy harvesting from 350 MHz to 3 GHz [TBSB13];

- Antennas and circuits for ambient RF energy harvesting in WBANs [BSGT13];

- Block acknowledgement and piggyback mechanisms for the optimization of channel use in wireless sensor networks with cognitive radio capabilities [BaVC13a].

Contributions were also given in the proposal of new innovative MAC sub-layer protocols employing RTS/CTS with packet concatenation as follows:

- A Block Acknowledgment (BACK) mechanism for the optimization of channel use in wireless sensor networks has been proposed resulting in a conference publication [BaVC13a] and a technical report was created [BaVC13b] in the context of a Short Term Scientific Mission (STSM) in the Department of Informatics, Alexander TEI of Thessaloniki, Greece, supported by COST IC0905 "TERRA";

- IEEE 802.15.4 MAC Layer Performance Enhancement by employing RTS/CTS combined with Packet Concatenation has been proposed in the context of this thesis resulting in a submission to a conference [BBVC14]. The extension of this work including the IEEE 802.15.4 by CSS PHY layer will be submitted for a publication in a Journal [BBVC13].

1.4 Structure of the Thesis

This Thesis is organized into 6 Chapters, including this one, and five Appendices.
Chapter 2 presents the application fields of WSNs showing the development of real WSNs applications and scenarios. It is divided into two main Sections. Section 2.1 addresses the hierarchical communication system that is employed to deliver the data from the WBAN that is installed in a pregnant woman to a Centralized Management of Resources (CMR), where the information can be accessed by the doctor later on. The development of the prototypes combines investigation in sensors, functional textiles, data mining and wireless communication networks in the context of human body. Section 2.2 addresses interdisciplinary research among Civil and Electrical Engineering, where a prototype has been developed allowing for remotely monitoring concrete structures. A WSN has been created based on IEEE 802.15.4 allowing for the creation of a continuous monitoring humidity and temperature system capable of sending the data wirelessly. The proposed solution has a tremendous potential in real time structural health monitoring, since it reduces the cost and prevents from the risks associated to monitoring systems (e.g., inaccuracy in the measured values or negative impact of dangerous environments) in the measurement procedure.
Chapter 3 addresses an energy self-sustainable WSN formed by nodes with Radio Frequency (RF) energy harvesting capabilities. The spectrum opportunities for RF energy harvesting have been identified through power density measurements from 350 MHz to 3 GHz . Based on the identification of the most promising opportunities, a dual-band band printed antenna operating at GSM bands (900/1800) is shown, enabling to harvest the electromagnetic energy. Besides, simulation and experimental results for the dimensioning of a 5-stage Dickson voltage multiplier for collecting RF energy are presented followed by the discussion of the results.
In Chapter 4 we present the state-of-the-art of the WSN hardware platforms that could be suitable for accommodating the MAC protocols developed in the context of this thesis. An evaluation criterion for choosing the best WSN platforms has been proposed enabling to choose the best among them. This assumes particular importance since energy efficient platforms and innovative MAC protocols are envisaged, enabling for the creation of an autonomous WSN with energy harvesting capabilities running in nearly perpetual operation with little or no maintenance.
Chapter 5 proposes IEEE 802.15.4 MAC layer performance enhancement by employing RTS/CTS combined with packet concatenation. One explores that the use of the RTS/CTS mechanism to enhance channel efficiency by decreasing the deferral time before transmitting a data packet. In addition, the SBACK-MAC protocol has been proposed, which allows the aggregation of several acknowledgment responses in one special *BACK Response* packet. The first one considers the SBACK-MAC protocol in the presence of *BACK Request* (concatenation) while the second one considers the SBACK-MAC in the absence of *BACK Request* (piggyback).
Finally, Chapter 6 presents the conclusions of the research carried out throughout the current thesis as well as, some final considerations and suggestions for further research. Further detailed information can be found in Appendices.

Appendix A discusses the IEEE 802.15.4 PHY and MAC layers in detail. Appendix B addresses the O-QPSK modulation employed by IEEE 802.15.4. Appendix C presents the energy consumption model enabling to evaluate the lifetime of the WSN platforms presented in Chapter 4. Appendix D shows the remaining characterization of the WSN platforms considered in Chapter 4. Finally, Appendix E presents the remaining results for the evaluation of the performance of the SBACK-MAC protocol.

Chapter 2

Fields of Application for Wireless Sensor Networks

This Chapter presents the instrumentation and applications proposed and tested in real Wireless Sensor Network (WSN) scenarios, and is organized into two parts. Firstly, a Wireless Body Area Network (WBAN) is presented where an innovative foetal movement monitoring application was developed in the framework of the Smart-Clothing Project. Secondly, an automatic wireless sensor monitoring system for civil engineering structures, developed in the framework of the INSYSM Project is addressed followed a summary and conclusions.

2.1 Applications for Wireless Body Area Networks

The increasing use of WSN and the constant miniaturization of electrical devices has empowered the development of Wireless Body Area Networks (WBANs). A WBAN consist of tiny intelligent devices (motes) attached on or implanted in the human body that are able to gather, process and wirelessly transmit the sensed data. These devices provide continuous health monitoring as well as real-time feedback to the user or medical personnel. Furthermore, the physiological measurements can be recorded in specialised medical servers in an unobtrusive manner to the patient. Next, we provide an overview of the work addressed in WBAN in the framework of the Smart-Clothing project that combines investigation in functional textile materials and wireless communication networks in the context of human body and methods for the data analysis and treatment.

2.1.1 Challenges

The main objective of the Smart Clothing for Health Monitoring and Sport Applications (Smart-Clothing) project is to monitor the foetal movements in the last four weeks of pregnancy in the context of WBANs. The pregnant women can be either at home or in the hospital. In the first stage of the project some tests were made using several types of sensors integrated into a belt. As so, we were able to identify the ones that are more reliable for the detection of foetal movements. Besides the integration of sensors in the garment, a hierarchical communication system was created allowing for deliver the data collected from the garment that the pregnant is wearing to the doctor. A bottom-up architecture formed by i) WSNs, ii) Wi-Fi, and iii) Ethernet (or WiMAX) was explored to facilitate healthcare monitoring anyway, anywhere and anytime, as shown in Figure 2.1. Although, the maternal perception is a relevant characteristic for the evaluation of the foetal health, this monitoring is hard to accomplish and could induce errors due to mother's anxiety and concentration. Therefore, counting the foetal movements felt by the mother is very important [KPTB06], [GrJa05].
From the WBAN perspective a network based on the IEEE 802.15.4 standard was developed, enabling to identify sudden changes in the foetus health, by monitoring its movements and the Foetal Heart Rate (FHR).

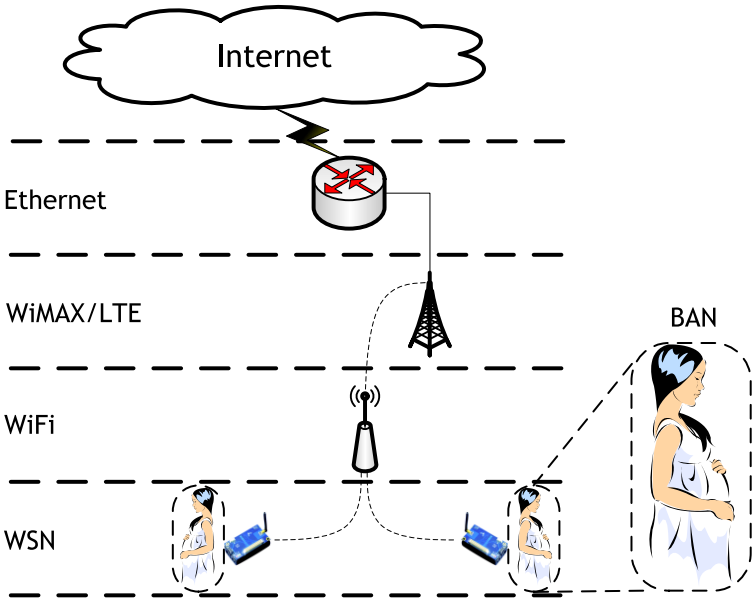

Figure 2.1: Hierarchical network considering the WBAN and other communication networks.

2.1.2 System description

In order to accomplish the communications task, instead of using wired connections, the data is transmitted through a WSN composed by MEMSIC® IRIS motes [IRIS13]. This WSN allows for receiving the collected data from the sensors in a computer and make the results available [BBVL09a]. The simplest device consists of a mote, a small battery and a set of sensors (i.e., flex sensors). These devices enable for continuous foetal health monitoring which traditionally is based on protocols where the foetal movements felt by the mother are counted. So a hybrid communication system is employed in order to deliver the data from the WBAN that is installed in the pregnant woman. All the data from our application is saved, by using a Structured Query Language (SQL) database. The SQL database helps avoiding redundant and outdated data, and solves security problems related with the malicious or unauthorized access. The data being collected from the belt of the pregnant woman must be protected from corruption [BBVL09a].

The block diagram for the acquisition system is presented in Figure 2.2. The IEEE 802.15.4 sensor network, whose primary function is the gathering of the vital data from the various sensors that are applied in the patient body remotely, allows for monitoring the foetal movements from a pregnant woman while transmitting the data to a mote interface board (Gateway) that is directly connected to our CMR. The CMR entity is formed by a base station, a personal computer, an application being responsible for showing the data and save all the records in a database, and a Wi-Fi module to transmit the data across a Wireless Local Area Network (WLAN), [BVFB09, SoMZ07], as shown in the Figure 2.3. There are two different possibilities to receive and send information. One uses an IEEE 802.15.4 network, while the other one considers two protocol layers (IEEE 802.15.4 and 802.11 ones). If the priority is to collect as much data as possible from the patient, some questions like energy consumption arise. Tradeoffs between energy consumption and processing and communication capabilities must be addressed [BVFB09].

The IEEE 802.15.4 standard was chosen because of its unique characteristics that lead to energy-efficient MAC protocols. It also facilitates the development of our application according to the patient needs, while ensuring an integrated and complete solution for sensor networking based

applications, including analog-to-digital conversion. One scenario addressed for this small scale wireless flex sensor belt network is a waiting room of the health centre or clinic, where a pregnant women waits to visit the obstetrician. In the second solution for this belt, another communication layer was considered allowing for sending and receiving information that is collected from the IEEE 802.15.4 network through an IEEE 802.11 wireless network, as shown in Figure 2.3. This solution was chosen because it constitutes a practical and interesting solution for network connectivity while offering some mobility, flexibility, and low cost of deployment. An example is transmitting the data from our CMR to any computer that is in its range and has an IEEE 802.11 (Wi-Fi) connection capability. The CMR may be controlled and monitored by a nurse that looks up for anomalies in the flex sensor belt data.

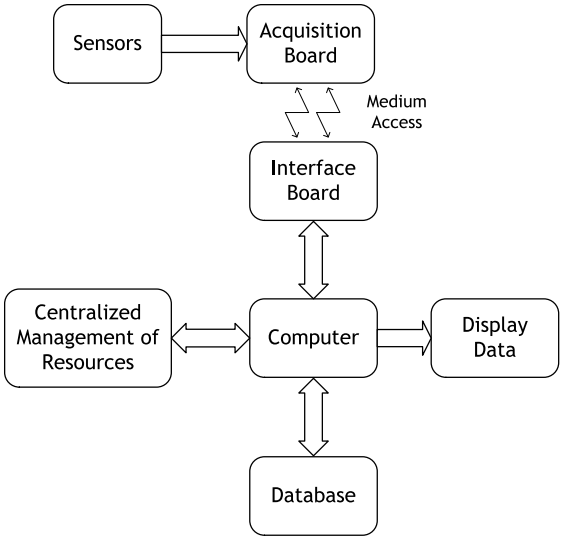

Figure 2.2: Block diagram for the acquisition system.

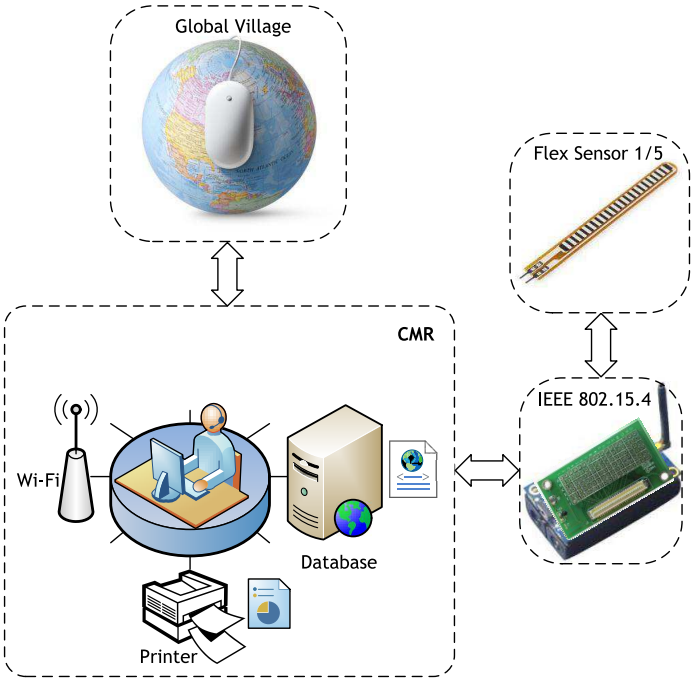

Figure 2.3: Patient monitoring and IEEE 802.15.4 wireless networking.

2.1.3 Experimental apparatus

Flex sensor belt

After the application scenarios had been defined in [BRVS08], the next step was to identify which types of sensors would be incorporated into the Smart-Clothing belt. To achieve this goal, several belts were made, tested and compared to see which sensors were capable of better detecting the foetal movements [BRVS08]. One of the Smart-Clothing belt prototypes is based on the flex sensor, while another one incorporates a piezoelectric sensor. The first version of the flex sensor belt incorporates eight flex sensors, as shown in Figure 2.4. A simple voltage divider, associated to a temperature compensated voltage reference, generates the input signal. The manufacturer proposes a correspondence of standard values of the flexion angle to a certain value of resistance. The acquisition system diagram is presented in Figure 2.5.

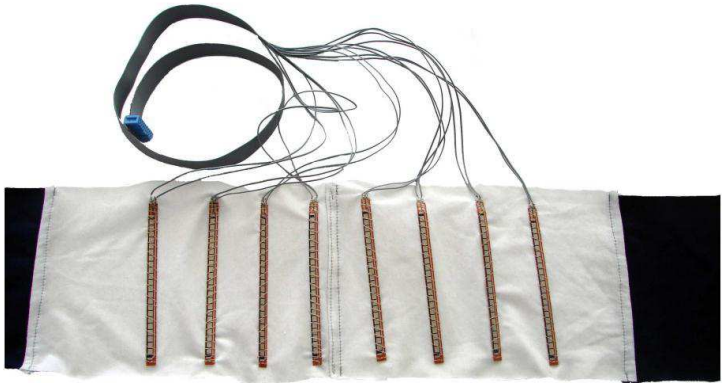

Figure 2.4: Flex sensor belt.

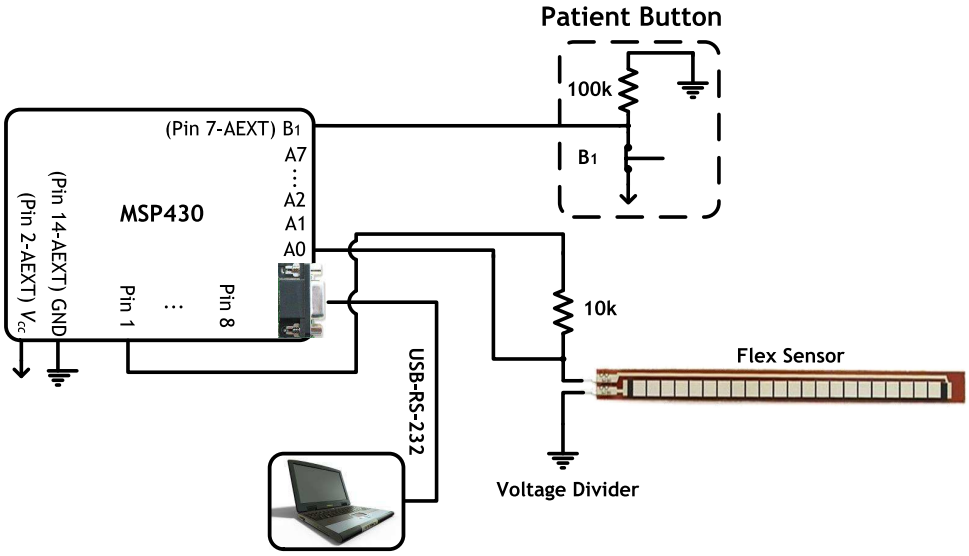

Figure 2.5: Flex sensor belt acquisition system diagram.

For the sake of simplicity just one flex sensor is presented. Besides the flex sensor, a button was incorporated in the system to be pressed by the pregnant woman (i.e., when she feels or detects

foetal movement). The recording of these events is very useful for comparison purposes, as they enable a comparison of personal detected movements with the movements automatically detected by the belt. A microcontroller was used for data acquisition and communication. For practical reasons, in a preliminary experimental context, we supplied the V_{cc} voltage to the voltage divider by using external pin from the MSP430 microcontroller (MSP430-F449STK2 module) and read the voltages from the voltage dividers using the Analog-to-Digital Converter (ADC) inputs of the microcontroller.

Figure 2.6 presents the theoretical and calibration curves for the flex sensor. The theoretical line is based on the resistance values and corresponding deflection angle supplied by the flex sensor manufacturer. The calibration curve results from an experiment where the flex sensor was bent from 0º to 90º and the resistance value measured with a protractor was registered at each 10º of bending increment. The mathematical formulations to compute the resistance value and the bend angle are presented in [BALR10].

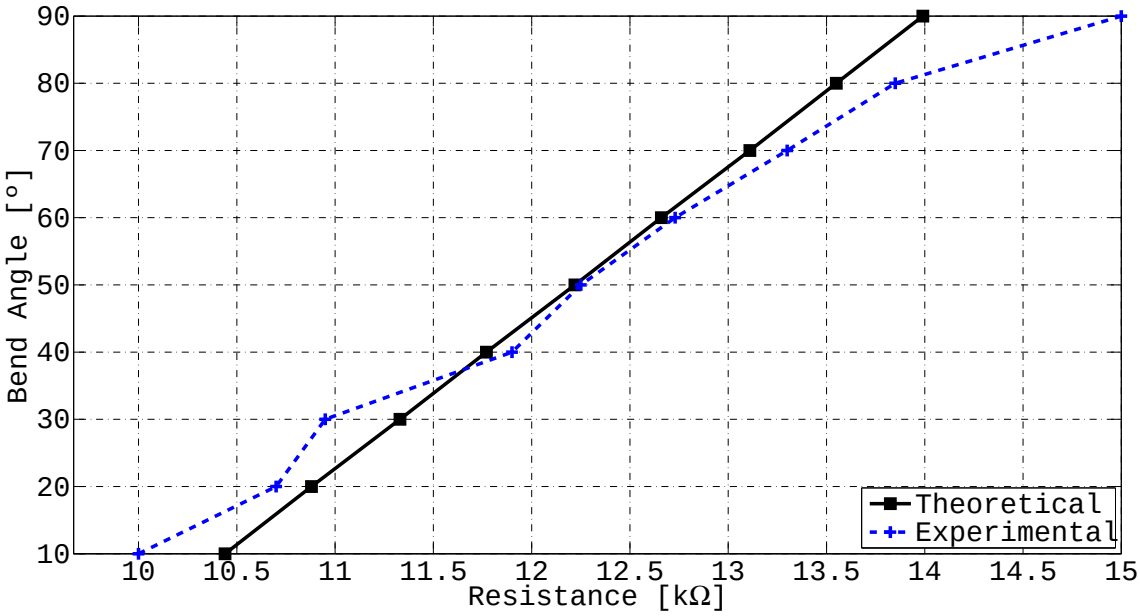

Figure 2.6: Theoretical and calibration curves for the flex sensor.

Figure 2.7 presents the algorithm for the acquisition system. If the reset option is not chosen then the algorithm will measure the voltage from the power supply, in order to compute later the corresponding voltage to a flexion angle. Then, if button B1 (located in the acquisition module) is pressed, a timer (of 100 ms) is set. After 100 ms, the algorithm starts reading all flex sensors. First, the flex sensor 1 voltage divider is powered up. Then, the algorithm waits 10 ms so that the ADC can read properly the voltage value from the voltage divider. Then, it computes the flexion angle depending on the read voltage value and extracts the state of the patient button (if the patient pressed the button it records the time and add one unit to the counter). This procedure is repeated for the other seven flex sensors. However, in the last one the data from all the flex sensors and patient counter is aggregated enabling to build the data packet while sending it to the computer. The flex sensor view program running presents the values of the different angles for each flex sensor.

The final version of the standalone flex sensor belt considers only one data packet to transmit the deformation angles of the eight flex sensors, according to the packet protocol established between the computer and the acquisition module. This data packet is sent at the end of the routine controlled by a timer in the microcontroller only, in order to maintain a constant data

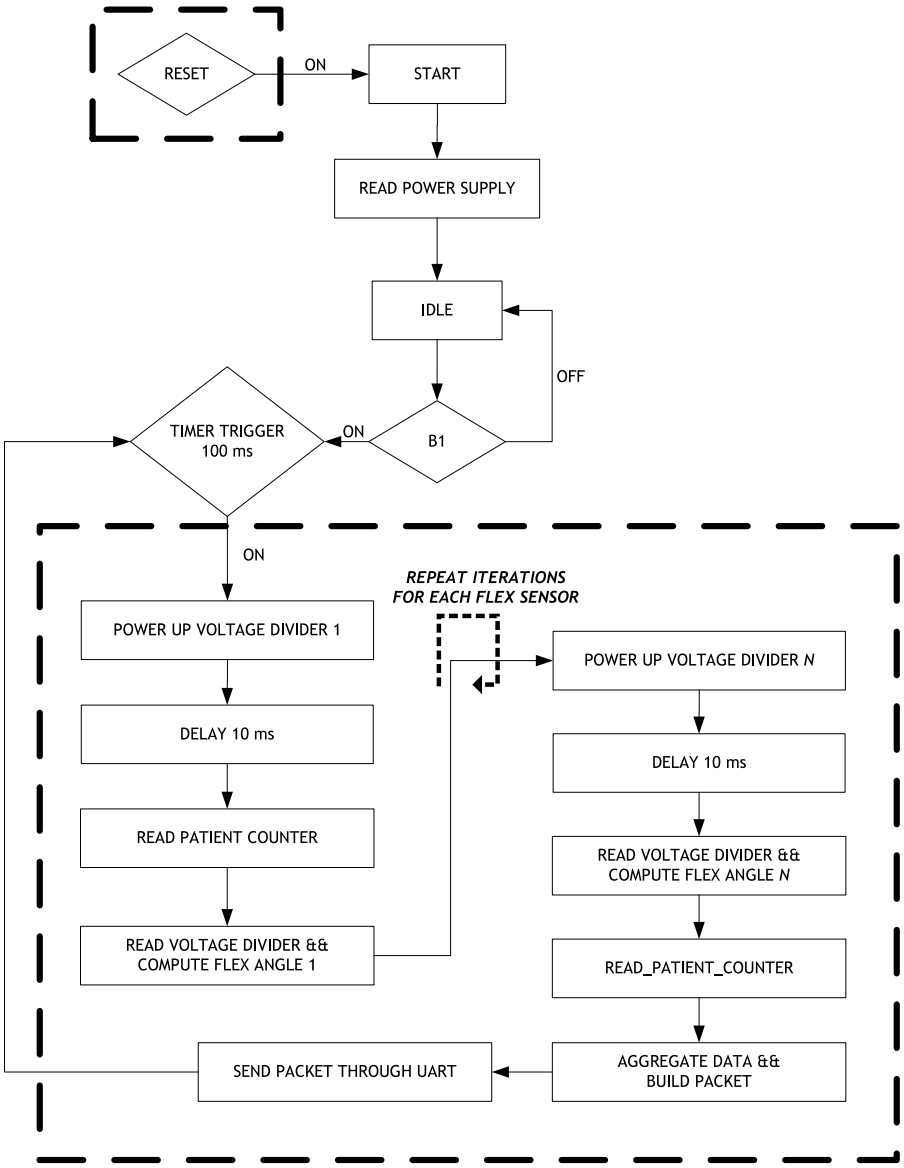

Figure 2.7: Algorithm diagram for the flex sensor acquisition system.

flow between the acquisition module and the computer. Moreover, a calibration routine was implemented in the microcontroller. Each calibration packet is sent from the program running in the computer to the acquisition module and has the ability to calibrate all the (eight) flex sensors (or only one).

Belt with piezoelectric sensors

In the context of the Smart-Clothing project we have developed another belt incorporating piezoelectric sensors. This type of sensor transduces the force to voltage (and vice-versa) allowing for the detection of the mechanical movements such as those originated from foetus in a pregnant woman. They have high sensitivity, are cheap and could be very small, being able to respond to a broad frequency range whilst not reacting to static forces. The integration of this type of sensor in the wearable belt was accomplished by using a plastic pre-encapsulated piezoelectric sensors with a BNC connector, being responsible for driving the electrical voltage signal to the signal processing circuit. This type of sensor, Figure 2.8, is used by PowerLabs data

acquisition system from ADInstruments [MLT109], at Health Science Faculty from Universidade da Beira Interior.

Figure 2.8: MLT1010 piezoelectric sensor (ADI Instruments).

Other healthcare monitoring devices are based in piezoelectric film sensors, as the one presented in Figure 2.9. This sensor is placed against the abdomen of the pregnant woman in order to detect slight surface deformations caused by the movements of the foetus.

Figure 2.9: A piezoelectric film sensor used in a preliminary Smart-Clothing belt.

Compared with other sensors this one presents a high sensitivity, reduced dimensions and does not need power supply to operate. Figure 2.10 shows the signals captured by the sensor above, during an experiment where the pregnant woman also holds a pressure switch that should be pressed when perceiving a foetal movement. In this experiment, only one sensor was used several times, placed in several positions in order to detect the foetal movements. Besides the detection of the foetal movement, the mother's breath movement is also felt as well as the movements due to the displacement of the sensor (motion artifacts). These movements represent an interference signal that should be eliminated [VPMS07], and are represented upon the curve in Figure 2.10.

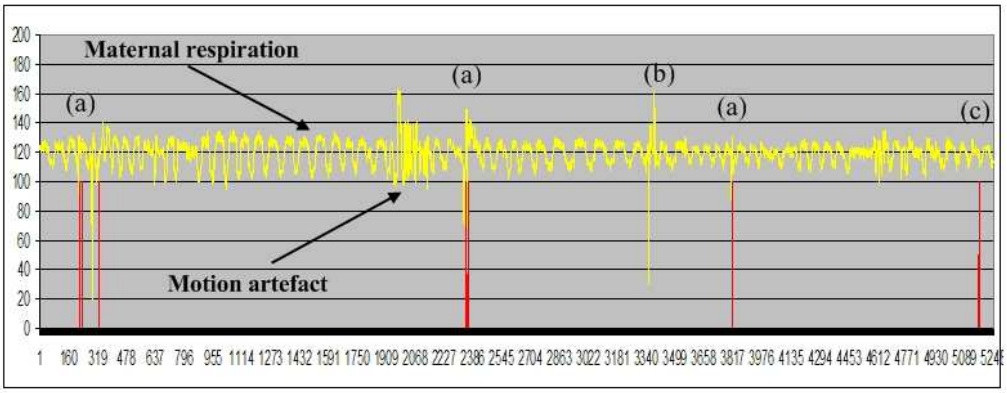

Figure 2.10: Foetal movement curves (upper=belt, lower=mother): (a) detected by mother and belt, (b) detected by belt only, and (c) detected only by the mother.

2.1.4 Experimental results

Flex sensor belt

Some initial results were extracted from the flex sensor belt with a patient that was not a pregnant woman. The objective of this test was to verify if the respiratory movements or

other type of motion artefact influence the angles of each flex sensor in the belt. It was verified that the respiration movements were slightly felt. If the patient moves quickly, the sensors may detect the deformation from the belt. After these preliminary tests, the flex sensor belt was tested in a pregnant woman, in order to detect foetal movements and compare these occurrences with those signalled when the pregnant woman presses the button. A good idea that can be extracted from these initial tests is to implement a routine which automatically defines the value for a detection threshold-trigger whose values will be tuned. This version enables the communication between the computer and the acquisition module by using a single interface a packet for all flex sensors.

The flex sensor view software was incorporated and its final version is presented in Figure 2.11. Examples are the capability to simultaneously show eight angles from the flex sensor belt, the patient counter and the option to save the data in a log file (for later treatment).

Figure 2.11: Main window for flex sensor view application.

Figure 2.12 presents the real-time view chart plot for the flex sensor belt, extracted from the application to display the deformation angles.

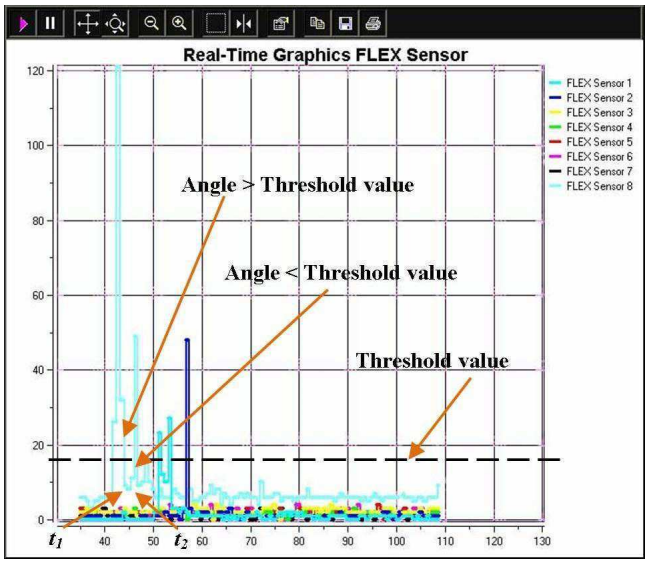

Figure 2.12: Real-time view chart plot for the flex sensor.

For each sensor, an independent threshold trigger can be defined individually or a unique threshold value can be defined (as a whole) for all the sensors. Therefore, even if the sensor detects some motion artefact, a boundary can be established in order to tune when the application should count the deformation angle as a foetal movement. In Figure 2.12, the value used for the global threshold is equal to 15º (angle deformation). This threshold was established by analysing the experimental data. This means that the automatic counter from each flex sensor counts a flexion as a movement when the instant value of the flex sensor angle is larger than the threshold value at one time instant and smaller at the next time instant. As an example of how the automatic counter works, considering flex sensor 8 in the view chart at time instant t_1 the angle value is equal to 28º. Hence, the counter will count a foetal movement if this value decreases at the next time instant. In time instant t_2 the angle value is equal to 8º; so, the automatic counter will add one unit to the counter of the flex sensor 8.
Some tests were made in a pregnant woman. During the test, the patient was sitting in a chair most of the time, as presented in Figure 2.13.

Figure 2.13: Pregnant woman sitting.

A calibration of the flex sensors has been made in the belt circuit before any test. A test was also made to verify on how curves vary if a sudden change of the pregnant woman position happens, as shown in Figure 2.14.

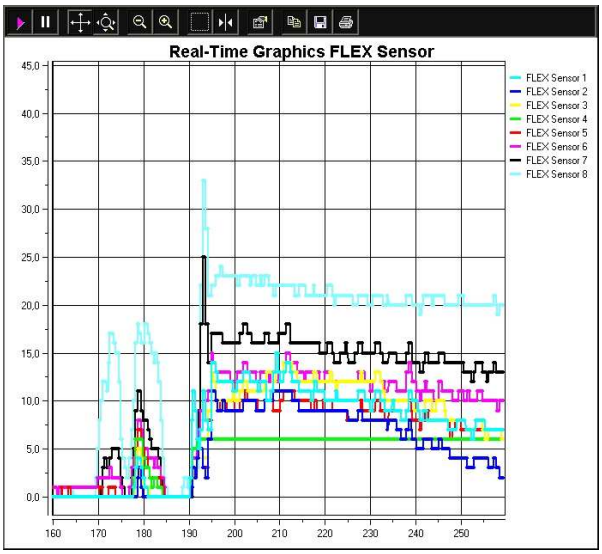

Figure 2.14: Results when patient stands up at time t = 190 s.

One may verify that the change of position occurred approximately at the time instant 190 s. There was a lot of artefact movement detected during the change of position, which causes the loss of the initial calibration.
Another test was made when the patient was sitting in a chair, as presented in Figure 2.15. A movement was detected by the system, while the patient claims to have detected two foetal movement occurrences. The time instant when the system and the patient detected the foetus movement simultaneously was $\approx$ 910 s. The system detected the movement at the Flex sensors 1, 2, 3, 4, 5 and 6, with a stronger intensity in the Flex sensor 3. The other movements the pregnant woman claimed to have felt a foetus movement was at time instant $\approx$ 895 s. However, the system did not detect any foetal movement. At the instant $\approx$ 925 s the system detected a foetus movement but it was considered a false positive, as the patient did not feel it.

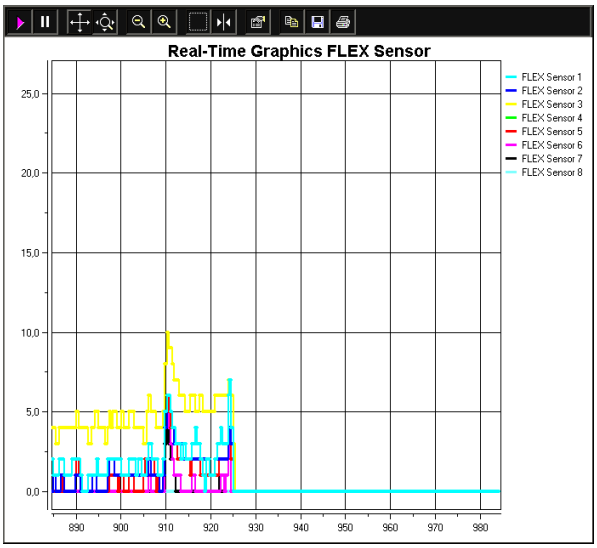

Figure 2.15: Results when patient is sited.

Belt with piezoelectric sensors

All the tests of the piezoelectric sensor belt were performed in Centro Hospitalar da Cova da Beira. A woman in her 38^{th} week of pregnancy wore a belt that incorporates three piezoelectric sensors (one central sensor and two on both sides), adjusted to the abdomen by an elastic belt. The signals obtained from the sensors were combined into only one signal, amplified, filtered and applied to an ADC converter, being sent to the computer via Universal Serial Bus (USB). At the computer, the signals were processed and graphically presented to the medical team. The pregnant woman had a manual event marker (patient button) to mark the foetal movements when she felt it, for redundancy purposes. Another device was also used, called Respisense [RESP12] and usually applied to detect the baby breathing. The signals of the event marker and Respisense were compared with those extracted from piezoelectric sensors. Figure 2.16 shows a block diagram of the circuit responsible for acquiring the signals from the sensors.
Figure 2.17 shows the Hospital environment in which the tests were performed, as well as the pregnant woman. The belt covers only a small part of the pregnant patient belly, contributing for non-ideal results. One envisaged scenario is the use of more piezoelectric sensors in a future version of the belt.

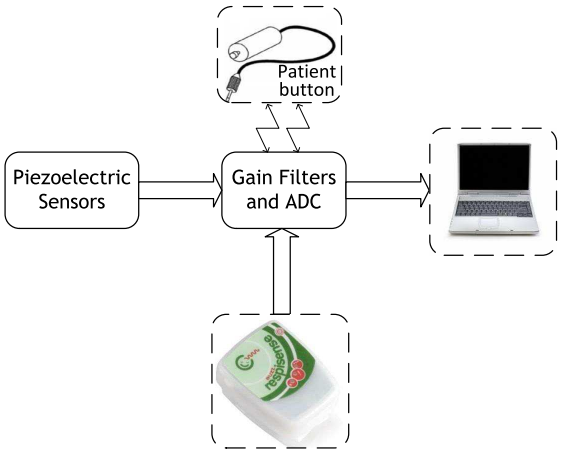

Figure 2.16: Diagram for the circuit to acquire the signals from the sensor.

Figure 2.17: Field tests for foetal movements' detection.

Figure 2.18 presents the experimental results. Different signals can be observed and distinguished by different colours:

- Red - original signal (piezoelectric sensors);
- Blue - filtered signal (finite impulse high-pass response filter);
- Brown - event marker;
- Green - detected foetal movements.

Figure 2.18 presents a screenshot from the program developed to display the signals from the sensors. It shows the: a) multiple foetal movements simultaneously detected by the mother and sensors, as well as b) some discrepancies caused by patient movements (like speaking, tossing), by the event marker detection forgotten by the patient, and due to the reduced number of piezoelectric sensors included. From the experimental results, we can conclude that the system has a high potential to detect foetal movements, isolating them from external interferences. However, weak foetal movements are easily hidden by signals with larger amplitude, such as maternal walking, speaking and even breathing. Filtering and interference reduction will be important topics that pose significant challenges and need further research. Also, using

more piezoelectric sensors inside of the belt, to cover a broader area of the pregnant woman abdomen, is one suggestion for future developments.

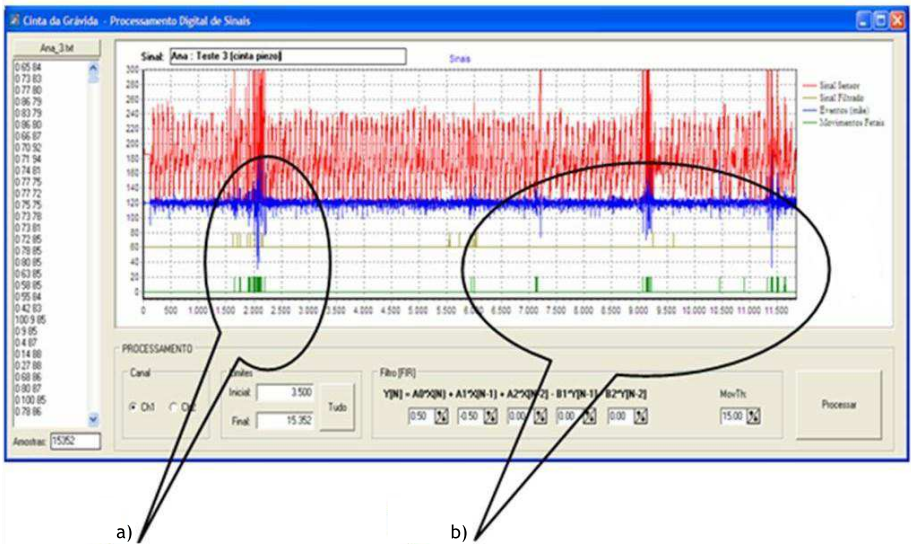

Figure 2.18: Test results for foetal movements' detection.

2.1.5 Summary and conclusions

This Section has presented two main versions of prototype sensor belts produced within the Smart-Clothing project, which aim at counting the movements of the foetus in a pregnant woman. Besides the standalone solution for the flex sensor belt, where data can be saved into a memory card, we developed a wireless flex sensor belt network based on the IEEE 802.15.4 standard. A hierarchical wireless network with a Wi-Fi layer on top of the sensor network will allow for extra flexibility in data communication. The system guarantees real-time and continuous foetal monitoring while creating effective interfaces for querying sensor data and store all the medical record (which can later be accessed by health professionals). Another belt developed has piezoelectric sensors incorporated onto it. The system has a high capacity to detect foetal movements, isolating them from external interferences. As future work, the objective is to propose and implement other types of communication systems that may work together with the existing ones. For example, create a webpage where we can scroll through all the data produced in real time while sharing the information with other medical institutions. Another proposal is to implement algorithms for signal source separation, noise and motion artefact signal suppression, as well as to implement advanced algorithms for data treatment and aggregation. Further work is needed to upgrade the signal conditioning circuitry, the processing software (to accomplish a real time filtering) and statistical techniques to detect the foetal movements in the piezoelectric belt. The data collected from the belt contains signals from the mother and foetus. An alternative approach to distinguish the different signals detected with the belt may be based on a spectral analysis instead of time domain analysis, facilitating the separation of the different signals, such as the mother respiration, foetus movements, mother's heart beat and motion artifacts. Other techniques may be based on the Fast Fourier Transform (FFT), which detects a peak from a signal composed by signals with different frequencies, or blind source separation.

2.2 Wireless Sensor Monitoring System for Civil Engineering Structures

It is now recognized that integrated monitoring systems and procedures have an important and promising role to play in the total management of concrete structures. Monitoring deterioration would provide an early warning of incipient problems enabling the planning and scheduling of maintenance programmes, hence minimising relevant costs. Furthermore, the use of data from monitoring systems together with improved service-life prediction models leads to additional savings in life cycle costs [BDKG08, McVe04].

Sensors and associated monitoring systems to assess materials performance form an important element in the inspection, assessment and management of concrete structures. There are more than fifty different types of sensor whose deployment into practical devices facilitates long-term monitoring of structural changes, reinforcement corrosion, concrete chemistry, moisture state and temperature [McVe04].

The development of new sensor concepts allows for a more rational approach to the assessment of repair options, and scheduling of inspection and maintenance programmes in different civil engineering structures. Currently, there is a growing number of recent studies for the development of sensors in concrete structures, to monitor earlier-age parameters to environmental conditions that can cause deterioration processes, some of which may be highlighted. In the work from [PrLi11], the authors studied an early-age concrete strength development miniaturized sensor system. The idea is to characterise the condition of the fresh concrete at very early stages. It consists of a reusable transducer being strong enough to easily detach from the hardened concrete structure, and to monitor the concrete strength development at early ages and initial hydration stages. The authors from [CLNL06] studied the performance of a fibre-optic sensor for monitoring cracks of concrete, masonry and bituminous elements. The proposed sensor does not require prior knowledge of the locations of cracks, which is significantly advanced over existing crack monitoring techniques. Moreover, according to the authors, several cracks can be detected, located and monitored using a single fibre. In the work from [DuFa09], the authors developed an integrated cost-effective sensor system to monitor the state of reinforced concrete structures from the corrosion point of view. The sensor provides measurements of the open circuit potential of rebars, corrosion current density of rebars, electrical resistivity of concrete, availability of oxygen, chloride ions concentration in the concrete, and temperature inside the structure [DuFa09]. Insertion of small sensors inside or at the surface of the concrete can be considered as one of the most promising development in order to monitor the long-term behaviour of concrete structures. Corrosion monitoring is possible using different sensors and methods that can work in the alkaline media of concrete for several years. Recorded data for potential corrosion and electrical concrete resistance obtained in real structures exposed to the environment can be used to determine the corrosion rate that corresponds to the concrete structure [MaAn09].

Embedded sensors in the concrete near the surface (depth of 50 mm) enable measurements of the spatial and temporal distribution of the electrical characteristics within the cover-zone. Thereby, it allows for an integrated assessment of its performance. Regular monitoring can enable cover-zone response to different ambient environments, namely changes in the temperature [MCSH10].

Advances in the study of concrete deterioration can be achieved if concrete technologists cooperate with scientists in the relevant sensor sciences, to take advantage of the development

of wireless low power smart sensor nodes capable of measuring behaviour, filtering, sharing and combining readings from a large variety of sensors.
Key issues are calibration of embedded sensors, robustness of sensors cast into concrete elements and durability of sensors which is related to the long live required for the structures [Buen11]. The monitoring of temperature and moisture level will provide crucial information about the hardening and setting process of concrete as well as the progress of deterioration mechanisms such as corrosion of steel reinforcement, freeze-thaw cycles, carbonation and alkali-aggregate reaction. A new technique to monitor the moisture level and temperature has recently been proposed in [NoSR08]. This innovative technique uses nanotechnology/Microelectromechanical Systems (MEMS) to measure temperature and internal relative humidity by using microcantilever beams and a moisture-sensitive thin polymer. Based on the obtained results, it was found that the proposed MEMS survived the concrete corrosive environment, as well as to internal and external stresses. Also it was found that the MEMS output reflects the change in the concrete properties and can be used to effectively measure moisture content and temperature, with high sensitivity. However, serious issues, such as long-term behaviour and repeatability of MEMS embedded into concrete, require further investigation [NoSR08]. Resulting from cross-disciplinary research between civil engineering and automatic control engineering, a new measurement technique was recently developed in [NoSR08], enabling direct, real-time measurements and continuous monitoring of concrete internal temperature and humidity via wireless signal transmission. The results are very promising with temperature/humidity sensors which monitor the internal temperature and humidity of concrete wirelessly, directly, in real-time and continuously. However, several limitations need to be overcome when embedding electronic components into concrete, such as the continuity and stability of signal transmission, protection of electronic components, as well as the design of encapsulation boxes [ChHu12].

2.2.1 Motivation and objectives

The main objective of the Intelligent Systems for Structures Strengthening and Monitoring (INSYSM) project is to develop a prototype for WSNs, allowing for remotely monitoring certain concrete structures. WSNs are formed by tiny devices, known as motes, that incorporate a microcontroller, sensors, memory, a power unit and a communication module. They are able to sense the environment and communicate the information gathered from the sensors to the sink node through wireless links. Their capabilities include reading the value of physical variables at a given location, detecting the events of interest, whilst performing collaborative signal processing. From the application perspective, WSNs are useful in situations that require quick or infrastructure-less deployment and continuously monitoring [Jurd07, Fried09, InMa09]. Besides this, the research work was focused on studying the behaviour of a concrete cube immediately after casting and at earlier ages, whilst monitoring all the temperature and moisture changes in real time. This is accomplished by using an IEEE 802.15.4 network, enabling a significant reduction of the installation time and costs. The experiments to be carried out, also aim at expanding the output from this research to the monitoring of other structures regardless the type of material, and to develop a prototype that facilitates to measure several parameters inside a real concrete structure, e.g., humidity and temperature.
In the context of WSNs applied to civil engineering structures it is important to create a monitoring device platform that is able to accommodate a wide range of sensors, depending on the needs, expandability and cost, while sharing the information across the network. For this pur-

pose, remote agents can be collectors of information either by storing the data into a microSD card, to be accessed later on, or by wirelessly transmitting this information, in real time, to a mote interface board (gateway) that is connected to a PC, allowing for a rapid intervention of civil engineers, if needed, as shown in Figure 2.19.

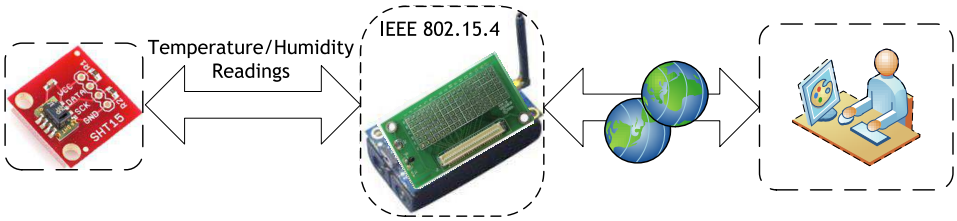

Figure 2.19: Wireless sensor network architecture for the monitoring of civil engineering structures.

Temperature is an important parameter during the curing and hardening of the concrete, since the concrete cannot be too cold or too hot. When the temperature decreases, the hydration reaction slows down. However, if the concrete temperature increases the reaction accelerates, creating an exothermic reaction (which produces heat), causing temperature differentials within the concrete. This temperature gradient can lead to cracking. Moreover, during the initial phase of the life of the concrete, it is essential to avoid cracking caused by the rapid drying due to increased temperature and the ongoing hydration reaction. The rate of strength development in the early life of the concrete is strongly related to its rate of hydration. As a consequence, it is worthwhile to study the impact of the temperature increase caused by the occurrence of the hydration reaction. Furthermore, structural health monitoring has been identified as a prominent application field for WSNs, since traditional wired-based solutions present some inherent limitations such as installation/maintenance cost, scalability and visual impact. In order to collect the data from the temperature sensors, a WSN was created facilitating the remote monitoring.
The properties of civil structures involve a significant amount of uncertainties in several parameters, caused by the effects from environmental factors, e.g., temperature and humidity. The deterioration process of the underlying structure is caused by these variations. At earlier ages, temperature and moisture plays an important role during the curing and hardening of the concrete, and can have long-term consequences. Both moisture and temperature at specific operational conditions promote concrete deterioration processes namely, occurrence of undesirable cracks, corrosion of the reinforcing steel, ingress of carbon dioxide and other chemical processes.

2.2.2 Experimental work

Negative temperature thermistor - temperature sensor

The first set of tests consisted of measuring the temperature with a Negative Temperature Thermistor (NTC) temperature sensor inside a concrete cube (common strength class C25/30, 10 cm length size), as shown in Figure 2.20.
The acquisition system consists of a sensor board and an IRIS mote, facilitating the creation of an IEEE 802.15.4 network whose primary function is to remotely collect the data from the NTC sensor inside the concrete cube.

Figure 2.20: On-going measurement of temperature with wireless sensors inside a concrete cube.

SHT15 humidity and temperature sensor

In the second set of tests, the SHT15 digital sensor was used, facilitating to measure both temperature and humidity with high accuracy in a single chip sensor. Figure 2.21 presents a schematic representation of process to measure the temperature and humidity within the concrete cube.

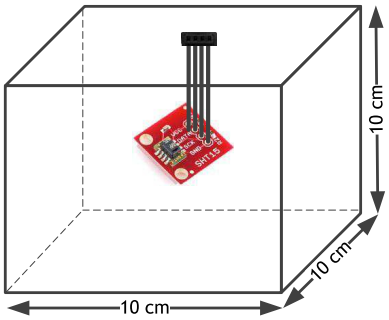

Figure 2.21: Schematic representation of temperature and humidity sensor inside a concrete cube (10 cm length size).

The conversion from the raw value returned by the SHT15 sensor, R_{xval}, to the temperature and humidity values is performed by using the following equations:

$$Temperature[^{o}C] = (R_{xval} \times 0.01) - 40 \tag{2.1}$$

$$Humidity[\%RH] = -4 + 0.0405 \times R_{xval} - 0.0000028 \times 2R_{xval} \tag{2.2}$$

Before inserting the sensor inside the concrete block, the following preparations have been made (as shown in Figure 2.22):

- the sensors were placed inside a small size cube (4 cm side length) made of cement mortar for its protection. The mortar was produced using low water content with a cement mortar ratio of 1:3 (the mortar works as shell that can protect sensor wire connections when placed inside concrete during casting; high porosity of this mortar shell easily allows moisture measures of involving concrete);
- coarse sand size was used avoiding fine particles, so that the sensors would not become obstructed.

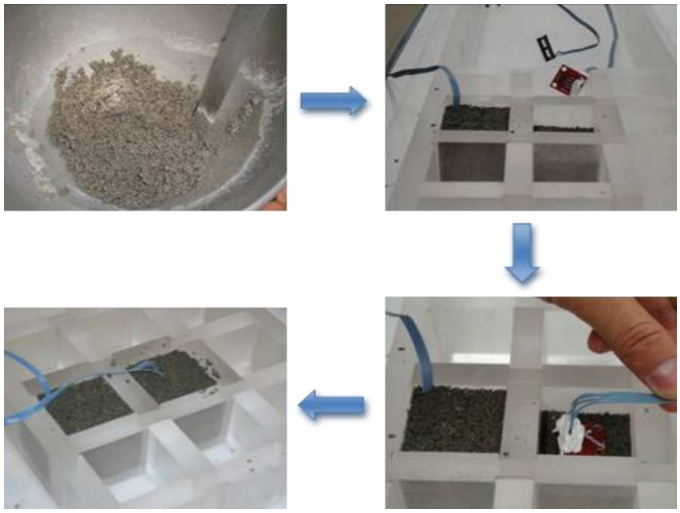

Figure 2.22: Preparation and placement of the temperature and humidity sensors inside a mortar cube for its protection.

SHT21S humidity and temperature sensor - standalone version

Besides the SHT15 (humidity/temperature) sensor, we tested the new Sensirion SHT21S (humidity/temperature) sensor. Before testing this sensor a cement mortar shell has been used for its protection. This sensor is an updated version of the previous one but with a smaller package. To test this sensor, an acquisition system was designed to facilitate the acquisition of the analogue signal while converting it for its digital representation. As previously mentioned we intend to measure both temperature and humidity inside the concrete block, from the early ages, during setting and hardening period.

The temperature and humidity values are obtained by using Equations (2.3) and (2.4), respectively:

$$Temperature[^{o}C] = -46.85 + 175.72 \times \frac{V_{SO}}{V_{DD}} \tag{2.3}$$

$$Humidity[\%RH] = -6 + 125 \times \frac{V_{SO}}{V_{DD}} \tag{2.4}$$

where, V_{DD} is the supply voltage at which the SHT21S sensor works, as presented in the datasheet of the sensor in the interface specifications. In this case, V_{DD}=3 V. Moreover, since the SHT21S output is a Sigma Delta Modulated (SDM) signal, normally this signal is converted to an analogue voltage signal by the means of a low-pass filter. The output of low pass filter provides a voltage value (V_{SO}) which is a portion of V_{DD}, depending on the measured humidity or temperature. The developed acquisition system (for the standalone SHT21S) incorporates a microSD module, responsible for storing the values acquired from the SHT21S sensor, as shown in Figure 2.23. The MSP430F449-STK2 module was used to convert the signal output from the RC-filter to the digital format. The algorithm running inside the microcontroller performs five readings (with a 100 ms interval between two consecutive readings for the temperature), storing the fifth reading in a buffer. Then, it switches to the humidity sensor, performing another five readings and conversions with the same duration between consecutive readings, storing the fifth reading in another buffer. Finally, after that it sends the commands to store

the temperature and humidity values in separated text files, into the microSD card.

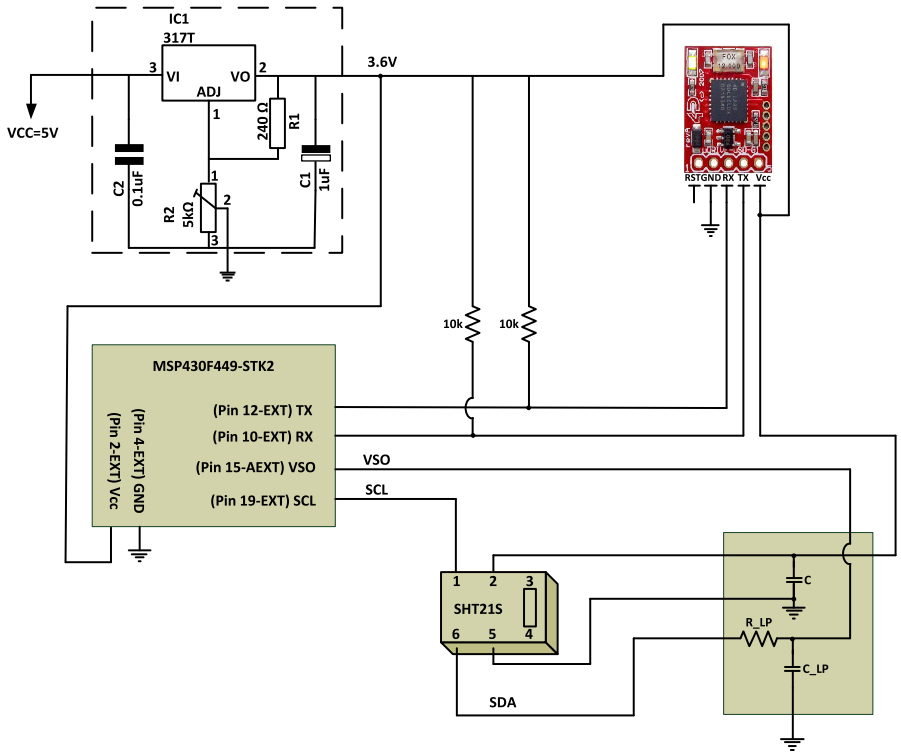

Figure 2.23: SHT21S acquisition system for the standalone version.

SHT21S humidity and temperature sensor - wireless version

The SHT21S wireless prototype aims at creating a Building Wireless Sensor Network (BWSN) capable of measuring temperature and humidity inside a concrete structure. It has two Integrated Circuits (ICs) interfaces via Serial Peripheral Interface (SPI), and an antenna allowing for connectivity with no additional hardware components. Besides this, it provides real-time data information and remote interaction with multiple devices (e.g., laptop, PDA, cell phone with ZigBee® capabilities). The MSP430F2274 ultra-low-power microcontroller controls the CC2500 radio transceiver (that operates at the 2.4GHz band) and establishes a basic wireless network with minimal power requirements, enabling to extend the system lifetime. Figure 2.24 presents the acquisition system used to read the signal from the SHT21S sensor. The computed temperature and humidity values are sent wirelessly to the Access Point (AP). The End Device (ED) reports periodically values each minute to the AP. The user, depending on the application scenario can change this reporting periodicity value.

Joint verification of shielded SHT15 and SHT21S sensors

The main purpose of shielding the SHT15 and SHT21S sensors is to protect the sensor from the concrete high relatively humidity alkaline environment that could affect the sensor inside the concrete. Besides this, the unique capacitive sensor element used to measure humidity as well as the band-gap sensor utilized to measure the temperature do not resist to the high relative humidity alkaline environment present in cement. To overcome this limitation, in the second series of tests we have decided to use a filter cap allowing for protecting the SHT15

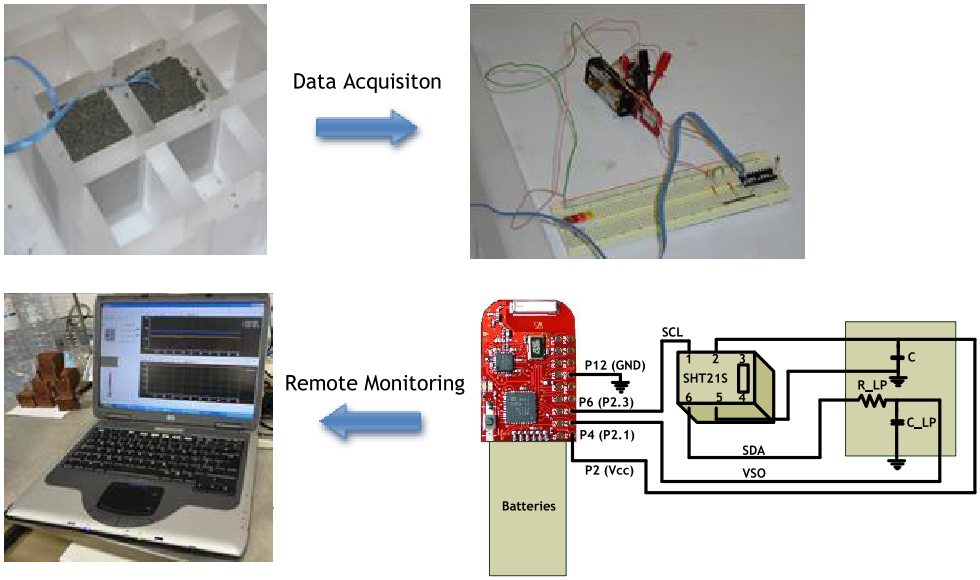

Figure 2.24: SHT21S wireless acquisition system.

and SHT21S humidity and temperature sensors against dust, water immersion, condensation, as well as contamination by particles. The cavity inside the filter cap is made such that the volume between the membrane and the sensor is kept minimal, which reduces the impact on the response time for the humidity measurements. The filter cap is made of a single piece of Polypropylene (PP) and a filter membrane welded to the single piece, Figure 2.25.

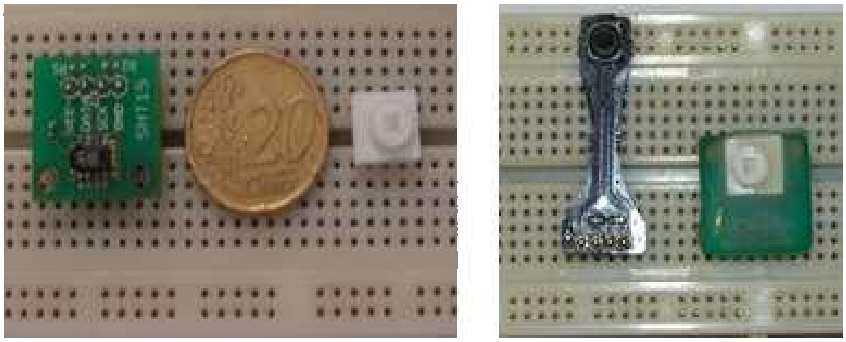

Figure 2.25: Filter cap protection for the SHT15 and SHT21S sensors.

Before inserting the filter cap for sensor protection, the following preparations have been made (as shown in Figure 2.26):

- the filter cap was mounted on the Printed Circuit Board (PCB) after soldering the SHT15 and SHT21S sensors by sticking the two openings in the PCB;
- the filter cap was fixed by adhesive (there is also the possibility of melting the pins from the back side by heating them up with a hot iron);
- an hermetic seal was applied, which is an adhesive added between the filter cap, sensor housing and PCB, providing higher security against water leakage, condensation inside the housing and corrosion of the soldering paths of the sensors.

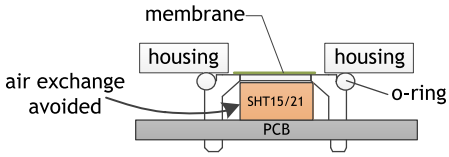

Figure 2.26: Mounting schematics of the filter cap protection for the SHT15 and SHT21S sensors.

After shielding the SHT15 and SHT21S sensors, we have decided to create different humidity and temperature environments and compare the obtained results with a standard climate sensor probe (Rotronic hygroclip probe, for all climatic measurements, operating range -40...100 °C, 0...100 % RH) in order to show the accuracy of the measurements, as presented in Figures 2.27.a), b), c) and d). We have decided not to include markers in the curves for the temperature and humidity variation, in order to facilitate their interpretation. The response of the sensors was tested in four different conditions. The first test consists of creating a controlled relative humidity of 75 % inside a desiccator. Therefore, the bottom of the desiccator was partially filled with sodium chloride saturated water solution (salt mixed with water), Figure 2.27.a). The test was performed during 23 hours, in which the standard climate sensor probe from Rotronic was used to confirm the measured values with SHT15 and SHT21S sensors.

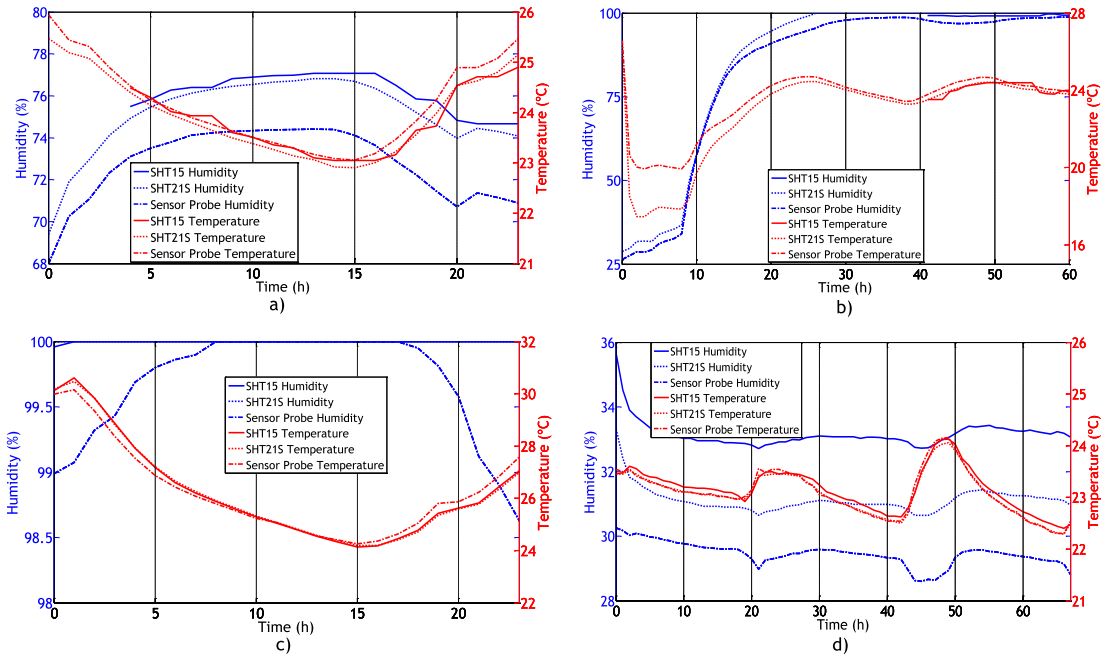

Figure 2.27: Results for the humidity and temperature obtained using the SHT15 and SHT21S sensors: a) humidity of 75 %, b) silica gel particles replaced by ice cubes, c) desiccator filled with water, and d) water replaced by silica gel particles.

During the first 4 hours, the SHT15 was not connected to the Arduino platform, so we did not measure any temperature and humidity value. After 4 hours, we powered up the SHT15 sensor and it started to measure both humidity and temperature values. Between the 4^{th} and 23^{rd} hours, by comparing the results obtained from the SHT15 and SHT21S sensors with the ones obtained from the sensor probe, we conclude that the results are similar. Moreover, after 7 hours, both humidity and temperature values started to have a constant behaviour, where the humidity is about 75 % and the temperature is about 23 °C. After 16 hours we decided to open the desiccator to observe if there is any variation in the temperature and humidity values. As

presented in Figure 2.27.a) there is a decrease in the humidity values and an increase in the temperature values.
In the second set of tests, Figure 2.27.b), the bottom of the desiccator, which was filled with a salt solution, was replaced by ice cubes. Therefore, during the first 3 hours there is a decrease of the temperature and an increase of the humidity values. After 30 hours the air inside the desiccator reaches the equilibrium, where the humidity is about 100 %, and the temperature is ambient dependent. The SHT15 sensor was connected only after 42 hours. Between the 42^{th} and 63^{th} hours, by comparing the results obtained from the SHT15 and SHT21S sensors with the ones from the sensor probe, we conclude that the results are similar. In Figure 2.27.c), the ice cubes inside the desiccator melted, and the bottom of the desiccator is filled with water. Therefore, as expected, the humidity inside the desiccator is around 100 % and the temperature is ambient dependent. In addition, there was an increase of the temperature during the day and a decrease during the night. Finally, the last test consists of replacing the bottom of desiccator, previously filled with water, by silica gel particles. As presented in Figure 2.27.d), there is a fast variation in terms of relative humidity inside the desiccator, especially during the first hour. The values for the humidity show an average standard deviation of 2 % by comparing the SHT15 and SHT21S sensors. This can be explained by the fact that the positions inside the desiccator are not the same, leading to small variation in the measurements of the humidity values. We have also noticed that there was an average standard deviation of 2 to 4 % between the relative humidity measured by the standard climate sensor probe from Rotronic and the SHT15 and SHT21S sensors, respectively. This is due to the fact that the sensor probe [Hygr12] is not as accurate as the digital humidity and temperature sensors when fast variations occur.

2.2.3 Results and discussion

Negative temperature thermistor - temperature sensor

The first experimental approach for reading temperature inside a concrete cube involves the use of a NTC thermistor and an IRIS mote. This setup foresees an automatic wireless monitoring system. The temperatures inside the concrete cube and environment have been compared. Figure 2.28 presents the values obtained by the probe for the temperature and calibrated sensors.
As shown in Figure 2.28, there is a difference of 5 ºC between the actual and measured temperatures. This is due to some failures during the calibration of the sensor, resulting in inaccurate values. Based on this fact, we can conclude that using a NTC sensor with an "unknown" behaviour is not the most adequate approach to the problem. However, this kind of sensor is not able to simultaneously measure temperature and humidity inside the concrete structures.

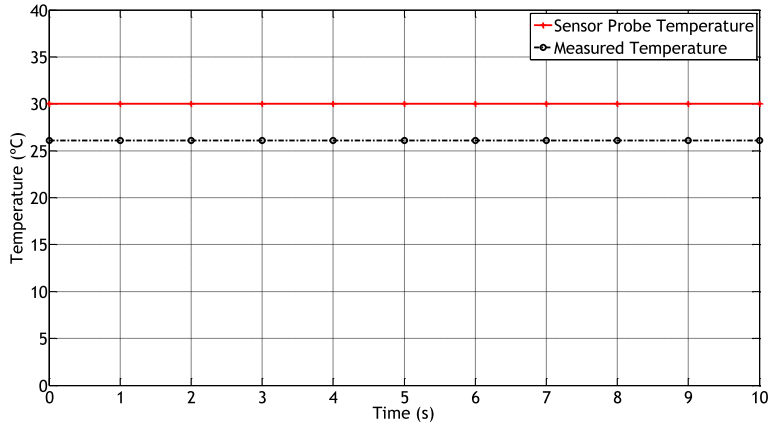

Figure 2.28: Verification of the sensor probe and measured temperatures inside the concrete cube by using an NTC temperature sensor.

SHT15 humidity and temperature sensor

The second set of tests considers the use of the SHT15 sensor, allowing for measuring both the humidity and temperature. Two solutions were tested, one with the PIC18F4680 microcontroller and another one using the Arduino platform. Before using the SHT15 sensor in a real scenario, some tests have been performed to verify the accuracy of the temperature and humidity readings. By using a temperature of 16.3 ºC inside a fridge chamber, and by comparing the results obtained from the sensor with the ones obtained from the sensor probe, we conclude that the results are very similar, as shown in Figure 2.29.

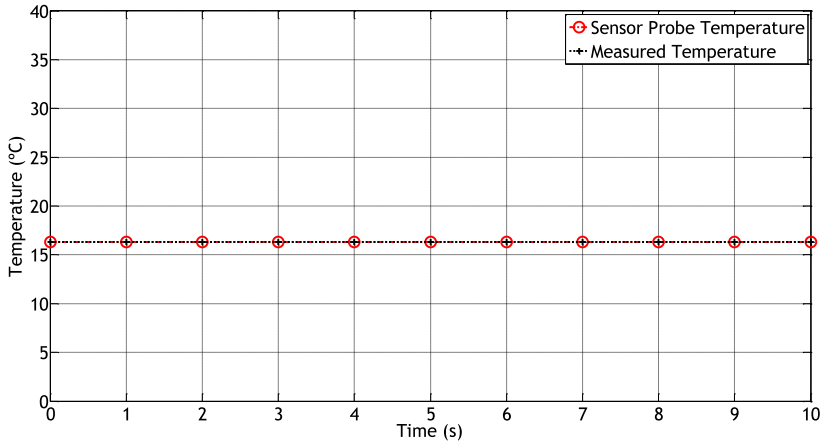

Figure 2.29: Sensor probe temperature versus measured temperature inside the fridge chamber by using an SHT15 temperature sensor.

To measure humidity we have placed the SHT15 sensor inside a small mortar cube for sensor protection, as explained in Section 2.2.2. When, the cubes were placed in a tray (with 2-3 mm water level), we observed the rise of water inside the cube by capillary, as shown in Figure 2.30. After around one minute, the humidity reaches a value of 98 % RH. The objective of this test was to verify the sensor integrity, as well as the porosity effect of its mortar shell. The results obtained from both PIC18F4680 and Arduino platforms were identical. The tests were carried out during several hours, to observe if any variation of humidity and temperature could be detected.

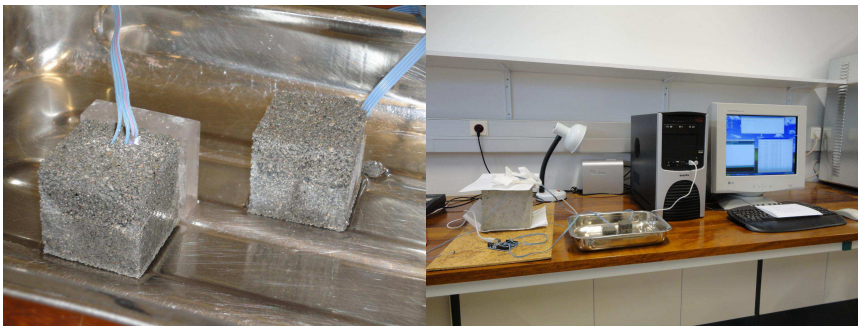

Figure 2.30: Setup to measure temperature and humidity using an SHT15 sensor inside a mortar cube for sensor protection.

In another experiment a SHT15 sensor with a mortar shell was fully immersed in water. One observes that as the temperature was decreasing the humidity was increasing, as expected. After 20 minutes of accurate measurements, we have decided to prolong the test during one week. However, after one day, the SHT15 temperature sensor went off. Then, after 4 days the same happened to the humidity sensor. It is believed that the primary reason for this occurrence is that some chemical reactions inside the mortar shell have affected the capacitance of the sensor. Sensor components might not resist to alkaline ions present in cement, namely calcium hydroxide, which can be released in water from its mortar shell during immersion. To solve this problem, instead of making a cement-based mortar shell it may be preferable to shield the sensor using other material, textile or polymer based.

SHT21S humidity and temperature sensor - standalone version

The SHT21S sensor protected by a mortar cube was placed inside a concrete cube during casting, as shown in Figure 2.31. The values measured by the sensor were recorded into the microSD card. The data collected from the sensor is shown in Figure 2.32. The measurements were performed in outdoor environmental conditions during summer. During the first 12 hours there is observed a constant and progressive variation; while between the 12thth and 16th hours a decrease in the temperature and humidity values is observed. After 16 hours, the sensor stopped reading the temperature values. Only the humidity values are measured beyond this time instant. As occurred with SHT15, the SHT21S sensor components have not resisted long time inside the concrete alkaline environment. To overcome this limitation, shielding of sensor is also advised in this case, e.g., with textile, polymer (Polybutylene Terephthalate) [Filt12] or even metal shielding.

Figure 2.31: Preparations to measure early age concrete temperature and humidity using a SHT21S sensor inside a mortar cube.

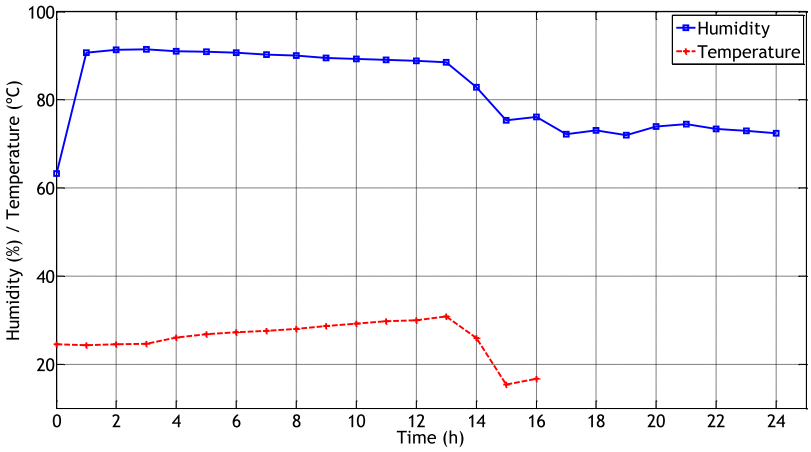

Figure 2.32: Results for the humidity and temperature for the SHT21S sensor obtained inside a mortar cube placed in outdoor environmental conditions during summer.

SHT21S humidity and temperature sensor - wireless version

In scenarios of remote monitoring, there is a need of extracting and recording the data gathered by the sensor nodes. To avoid the need of regularly visiting, remote access to the collected data is essential. Moreover, solutions involving WSNs have a tremendous potential in real time structural health monitoring, since they potentially reduce costs.
The SHT21S wireless version allows for collecting the information from any given structure. Figure 2.33 presents the SHT21S eZ430-RF2500 C++ software program responsible for the acquisition of the values from the SHT21S sensor. The acquired values are shown in two different ways, either plotted in a chart as a function of time, or by the instantaneous observation of the values in a segment display (while the AP receives the data packets). To analyse the acquired values we export the data to a Matlab® file.

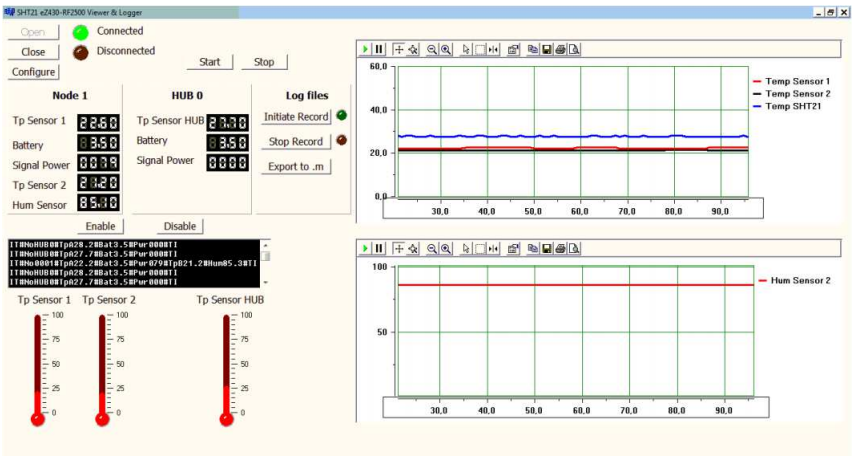

Figure 2.33: Software program for the acquisition of the SHT21S eZ430-RF2500 sensor data.

As shown in Figure 2.33, the results obtained for temperature and humidity are quite accurate. Therefore, the use of a porous cement mortar as protective shell does not affect the sensor readings. This method of protection of the sensor is similar to those developed by the authors in [ChHu12] and recently published, although unknown to authors during the experimental phase. However, the presented solution does not consider an encapsulation box for the electronic acquisition system components (since it is outside the "brick"), as presented in Figure 2.24.

This way we are able to obtain more accurately values for the temperature and humidity, since the sensor is placed as close to the environment as possible. By using an encapsulation box the detected temperature and humidity may not be the actual structure temperature and humidity, as stated in [ChHu12]. Moreover, in the work developed in [ChHu12] the Radio Frequency Integrated Circuit (RFIC) transmitter is inside the brick, being the maximum effective reception range bellow 20 m. The research conducted by the authors in [QuKe10], also considers a package to protect the sensor from the aggressive environment. Preliminary results show that the transmission distance is strongly affected by the steel backed formwork, showing that the maximum distance achieved without the formwork is 7.5 m. In our case, by considering the open field scenario (since the acquisition systems is outside the "brick") the eZ430-RF2500 can achieve a minimum effective reception range of 35 m. In this experiment, the SHT21S sensor temperature readings have been successfully performed during the first 16 hours, while the humidity values were successfully obtained during the first 21 hours.
After this period, the sensor went off, possibly also caused by the alkaline concrete environment that stopped the sensor operation.

Joint verification of shielded SHT15 and SHT21S sensors

In this set of experiments, the SHT15 and SHT21S sensors previously shielded were inserted into two small size mortar cubes (4 cm of side length) before being inserted into the concrete block. To test the accuracy of the measurements, the mortar cubes were first placed in a tray with water. After some time, we observed the rise of water inside the cube by capillarity. Then, the cubes were removed for drying purposes and the results are illustrated in Figure 2.34.

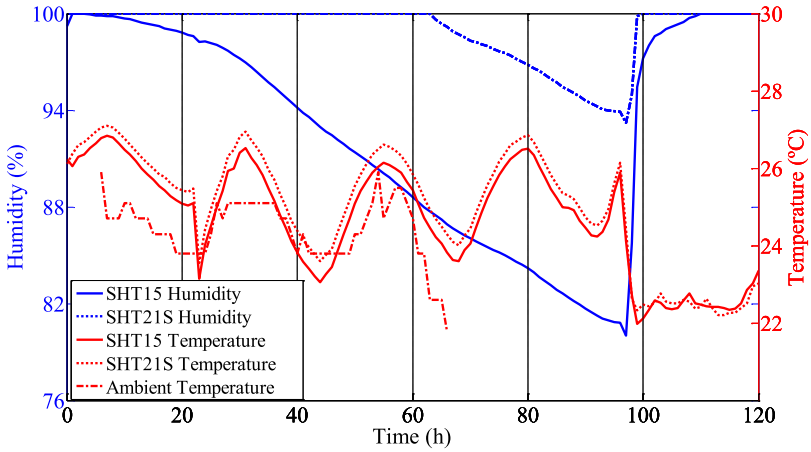

Figure 2.34: Results for the humidity and temperature obtained using the SHT15 and SHT21S sensors during 5 days.

The cube containing the SHT15 sensor initiated the drying process after 10 hours, while the cube containing the SHT21S sensor started the drying process after 60 hours. After 97 hours, we have repeated the test of placing the cubes in a tray with water, in order to observe the increase of the humidity values. The standard deviation between the humidity measured by the SHT15 sensor and the SHT21 sensor is explained by the fact that the small cubes are not exactly the same, so some variations in terms of humidity may exist during the drying process. Furthermore, if the SHT21S is exposed to conditions outside the normal operation range (humidity >80 %), an offset could exist. Therefore, in high relative humidity environment it is advised to use the SHT15 sensor. The measured temperature is similar to the ambient temperature, in which

the small variations are also due to the drying process. Then, the SHT15 and SHT21S sensors previously shielded and protected by a mortar cube were placed inside a concrete cube during the casting, as shown in Figure 2.35.

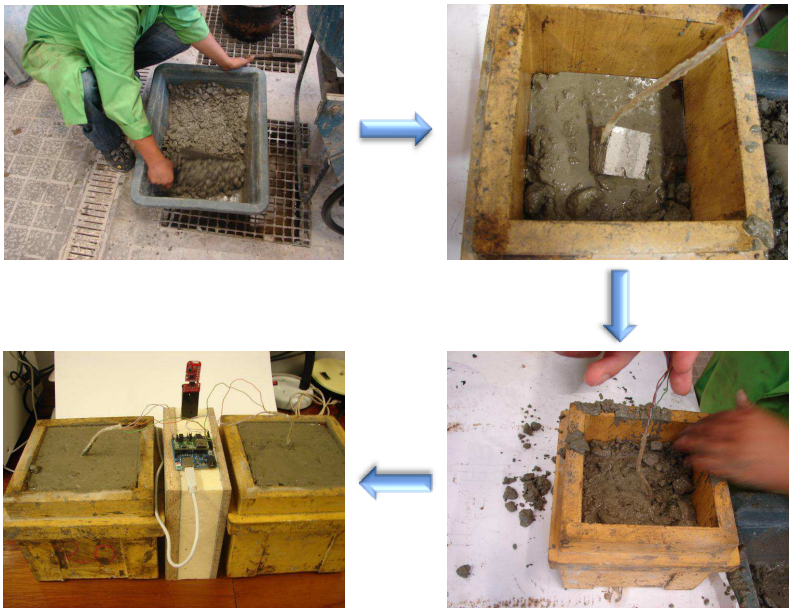

Figure 2.35: Preparations to measure early age concrete temperature and humidity using the SHT15 and SHT21S sensors inside a mortar shell.

The values measured by the sensors were recorded into the microSD card. The data collected from the sensors is shown in Figure 2.36. The tests were performed during 6 days. During the first 12 hours there is an increase of the humidity for the cube containing the SHT15 sensor, while the humidity inside the cube containing the SHT21S sensor achieves the maximum value (i.e., 100 %). Moreover, during the curing process the temperature inside the cubes was about 37 ºC after the first 11 hours. These results are similar to the ones presented in Figure 2.32. Therefore, we may conclude that by using a filter cap (shielding the sensors) as shown in Figure 2.25, we protect the humidity and temperature sensors, allowing for the creation of a long-term solution, which is one of the objectives of these experiments. Finally, it was verified that both sensors were performing measurements inside the concrete after 2 months of experiments.

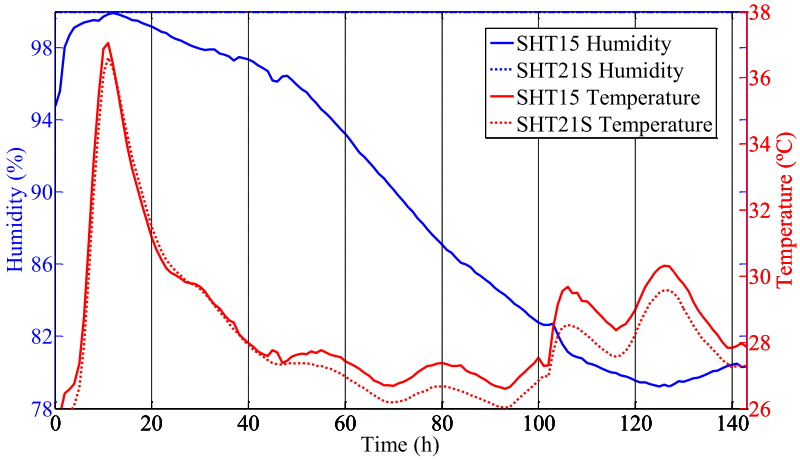

Figure 2.36: Results for the humidity and temperature obtained using the SHT15 and SHT21S sensors inside a mortar shell for 143 hours.

2.2.4 Limitations and challenges

In this work, we proposed several tiny systems, capable of (but not limited to) measuring both temperature and humidity, within concrete structures. In the context of sensing devices (i.e., the SHT15 and SHT21S sensors) only the sensor is inside the structure (the instrumentation, test control, and data acquisition is outside the structure allowing for using the same sensor and different acquisition systems, if needed). However, the proposed systems are battery operated. Hence, the service lifetime of the electronic components could be a major concern if there is no possibility to replace batteries and energy harvesting is not exploited in the mote. The need for a system with long-term lifetime is a major concern. To overcome the service lifetime limitation of the electronic components, energy harvesting systems must be addressed facilitating to extend the service lifetime (e.g., by using solar panels or thermal energy scavengers). In remote monitoring scenarios, the data needs to be transmitted wirelessly. Hence, there is a need to study the influence of the concrete material in the transmission of data (e.g., interference of electromagnetic field of steel bars), in order to provide a general-purposed solution that could be applied not only to new structures but also in the existing ones. From the experimental point of view, we only have measured the humidity and temperature in a single point inside the concrete cube. So, the creation of a system allowing for a distributed multipoint humidity and temperature measurement set up is envisaged as future research.

2.2.5 Summary and conclusions

This Section has addressed the development of an automatic measurement system allowing for monitoring the temperature and humidity within civil engineering structures. This system can be very useful when carrying out large works in concrete, such as dams or bridges where the volume of concrete involved is massive. Since the curing process is the process that defines the concrete quality, if the values of humidity and temperature are known, the premature drying of the concrete surface can be avoided by hydrating it. This decreases cracking and increases concrete quality. Moreover, this system can be implemented in existing structures where the concrete is going to be applied in an aggressive environment, therefore preventing corrosion of the reinforcement steel. Several types of hardware implementation have been conceived in order to read the temperature and humidity inside a concrete cube. A WSN has been created based on the IEEE 802.15.4, allowing for the creation of a continuous monitoring system capable of sending data wirelessly. In this network, the motes used two types of sensors, the SHT15 and SHT21S ones, to read both humidity and temperature, in real-time and continuous monitoring basis. The obtained results show two types of sensors and the measurement procedure have highly potential for inexpensive concrete structure monitoring. However, during the first set of experiments, the SHT15 temperature sensor stopped working after one day. After four days, the same happened to the humidity sensor. The temperature readings from the SHT21S sensor have been successfully performed during the first 16 hours of the experiment, while the humidity values were successfully obtained for the first 21 hours. After this period the sensor went off. The initial sets of results were very promising, although SHT15 and SHT21S sensors went off after some time inside concrete. This is explained by the fact that the components of the sensors do not resist to concrete high relative humidity alkaline environment. The experiments carried on have also shown that a porous cement mortar could be used as shell to protect sensor wire connections. High porosity of this mortar shell easily allows moisture and temperature measures of involving concrete. However, this solution still does not protect sensors of the

alkaline environment. Hence, it is advised to shield the sensors before using them within the structure, especially during the construction phase. It is also advised to use sensors that can resist in concrete alkaline environment. In the second set of experiments, the SHT15 and SHT21S sensors were shielded by a filter cap, so that they are not affected by the alkaline environment, allowing for real-time and continuous monitoring basis. The SHT15 and SHT21S sensors are working since the beginning of this second phase of the experimental research work, for more than two months. One verifies that there is a perfect match between the measured values for the humidity and temperature and the ones obtained by the sensor probe, which confirms the potential of the proposed wireless sensor monitoring approach. Finally, it is worth mentioning that the solutions involving WSNs have a tremendous potential in real time structural health monitoring, since it reduces the cost and prevents from the risks associated to monitoring systems (e.g., inaccuracy in the measured values or negative impact of dangerous environments) in the measurement procedure.

2.3 Final remarks

This Chapter addressed two use cases for real time WSN applications. The Smart Clothing application comprises a WBAN where an innovative monitoring application was developed to monitor the foetal movements in the last four weeks of low risk pregnancies. The structural health monitoring application for civil engineering structures is also addressed in this work, allowing for monitoring possible crackings in a concrete structure is a contribution for the INSYSM project.

Chapter 3

Energy Self-sustainable Wireless Sensor Networks

The major limitation for the adoption of WSNs is the energy available for power supplying the wireless sensor nodes imposed by the finite battery capacity. Since nodes may be deployed in a hostile environment, replacing batteries is often not feasible. Therefore, in order to prolong the network lifetime, users must limit the application's duty cycle, or use batteries with higher capacity. Other possibility is to use low-power hardware like a low-power processor and radio, at the cost of lesser computation ability and lower transmission ranges [SuKu11]. Energy harvesting will allow for recharging batteries or supercapacitors, and will have a great impact on the lifetime of WSNs. This poses a significant importance as the network size increases, since, for the typical situation, the replacement of the batteries is not practical. The common sources of energy harvesting include (and not limited to) the following ones [YiFC10]: mechanical, thermal, electromagnetic, natural (wind, solar and other) and human body energy. Nowadays, energy harvesting devices efficiently and effectively capture, accumulate and store energy, to power up the sensor nodes for short periods of time, in order to perform helpful tasks. However, in a not too distant future, they will enable to power supply all the WSN nodes without the need of replacing batteries. In a hazardous situation, if a battery or a solar-collector/battery package completely fails, harvesting the energy from the electromagnetic RF waves will enable the system operation, whilst potentially maintaining critical functionalities [NMLC12].

3.1 Challenges

A smart environment is a physical space populated by sensors, actuators, embedded systems, user terminals and any other type of communicating devices, which cooperatively share all types of resources such as radio spectrum or energy. Radio communications clearly constitute an essential element of smart environments. The main challenge of Prototypes for Efficient Energy Self-sustainable Wireless Sensor Networks (PROENERGY-WSN [PROE13]) is the development of an energy self-sustainable WSN formed by nodes with energy harvesting capabilities. Therefore, energy efficient platforms and harvesting techniques are envisaged to create an autonomous WSN running in nearly perpetual operation with little or no maintenance (i.e., without replacing batteries or other type of power supply source). Since WSN have scarce energy and processing resources, joint optimization and design of networking layers, i.e., cross-layer design must be addressed, improving the efficiency and interaction between the protocols in a WSN by combining two or more layers of the protocol stack. At the PHY layer, energy-efficiency can be obtained by using shorter active periods (i.e., by reducing the duty cycle) and by using efficient modulation schemes (e.g., O-QPSK). Moreover, using low-power modes for the processor or disabling the radio transceiver during the idle periods is also advantageous. At the Data Link Layer (DLL) energy-efficient MAC protocols will be addressed being responsible for timing the transmissions, allowing for multiple sensor nodes to share the same communication medium, as well as to determine and change the operation mode of the radio transceiver. As a consequence, an efficient management of transmission, reception and sleep modes should be implemented in

each individual WSN device. It is worthwhile to note that, MAC protocols are always restricted by hardware constraints. Moreover, long periods for switching the radio between the radio states (i.e., RX, TX and SLEEP) could result in significant energy spent [BaGV13].

3.2 Energy harvesting sources

Like any other wireless devices, WSNs are powered by energy sources. Therefore, in order to create a self-sustainable WSN, energy efficient harvesting and management techniques must be addressed. One of the major limitations of nodes is the finite battery capacity. Nodes could possibly use batteries with higher capacity for increasing the lifetime. However, this solution implies having to deal with increased size, weight and cost. Nodes may also optimally use low-power hardware like a low-power processor and radio transceiver, at the cost of lesser computation ability and lower transmission ranges. With the growing demanding of WSN-based applications (e.g., structural health monitoring and human health monitoring), the need to adopt inexpensive, energy efficient and long-term solutions has lead to a new paradigm. Therefore, new energy harvesting devices should be designed enabling a long-term and self powered wireless sensing solution. Figure 3.1 presents the most widely used portable energy systems for powering up the WSN nodes.

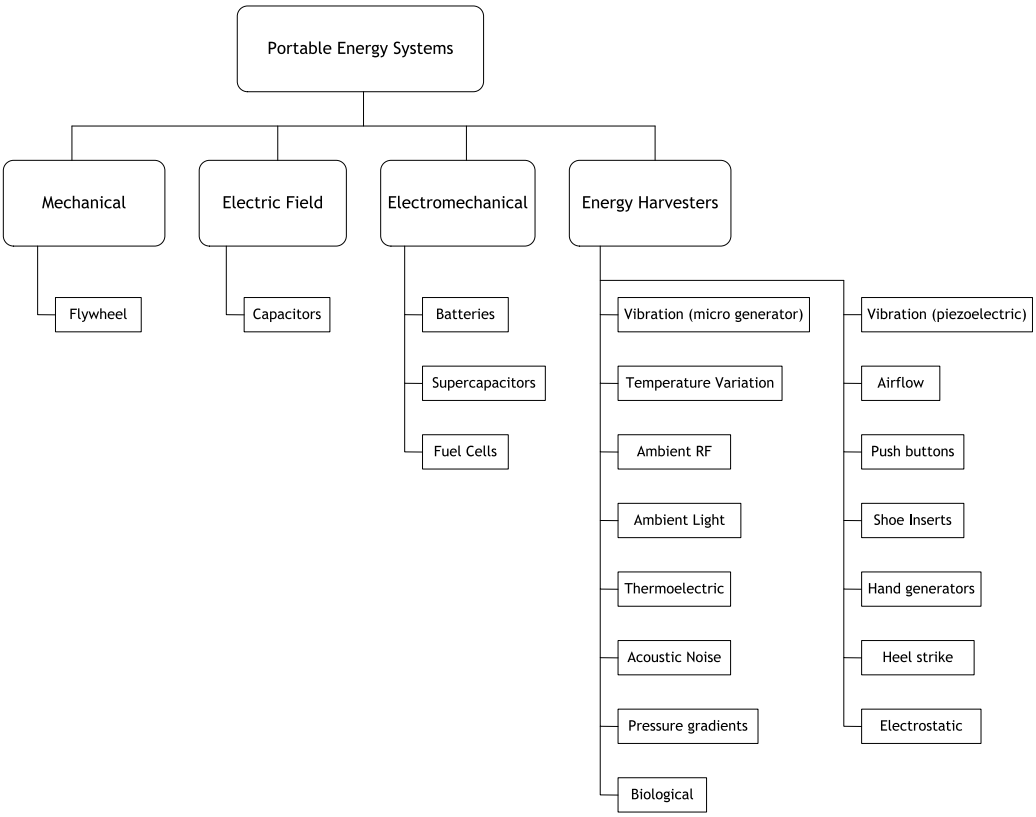

Figure 3.1: Portable energy systems.

Since there is a broad range of different energy harvesting opportunities within the surrounding environment, the opportunities are vast [Harb11]. However, it is difficult to generalize regarding the typical energy power levels available which is the most suitable energy source for energy harvesting. Table 3.1 presents the power density measurements for different energy harvesting

sources [YiFC10]. It is clear that in terms of power density, solar power in outdoor conditions achieves the best results. However, solar energy is what is called an intermittent source, which means it is not always available. When it is cloudy or raining, the sun is unavailable to provide light, and solar energy systems are unable to harvest energy. Therefore, this kind of energy source will need a backup energy system like a battery when there is no available solar energy for harvesting. Kinetic energy could be used by exploiting vibrations, however as presented in Table 3.1 the source vibration spectra varies depending on the application. Moreover, as stated in [BeWi10] generating power from human movement requires a totally different solution to the design of a generator for harvesting machinery vibrations.

Table 3.1: Power Density and Performance for different Harvesting Methods.

Energy Source	**Power Density & Performance**
Acoustic Noise	0.003 μ W/cm^3 @ 75 dB 0.96 μ W/cm^3 @ 100 dB
Temperature Variation	10 μW/cm^3
Finger motion	2.1mW
Breathing	0.83W
Ambient RF	1 μW/cm^2
Ambient Light	100 mW/cm^2 (direct sun) 100 μW/cm^2 (illuminated office)
Thermoelectric	60 μW/cm^2
Vibration (micro generator)	4 μW/cm^3 (human motion - Hz) 800 μW/cm^3 (machines - kHz)
Vibration (piezoelectric)	200 μW/cm^3
Blood Pressure	0.37 W
Airflow	1 μW/cm^2
Shoe Inserts	330 μW/cm^2
Heel strike	7 W/cm^2
Hand generators	30 W/kg
Heel strike	7 W/cm^2

Our vision is that energy harvesting from RF electromagnetic holds a promising future for power supply wirelessly electronics devices. Nowadays, RF energy is currently broadcasted from billions of radio transmitters (e.g., mobile communications base stations and television/radio stations) that can be collected from the ambient or from dedicated sources, enabling wireless charging to power supply the low-power devices. Additionally, RF transmitters and receivers can be used when other potential intermittent energy scavenging sources (e.g., solar, vibration and heat) are not available. Hence, by adding new energy harvesting capabilities to the sensor nodes, we provide a predictable and reliable power system that uses controlled broadcasted RF energy for wirelessly charge the battery systems.
Powercast offers several Powerharvester receivers [Powe13] modules that have been designed for charging batteries, energy storage devices and for direct power applications. The P2110 Powerharvester long range receiver module has the following characteristics:

- Low RF input for longer range operation;
- RF scavenging range down to -11 dBm input power;
- Frequency range from 850 to 950 MHz;
- Configurable regulated output voltage up to 5 V;
- RSSI and data output.

According to the experiments conducted in [VeMu12], Table 3.2 shows the time to charge a battery with a capacity of 1150 mAh using the P2110 module at a given distance (P is the power and I is the current). One advantage of collecting RF energy is that it is essentially "for free" and it is universally present over an increasing range of frequencies and power levels, especially in highly populated urban areas. These radio waves represent a unique and widely available source of energy if it can be effectively and efficiently harvested. Moreover, the growing number of wireless transmitters is naturally increasing RF power density and availability. Dedicated power transmitters will enable engineered and predictable wireless power solutions.

Table 3.2: Amount of Power Harvested by the P2110 Harvester using a Patch Antenna [VeMu12].

Distance (m)	P (μW)	I (μA)	Recharging Time (h)
1.52	1925	1604	42.24
3.05	386	322	210.5
4.57	189	158	429.4
5.49	131	109	618.5
6.10	102	85	797.5
7.62	50	41	1639
9.14	19	16	4353
10.67	5	4	15517
10.97	1	1	70019

Since the power consumption of wireless devices is decreasing and the sensitivity of passive RF harvesting receivers is increasing, the applications for wireless charging by means of RF-based wireless power and energy harvesting will continue to grow. Therefore, ubiquitously available RF sources, operating at different bands could be exploited for RF electromagnetic energy harvesting purposes.

3.3 Indoor and outdoor spectrum opportunities for RF energy harvesting

One of the main contributions of the current work is the identification of spectrum opportunities through power density measurements from 350 MHz to 3 GHz. The field trials were performed by using the NARDA-SMR spectrum analyser with measuring antenna [Nard13]. By analysing the power density measurements in 36 different indoor/outdoor locations in Covilhã, we have been able to identify the best opportunities that may be taken in order to conceive wideband or multi-band antennas for electromagnetic energy harvesting.

3.3.1 Average received power

By analysing the power density measurements in 36 different locations, we intend to find the best frequencies for RF energy harvesting. Besides this, the identified spectrum opportunities are being considered to conceive multi-band antennas. The location for the measurements is shown in Figure 3.2. To determine the received power, P_r, of the spectrum analyser, we multiply the power density, P_d, by the effective receiving area of the antenna, A_e, and gain, $G = 1$, as follows:

$$P_d \left[\frac{W}{m^2}\right] = \frac{|E^2|}{120\pi} \tag{3.1}$$

$$\overline{P_r}[dBm] = 10 \times log\left(P_d \frac{\lambda^2 G}{4\pi}\right) + 30 \tag{3.2}$$

where E is the electric field and λ is the wavelength.

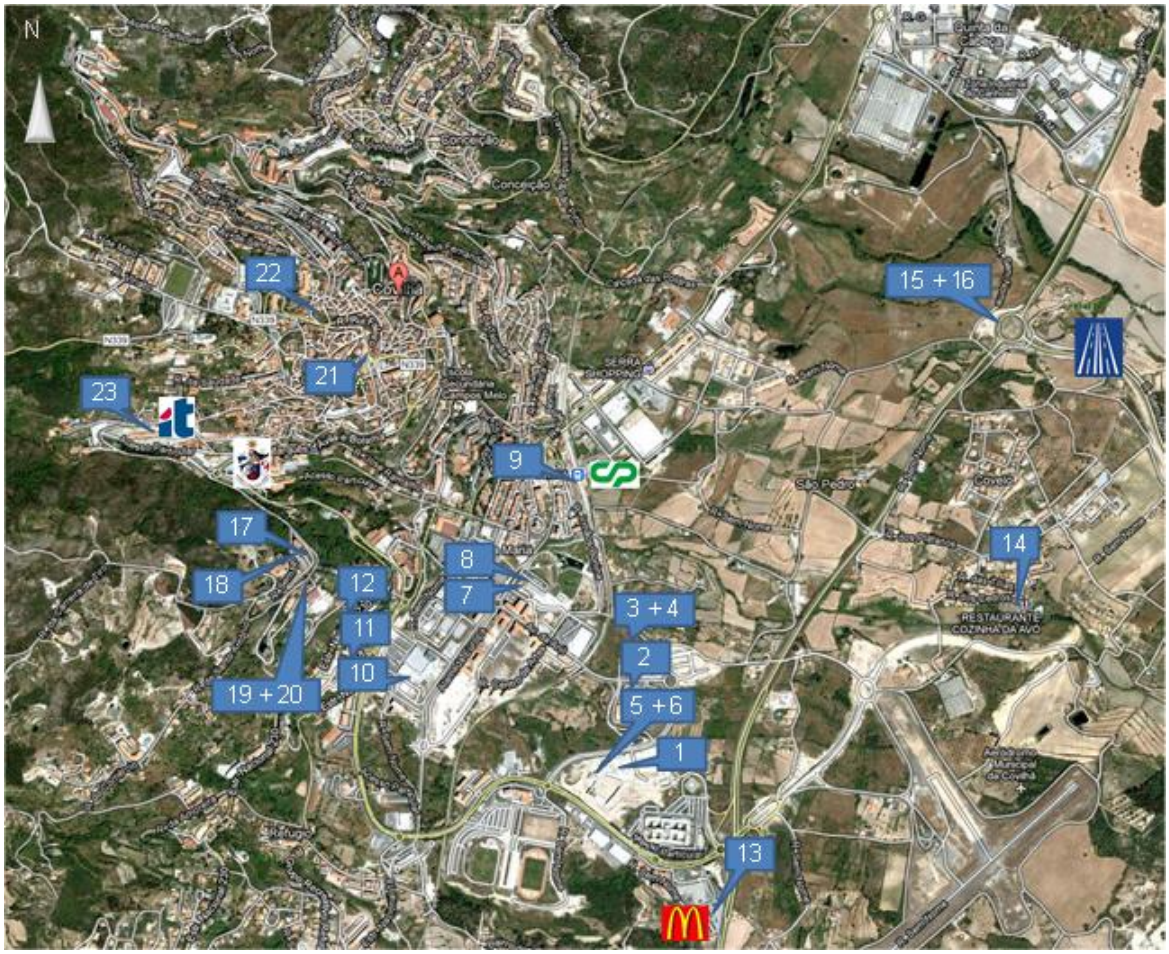

Figure 3.2: Locations of the measurements in Covilhã, Portugal.

To decide the best frequency bands for electromagnetic energy harvesting, we have determined the average of each of the n values of the received power, P_{ri} [W] in linear units, in five different locations, where n is the number of taken measurements, for each frequency. The average received power, in dBm, is given as follows:

$$\overline{P_r}[dBm] = 10 \times log\left(\frac{\sum_{i=1}^{n} P_{ri}[W]}{n}\right) + 30 \tag{3.3}$$

3.3.2 Indoor opportunities

Figure 3.3 presents the indoor spectrum opportunities for the higher education institution in Covilhã, the set of frequencies with high energy available for harvesting comprises the range from 934 to 960 MHz (GSM900), 1854 to 1892 MHz (GSM1800), 2116 to 2160 MHz (UMTS), 2359 MHz (amateur, SAP/SAB applications, video) and 2404 to 2468 MHz (Wi-Fi).

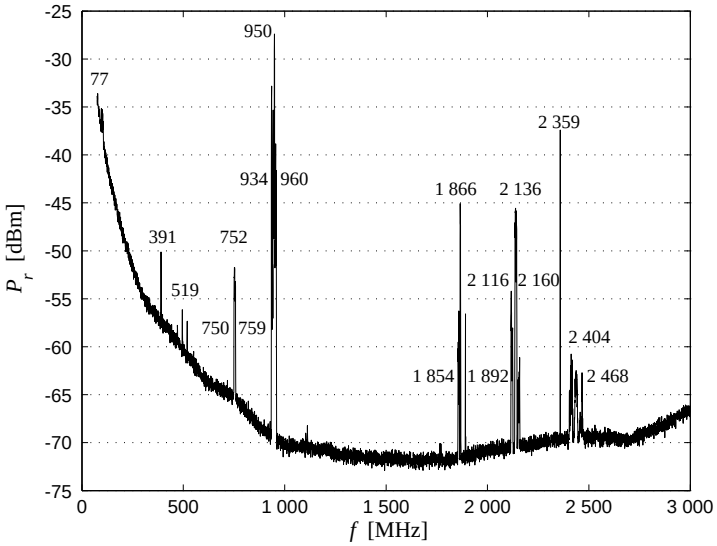

Figure 3.3: Average received power as a function of the frequency for the University scenario (indoor).

3.3.3 Outdoor opportunities

The location of public places in the outdoor scenario for the field trial results are identified in Figure 3.2, for the locations numbers 8, 9, 12, 13, 14, 21 and 22. The corresponding values of the average received power are shown in Figure 3.4. 3. The set of frequencies with more energy available for harvesting are in the range from 79 to 96 MHz (mobile/radio broadcast stations), 391 MHz (emergency broadcast stations), 750 to 759 MHz (television broadcast stations), 935 to 960 MHz (GSM 900 broadcast stations), 1854 to 1870 MHz (GSM 1800 broadcast stations) and 2115 to 2160 MHz (UMTS broadcast stations).

3.4 Antennas for RF energy harvesting

In the previous Section we have identified the most promising bands for RF energy harvesting. From the measures taken it is clear that the best frequency bands for energy harvesting purposes are the GSM900 and GSM1800 frequency bands. Therefore, in the context of the PROENERGY-WSN project [PROE13] we propose the design of energy efficient single- and dual-band monopole textile antennas suitable to be introduced within clothes for body-worn applications.

3.4.1 Single-band antenna

The single band antenna has the ability to harvest energy in the GSM900 band that, in Europe, covers frequencies from 880 to 960 MHz. The proposed single-band antenna design is shown in

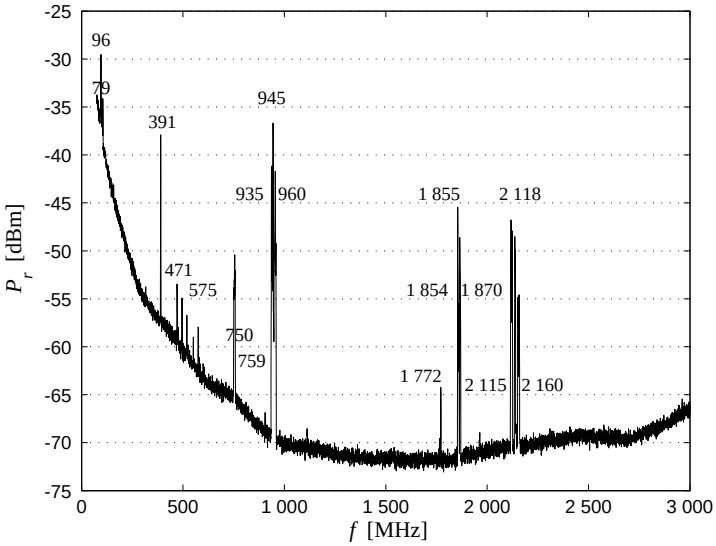

Figure 3.4: Average received power for the outdoor scenario.

Figure 3.5. Table 3.3 presents the corresponding dimensions.

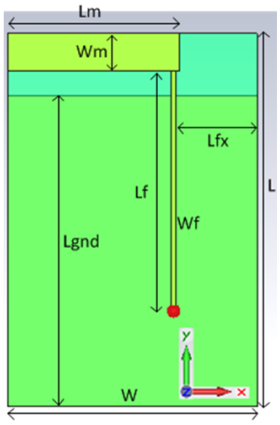

Figure 3.5: Proposed single-band antenna geometry.

Table 3.3: Proposed single-band antenna dimensions.

Parameter	Dimension [mm]
L, Lgnd, Lf	120, 100, 78
Lm, Lfx	55, 26
W, Wf, Wm	80, 1.5, 12

A Cordura® cloth type was considered, it presents a permittivity, ε_r, of 1.9 and a loss tangent, tan δ, of 0.0098, having a relative height of 0.5 mm. For the conductive sections of the antenna, an electrotextile (Zelt), with an electric conductivity 1.75×10^5 S/m was considered. The return loss obtained from numerical simulations of the proposed single-band antenna is presented in 3.6. By Considering a return loss $S_{11} < -10$ dB, this antenna presents an operating frequency range from 850 to 1150 MHz, covering completely the E-GSM band.

Since the privileged direction of signal reception is not known, the best possible radiation pattern for the antenna is an omnidirectional radiation one. The obtained radiation pattern in

the YZ and XZ planes (see Figure 3.5) for the proposed antenna, based on numerical simulations is depicted in Figure 3.7. Although a slight bend in the radiation pattern is noticeable, which is due to the geometry of the antenna, the obtained radiation pattern is clearly omnidirectional.

In energy harvesting applications, to achieve the best performance possible, the antenna

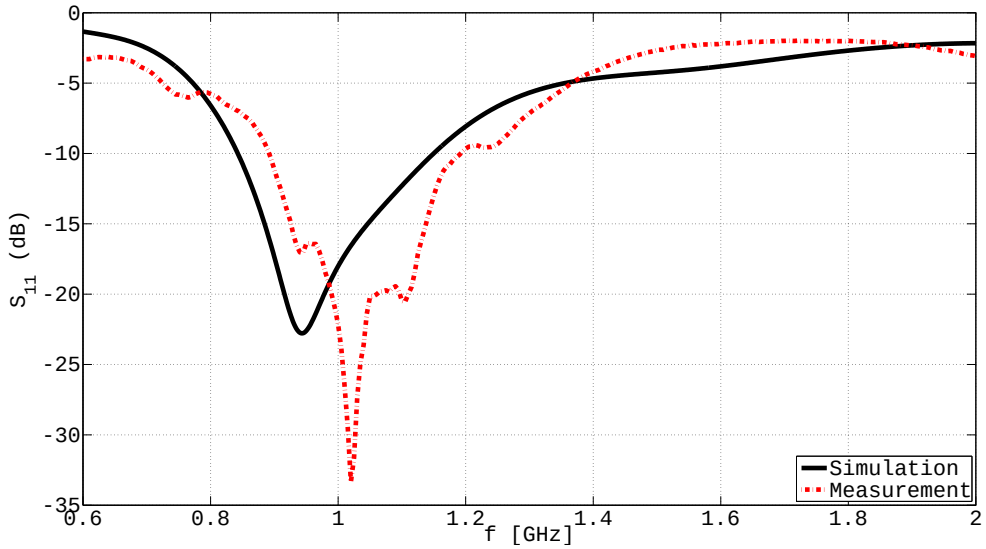

Figure 3.6: Simulated and measured return loss for the proposed single-band antenna.

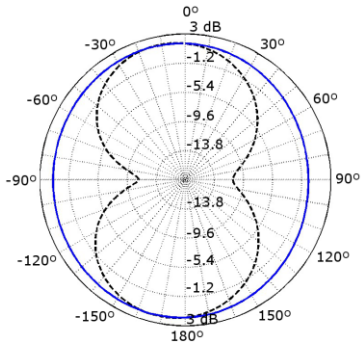

Figure 3.7: Simulated radiation pattern for the single-band antenna in the YZ plane (dashed) and XZ plane (blue solid).

should present the highest gain and the highest efficiency possible. The gain obtained from numerical simulation to the proposed antenna is about 2.05 dBi, allied with 84 % radiation efficiency, values which are adequate results for this type of antenna.

3.4.2 Dual-band antenna

As in the DCS1800 band the power level from radio waves is also quite considerable, some changes in the previous model have been explored, in order to facilitate the simultaneous operation at both GSM900 and DCS1800 bands (dual-band). As so, a second monopole antenna is considered, based on the same materials as for the single-band one, according to the geometry presented in Figure 3.8, and the dimensions from Table 3.4. The return loss obtained from numerical simulations for the dual-band proposed antenna is shown in Figure 3.9, from which both the antenna's operating frequency bands are clear. The lowest band is from 820 MHz to 1000 MHz, covering the entire E-GSM band, while the highest band is from 1690 MHz to 1930

MHz, covering the entire DSC1800 band (1710 to 1880 MHz). In the lowest operating frequency (900 MHz), the radiation patterns from the dual- and single-band antennas shown in Figure 3.10 are similar. However, the radiation pattern for the dual-band antenna suffers a deformation at 1800 MHz.

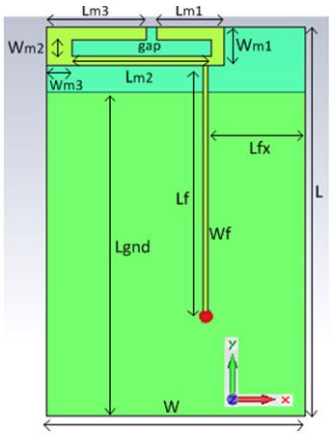

Figure 3.8: Proposed dual-band antenna geometry.

Table 3.4: Proposed dual-band antenna dimensions.

Parameter	Dimension [mm]
L, Lgnd, Lf, Lfx	120, 100, 78, 30
Lm1, Lm2, Lm3, gap,	21, 43, 31, 3
W, Wf, Wm1, Wm2, Wm3	80, 1.5, 12, 5, 8

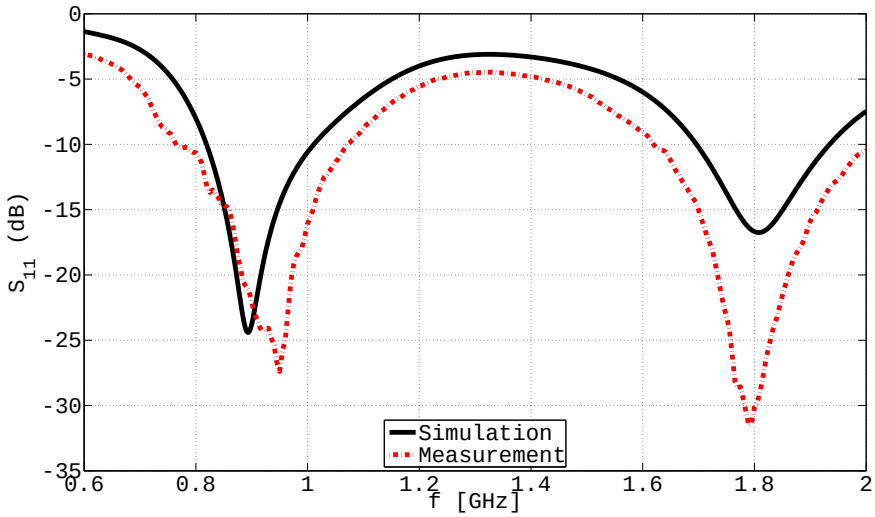

Figure 3.9: Simulated and measured return loss for the proposed dual-band antenna.

The gains for the dual-band antenna are about 1.8 dBi and 2.06 dBi, for the lowest and highest operating frequency bands, respectively. As in the previous case, these gains are fairly good for the proposed antenna type. The radiation efficiency determined by numerical simulation is also high, with 82 % and 77.6 % radiation efficiency for the lowest and highest operating frequency bands, respectively.

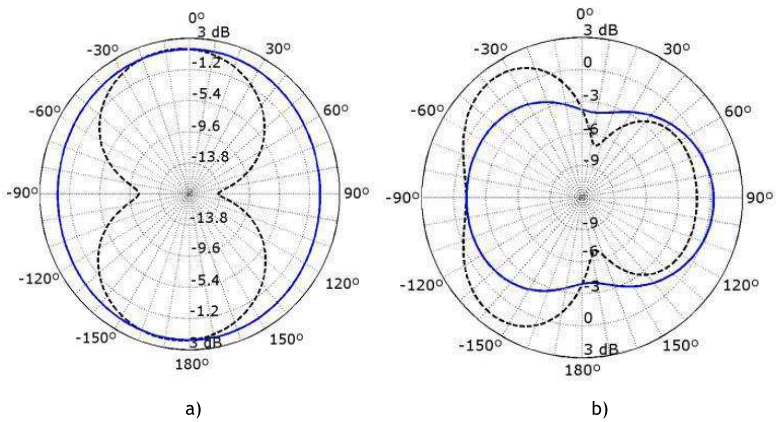

Figure 3.10: Simulated radiation pattern for the dual-band antenna in the YZ plane (dashed) and XZ plane (blue solid), at (a) 900 MHz and (b) 1800 MHz.

3.5 RF energy harvesting circuits

One of the main factors that influence RF energy harvesting is the path loss. The Friis free-space equation relates the received power, P_r, at a distance, d, with the transmitted power, P_t, as follows:

$$P_r = P_t \times G_t \times G_r \times \left(\frac{\lambda^2}{4\pi d}\right) \tag{3.4}$$

where, G_t and G_r are the antenna gains of the transmitter and receiver, respectively. Based on Equation (3.4), we can observe that, the received power depends on the frequency (the higher the frequency is the lower the received power is), and decreases with the square of the distance (path-loss exponent equal to 2).To conceive an RF energy efficient rectifier which enables to rectify and amplify the input voltage (corresponding to P_r), the Cockcroft-Walton and Dickson voltage multiplier circuits can be considered, as shown in Figs. 3.11.a) and b). This work only addresses the Dickson voltage multiplier since, according to [YMAV05], since both topologies have a similar performance.

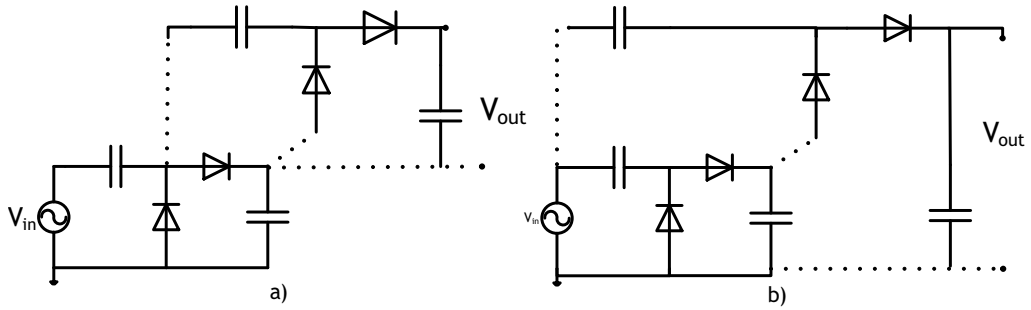

Figure 3.11: Voltage multiplier circuits with two stages: a) Cockcroft-Walton and b) Dickson.

In order to have a self-sustainable WBAN, energy efficient harvesting and management techniques must be considered. However, one of the drawbacks of wireless sensor devices is the finite battery capacity, as well as the voltage generated by the RF energy harvesting circuit, since it may be insufficient to drive the motes (at least 1.8V is needed for the IRIS mote). By means of simulation, we have addressed the main aspects and parameters that influence the performance of the Dickson voltage multiplier, e.g., the choice of diodes, the number of

stages and the load impedance. We have used the Advanced Design System (ADS) software [ADSS13] from Agilent and varied the RF received power, P_r, from -50 dBm to 20 dBm. The considered centre frequency is equal 945 MHz, since we have identified the GSM900 band as the most promising one for RF energy harvesting. The Dickson voltage multiplier presented in Figure 3.11 b) is mainly formed by diodes and capacitors in parallel (instead of being in series, as for the Cockcroft-Walton voltage multiplier). As the input peak voltage from the antenna signal is usually much lower than the diode forward conduction voltage [YMAV05], diodes with low turn-on voltage have been considered. Therefore, we considered HSMS-2850 Schottky diodes from Avago Technologies optimized for low power applications. The number of rectifier stages has a major impact on the output voltage of the Dickson voltage multiplier. According to [KaFi03], the output Open Circuit Voltage (OCV) of an *N*-stage Dickson voltage multiplier is given as follows:

$$V_{out} = 2 \times N \times (V_{in} - V_t) \tag{3.5}$$

where *N* is the number of stages,V_{in} is the input voltage amplitude and V_t is the forward conduction voltage of diodes. As shown in Equation (3.5), the output voltage is directly proportional to the number of stages. However, practical restrictions (e.g., conversion efficiency) limit the number of permissible stages. The conversion efficiency, η_c , of a Dickson voltage multiplier is responsible for providing a representation of the overall performance of the circuit, and defines the relationship between the output DC power, P_{DC} , and the RF received power, P_{RF}, as follows:

$$\eta_c = \frac{P_{DC}}{P_{RF}} \tag{3.6}$$

where, the output DC power is given by:

$$P_{DC} = V_{DC} \times I_{DC} \tag{3.7}$$

To show the impact of number of stages on conversion efficiency and output voltage in terms of simulation, we have also used the ADS software. Figures 3.12 and 3.13 analyse the impact of the number of stages (3, 5 or 8) on the output voltage and conversion efficiency of the Dickson voltage multiplier, by assuming a load impedance of 100 kΩ. The simulation results were obtained through an harmonic balanced analysis (i.e., a frequency domain method) that evaluates the steady state solution of a nonlinear circuit. By analysing Figure 3.12, we conclude that by increasing the number of stages we increase the output voltage. The saturation values are theoretically obtained by multiplying the number of stages by the reverse breakdown voltage (i.e., 3.8V for HSMS-2850). By considering the number of stages equal to 3, 5 or 8, the maximum output voltage obtained by simulation is approximately 11, 18 and 29 V, respectively, which corresponds to RF input received powers of 10, 12 and 15 dBm.
Figure 3.13 presents the effect of the RF received power on the conversion efficiency. By adding more stages, the peak of the conversion efficiency curve shifts towards the higher received power region. These results are similar to the ones presented by the authors in [NMLC12]. As a consequence, we have chosen the 5-stage Dickson voltage multiplier as the best circuit for RF energy harvesting for WBANs. This is explained by the fact that more than 5 stages will not bring substantial improvement for the power levels considered, due to energy losses along the chain [YMAV05].

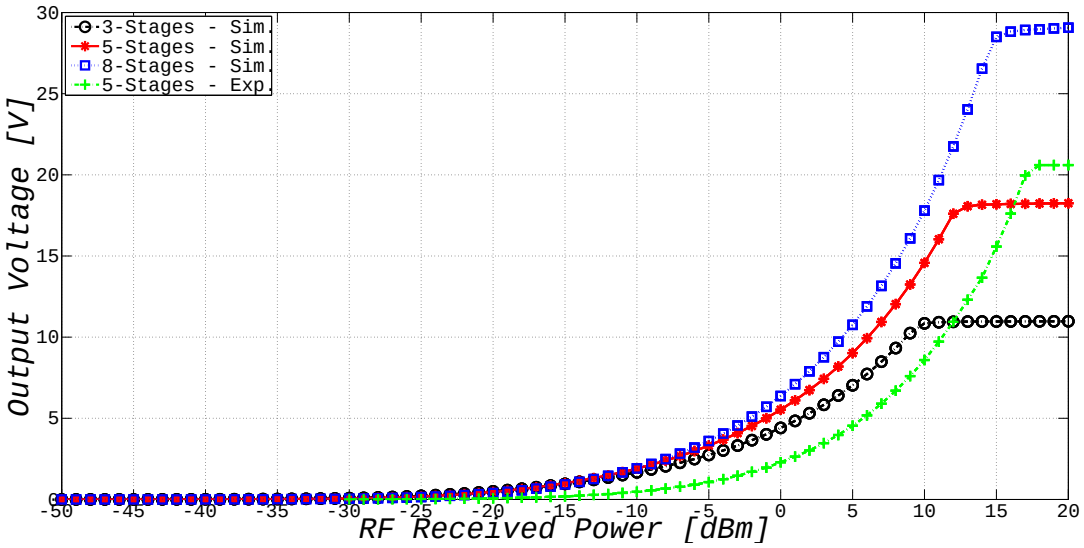

Figure 3.12: Impact of the number of stages on the output voltage for an *N*-stage Dickson voltage multiplier with a load impedance of 100 kΩ.

Moreover, since the wireless sensor nodes need at least 1.8V for operation (i.e., approximately -10 dBm RF input power from simulated results), the 5-stage Dickson voltage multiplier is the one which presents the best performance in terms of conversion efficiency. Based on the previous conclusions we have decided to conceive a 5-stage Dickson voltage multiplier prototype in a PCB fabricated with two layers by using a FR-4 epoxy glass substrate. The performance was evaluated by using the E8361C PNA Microwave Network Analyser and the Agilent E4433B Signal Generator.

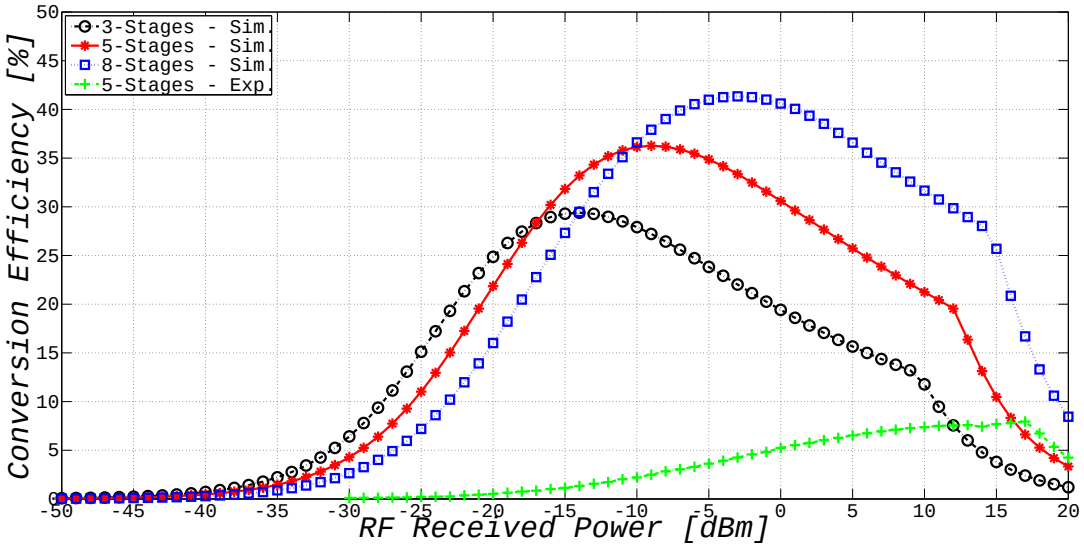

Figure 3.13: Impact of the number of stages on the conversion efficiency for an *N*-stage Dickson voltage multiplier with a load impedance of 100 kΩ.

By comparing the simulation (Sim.) and the experimental (Exp.) results, we conclude that there is an average deviation of 59 % between the simulation and experimental results for the output voltage, whereas the experimental saturation value occurs at the RF input received power of 16 dBm. Moreover, there is an average deviation of 75 % between the simulation and experimental results for the conversion efficiency. The maximum conversion efficiency is

approximately 8 %. By analysing the experimental and simulation results we conclude that the deviations for the output voltage and conversion efficiency can be explained by the impedance mismatching between the antenna and the 5-stage Dickson voltage multiplier prototype as shown in Figure 3.14. The prototype measured impedance is $Z_{in} = 262.49 + j401.65\Omega$ at 945 MHz. The measured return loss is presented in Figure 3.14.

Since, the measured return loss coefficient, S_{11}, is extremely high, it will induce significant amount of reflection. Therefore, there is a need to design a match impedance circuit to cancel the losses due to reflection. One solution is to use a single stub matching circuit for improving both the output voltage and conversion efficiency, like in [ZhFR12].

Figure 3.15 presents the impact of the load impedance on the conversion efficiency of the 5-stage Dickson voltage multiplier by analysing its dependence on the RF received power through a simulation approach.

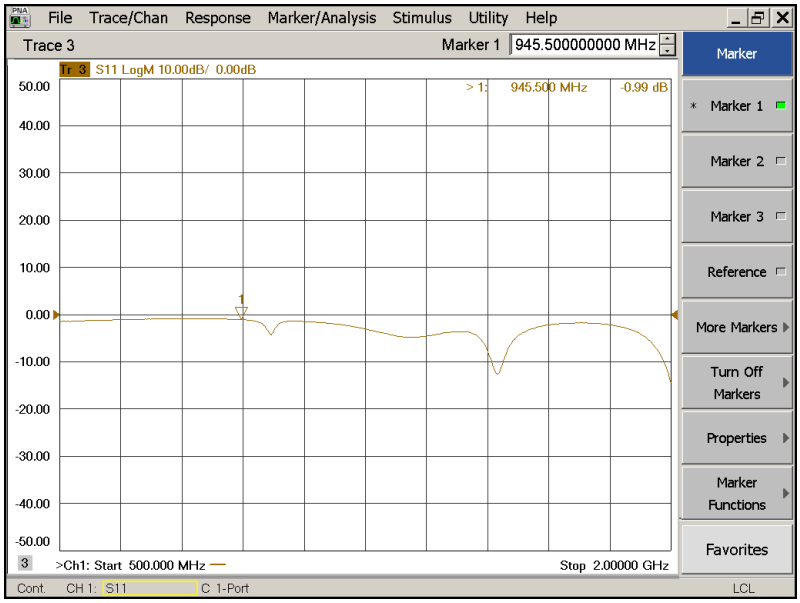

Figure 3.14: Experimental measured return loss (S_{11}) from E8361C PNA Microwave Network Analyser.

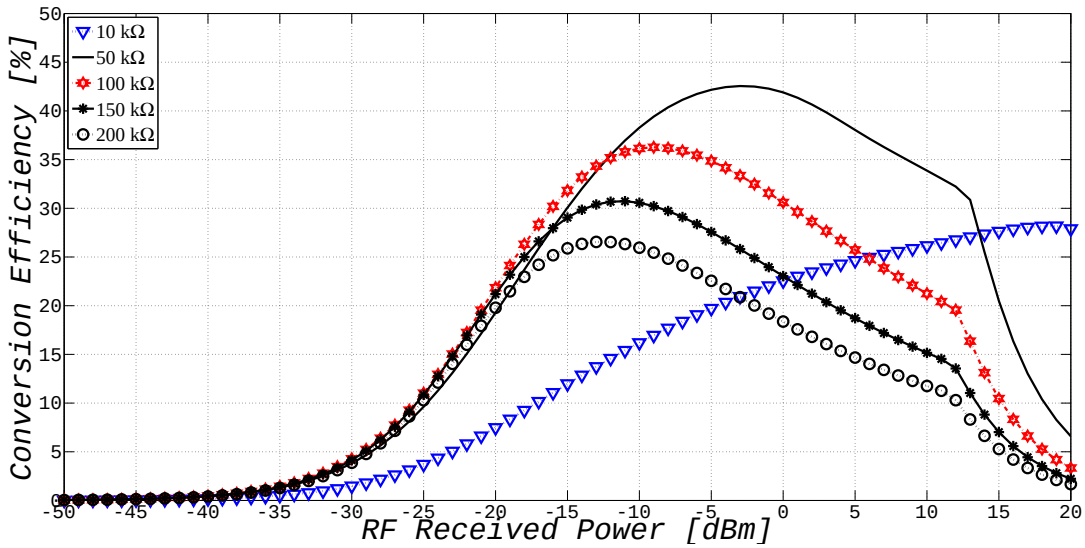

Figure 3.15: Variation of the conversion efficiency with the RF received power for the 5-stage Dickson voltage multiplier with the load impedance as a parameter.

Based on the simulation results we can conclude that the optimal conversion efficiency is achieved when the load impedance is 50 kΩ. If the resistive load value is too low or too high, the conversion efficiency greatly decreases. In WBAN the nodes equivalent impedance is different for each radio operation state (i.e., RX, TX and SLEEP). According to [NMLC12], the value of the impedance from Mica2 mote in the deep sleep state is 100 kΩ. This value is considered as the impedance reference load for the IRIS motes.

3.6 RF wireless charging and energy harvesting

Nowadays, RF energy is being transmitted from billions of radio transmitters around the world, including mobile cell phones, handheld radios, mobile base stations, and television/radio broadcast stations. There are therefore plenty of opportunities for harvesting this RF energy for power supply nodes from WBANs. Although the opportunities for energy harvesting are vast, the amount of energy collected could not be enough to power supply the wireless nodes of a WBAN.
In previous Sections, it has been shown that it is possible to harvest RF electromagnetic energy from multiple sources. However, nodes typically need to be power supplied by a source able to provide at least 1.8 V, i.e., -10 dBm by simulation and -1 dBm experimentally by considering a 5-stage Dickson voltage multiplier like the one previously presented. Therefore, by combining the TX91501 Powercast® RF transmitter with a power output of 3 W and the *N*-stage Dickson voltage multiplier, we can add new energy harvesting capabilities to the sensor nodes, providing a predictable and reliable power system that uses controlled broadcasted RF energy for wirelessly charge battery-based systems. Figure 3.16 presents the available received power for RF energy harvesting by considering Equation (3.4), where the Effective Isotropic Radiated Power (EIRP), $P_t \times G_t$, is 3W, G_r is 3.98 and the operation frequency is 945 MHz.

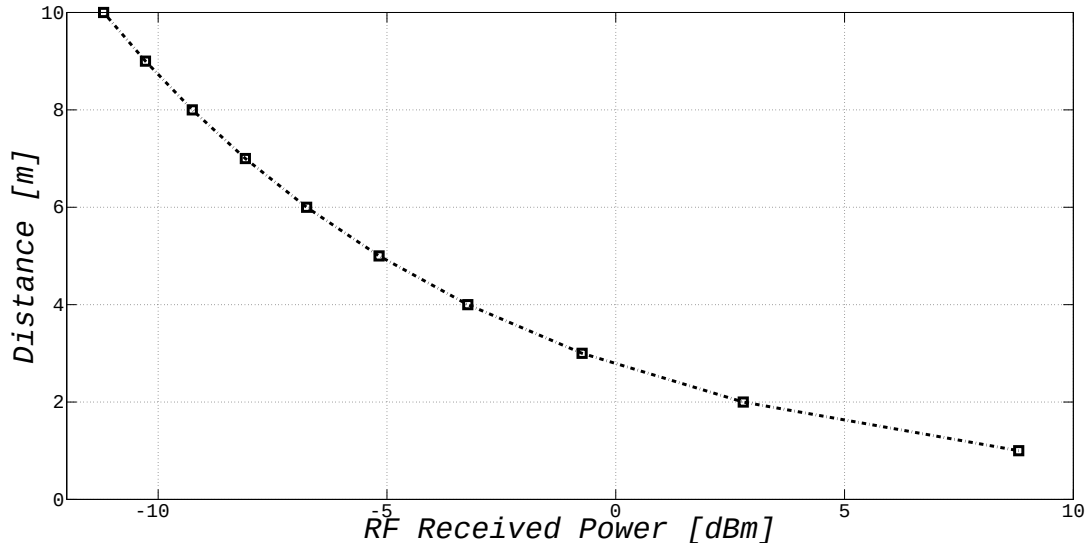

Figure 3.16: Distance between wireless sensors versus amount of power harvested by the 5-stage Dickson voltage multiplier.

By analysing the obtained simulated results, one may conclude that dedicated power transmitters can be used to wirelessly power the sensor nodes located at less than 9 m away from each other corresponding to the received power higher than -10 dBm.
However, since our 5-stage Dickson voltage multiplier prototype does not considers the use of a

match impedance circuit to cancel the losses due to reflection, we are only able to wirelessly power the sensor nodes located at less than 3 m away from each other, corresponding to the received power higher than -1 dBm.

By analysing Figures 3.13 and 3.15 the range of power (higher than -10 dBm by simulation) corresponds to values of the conversion efficiency in the descendent part of the curves (with load impedance of 100 kΩ). For short-range applications, the 5-stage Dickson voltage multiplier could be used for store the RF energy directly into a battery. However, for longer-range applications, it is advised to accumulate the energy in a supercapacitor before directly powering up circuits or charging batteries, since it is only possible obtain intermittent pulses of energy. The use of supercapacitors allows faster charging times, better discharge performance and "unlimited" virtually life cycles. The choice of the supercapacitors is justified by the fact that batteries suffer from some non-linear characteristics, such as degradation and saturation (due to high constant current drain). Note however that the main disadvantage of supercapacitors is their high "self-discharge" characteristic. Based on the presented characteristics, a system is envisaged where both batteries and supercapacitors are used, enabling to overcome the saturation and degradation problem from the batteries, if they are only used during the mote's sleep state (i.e., very low current drain), whilst the supercapacitors are being charged. During the active state, nodes can be power supplied by supercapacitors, turning off the batteries. This way, higher current consumptions will not degrade batteries, increasing the network lifetime. Moreover, we can also conclude that the spectrum opportunities presented in Section 3.3 may not be enough to power supply the current WBANs platforms. This is due to the insufficient energy available, which corresponds to powers in the range of -27 dBm to -37 dBm. To mitigate this very low received power we envisaged the use of highly efficient DC-to-DC boost converter (e.g., BQ25504 highly efficient DC-to-DC boost converter [BQ2513]) placed between the rectifying antenna circuit and the storage device. This device manages power from a variety of sources (such as solar, thermal electric, electromagnetic and vibration energy) in the range between microwatts (μW) and milliwatts (mW).

3.7 Wireless Body Area Networks with electromagnetic energy harvesting and Cognitive Radio capabilities

The next generation of CR networks will be supplied by renewable energy from natural resources, such as solar, wind and RF energy [LeMF08]. This energy could be used overnight to increase the battery charge, or to prevent power leakage. In a hazardous situation, if a battery or a solar-collector/battery package completely fails, harvested energy from radio waves can enable the system to transmit a wireless distress signal, whilst potentially maintaining critical functionalities [BFBT12].

MAC and routing protocols also play an important role in the network performance of the WBAN. The MAC protocols are responsible for managing the radio transmission and reception through the shared wireless link, whereas the routing protocols are responsible for the selection of the best path in order to send packets from one source to one single-destination or multi-destination. Hence, choosing the best ones has a high effect on the overall network performance as well as on the energy consumption. Driven by the intense usage of some frequency bands, while others are being liberated (e.g., white spaces left by analogue television discontinuation) investigation on multi-hop CR networks has experienced an evolution in the

latest years. The authors from [ZLWZ09] use graph theory for the routing algorithms, where the CR aspects are considered by assigning a different colours to each considered frequency band. The developed algorithm is not computationally heavy and based on hop-count for the routing. However, as pointed by the authors, they were not able to mitigate the interference between neighbours. In [XiZW10], the authors aim to minimise the interference between nodes. To achieve this objective, they propose the use of relays, with visible gains in the channel utilisation, energy consumption and delay.

Dynamic Spectrum Access (DSA) can be used to mitigate spectrum scarcity. This is accomplished by enabling an unlicensed user (i.e., secondary user) to adaptively adjust its operating parameters and exploit the spectrum which is unused by licensed users (i.e., primary users), in an opportunistic manner. Therefore, CR allows for Secondary Users (SUs) to seek and utilize "spectrum holes" in a time and location varying radio environment as long as they do not cause interference to the Primary Users (PUs) [AkKE09]. This opportunistic use of the spectrum poses new challenges, making the network protocols to adapt to the varying available spectrum. The extreme flexibility of CR has significant implications in the design of network algorithms and MAC protocols at both local/access network and global inter networking levels.

Therefore, we envisage new cross-layer algorithms which can adapt to the changes in the transmission link, based on the quality of the received signal, radio interference, radio node density, network topology or traffic demand. Hence, it may be required an advanced control and management framework with support for cross-layer information and internode collaboration [RJSL08]. Figure 3.17 shows a typical WBAN scenario with CR. Depending on the spectrum availability, sensor nodes transmit their results from the sensing, to the next hops and ultimately to the sink [AkKE09] in an opportunistic manner.

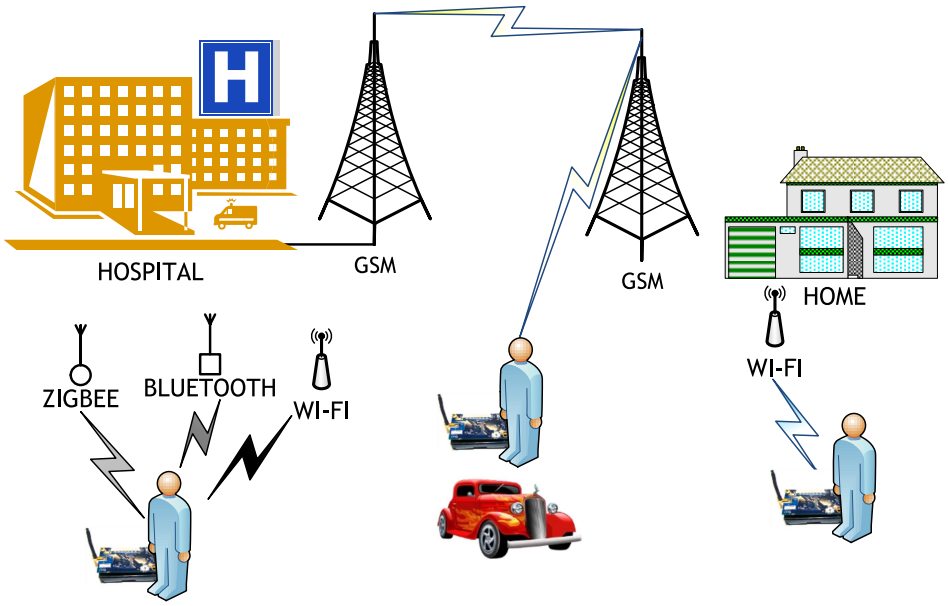

Figure 3.17: Wireless body area networks scenario with electromagnetic energy harvesting and CR capabilities.

A DSA entity will be used to identify the CR opportunities, in which nodes can be equipped with Powerharvester receivers [Powe13], facilitating to collect energy by converting the harvested energy, from the radio frequency waves, within other frequency bands from the CR opportunities, to DC power. By using RF-based wireless scavenging devices, we intend to eliminate the cost of replacing batteries of wireless sensors, as well as eliminate the service downtime

caused by depleted batteries. Future improvements in RF energy harvesting technology will allow for the creation of a network with no need of a dedicated transmitter to a single-sided system. This is accomplished by enabling the capture of radio frequency waves transmitted from existing and commonly used ambient RF energy sources, such as mobile base stations, TV and radio transmitters, microwave radios, and mobile phones, as presented in Figure 3.17. Future improvements in the performance of the electronic components will lead to a decrease of the power consumption which results in faster charge times and more frequent broadcasts of data, enabling the creation of a always connected Ubiquitous Wireless Power Sensor Network (UWPSN).
Moreover, a system that cognitively seeks the best signal available from multiple frequency bands for collecting energy, and simultaneously finds the best transmission opportunities is envisaged, possibly employing multi-band antennas. In terms of channel access an Adaptive Frequency Hopping (AFH) algorithm could be implemented, containing a blacklist of the bands which contain interference caused by the same/other protocols to exploit the temporal opportunities (i.e., temporal "white spaces"). By considering that the primary user flow is bursty and there will be inactive periods between transmissions. These inactive periods can used by the secondary users CR entity to send their own traffic.

3.7.1 Topology aspects

Depending on the application, the scavenging WBANs with CR capabilities may be applied to different scenarios, as follows:

- **Static Networks**: In ad hoc networks, nodes send their readings to the gateway node in a multi-hop manner. In addition, the bandwidth availability and computing resources (e.g., hardware and battery power) are restricted. Therefore, to overcome these limitations joint optimization between the MAC and PHY layers, to maximize energy efficiency, must be addressed. In the scenario presented in Figure 3.17, a CR node senses several channels simultaneously and chooses the best ones to transmit data to the receiver. By considering the PHY layer measurements, RF-based scavenged device can be used, to power the sensor nodes based on local measurements (e.g., by using WiFi inside the hospital).
- **Mobile Networks**: In static networks, node position can be determined once during initialization. However, in a mobility scenario, since nodes frequently change position, some adjustments in the transmission power may be required (e.g., when nodes are closer to each other, their transmission power can be lowered). The challenge in node mobility is how to cope with motion on different speeds, which dictates the frequency of transmission power updates. Besides, our CR system must be capable to adapt to the frequent changes in the control and data channels that may vary in different clusters. This requires additional time and energy, as well as the availability of a rapid localization service. Since frequent updates have a great impact in the network performance, we can collect the electromagnetic energy from RF signals by using available the spectrum opportunities.
- **Hybrid**: In a hybrid ad hoc WBAN, nodes are mobile and stationary. Therefore, they are able to form connections at both MAC and network layers. When mobile nodes are inserted into the static network, in order to maintain the connectivity of the network, route information must be set up, which increases the drain of the power source. Hence, mobility-aware dynamic spectrum management CR solutions must be considered to overcome the challenges covered by this additional source of complexity. Spectrum sensing

parameters include SNR, frequencies available and RF energy harvesting opportunities, based on the energy detection performed at the PHY layer.

3.7.2 Cognitive sensor node hardware

The cognitive sensor node hardware of the WBANs is composed by four sub-systems: i) communication, ii) computational and storage, iii) sensing and actuation, and iv) power. Figure 3.18 presents the general hardware architecture.

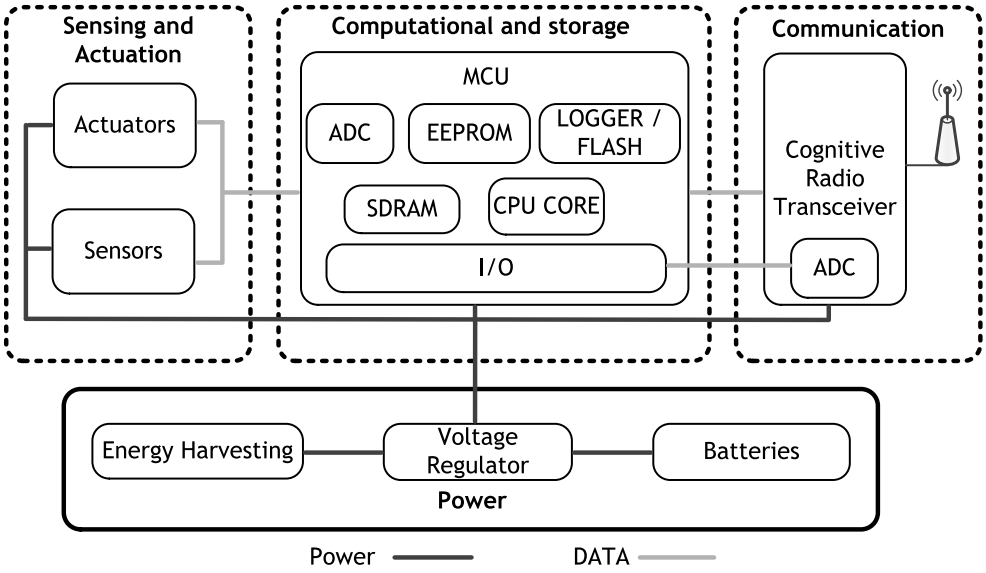

Figure 3.18: Hardware structure and sub-systems for cognitive radio sensor nodes.

The description of each sub-system is as follows:

- **Communication**: The communication sub-system consists of a radio transceiver and an antenna which enables the wireless communications between neighbouring nodes.
- **Computational and storage**: This sub-system allows for data processing and the management of the nodes functionalities.
- **Sensing and Actuation**: The interfaces between the environment and the WBAN are the sensors and the actuators. Basic environmental sensors include, but are not limited to, light, temperature, humidity, pressure, acceleration/seismic, acoustic, magnetic and sound. Basic environmental actuators include, but are not limited to, light-emitting diodes, speakers and buzzers.
- **Power**: The appropriate energy infrastructure to supply the nodes, includes the batteries and the energy scavenging systems, which allows for supporting the operation of the nodes from a few hours to months or years.

The inclusion of a cognitive radio transceiver in the communication sub-system is the main difference between the hardware structure of CR sensor and classic sensors.

3.8 Communication aspects of WBANs with CR capabilities

This subsection investigates the specific cross-layer design aspects, between the PHY, MAC and network layers of a cognitive radio sensor node [BBTV13].

3.8.1 Physical layer aspects

The PHY layer acts as a mediator between the data link layer and the physical wireless environment. Since cognitive radios need to sense the spectrum in order to find spectrum opportunities, the PHY layer is also responsible for spectrum sensing, reporting it to the microprocessor of the CR node. As presented in Figure 3.19, the PHY layer also aims at the reconfiguration of the transmission parameters according to the decisions from the microprocessor. WBANs which

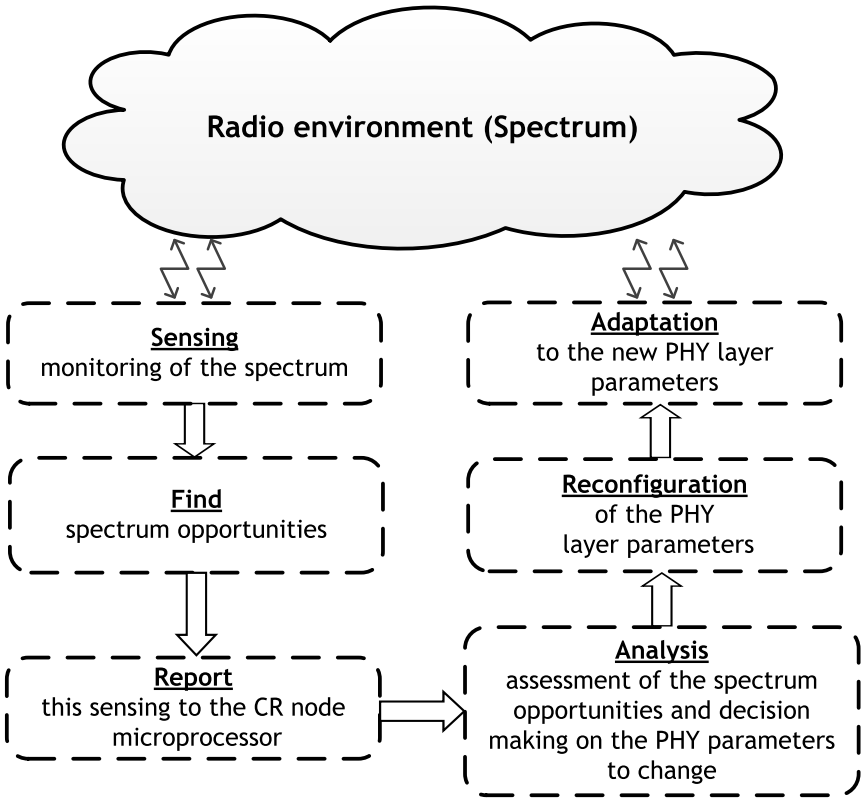

Figure 3.19: Tasks related with spectrum sensing at the physical layer.

do not consider CR capabilities impose environmental and propagation constraints that must be taken into account in system design:

- Current draw is 400 μA and 1 μA for the active and idle modes, respectively [JRPC01];
- Typically, the sensor nodes are placed near the human skin, which imposes restrictions to the transmitter power from the radio transceiver, as the radiation caused by the large wireless transmission power may possibly harm human health. The IEEE 802.15.6 WG, which is focused in WBANs, already foresees and advises these thresholds. Safe transmitter power thresholds are depend according to the location of the sensor node relatively to the human body;
- The surrounding environment of WBANs produces situations such as the phenomena of body shadow effect already identified by the authors from [CoSa07]. This effect is due

to the propagation of signal over the human body;

- The multi-path effect leads to interference due to the reflection of the radiated signal. This is caused by the ground and surrounding objects. In WBANs the values of reflection signal depends on the position of the sensor node in the human body [FRDD06];

- The antenna characteristics cause some negative impact in the overall performance of WBANs. The coupling effect appears and depends much on the relative positions of the sensor nodes in human body.

WBANs with no CR capabilities must be able to cope with the majority of the aforementioned effects in order to properly receive the low power signal. Therefore, the use of CR capabilities in WBANs must also consider these design requirements of the system in order to be efficient. In addition, to the environmental and propagation constraints, the CR transceiver hardware must be suitable to enable CR operations in WBANs. The ability of the CR to reconfigure the PHY layer parameters (i.e., modulation, channel coding, transmitting power) is the main difference between the WSN and the Cognitive Radio Sensor Network (CRSN) PHY layer.
This *in situ* reconfiguration does not require any hardware replacement. To accomplish this reconfiguration, Software Defined Radio (SDR) based RF front-end transmitters and receivers are needed. Special attention is needed in the use of SDRs due to the nodes' scarce power supply in WBANs. Energy harvesting is a solution to complement the power supply requirements in the context of SDR in CR sensor nodes. A preferable solution is the development of SDRs specifically designed to energy-efficient CR sensor nodes.
The spectrum sensing task of the CR sensor nodes is a challenging issue due to its limited processing capabilities. Spectrum sensing is a highly demanding signal processing task, since the radio signals in WBANs are weak and with possible large background noise. Digital Signal Processing (DSP) hardware and algorithms can be added to the CR sensor node to achieve more efficient wideband spectrum opportunities sensing and detection. Furthermore, if conventional SDRs applied to CR sensor nodes are not considered, it is impossible to support different modulations schemes, waveforms or supporting wideband spectrum sensing, due to the limited processing capabilities of the CR sensor node. Another design consideration aspect in WBANs with CR capabilities is the development of transmission power and interference adaptive algorithms that cope with interference in the deployment of CR sensor nodes over the human body.

3.8.2 MAC layer aspects

The MAC protocols are responsible to determine and change the operation mode of the radio transceiver, allowing for nodes to access the medium in a more fair and efficient manner. Compared to conventional WSNs, the MAC layer of a CRSN nodes must handle additional challenges such as silent spectrum sensing periods and the need for high-priority access mechanism for the distribution of spectrum sensing and decision results [AkKE09]. In WBANs with CR capabilities, sensor nodes may use a Control-Channel-Request-To-Send/Control-Channel-Clear-To-Send (CRTS/CCTS) handshake mechanism to negotiate on the channel before transmitting packets [WaQZ08]. The use of a CRTS/CCTS mechanism on a separated control channel packets allows for decreasing the number of collisions, whereas the DATA and ACK packets could be transmitted in a group of frequency bands, as shown in Figure 3.20.
Therefore, compared to conventional WSNs, the MAC layer of WBANs with CR capabilities must

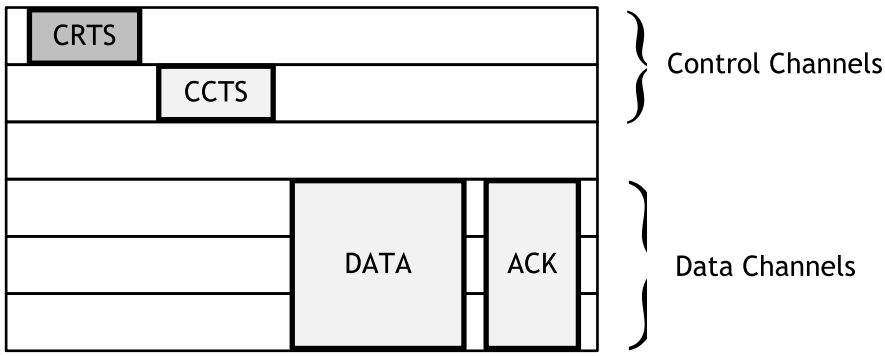

Figure 3.20: CRTS/CCTS/DATA/ACK handshake.

address additional challenges regarding the coordination of dynamic spectrum access, as follows:

- **Spectrum sensing and decision results**: Cooperative sensing [GaLi05] and decision results are used to increase sensing accuracy and sharing efficiency. Therefore, nodes must share extra control information. The CR MAC protocol must include mechanisms to share information with higher priority;
- **Minimum overhead**: The wide range of MAC protocols for WBANs use control packets. This type of packets can be received by all nodes within radio range of the sender, resulting in an increase of the power drain in a potentially large number of nodes. Since nodes are required to remain awake in order to receive control packets, the battery life can be significantly reduced. Therefore, it is envisaged a CRSN with minimum exchange of control packets and without the need of having additional hardware requirements (i.e., an extra transceiver or GPS for synchronization). This can be accomplished by using a BACK policy feature [CaSV09]. This way every time a node accesses to the medium, it optimizes the transmission time by reducing the amount of overhead, whilst increasing the channel capacity. The Piggyback Mechanism (PM) could also be used, in which a receiver station is allowed to piggyback a data frame to a sender station once if the receiver station has a frame to send to the sender [Xiao05].
- **Adaptive duty cycle**: Since the spectrum opportunities are time and location variant, self-adaptive mechanisms must be introduced. Therefore, based on the spectrum sensing measurements we can increase the duty cycle, which means more opportunities to cover multiple neighbors with one forwarding. Besides, since collecting RF energy to power the sensor nodes is foreseen based on the available energy and CR opportunities, a threshold can be implemented to send packets based on the existing energy scavenging opportunities versus interference metrics.

3.8.3 Network layer aspects

Cognitive networks and its design aspects are very challenging for the network layer design. In traditional wireless networks, the nodes use the same frequency to communicate with each other. Thus, routing is performed by considering only one link between neighbours. In cognitive radio networks, the network layer is responsible for choosing the best next hop as well as the frequency to use. This arises an extra load to the routing algorithm, since it must also take

into account the readings from the spectrum to decide the routes for the packets to follow. Therefore, the first challenge is how to have available information on the spectrum usage. This information must be provided by an external (to the routing) entity that constantly monitors the communication bands and evaluates its interference or not. This can be performed by the node locally, using its own sensing capacities, can be provided by an external entity dedicated to that task, or by a combination of these two, in which neighbouring nodes exchange information about their spectrum sensing.
The second challenge is how to combine the information gathered and choose the optimal path for the packets to be sent. Traditional approaches use hop-count, RSSI strength or QoS metrics to decide the best routes for the packets; however in CR networks the frequency to be used must also be included in the algorithm. With the dynamic nature of the spectrum, and constant frequency usage by other entities, the algorithm will have to adapt the paths to the current conditions of the channel.
However, open research issues are still open, and must be addressed in order to have a complete network solution as follows:

- **Spectrum aware routing**: When nodes send packets through the network, spectrum sensing techniques must be addressed to opportunistically route data packets across paths avoiding spectrum congested areas. To achieve this goal, innovative awareness mechanisms (that facilitate to know about the presence, characteristics and requirements of other wireless devices in the same area) that consider spectrum mobility and resource constraints must be employed to find the optimal traffic according to the available spectrum resources;
- **Adaptive and QoS routing**: Cross-layer mechanisms will be responsible for providing up-to-date local QoS information for the adaptive routing protocol. Hence, new techniques based on varying channel conditions must be taken into consideration for real time communication in CRSNs;
- **Multi-hop routing maintenance and reparation**: In a multi-hop CR scenario the sudden appearance of a PU in a given location where may impose an unusable channel for the SUs, leading to unpredictable route failures. Therefore, effective signalling mechanism must be addressed to restore the paths with minimal effect on the network performance.

3.9 Summary and conclusions

This Section has addressed the development of an energy self-sustainable WSN by considering RF energy harvesting as the primary energy source. The spectrum opportunities for RF energy harvesting to power supply the wireless sensor nodes in real indoor/outdoor scenarios have been identified. The set of indoor/outdoor most promising frequency bands are 79 to 96 MHz (mobile/radio broadcast stations), 391 MHz (emergency broadcast stations), 750 to 758 MHz (digital television broadcast stations), 935 to 960 MHz (GSM 900 broadcast stations), 1855 to 1868 MHz (GSM 1800 broadcast stations) and 2115 to 2160 MHz (UMTS broadcast stations). For the GSM (900/1800) frequency bands, a dual-band printed antenna has been proposed, with gains of the order of 1.8-2.06 dBi and 77.6-84 % efficiency respectively. The design of RF energy harvesting circuits have also been analysed. We have also simulated the behaviour of a 5-stage Dickson voltage multiplier for power supplying an IRIS mote, which can perpetually operate if the RF received power is at least -10 dBm. However, the transmission opportunities must be

carefully selected according to the estimated battery lifetime based on the electromagnetic RF energy harvested. A scenario where RF dedicated transmitters are used has been briefly analysed in the PROENERGY-WSN [PROE13]. It enables future WBAN to operate without the need of replacing batteries. The PHY, MAC and network layers aspects of WBANs with electromagnetic energy harvesting and CR capabilities has also been addressed. Showing that CR offers a viable and future proof solution for addressing both scalability and coexistence issues.

Chapter 4

Wireless Sensor Node Platforms

4.1 Introduction

To demonstrate the feasibility of the existing MAC protocols, the analysis of several implementations in real-world platforms must be carried out, allowing for implementing and testing the developed MAC protocols. A vast diversity of platforms can be found on the market, where the majority employs IEEE 802.15.4 compliant radio transceivers and a few employ their own standards and protocols. Several platforms try to achieve high computing performance while others try to minimize the overall power consumption of the platform components. Depending on the application, requirements and selected tradeoffs, some platforms may be a preferable choice than the others. This means that the hardware platform must be carefully selected since it significantly affects the network performance. Even if the MAC protocol is designed to be energy-efficient, if the hardware platform does not allow for minimizing the energy consumption in the idle and sleeping states (which limits the network lifetime), the goal of energy efficiency will not be achieved. In the same way, some companies present better solutions for easier and/or more complex deployments, both in terms of programming as well as the deployment of vast sets of compatible sensors and actuators that can be attached to them. Based on the aforementioned issues a state-of-the-art for the WSN platforms hardware that will accommodate the MAC protocols developed is given bellow.

4.2 Platform components

In an effort to create inexpensive (ubiquitous) wireless devices, the market industry players are seeking new ways to add cheaper hardware components in order to build low-cost smart sensors to be used in future wireless applications. As a result, WSNs have become a leading solution, in many important applications such as intrusion detection, target tracking, industrial automation, smart building and so on [HXSM12]. Moreover, advances in MEMS-based sensor technology has led to the development of miniaturized and cheap sensor nodes, capable of communicating wirelessly, sensing and performing computations [FaKu11].
The three main components of a wireless sensor platform are the following ones:

- **Wireless sensor devices or motes**: a mote usually consists of a communication, computing, sensing and power unit. Its functionalities include collecting and processing the sensing data from the sensor unit, as well as managing the connections established in the network. A wide variety of platforms have been developed in recent years such as: MICAz [MICz13], TelosB [Telo13], Imote2 [Imot13], SunSPOT [SUNS13], IRIS [IRIS13], LOTUS [LOTU13], Waspmote [WASP13], WirelessHart LTP5902 [WIHA13], T-MOTE Sky [TMOT13], Tinynode [Tiny13], Z1 [ZNOD13], BTnode [BTNO13] and EZ430-RF2500 [EZTI13].

- **Sensor board**: the sensor board is attached on the mote and is responsible for collecting the data from the various sensors. The sensor board may also include a prototyping area,

which may be used to connect additional sensors. Existing sensor boards include the MTS400/420 and MDA100/300 compatible with the MICA and IRIS wireless modules.

- **Programming board**: also known as "gateway", provides multiple interfaces such as Ethernet, Wi-Fi, Universal Asynchronous Receiver/Transmitter (UART) and USB for both programming and data communication. Their function includes working as base station for WSNs. Existing programming boards include the MIB510, MIB520 and MIB600. Some advanced features include Over The Air Programming (OTAP) that allows for reprogramming the gateways over Radio Frequency (RF).

The wireless sensor devices hardware for WSNs are composed by four sub-systems: a) communication, b) computational and storage, c) sensing and actuation and d) power. The general hardware architecture is presented in Figure 4.1.

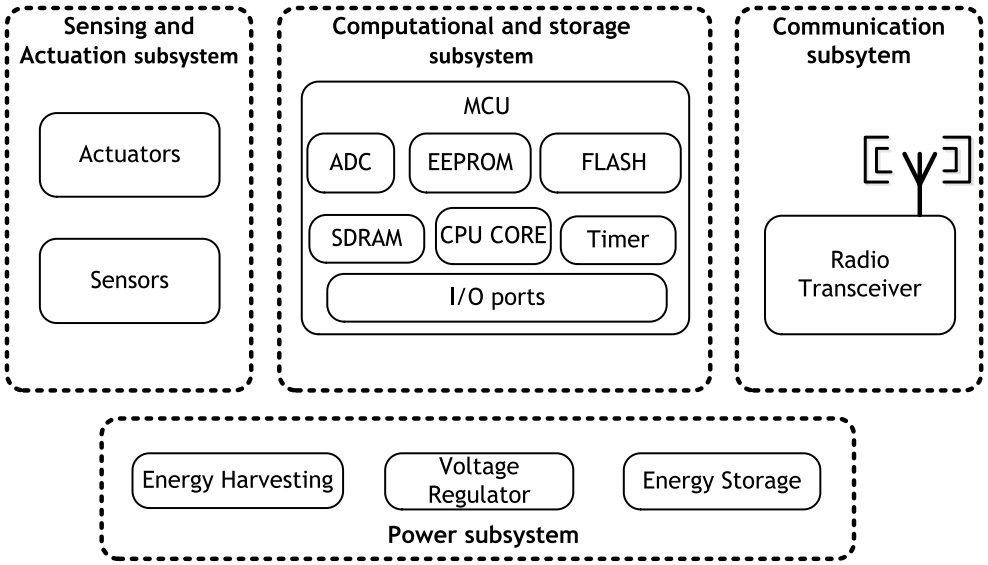

Figure 4.1: Wireless sensor node hardware architecture.

A. Power subsystem

The power subsystem is responsible for power supplying all the sensing systems. It includes a voltage regulator, batteries and may include an energy harvesting unit (an possibly a supercapacitor). The voltage regulator is responsible for providing the right amount of supply voltage for each individual hardware component. The energy provided to the voltage regulator can be from a non-rechargeable battery (primary source) or from an energy harvesting system (secondary source). For the latter case, energy can be stored in a supercapacitor. Supercapacitors can be charged and discharged hundreds of thousands (and millions) of cycles without losing performance. A battery is only suitable for a limited amount of charge and discharge cycles. Since energy is typically generated in peaks during short periods of time and the amount of stored energy can be relatively low [BSGT13], supercapacitors are suitable to be used with an energy generator.

B. Computational and storage subsystem

The computational and storage subsystem is responsible for performing local computations based on the data acquired by the different sensors. It consists of a Microcontroller Unit (MCU), which integrates a Central Processing Unit (CPU) core, input/output ports, Analog-to-Digital

converters and data memory.

C. Sensing and actuation subsystem

The sensing and actuation subsystem which, includes the sensors and the actuators, is the interface to the physical world and is close to the sensed phenomenon. The sensors are responsible for monitoring a certain phenomenon within their sensing ranges as well as reporting the measurements to the gateway nodes where the end-user can access the data. Existing sensors include temperature, humidity, light, CO_2, acoustic, vibration and pressure. The actuators are controlled by a WSN node and they typically control a mechanical device like a servo drive, or may might switch some electrical appliances by means of an electrical switch, like a lamp or a similar device.

D. Communication subsystem

The communication subsystem consists of a radio transceiver and an antenna. The four operating modes of a radio transceiver are: transmit, receive, idle and sleep. Owing to the hardware design principles sometimes, in the receive state, the transceiver can consume even more energy than in the transmit state, due to the CCA procedure.

4.3 Comparison of Wireless Sensor Network platforms

In order to choose the most appropriate hardware platform for WSNs, we have established an evaluation criteria for the most "well known" WSNs platforms. Next we present two WSN platforms (i.e., MICAz and Imote2) and discuss then the main features and technical characteristics. The platforms operate in the Industrial, Scientific and Medical (ISM) 2.4 GHz band and are compliant with the IEEE 802.15.4 standard. They include the CC2420 [CC2420] transceiver chip from Chipcon, which is currently the most popular radio chip on wireless sensor nodes. Specific information related with other WSNs platforms (e.g., Waspmote) has been extracted from their datasheets and is presented in Appendix D.

A. MICAz

The MICAz platform [MICz13] presented in Figure 4.2 is part of the MICA family including the Mica2 (Cricket) and Mica2Dot, that are one of the most "well known" wireless sensor platforms for WSNs. It has a single processor board (MPR2400) based on the ATmega128L microprocessor that can be configured to run the sensor application/processing and the network/radio communications stacks simultaneously. The radio transceiver has a data rate of 250 kb/s, and uses a wide-band Direct Sequence Spread Spectrum (DSSS) modulation scheme allowing for providing better tolerance against noise and interferences. To add additional sensing capabilities, sensor data acquisition boards can be attached by using the expansion connector. The acquisition boards include the MTS300, MDA100 and MDA500 sensor boards. Table 4.1 summarizes the characterisation parameters from the datasheet.

Figure 4.2: MICAz platform.

Table 4.1: MICAz characterisation parameters.

Computational and storage subsystem		**Interfaces**	
Microcontroller	Atmega 128L	Analog Inputs, Digital I/O, I2C, SPI,	
RAM	4 kB	UART, 8 ADC (10 bit)	
Program Flash Memory	128 kB FLASH		
Speed	7.37 MHz		
Operating System	TinyOS		
Communication subsystem		**Miscellaneous**	
Transceiver	CC2420	**Power Source**	2 AA type batteries (3V)
Operating Frequency	2.4 GHz	P_{Sleep}	3 μW
Data Rate	250 kb/s	$P_{Receive}$	59.1 mW
Modulation Scheme	O-QPSK	$P_{Transmit}$	52.2 mW
Protocol	IEEE 802.15.4 compliant		
Range	$\simeq$ 75-100 m outdoor $\simeq$ 20-30 m indoor		

B. Imote2

The Imote2 is an advanced platform for WSN applications that require higher CPU/DSP and wireless link performance as well as higher reliability [Imot13]. It was built around the low power PXA271 XScale processor which integrates an IEEE 802.15.4 radio transceiver operating in the ISM 2.4 GHz band. The platform can be expanded by using extension boards enabling to customize the system to a specific application. The extension sensor boards provide both analog and digital interfaces. A battery board is responsible for power supply the system, or it can be powered via the integrated USB interface. Figure 4.3 presents the Imote2 platform, and Table 4.2 presents the characterisation parameters for the functional and physical characteristics of the sensor platform.

Figure 4.3: Imote2 platform.

Table 4.2: Imote2 characterisation parameters.

Computational and storage subsystem		**Interfaces**	
Microcontroller	Intel PXA271	GPIOs 2x, SPI 3x, UART, I2C, SDIO,	
RAM	256 kB SRAM 32 MB SDRAM	USB host, USB client, AC'97, Camera	
Program Flash Memory	32 MB FLASH		
Speed	13 MHz - 416 MHz		
Operating System	TinyOS		
Communication subsystem		**Miscellaneous**	
Transceiver	CC2420	**Power Source**	3 AAA type batteries (4.5V)
Operating Frequency	2.4 GHz	P_{Sleep}	4.5 μW
Data Rate	250 kb/s	$P_{Receive}$	88.65 mW
Modulation Scheme	O-QPSK	$P_{Transmit}$	78.3 mW
Protocol	IEEE 802.15.4 compliant		
Range	$\simeq$ 20-30 m outdoor $\simeq$ 75-100 m indoor		

4.3.1 Groups of evaluation criteria

There is a set of very "well know" WSN platforms, which operates in the 2.4 GHz band, and are compliant with IEEE 802.15.4. In the framework of this thesis, we have established an evaluation criteria for the platforms presented in the previously Section as well as in Appendix D. Each criterion includes a description and a scale for interpreting the possible values. The proposed scale comprises four categories, integer values ranging from 1 to 4, and must be interpreted as presented in Table 4.3.

Table 4.3: Evaluation criteria.

Criteria	**Value**
Very good	4
Good	3
Average	2
Bellow Average	1

Furthermore, in order to obtain the overall performance of the hardware platforms, three different groups of criteria have been identified: i) main characteristics, ii) power requirements and iii) expansibility, programming and community resources. The importance of each group in terms of percentage, to evaluate the overall performance is shown in Table 4.4
As presented in Table 4.4, the power requirements have an impact of 50 % in the total overall performance. We assume that this is the most important group of criterion to evaluate the WSNs platforms, since energy efficiency is one of the main goals associated with WSNs. The other two groups cause an impact of 25 % in the total overall performance, since both processing and computation as well as the number of sensor boards available to develop our own applications and easiness of programming are equally important.

Table 4.4: Impact on the overall performance based on the group for evaluate the WSN platforms.

Group of criteria	Evaluation parameters	Impact on the overall performance
Main characteristics	Standard	25%
	Topology	
	Number of nodes	
	Price per node	
	Program flash memory	
	Random access memory	
	Data rate	
Power requirements	Lifetime	50%
	Indoor distance range	
	Outdoor distance Range	
Expansibility, programming	Expansibility	25%
	Object oriented programming	
	Easy to use programm environment	
	Community support	
	Documentation	

4.3.2 Main characteristics

A. Standard

Standardization is the process of developing and implementing a technical specification, called a standard. By using standardization, wireless sensor nodes can easily communicate through a set of primitives which allows for interoperability among different nodes that operate within the same standard. Table 4.5 presents the range of variation for the criterion that is related with the standard.

Table 4.5: Range of values for the standard criterion.

Standard/Alliance	Value
ZigBee®	4
IEEE 802.15.4	3
Average	2

B. Topology

Depending on the application requirements different topologies can be considered. The choice of the topology depends on the number of wireless sensor nodes being used, cost and the requirements in terms of QoS. Table 4.6 presents the range of variation for the criterion related to the topology.

Table 4.6: Range of values for the topology criterion.

Topology	Value
Mesh	3
Star	2
Linear	1

C. Number of nodes

This refers to the maximum number of nodes allowed to be added to the network. Depending on the hardware constraints of each wireless sensor node, the network can support a higher or a lower number of devices. The number of wireless sensor nodes required is application-dependent. Table 4.7 presents the range of variation for the criterion related to the number of nodes.

Table 4.7: Range of values for the number of nodes criterion.

Number of nodes	Value
$\geqslant$ 65533	3
$<$ 65533	2

D. Price per node

Since WSNs may contain hundreds or thousands of sensor devices, the price of each node is important. Table 4.8 presents the range of variation for the criterion related to the unitary price per node.

Table 4.8: Range of values for the unitary price per node criterion.

Unitary price per node	Value
$<$ 10 €	4
[10, 50] €	3
]50, 150] €	2
$>$ 150 €	1

E. Programm flash memory

The wireless sensor node MCU includes a program flash memory being used primarily for the storage of the programm and read-only constants. In most of the applications the flash memory is used to log the sensor readings for later analysis. Table 4.9 presents the range of variation for the criterion related to the available program flash memory.

Table 4.9: Range of values for the available program flash memory criterion.

Memory size	Value
]8, 64] MB	4
]0.512, 8] MB	3
]128, 512] kB	2
[16, 128] kB	1

F. Random access memory

The wireless sensor node Microcontroller Unit(MCU) is equipped with a RAM that is a very constrained resource (i.e., nodes typically only have a few kilobytes). This memory can be accessed in a few processor cycles, whereas the programm flash memory takes several milliseconds to read or write. Table 4.10 presents the range of variation for the criterion related to the available RAM.

Table 4.10: Range of values for the available RAM criterion.

Memory size	Value
> 256 kB	4
]64, 256] kB	3
]10, 64] kB	2
[1, 10] kB	1

G. Data rate

The data rate can be defined as the average number of bits transferred among the wireless sensor nodes per second. Higher data rates allow to transfer the same amount of information quicker.

Table 4.11 presents the range of variation for the criterion related to the data rate in kb/s.

Table 4.11: Range of values for data rate criterion.

Data rate	Value
> 250 kB	3
[20, 250] kb/s	2
< 20 kb/s	1

4.3.3 Power requirements

A. Lifetime

The very low energy consumption is a mandatory characteristic of WSNs because there are strong limitations to power supply the WSN devices. Furthermore, since WSNs are battery operated, one of the most important issues is the energy conservation and the possibility of using rechargeable batteries as a secondary power source. Therefore, in order to choose the best WSN platform, the power consumption of the whole systems must be taken into account. To determine lifetime of the WSNs nodes we have considered the energy consumption model for lifetime evaluation presented in Appendix C. This model accounts both the energy consumption of the radio transceiver and the MCU. The Peukert's Law [RaVr01], has been considered, enabling to define the non-linear relationship between the battery lifetime and the discharge rate without modelling the recovery effect. Table 4.12 presents the range of variation for the criterion related to the lifetime in days by considering a duty cycle of 1 %.

Table 4.12: Range of values for the lifetime criterion.

Lifetime	Value
> 3 years	4
[2 - 3] years	3
[1 - 2[years	2
< 1 year	1

B. Indoor distance range

The indoor distance range defines the maximum distance required between wireless sensor nodes to work properly inside a building. Table 4.13 presents the range of variation for the criterion related to the indoor distance range in meters.

Table 4.13: Range of values for the indoor distance range criterion.

Range (indoor)	Value
> 150 m	4
[60 - 150] m	3
[40 - 60[m	2
< 40 m	1

C. Outdoor distance range

The outdoor distance range defines the maximum long range at acceptable error rates by considering Line-of-Sight (LoS) between the sender and receiver. Table 4.14 presents the range of variation for the criterion related to the outdoor distance range in meters.

Table 4.14: Range of values for the outdoor distance range criterion.

Range (outdoor)	Value
> 250 m	4
[150 - 250] m	3
[70 - 150[m	2
< 70 m	1

4.3.4 Expansibility, programming and community resources

A. Expansibility

The expansibility refers to the existence of sensors and sensor boards well developed that can be easily added to the wireless sensor nodes. Table 4.15 presents the range of variation for the criterion related to the expansibility.

Table 4.15: Range of values for the expansibility criterion.

Expansibility	Value
Well developed sensors and sensor boards that can be easily added	3
There are only a few sensors and sensor boards	2
There are only on-board sensors	1

B. Object oriented programming

The object oriented programming defines the use or not of an object-oriented language, enabling to write large-scale programs. Table 4.16 presents the range of variation for the criterion related to the objected oriented programming.

Table 4.16: Range of values for the objected oriented programming criterion.

Object oriented programming	Value
Yes	2
No	1

C. Easy to use programm environment

The easy to use programm environment defines the easiness to work with the Integrated Development Environment (IDE) environment. Table 4.17 presents the range of variation for the criterion related to the easy to use programm environment.

Table 4.17: Range of values for the easiness to use programm environment criterion.

Easiness of use	Value
Yes	2
No	1

D. Community support

The community support refers to the different sources of information that are available for each individual WSN platform, for example, the manufacturer web site, research projects or forums. Table 4.18 presents the range of variation for the criterion related to the community support.

Table 4.18: Range of values for the community support criterion.

Community support	Value
Enough information, easy to find and get access. Researchers work with the modules. There are forums where people can comment and resolve their research issues.	2
The information is not easy to find and access, but there are some forums related with the module	1

E. Documentation

The documentation refers to the quality of the datasheets and how well the information is organized. Table 4.19 presents the range of variation for the criterion related to the documentation.

Table 4.19: Range of values for the documentation criterion.

Documentation	Value
Documentation is clear and organized, there is enough information to work with the WSN platforms with "no problems" and there are enough examples.	2
Documentation is neither clear, nor complete and there are not enough examples.	1

Next, we present all the WSN platforms and a comparison is made based on the evaluation criteria previously defined for each different group. It is worthwhile to mention that, in the Tables present bellow, the gray rows represent the value given for each criterion.

Comparison of the main platforms

In order to have an overview from the WSN platforms that considers the criteria previously defined, next we present all the groups and the sum of all scores added to a given platform. Figure 4.4 presents the sum of the evaluation criteria related with the main characteristics group.Therefore, we conclude that Lotus and Sun SPOT platforms are the ones that achieve the best performance in terms of **main characteristics**, whereas the eZ430-RF2500 platform is the one that presents the worst results.

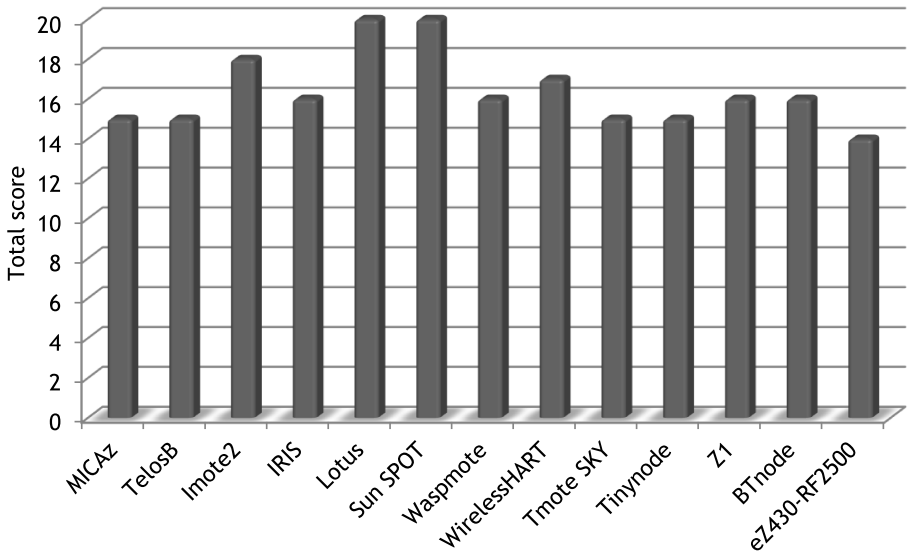

Figure 4.4: Main characteristics of the WSN platforms.

Table 4.20: Main Characteristics of the WSN Platforms.

Criterion		MICAz	TelosB	Imote2	IRIS	Lotus
Standard		IEEE 802.15.4	IEEE 802.15.4	IEEE 802.15.4 / ZigBee® compliant	IEEE 802.15.4 / ZigBee® / 6LoWPAN compliant	IEEE 802.15.4 / ZigBee® compliant
		3	3	4	4	4
Topology		Star Mesh	Star Mesh	Star Mesh	Star Mesh	Star Mesh
		3	3	3	3	3
Number of nodes		65,533	65,533	65,533	65,533	65,533
		3	3	3	3	3
Price		90	87	280	92	92
		2	2	1	2	2
MCU	Chip	Atmega 128L	TI MSP430	Intel PXA271	Atmega 1281	ARM® Cortex-M3
	Type	8 MHz, 8 bit	8 MHz, 16 bit	13-416 MHz, 16 bit	8 MHz, 8 bit	100 MHz, 32 bit
	Program flash memory	128 kB	48 kB	256 kB (SRAM) 32 MB (SDRAM)	128 kB	512 kB (Flash) 64 Mb (Serial Flash)
		1	1	3	1	4
	RAM (kB)	4	10	256	8	64
		1	1	3	1	2
Power source	Type	2 AA batteries	2 AA batteries	3 AAA batteries	2 AA batteries	2 AA type batteries
	Capacity (mAh)	2850	2850	500	2850	2850
RF transceiver	Chip	CC2420			AT86RF230	LPR2400
	Frequency band (GHz)	2.4				
	Data rate (kb/s)	250	250	250	250	250
		2	2	2	2	2
Total		15	15	18	16	20

Table 4.21: Main Characteristics of the WSN Platforms (cont.).

Criterion		Sun SPOT	Waspmote	WirelessHART	Tmote SKY	Tinynode
Standard		IEEE 802.15.4 / ZigBee® compliant	IEEE 802.15.4 / ZigBee® compliant	IEEE 802.15.4 / ZigBee® compliant	IEEE 802.15.4	IEEE 802.15.4
		4	4	4	3	3
Topology		Star Mesh	Star Mesh	Star Mesh	Star Mesh	Star Mesh
		3	3	3	3	3
Number of nodes		65,533	65,533	65,533	65,533	65,533
		3	3	3	3	3
Price per node		318 €	130 €	-	77 €	109 €
		1	2	-	2	2
MCU	Chip	AT91RM9200	ATmega1281	ARM® Cortex-M3	TI MSP430	TI MSP430
	Type	180 MHz, 32 bit	8/14.7 MHz, 8 bit	100 MHz, 32 bit	8MHz, 16 bit	8 MHz, 16 bit
	Program flash memory	8 MB	128 kB	512 kB	48 kB	48 kB
		3	1	2	1	1
	RAM (kB)	1024	8	72	10	10
		4	1	3	1	1
Power source	Type	2 AA batteries	2 AA batteries	2 AA batteries	2 AA batteries	2/3 AA type batteries
	Capacity (mAh)	3000	13000/6600	3000	3000	3000
RF transceiver	Chip	CC2420	Xbee-802.15.4	M2510 RF	CC2420	Semtech XE 1205
	Frequency band (GHz)	2.4				0.868/0.915
	Data rate (kb/s)	250	250	250	250	250
		2	2	2	2	2
Total		20	16	17	15	15

Table 4.22: Main Characteristics of the WSN Platforms (cont.).

Criterion		Z1	BTnode	eZ430-RF2500
Standard		IEEE 802.15.4 / ZigBee® / 6LoWPAN	IEEE 802.15.4	-
		4	3	-
Topology		Mesh Star	Star Mesh	Star Mesh
		3	3	3
Number of nodes		65,533	65,533	65,533
		3	3	3
Price per node		100 €	81 €	42 €
		2	2	3
MCU	Chip	MSP430F2617	ATmega 128L	MSP430F2274
	Type	8 MHz, 16 bit	8 MHz, 8 bit	16 MHz, 16 bit
	Program flash memory	92 kB	128 kB	16 kB+ 256B
		1	1	1
	RAM (kB)	8	64+180	1
		1	3	1
Power source	Type	2 AA batteries	2 AA batteries	2AAA batteries
	Capacity (mAh)	3000	3000	1200
RF transceiver	Chip	CC2520	CC1000	CC2500
	Frequency band (GHz)	2.4	430-915MHz	2.4
	Data rate (kb/s)	250	9.6	(250/500)
		2	1	3
Total		16	16	14

Table 4.23: Power Requirements

Criterion	MICAz	TelosB	Imote2	IRIS	Lotus
Transmited power (dBm)	0, -1, -3, -5, -7, -10, -15, -25	0, -1, -3, -5, -7, -10, -15, -25	0, -1, -3, -5, -7, -10,	3, 1, -3, -17	0, -1, -3, -5, -7, -10, - 15, -25
RF transceiver	(@ 3 V & 0 dBm) TX: 17.4 mA RX/Idle: 19.7 mA Sleep: 1 μA	(@ 3 V & 0 dBm) TX: 17.4 mA RX/Idle: 23 mA Sleep: 1 μA	(@ 4.5 V & @13 MHz & 0 dBm) TX: 17.4 mA RX/Idle: 19.4 mA Sleep: 1 μA	(@ 3 V & 3 dBm) TX: 17 mA RX/Idle: 16 mA Sleep: 0.02 μA	(@ 3 V & 3 dBm) TX: 17 mA RX/Idle: 16 mA Sleep: 0.02 μA
Processor (CPU)	Active: 5 mA Sleep: 15 μA	Active: 1.8 mA Sleep: 4.1 μA	Active: 31 mA Sleep: 390 μA	Active: 8 mA Sleep: 8 μA	Active: 50 mA Sleep: 10 μA
Lifetime (years)	1.21	1.36	0.16	1.21	0.43
	2	2	1	2	1
Receiver sensitivity (dBm)	-94	-94	-94	-101	-101
Indoor distance range	20-30 m indoor	20-30 m indoor	20-30 m indoor	>50 m indoor	>50 m indoor
	1	1	1	2	2
Outdoor distance range	75-100 m outdoor	75-100 m outdoor	75-100 m outdoor	>300 m outdoor	>300 m outdoor
	2	2	2	4	4
Supply voltage (V)	3	3	4.5	3	3
Total	5	5	4	8	7

Table 4.24: Power Requirements (cont.).

Criterion	Sun SPOT	Waspmote	WirelessHART	Tmote SKY	Tinynode
Transmited power (dBm)	0, -1, -3, -5, -7, -10, -15, -25	0, -2, -4, -6, -10,	0, 8	0, -1, -3, -5, -7, -10, -15, -25	0, +5, +25
RF transceiver	(@ 3.7 V & 0 dBm) TX: 18 mA RX/Idle: 20 mA Sleep: 1 μA	(@ 3 V & 0 dBm) TX: 15 mA RX/Idle: 15 mA Sleep: 0.06 μA	(@ 3 V & 0 dBm) TX: 4.4 mA RX/Idle: 4.5 mA Sleep: 1.2 μA	(@ 3 V & 0 dBm) TX: 17.7 mA RX/Idle: 20 mA Sleep: 1 μA	(@ 3 V & 0 dBm) TX: 24.9 mA RX/Idle: 14.9 mA Sleep: 1 μA
Processor (CPU)	Active: 25 mA Sleep: 33 μA	Active: 8 mA Sleep: 8 μA	Active: 2.4 mA Sleep: 1.2 μA	Active: 1.8 mA Sleep: 4.1 μA	Active: 2.1 mA Sleep: 6.5 μA
Lifetime (years)	0.124	3.4	4.6	1.45	1.36
	1	4	4	2	2
Receiver sensitivity (dBm)	-90	-92	-95	-94	-101
Indoor distance range	20-30 m indoor	100 m indoor	100 m indoor	50 m indoor	40 m indoor
	1	3	3	2	2
Outdoor distance range	75-100 m outdoor	500 m outdoor	300 m outdoor	>125 m outdoor	200 m outdoor
	2	4	4	2	3
Supply voltage (V)	3.7	3	3	3	3
Total	4	11	11	6	7

Table 4.25: Power Requirements (cont.).

Criterion	Z1	BTnode	eZ430-RF2500
Transmited Power (dBm)	0, -1, -3, -5, -7, -10, - 15, -25	10, 5, 0, -5, -20,	1, 0, -6, -12
RF transceiver	(@ 3 V & 0 dBm) TX: 17.4 mA RX/Idle: 20 mA Sleep: 1 μA	(@ 3 V & 0 dBm) TX: 34.1 mA RX/Idle: 34.1 mA Sleep: 3.3 mA	(@3 V & 0 dBm) TX: 21.2 mA RX/Idle: 18.8 mA Sleep: 0.4 μA
Processor (CPU)	Active: 10 mA Sleep: 0.1 μA	Active: 1.8 mA Sleep: 4.1 μA	Active: 2.7 mA Sleep: 0.9 μA
Lifetime (years)	1.05	0.074	0.647
	2	1	1
Receiver sensitivity (dBm)	-94	-94	-87
Indoor distance range	20-30 m indoor	20-30 m indoor	>50 m indoor
	1	1	2
Outdoor distance range	75-100 m outdoor	75-100 m outdoor	>50 m outdoor
	2	2	1
Supply voltage (V)	3V	3V	3V
Total	5	4	4

Table 4.26: Expansibility, Programming and Community Resources.

Criterion		MICAz	TelosB	Imote2	IRIS	Lotus
Expansibility		**Sensor Boards** **MTS101:** Light and temperature sensors, and prototyping area. **MTS300:** MTS101 sensors+microphone and buzzer. **MTS400**: Ambient light, relative humidity and temperature sensors, 2-axis accelerometer and barometric pressure. **Others: MTS 310/400** **Others: MDA 100/300**	**Features** On-board sensors: infrared light, humidity and temperature. **Sensor Boards** **SBT80:** Infrared, acoustic, temperature, dual-axis magnetometer and dual-axis accelerometer sensors.	**Sensor Boards** ITS400CA: Light, humidity and temperature sensors and on-board 3-Axis accelerometer.	**Sensor Boards** **MTS101:** Light and temperature sensors, and prototyping area. **MTS300:** MTS101 sensors+microphone and buzzer. **MTS400**: Ambient light, relative humidity and temperature sensors, 2-axis accelerometer and barometric pressure. **Others: MTS 310/400** **Others: MDA 100/300**	**Sensor Boards** **MTS101:** Light and temperature sensors, and prototyping area. **MTS300:** MTS101 sensors+microphone and buzzer. **MTS400**: Ambient light, relative humidity and temperature sensors, 2-axis accelerometer and barometric pressure. **Others: MTS 310/400** **Others: MDA 100/300**
		3	3	3	3	3
Language capabilities	Object oriented programming	No (nesC)	No (nesC)	No (c# micro framework)	No (nesC)	No (nesC)
		1	1	1	1	1
	Easy to use program environment	No	No	No	No	No
		1	1	1	1	1
Programming	Community support	Enough information	Enough information	Enough information	Enough information	Enough information
		2	2	2	2	2
	Documentation	Clear and organized	Clear and organized	Clear and organized	Clear and organized	Clear and organized
		2	2	2	2	2
Total		9	9	9	9	9

Table 4.27: Expansibility, Programming and Community Resources (cont.)

Criterion		Sun SPOT	Waspmote	WirelessHART	Tmote SKY	Tinynode
Expansibility		**Sensor Boards** Accelerometer, temperature and light sensors.	**Sensor Boards** **EVENTS:** Pressure, bend, vibration, impact, hall effect, tilt, temperature, liquid presence, liquid level, luminosity, presence and stretch sensors. **Others: GASES**, **SMART CITIES**, **SMART PARKING**, **RADIATION**, **SMART METERING**, **AGRICULTURE, VIDEO.** Prototyping Area. >60 Sensor+Libraries.	**Features** **On-board:** temperature sensor.	**Features** **On-board:** temperature, humidity, radiation, light sensors. Prototyping Area.	**Features** **On-board:** temperature, sensors. Prototyping Area. Extension Board.
		2	3	1	2	2
Language capabilities	**Object oriented programming**	Yes (Java)	Yes (C/C++)	-	No (nesC)	No (nesC)
		2	2	-	1	1
	Easy to use program environment	Yes	Yes	-	No	No
		2	2	-	1	1
Programming	**Community support**	Enough information	Enough information	Not enough information	Enough information	Enough information
		2	2	1	2	2
	Documentation	Clear and organized	Clear and organized	Unclear and organized	Clear and organized	Clear and organized
		2	2	2	2	2
Total		10	11	4	8	8

Table 4.28: Expansibility, Programming and Community Resources (cont.)

Criterion		Z1	Btnode	eZ430-RF2500
Expansibility		**Features** On-board sensors: Temperature, accelerometer. 52-pin expansion.	**Features** Generic sensor board for extensions. FPGA extension board.	**Features** On-board sensors: Temperature.
		2	2	2
Language capabilities	Object oriented Programming	No (nesC)	No (nesC)	No (C)
		1	1	1
	Easy to use program environment	No	No	No
		1	1	1
Programming	Community support	Not enough information	Not enough information	Enough information
		1	1	2
	Documentation	Clear and organized	Not clear and organized	Clear and organized
		2	1	2
Total		7	6	8

Figure 4.5 presents the sum of the evaluation criteria related with the **power requirements** group. Hence, we conclude that Waspmote and WirelessHART platforms are the ones that have the best performance in terms of power requirements and the Sun SPOT platform is the one that presents the worst results.

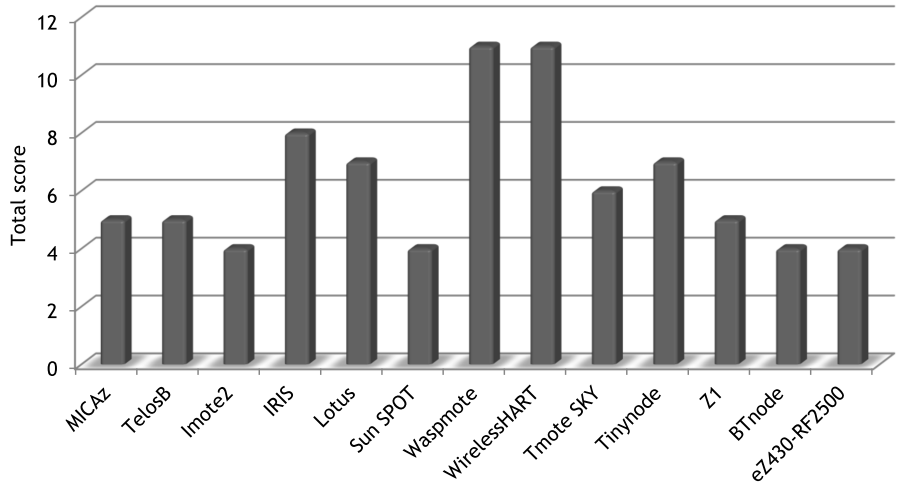

Figure 4.5: Sum of the criteria related to the power requirements of the WSN platforms.

Figure 4.6 presents the sum of the evaluation criteria related with the expansibility, programming and community resources group. Thus, we conclude that Waspmote and Sun SPOT platforms are the ones that have the best performance in terms of expansibility, programming and community resources requirements. The WirelessHART platform is the one that presents the worst results.

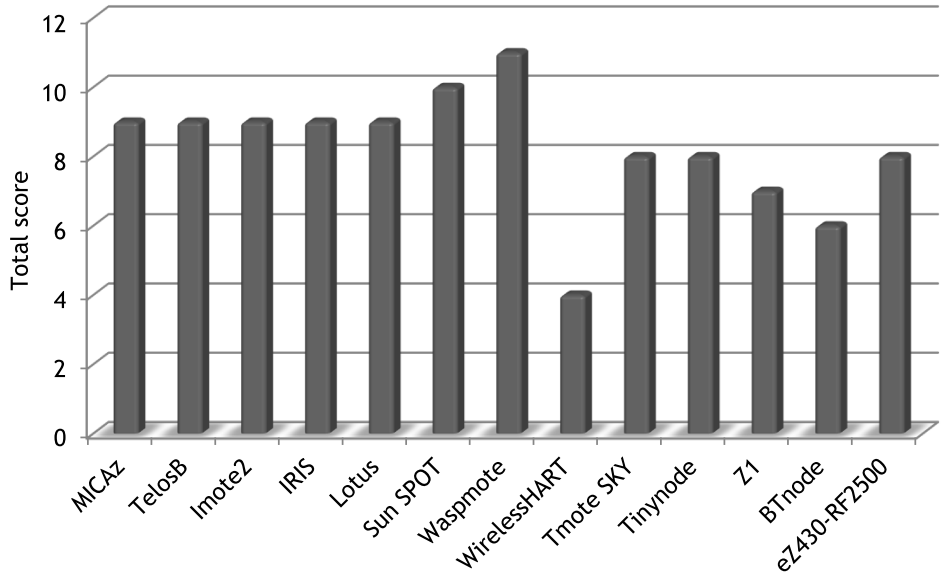

Figure 4.6: Sum of the criteria related to expansibility, programming and community resources of the WSN platforms.

Figure 4.7 and Table 4.29 present the total performance sum of the evaluation criteria metrics related with the overall performance for each platform, based on the impact of each group presented in Table 4.4. Therefore, we conclude that the Waspmote platforms are the one that have the best performance in terms of the overall performance based on the criteria previously

defined, while the BTnode and eZ430-RF2500 are the platforms whose results are the worst.

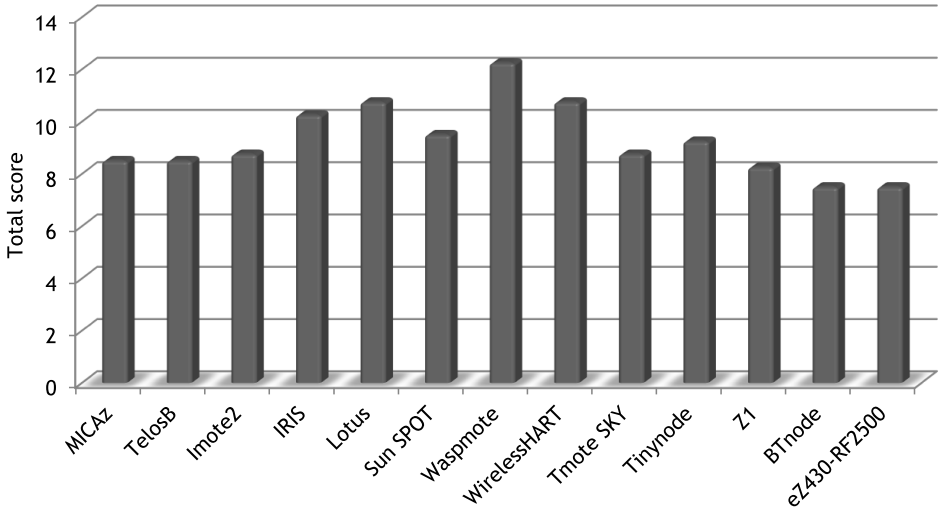

Figure 4.7: Overall performance of the WSN platforms.

Table 4.29: Overall performance

Mote	Main Characteristics	Power Requirements	Expansibility, Programming and Community Resources	Overall Performance
MICAz	15	5	9	8.5
TelosB	15	5	9	8.5
Imote2	18	4	9	8.75
IRIS	16	8	9	10.25
Lotus	20	7	9	10.75
Sun SPOT	20	4	10	9.5
Waspmote	16	11	11	12.25
WirelessHART	17	11	4	10.75
Tmote SKY	15	6	8	8.75
Tinynode	15	7	8	9.25
Z1	16	5	7	8.25
BTnode	16	4	6	7.5
eZ430-RF2500	14	4	8	7.5

4.4 Concluding remarks

In this Chapter, we have evaluated different parameters related with WSN platforms. These parameters were addressed by taking into account three different groups of criteria: i) main characteristics, ii) power requirements and iii) expansibility, programming and community resources. By analysing each criterion separately, we conclude that, in terms of main characteristics the Lotus and Sun SPOT platforms are the ones that present the best performance, whilst the eZ430-RF2500 platform is the one that presents the lower performance. Moreover, by analysing the main characteristic in respect to the radio transceiver being used, we also conclude that almost half of the evaluated WSNs platforms consider the CC2420 radio transceiver (MICAz, TelosB, Imote2, SunSPOT, Tmote SKY). This in turn, dictates the popularity of this radio transceiver among researchers, being used in several simulation frameworks for WSNs

(e.g. MiXiM) allowing for estimate the power consumption of the nodes based on is characteristics (e.g., switching delay times and energy spent in the TX, RX and SLEEP states). In terms of power requirements, the Waspmote and WirelessHART platforms are the ones that have the best energy performance, while Sun SPOT platform presents the worst energy performance. In terms of expansibility, programming and community resources, the Waspmote and Sun SPOT platforms are the ones that present the best results, whereas the WirelessHART is the one with the lowest performance.

Since we have previously defined that the power requirements group is the one that has higher impact in the overall performance, and the Waspmote is the WSN platform that globally is ranked as the one that presents the best performance, we conclude that, currently, in general, the best platform is the Waspmote. It is worthwhile to mention that, since some criteria are more important than others, choosing the best platform for WSNs depends on the criteria taken into account, as well as the applications requirements.

Chapter 5

MAC Sub-layer Protocols Employing RTS/CTS with Packet Concatenation

5.1 Introduction

Packet concatenation facilitates the aggregation of several consecutive packets by means of channel reservation and different types of acknowledgment and/or Network Allocation Vector (NAV) procedures. In this context, the RTS/CTS mechanism enables to reserve the channel and avoids to repeat the backoff phase for every consecutive transmitted packet, probably reducing overhead. In the presence of RTS/CTS two solutions are considered, one with DATA/ACK handshake and other with no ACKs, simply relying in the establishment of the NAV.
In particular, the Sensor Block Acknowledgment MAC (SBACK-MAC) protocol allows the aggregation of several acknowledgment responses into one special packet *BACK Response* being compliant with the IEEE 802.15.4 standard. Two different solutions are addressed. The first one considers the SBACK-MAC protocol in the presence of *BACK Request* (concatenation mechanism), while the second one considers SBACK-MAC in the absence of *BACK Request* (the so-called piggyback mechanism).
Therefore, we reduce the overhead, which is one of the fundamental problems of MAC inefficiency. The proposed protocol uses detailed information from the PHY (collision detection, data frame synchronization, CCA and state of the radio transceiver) and data link layers (carrier sense control, radio duty cycle control, use of fragmentation and retransmissions).The throughput and delay performance is mathematically derived under ideal conditions (a channel environment with no transmission errors) and non ideal conditions (presence of interference). The SBACK-MAC will also be evaluated in terms of bandwidth efficiency and energy consumption, and the proposed schemes are compared against IEEE 802.15.4 with and with no RTS/CTS by means of extensive simulations by employing the OMNeT++ simulator.

5.2 Motivation

The design of WSNs MAC protocols envisages satisfying application-specific QoS requirements, whilst maximizing the network lifetime. Considerable energy savings can be achieved by placing nodes into the sleep state during the periods when they are not receiving or transmitting. These nodes opportunistically enter into the sleep mode after successfully receiving RTS/CTS control packet reservation messages. In WSNs, the use of ACK packets introduces overhead. Since the length of these packets may be similar to the one of the data packets, they will increase the collision probability inside a given cluster. Moreover, nodes are battery operated; therefore the transmission of such packets also leads to energy decrease whilst reducing the number of data packets transmitted containing useful information. Based on Sensor-MAC (S-MAC) [YeHD04], an innovative MAC protocol that uses a BACK mechanism is proposed, i.e., the SBACK-MAC protocol. The main difference from SBACK-MAC relatively to S-MAC is the way it treats ACK control packets and the fact of being totally compliant with IEEE 802.15.4, e.g., in terms of

interframe spacing. By using a BACK mechanism we improve channel efficiency by aggregating several ACK frames into one special ACK frame (*BACK Response*). This way, energy consumption may be significantly reduced when a series of data messages needs to be transmitted, because it is not necessary to transmit and receive several ACK control packets (one for each data packet) which would lead to an extra energy waste while increasing the delay and decreasing the throughput as well as bandwidth efficiency. Moreover, these extra control signalling packets are considered to be overhead and do not directly result in the communication of information. Likewise other MAC protocols [WLAN05, WPAN11, KhAli11], SBACK-MAC is a contention-based MAC protocol that considers a duty cycle scheme in order to reduce the energy consumption. It considers the IEEE 802.15.4 nonbeacon-enabled mode and uses unslotted carrier sense multiple access with CSMA-CA for transmitting frames. When nodes have data to send, they will contend for the wireless channel, whereas if a collision occurs, or the medium is found to be busy, nodes will perform backoff for a random duration of time before attempting again to access the channel later on.

5.3 Design considerations for IEEE 802.15.4 nonbeacon-enabled mode with Packet Concatenation

The IEEE 802.15.4 standard has been widely accepted as the *de facto* standard for WSNs, enabling to provide ultra-low complexity, cost and power for low-data rate wireless connectivity for wireless sensors. Due to its low power, it has been used as a basis for ZigBee®, WirelessHart and MiWi applications. Moreover, it represents a significant breakthrough from the "bigger and faster" standards that the IEEE 802 organization continues to develop and improve: instead of higher data rates and more functionality, this standard addresses the simple and low-data universe, in terms of control and sensor networks, which existed without global standardization through a series of proprietary methods and protocols. The IEEE 802.15.4 standard can operate in the beacon-enabled and nonbeacon-enabled modes, which is presented in more detail in Appendix A. In this thesis, we assume that the IEEE 802.15.4 nonbeacon-enabled CSMA-CA algorithm for the basic access mode is employed by the SBACK-MAC protocol. Next we address the design considerations of the PHY and MAC layer aspects for IEEE 802.15.4 and SBACK-MAC.

5.3.1 PHY Layer

The PHY layer is responsible for providing status information for the MAC layer, switch between different radio states (i.e., RX, TX and SLEEP), send/receive/listen packets to/from channel, provide hooks for statistical information and configurable settings. The information can be passively (e.g., current channel state) or actively provided to the MAC layer (e.g., packet transmission complete) based on events. Some information must be provided on demand, as follows:

- Channel state (busy/idle) and Received Signal Strength Indicator (RSSI);
- Current radio state (e.g., RX, TX and SLEEP);
- Control information (e.g., transmission over and send).

Figure 5.1 presents the state transition diagram for switching between the different radio states. The time for switching mainly depends of the IEEE 802.15.4 compliant transceivers.

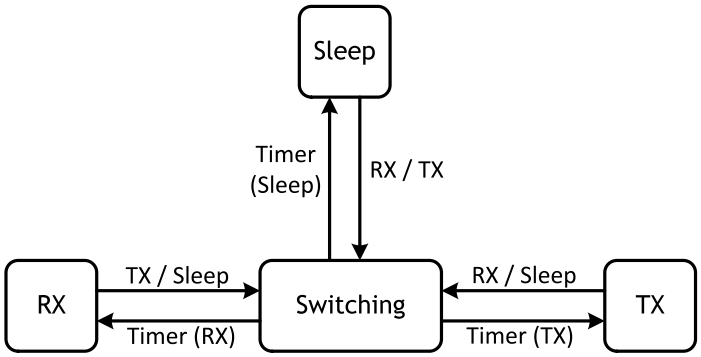

Figure 5.1: State transition diagram for the switching between different radio states.

In order to maintain a simple interface, both MAC and PHY layers share a common packet structure, as presented in Figure 5.2. This type of packet is known as the PHY Protocol Data Unit (PPDU), being responsible for the encapsulation of all data structures from the higher layers of the protocol. The packet is divided into three basic components: Synchronisation Header (SHR), PHY Header (PHR) and variable length payload, which contains the PHY Service Data Unit (PSDU) as follows:

- The SHR consists basically of two fields, a preamble sequence and a start of frame delimiter. The preamble field has a length of 4 bytes, allowing for achieving chip and bit synchronisation. The Start of Frame Delimiter (SFD) has a length of 1 byte and allows a receiver to set up the beginning of a packet;
- The PHR field has a length of 1 byte, where the Most Significant Bit (MSB) is reserved and the other 7 bits are used to specify the frame length information, enabling to have packets with a total length of 127 bytes;
- The PHY payload contains one field called PSDU that carries the data payload from the PPDU.

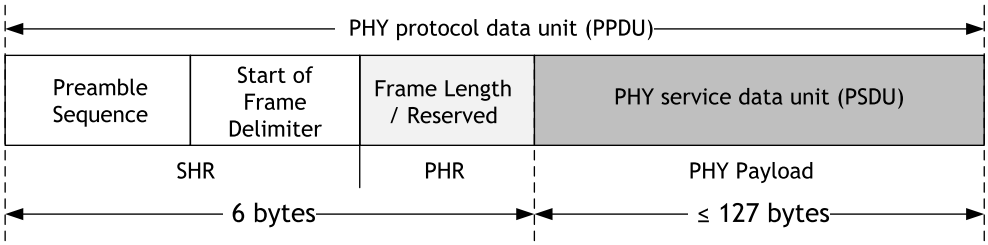

Figure 5.2: IEEE 802.15.4 PHY protocol data unit.

The IEEE 802.15.4 [WPAN11] PHY layer, (implemented in the OMNeT++ Network Simulation Framework [OMNe13]) operates in the 2.4 GHz band and considers an O-QPSK modulation, offering extremely low BER performance, in the presence of a low SNR. The O-QPSK modulation is presented in detail in Appendix B.
The BER is addressed by considering an interference signal similar to Additive White Gaussian Noise (AWGN). The radio transceivers operating in the 2.4 GHz band employ a DSSS spreading technique. As a consequence, the transmitter signal takes up more bandwidth than required to transmit the information signal being modulated. The name "spread spectrum" derives from the fact that the carrier signals occur over the full bandwidth (spectrum) of the

sensor nodes transmitting frequency band. The modulation and spreading technique uses a 16-ary quasi-orthogonal modulation, where four information bits are used to select one of 16 nearly orthogonal Pseudo-Random Noise (PN) sequences to be transmitted. Therefore, we use a power-efficient modulation method that achieves low SNR and Signal-to-Interference Ratio (SIR) requirements.

The O-QPSK modulation uses a chip rate, R_c, of 2 Mchip/s and a bit rate, R_b, of 250 kb/s, by using a codebook of M = 16 symbols. The conversion from SNR to the noise density, (E_b/N_0) assumes a matched filtering and a half-sine pulse shaping, as shown in Equation 5.1:

$$\frac{E_b}{N_0} = \frac{0.625 \cdot R_c}{R_b} SNR = \frac{0.625 \times 2000000}{250000} SNR = 5 \cdot SNR \tag{5.1}$$

Equation (5.2) presents the conversion of these ratios from bit noise density, E_b/N_0, to symbol noise density, E_s/N_0:

$$\frac{E_s}{N_0} = log_2(M) \frac{E_b}{N_0} = 4 \cdot \frac{E_b}{N_0} \tag{5.2}$$

As shown in [Skla98], the probability of Symbol Error Rate (SER), P_s, is computed by using the following equation:

$$P_s = \frac{1}{M} \sum_{j=2}^{M} (-1)^j \binom{M}{j} e^{\left(\frac{E_s}{N_0}\left(\frac{1}{j}-1\right)\right)} \tag{5.3}$$

Finally, for an M-ary orthogonal signal, the conversion from P_s to the probability of bit error, P_b, is given by:

$$P_b = P_s \left(\frac{M/2}{M-1}\right) = P_s \left(\frac{8}{15}\right) \tag{5.4}$$

By combining Equations (5.1) to (5.4), one obtains the BER function:

$$BER = \left(\frac{8}{15}\right) \left(\frac{1}{16}\right) \sum_{j=2}^{M} (-1)^j \binom{M}{j} e^{\left(\frac{E_s}{N_0}\left(\frac{1}{j}-1\right)\right)} \tag{5.5}$$

Since the modulation and spreading technique consists of using a 16-ary quasi-orthogonal modulation technique, one obtains the following equation for BER.

$$BER = \left(\frac{8}{15}\right) \left(\frac{1}{16}\right) \sum_{j=2}^{M} (-1)^j \binom{16}{j} e^{\left(20 \cdot SNR\left(\frac{1}{j}-1\right)\right)} \tag{5.6}$$

Figure 5.3 presents the BER as a function of the SNR for both SBACK-MAC and IEEE 802.15.4 (by considering the 2.4 GHz band). The Signal-to-Interference-plus-Noise Ratio (SNIR) values correspond to the BER lower bound, and are lower than 1×10^{-8}. In our simulator, this value is used as a parameter for the network.

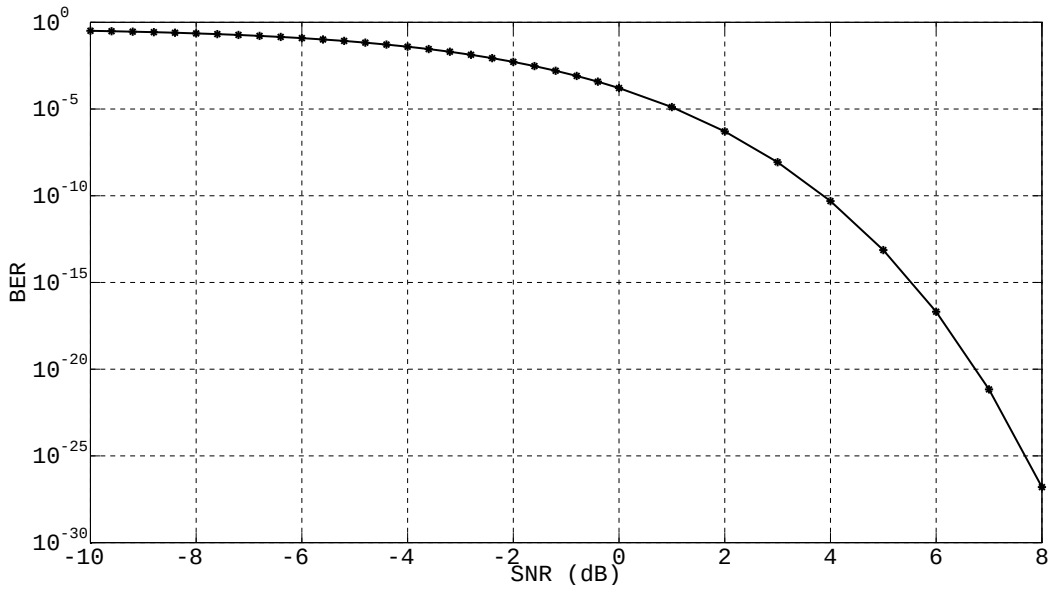

Figure 5.3: BER as a function of the SNR for IEEE 802.15.4 and SBACK-MAC.

The Packet Success Rate (PSR), is defined in [KaWi05] as the probability that the frame has no errors, and is given by:

$$PSR = (1 - BER)^{(nBits-1)} \tag{5.7}$$

where $nBits$ is the length of the frame, in bits.
The Packet Error Rate (PER) for a given packet is given by:

$$PER = (1 - PSR) \tag{5.8}$$

Figure 5.4 shows the PERs for different SNRs by considering 2 different data packets lengths with data payload of 118 bytes and 18 bytes respectively, and an ACK control packet with length of 11 bytes.

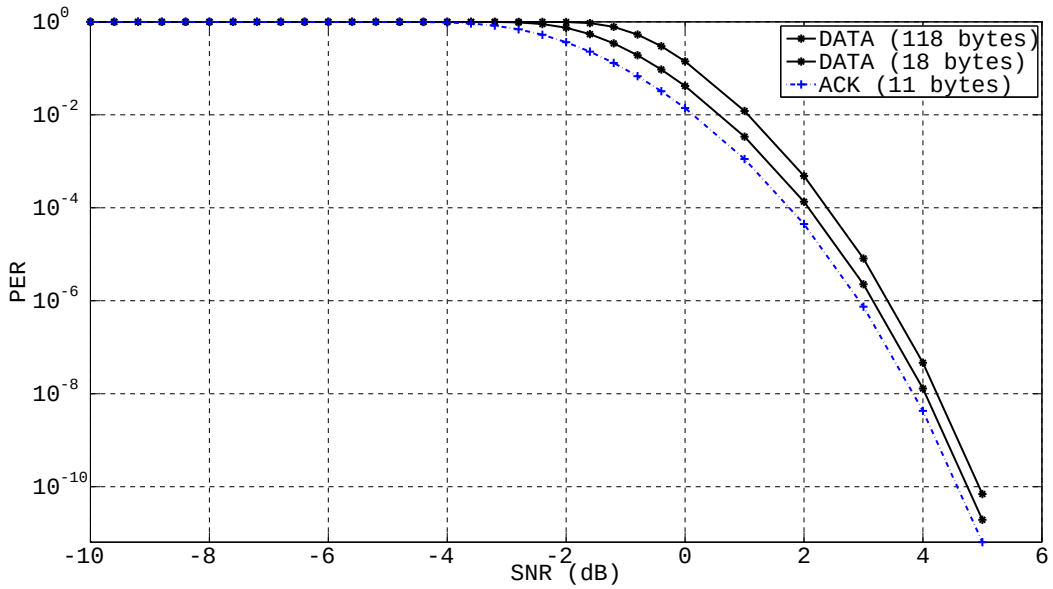

Figure 5.4: BER as a function of the SNR for IEEE 802.15.4 and SBACK-MAC.

By analysing Equation (5.8) and Figure 5.4, one concludes that, by increasing the SNR, the ratio between the received power and noise is increased, so that the PER decreases. Moreover, for longer packet lengths (i.e., for data packets) the PER is higher. In [BVLN14] the authors have proposed a reliability based decider to improve the packet reception rate at the PHY layer which is characterized by metrics like the SNIR, BER, SER, PER, and outage probability, whose implementation in the MiXiM framework of the OMNeT++ simulator is considered here.

5.3.2 MAC Sub-layer

In the IEEE 802.15.4 [WPAN11] basic access mode, nodes use a nonbeacon-enabled CSMA-CA algorithm for accessing the channel and transmit their packets. The backoff phase (N.B., this time period is not generally called contention window in IEEE 802.15.4) algorithm is implemented by considering basic units of time called backoff periods. The backoff period duration is equal to $T_{BO} = 20 \times T_{symbol}$ (i.e., 0.32 ms), where $T_{symbol} = 16\,\mu$s is the symbol time [WPAN11]. Before performing CCA, a device shall wait for a random number of backoff periods, determined by the backoff exponent (BE). Then, the transmitter randomly selects a backoff time period uniformly distributed in the range $[0, 2^{BE} - 1]$. Therefore, it is worthwhile to mention that even if there is only one transmitter and one receiver, the transmitter will always choose a random backoff time period within $[0, 2^{BE} - 1]$. Initially, each device sets the BE equal to $macMinBE$, before starting a new transmission and increments it, after every failure to access the channel. In this work we assume that the BE will not be incremented since we are assuming ideal conditions.
Table 5.1 summarizes the key parameters for both the IEEE 802.15.4 standard and the SBACK-MAC protocol for the 2.4 GHz band, by considering the DSSS PHY layer with the O-QPSK modulation, which is described in detail in Appendix A.
IEEE 802.15.4 [WPAN11] nodes support a maximum over-the-air data rate of 250 kb/s. However, in practice, the effective data rate is lower due to the protocol timing specifications, [WPAN11]. This can also be explained by the various mechanisms that are employed to ensure robust data transmission, including channel access algorithms, data verification and frame acknowledgement. In this thesis we address unicast data transmissions with ACKs, being the channel access time a dominant factor in the overall performance of the network. The regular procedure of the IEEE 802.15.4 nonbeacon-enabled mode is presented in Figure 5.5. When a device wishes to transfer data, it simply transmits its data frame, using unslotted CSMA-CA, to the coordinator. The coordinator acknowledges the successful reception of the data by transmitting an ACK control packet.

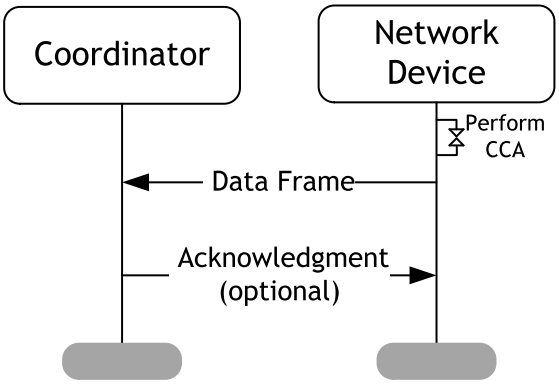

Figure 5.5: IEEE 802.15.4 - Communication to a coordinator in a nonbeacon-enabled PAN.

Table 5.1: Parameters, symbols and values for the IEEE 802.15.4 standard and the proposed MAC sub-layer protocols employing RTS/CTS with packet concatenation for the 2.4 GHz band, by considering the DSSS PHY layer with the O-QPSK modulation.

Description	Symbol	Value
Symbols per octet for the current PHY	$phySymbolsPerOctet$	2 symbols
PHY SHR length	L_{SHR}	10 symbols
RX/TX or TX/RX maximum turnaround length	$aTurnaroundTime$	12 symbols
Backoff period length	$aUnitBackoffPeriod$	20 symbols
Symbol period	T_{symbol}	16 μs
Backoff period duration	T_{BO}	320 μs
PHY SHR duration	T_{SHR}	160 μs
CCA detection time	T_{CCA}	128 μs
Setup radio to RX or TX states [RoAO09]	$rxSetupTime$	1720 μs
Time delay due to CCA	$ccaTime$	1920 μs
TX/RX or RX/TX switching time	T_{TA}	192 μs
PHY length overhead	L_{H_PHY}	6 bytes
MAC overhead	L_{H_MAC}	9 bytes
DATA payload	L_{DATA}	3 bytes
DATA frame length	L_{FL}	18 bytes
ACK frame length	L_{ACK}	11 bytes
Short Interframe Spacing (SIFS) time	T_{SIFS}	192 μs
Long Interframe Spacing (LIFS) time	T_{LIFS}	640 μs
ACK transmission time	T_{ACK}	352 μs
Request-To-Send (RTS) transmission time	T_{RTS}	352 μs
Clear-To-Send (CTS) transmission time	T_{CTS}	352 μs
RTS ADDBA transmission time	T_{RTS_ADDBA}	352 μs
CTS ADDBA transmission time	T_{CTS_ADDBA}	352 μs
BACK Request transmission time	$T_{BRequest}$	352 μs
BACK Response transmission time	$T_{BResponse}$	352 μs
ACK wait duration time	T_{AW}	560 μs
Number of TX frames	n	1 to 112
Data Rate	R	250 kb/s

In this research work, we only consider the nonbeacon-enabled mode. The beacon-enabled mode is not considered because collisions can occur between beacons or between beacons and data or control frames, making a multi-hop beacon-based network difficult to be built and maintained [SuSu10]. Another important attribute is scalability, due to changes in terms of network size, node density and topology. Nodes may die over time. Other nodes may be added later and some may move to different locations. Therefore, for such kind of networks, the nonbeacon-enabled mode seems to be more adapted to the scalability requirement than the beacon-enabled mode. In the former case, all nodes are independent from the PAN coordinator and the communication is completely decentralised.

Moreover, for beacon-enabled networks [WPAN11], there is an additional timing requirement for sending two consecutive frames, so that the ACK frame transmission should be started between the T_{TA} and T_{TA}+T_{BO} time periods (and there is time remaining in the Contention Access Period (CAP), for the message, appropriate interframe space, Interframe Space (IFS) and ACK). Figure 5.6 presents the timing requirements for transmitting a packet and receiving an ACK for the beacon and nonbeacon-enabled modes, respectively.

In IEEE 802.15.4 [WPAN06, WPAN11], the CSMA-CA algorithm is significantly different from the one used in IEEE 802.11e [WLAN05]. The main differences are related to the backoff algorithm. In IEEE 802.11e [WLAN05], the value of the Contention Window (CW) depends on the number

of failed retransmissions for the packet, whereas, in the basic access mode for IEEE 802.15.4, this value (denoted as backoff phase) depends on the backoff exponent (BE), and number of backoffs (NB). Moreover, in IEEE 802.11e, the backoff time counter (BO_c) is decreased as long as the channel is sensed idle and is frozen when a transmission occurs. In the IEEE 802.15.4 basic access mode, nodes do not continuously monitor the channel during the backoff phase and the sensing phase (i.e., CCA) only occurs at the end of the backoff phase.

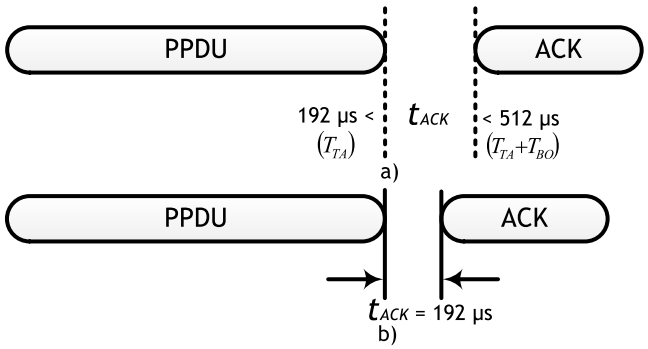

Figure 5.6: IEEE 802.15.4 acknowledgment frame timing: a) beacon and b) nonbeacon-enabled modes.

According to the IEEE 802.15.4 standard [WPAN06], a sensor node that sends a data or a MAC command frame with its ACK Request subfield set to one shall wait for at most an ACK wait duration period, T_{AW}, for the corresponding ACK frame to be received. The T_{AW}, already includes the time for the ACK frame itself. The transmission of an ACK frame in a nonbeacon-enabled PAN or in the Contention Free Period (CFP) shall start $aTurnaroundTime$ symbols (i.e., 192 μs) after the reception of the last symbol of the DATA or MAC command frame ([WPAN06], Section 7.5.6.4.2).
The ACK wait duration period, T_{AW}, is calculated as follows:

$$T_{AW} = T_{Symbol} + T_{TA} + T_{SHR} + [6 \times T_{symbol} \times phySymbolsPerOctet] \quad (5.9)$$

By considering the DSSS PHY layer for the 2.4 GHz band, the maximum ACK wait duration period, T_{AW}, is given by:

$$T_{AW} = 16\,\mu s + 192\,\mu s + 160\,\mu s + 192\,\mu s = 560\,\mu s \quad (5.10)$$

Figure 5.7 presents the ACK timing required for the IEEE 802.15.4 standard, by considering the DSSS PHY layer for the 2.4 GHz band at 250 kb/s. The receivers start transmitting the ACK, 192 μs (i.e., T_{TA}) after the reception of the DATA frame. By assuming a DATA and an ACK frame with 18 and 11 bytes, respectively (including the PHY and MAC overhead), the transmission time is 576 μs and 352 μs, respectively. As reference, Figure 5.7 also includes the ACK wait duration period, T_{AW}.

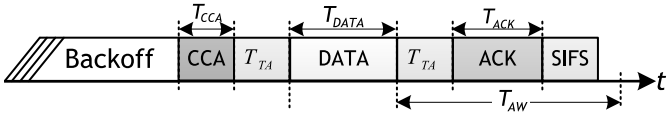

Figure 5.7: Acknowledgement process timing.

For every DATA packet transmitted, there is a random deferral time period, D_T, before trans-

mitting, which is given by:

$$D_T = Initialbackoff Period + ccaTime + T_{TA} \tag{5.11}$$

The initial backoff period, $Initialbackoff Period$, is given as follows:

$$Initialbackoff Period = CW_{NB} = (2^{BE} - 1) \times T_{BO} \tag{5.12}$$

The time delay, due to CCA, is given by:

$$ccaTime = rxSetupTime + T_{CCA} \tag{5.13}$$

The $rxSetupTime$ is the time to setup the radio from a previous state to the transmission or reception states and it mainly depends on the radio transceiver used. During the T_{CCA}, the radio transceiver must determine the channel state within a 8 symbol duration (i.e., 128 μs, which corresponds to one symbol duration of 16 μs). In a normal transmission, for every DATA packet sent an ACK must be received, as shown in Figure 5.8.

Figure 5.8: IEEE 802.15.4 basic access mode.

5.3.3 Analytical model for the maximum throughput and minimum delay

One of the fundamental reasons for the IEEE 802.15.4 standard MAC inefficiency is overhead. In this thesis, we consider the unslotted (nonbeacon-enabled mode) version of the protocol for the 2.4 GHz band. The 2.4 GHz band allows having more channels at the highest data rate. Besides, the unslotted version is the one that has the least overhead as explained in the previous Section (Figure 5.6). The IEEE 802.15.4 sources of overhead are as follows:

- **Interframe Spaces** - For every IEEE 802.15.4 transmission, there is an idle period before accessing the medium. This idle period is called IFS. In IEEE 802.15.4 in the basic access mode for IFS, SIFS is used when MAC Protocol Data Unit (MPDU) (i.e., $F_{H\_MAC} + L_{DATA}$) is less or equal than 18 bytes; otherwise, LIFS is considered. The purpose of IFS is to regulate the data exchange flow and provide priority for certain types of transmissions;

- **Backoff Period** - When IEEE 802.15.4 nodes contend for accessing the wireless medium, they use a backoff algorithm. This process ultimately reduces collisions and allows for achieving QoS prioritization. The random backoff time represents a number of "slots" (i.e., periods of time) when the wireless medium must be idle;

- **PHY and MAC Headers** - In IEEE 802.15.4 in the basic access mode the PPDU must contain the SHR and the PHR fields in order to achieve reliable reception of frames. The MAC header contains information about how to coordinate nodes, and provide a fair mechanism to share the medium access among other nodes, being responsible for how and when it should use the PHY functions for accessing the shared physical medium by the nodes. Although the described headers are necessary, they introduce overhead and are responsible for decreasing the throughput;

- **Acknowledgements** - The lossy and inherently unreliable wireless medium imposes the use of ACK control packets in order to confirm that packets have successfully reached the destination. However, ACK packets are also considered as overhead, since from the point of view of the communication, they do not contain any useful information;

- **Interference** - In a very generic sense, all sources of interference create overhead, since IEEE 802.15.4 nodes must perform a CCA procedure to determine whether the wireless medium is busy or idle;

- **Retransmissions** - When a transmitted frame is not received by the intended node, i.e., there is no ACK response, retransmissions are required. Transmitting a frame more than once creates more overhead, e.g., repetition of the backoff phase, IFS, etc. Therefore, retransmissions are one of the most "problematic" sources of overhead, which are mitigated by using efficient retransmission mechanisms.

Next, we will analyse the maximum average throughput (S_{max}) and the minimum average delay (D_{min}) for the IEEE 802.15.4 standard. S_{max} is defined as the number of data bits generated from the MAC layer that can be transmitted per second on average to its destination including the ACK reception, on average. D_{min} is the time needed to transmit a packet and the successfully reception of the ACK or *BACK Response*, on average. In this analytical model, we will only consider the nonbeacon-enabled version of the protocol. Although, we are considering the 2.4 GHz band, the proposed formulation is also valid for other different frequency bands as well as different PHY layer.
As explained before, initially, nodes uses the same backoff procedure like IEEE 802.15.4 basic access mode. Therefore, BE is set to $macMinBE$ (which corresponds to the minimum value of the backoff exponent, in the CSMA-CA algorithm). By considering the default value $BE = 3$ for $macMinBE$, and assuming that the channel is free, the worst-case channel access time that corresponds to the maximum backoff windows is given by Equation (5.12).
The average backoff window is given by:

$$\overline{CW} = \left(\frac{2^{BE} - 1}{2}\right) \times T_{BO} \tag{5.14}$$

S_{max} and the D_{min} can be determined for the best scenario, i.e., the channel is an ideal channel with no errors. During one transmission cycle, there is only one active node that has always a frame to be send, whereas the other neighbouring nodes can only accept frames and provide ACKs. An analytical model to evaluate S_{max} and D_{min}, is proposed. Table 5.1 presents the key parameters, symbols and values. Hence, there is no need to redefine every parameter after every equation again. The transmission times for the DATA and ACK frames are given as follows:

$$T_{DATA} = 8 \times \frac{L_{H\_PHY} + L_{H\_MAC} + L_{DATA}}{R} \tag{5.15}$$

$$T_{ACK} = 8 \times \frac{L_{H\_PHY} + L_{ACK}}{R} \tag{5.16}$$

The minimum average delay, D_{min}, in seconds, is given by:

$$D_{min} = \left(\overline{CW} + ccaTime + T_{TA} + T_{DATA} + T_{TA} + T_{ACK} + T_{IFS}\right) \tag{5.17}$$

For IFS, SIFS is considered when the MAC protocol data unit, MPDU ($= L_{H\_MAC} + L_{DATA}$), is less or equal than 18 bytes; otherwise LIFS is considered.
In IEEE 802.15.4 basic access mode, the maximum average throughput, S_{max} , in bits per second, is given by:

$$S_{max} = \frac{8L_{DATA}}{D_{min}} \tag{5.18}$$

By analysing Equations (5.17) and (5.18), we conclude that, if a short frame is transmitted, then the data transmission time is relatively short when compared to the associated overhead time, resulting into relatively low throughput. When a long frame is transmitted (by increasing the payload) data transmission time increases. This way, IEEE 802.15.4 is capable of achieving a much higher throughput.
Previously we have presented results for the channel with no errors for IEEE 802.15.4 basic access mode. However, data collisions may occur between neighbouring nodes if two or more nodes during the CSMA-CA perform CCA simultaneously, the channel is found to be idle and packet transmissions occur at the same time. Therefore, there is a need to study the impact of retransmissions in IEEE 802.15.4 networks by considering an erroneous channel. The flowchart of the CSMA-CA algorithm for the nonbeacon-enabled mode is presented in Figure 5.9. The CSMA-CA algorithm requires listening to the channel before transmitting in order to reduce the collision probability (which is used before the transmission of data frames within the CAP) unless the frame can be quickly transmitted due to an ACK of a data request command.
The IEEE 802.15.4 nonbeacon-enabled CSMA-CA algorithm in the basic access mode, maintains two variables for each packet as follows:

1. **Number of Backoffs (NB):** number of times the CSMA-CA algorithm was required to experience backoff due to unavailability. It is initialised to zero before each new transmission attempt.

2. **Backoff Exponent (BE):** enables the computation of the backoff delay, and represents the number of backoff periods that need to be clear of channel activity before a transmission can occur. The backoff delay is a random variable in the range $[0, 2^{BE} - 1]$.

The CSMA-CA algorithm can be summarised in four steps as follows:

1. In the first step, after initialization of the NB and BE, the MAC layer will delay the activity based on a backoff time counter (BOc) uniformly distributed in the range $[0, CW_{NB}]$, where $CW_{NB} = [2^{BE} - 1]$ is the dimension of the initial contention window and NB ranges from $[0, NB_{max} = macMaxCSMABackoffs]$. The $macMaxCSMABackoffs$ [WPAN06], represents the maximum number of backoffs the CSMA-CA algorithm will experience before declaring a channel access failure.

2. In the second step, the node will perform CCA during the $ccaTime$ time period.

3. In the third step, if the channel is found to be busy, both the NB and BE (BE is less or equal than BE_{max}) will be incremented by one unit. If the value of NB is larger than NB_{max}, then the CSMA-CA algorithm will finish by entering in the "Failure" state, which means that the node does not succeed in accessing the channel.

4. In the fourth step, if the channel is found to be idle during the CCA procedure, the MAC layer starts immediately transmitting its current frame, and the algorithm will finish by

entering in the "Success" state, which means that the node has success in accessing the channel.

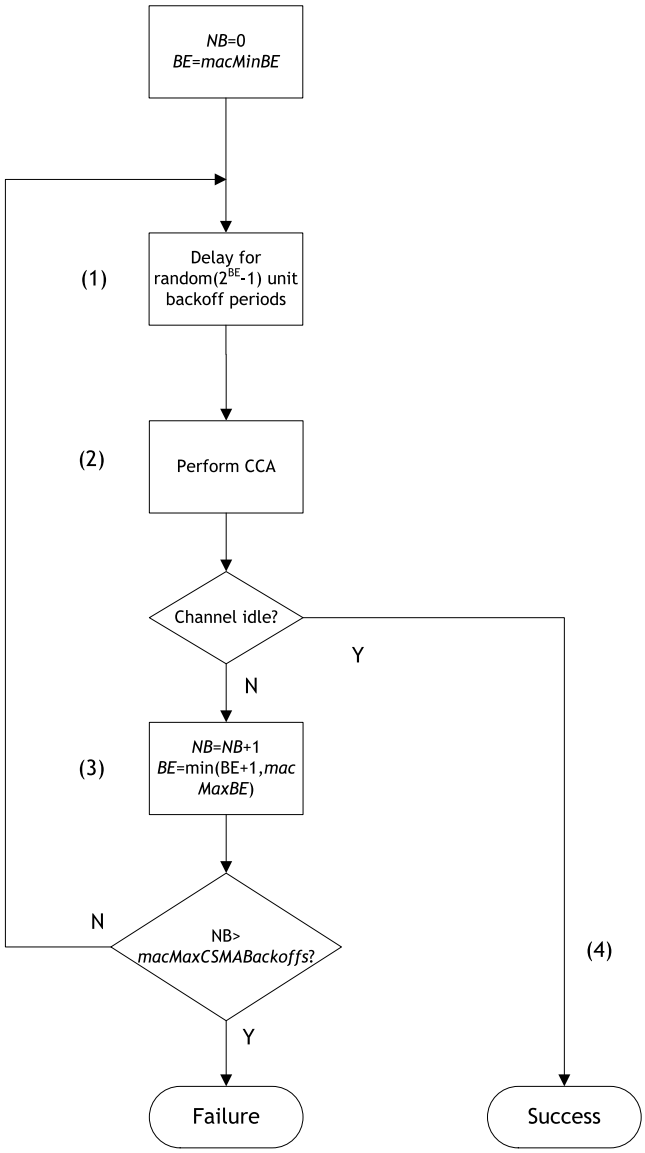

Figure 5.9: IEEE 802.15.4 and SBACK-MAC CSMA-CA algorithm for the nonbeacon-enabled mode.

By considering the same assumptions from the model presented in [BuVe09], one can model the backoff procedure by a dimensional process $Q(t) = \{BO_c(t), BO_s(t)\}$, where according to [BuVe09], t is an integer, which represents the time slot. More precisely, the j^{th} slot (varying from $j \cdot T_{BO}$ to $(j+1) \cdot T_{BO}$) is denoted by $t = j$. The variables $BO_c(t)$ and $BO_s(t)$ represent the backoff time counter and the backoff stage at slot t, respectively.
Since the $BO_c(t)$ is not a memoryless process, the dimensional process given by the $BO_c(t)$ and $BO_s(t)$ cannot be derived by considering a Markovian chain [BuVe09]. Moreover, as explained before, the BE is dependent of the $BO_s(t)$. By analysing the possible combinations between the pair (NB, BE) one concludes that there are $NB_{max} + 1$ different backoff stages, where NB_{max} represents the maximum number of backoffs allowed by the CSMA-CA algorithm.
Table 5.2 presents the different values for the backoff stage and the corresponding CW_{NB} by assuming the combination pair $(NB_{max} = 4, BE_{max} = 5)$.

Table 5.2: Backoff stages for IEEE 802.15.4 and SBACK-MAC.

NB	BO_s	BE_i	$CW_{NB} = [2^{BE_i} - 1]$	$\overline{CW}_{NB}$
0	0	3	$CW_0 = 7$	3.5
1	1	4	$CW_1 = 15$	7.5
2	2	5	$CW_2 = 31$	15.5
3	3	5	$CW_3 = CW_2 = 31$	15.5
4	4	5	$CW_4 = CW_2 = 31$	15.5

As shown in Figure 5.10.a), for each transmission attempt in the basic access mode of IEEE 802.15.4, nodes perform a random backoff from a uniform distribution over $[0, CW_{NB}]$. The $CW_{NB} = \left[2^{BE_i} - 1\right]$ represents the backoff delay before performing CCA. The BE_i value depends on the $BO_s(t)$. After performing CCA, if the channel is found to be idle there will be a data transmission. Otherwise, if the channel is found to be busy, nodes will defer the data transmission for a random backoff period defined by BE_i in the next backoff stage.

The backoff contention window is doubled whenever the channel is determined busy during CCA until BE_i reaches its maximum value and it cannot be increased any further. Thus, the backoff window remains the same until the maximum retry limit (e.g., $NB_{max} = 4$) is reached [WPAN11]. In the last retransmission case, if the channel is found to be busy, and nodes cannot succeed in sending the packet, the packet will be deleted from the MAC queue. Then, a new transmission cycle will start again, with a backoff delay defined by (e.g., $CW_0 = 7$) for the next data packet to be transmitted, and the CSMA-CA algorithm is repeated.

In case the channel is found to idle during CCA following the backoff phase and an ACK is not received within the ACK wait duration period, T_{AW}, nodes shall conclude that the transmission attempt has failed. For this case, nodes shall repeat the DATA/ACK handshake process and the backoff window is given by the first backoff phase, i.e., first contention window, CW_0, as shown in Figure 5.10.b).

To determine the maximum average throughput, S_{max}, in an erroneous channel, first one needs to determine the minimum average delay, D_{min}. D_{min} is obtained by taking into account, the channel state (i.e., idle or busy) during CCA and the number of retransmissions for the non-received ACK control packets, by considering packet collisions and channel errors. In IEEE 802.15.4 basic access mode, the minimum delay due to CCA, D_{min_CCA} is given as follows:

$$D_{min\_CCA} = \sum_{i=1}^{n} \sum_{k=0}^{k \leqslant NB} \left(\overline{CW_k} + ccaTime\right) \quad , \quad NB \in [0, NB_{max}] \tag{5.19}$$

Equation (5.19), provides the minimum delay resulting from the number of times the channel state (i.e., busy or idle) is determined during CCA. Every time the channel is found to be busy both NB and BE are increased by 1, as shown in Table 5.2. When BE reaches its maximum value, there is no more increase. By analysing Table 5.2, we conclude that, when $BO_s = 4$, and by considering $NB = NB_{max} = 4$, the BE cannot be increased any further. If $NB > NB_{max}$ the CSMA-CA algorithm will finish by entering in the "Failure" state, which means that the node does not succeed in accessing the channel. Equation (5.19) also accounts each transmitted packet ranging from 1 to n, where n represents the total number of transmitted packets for each active period. The number of times the CW will be doubled for each transmitted packet depends on the channel state determined during CCA (i.e., busy or idle).

The minimum delay due to packet retransmissions, $D_{min\_Data\_Ret}$, when the channel is found to be idle during CCA, after the backoff phase, where there is a data transmission and an ACK

is not received within the ACK wait duration period, defined by T_{AW}, is given as follows:

$$D_{min\_Data\_Ret} = \sum_{i=1}^{n} K_i \quad , \quad K_i \quad = \quad \begin{cases} H_1 & , j = 0 \\ H_2 + (j-1) \times H_4 + H_3 \ , \ j \in [1, MaxRet] \end{cases} \tag{5.20}$$

where j is the number of packet retransmissions, and could range between 0 and the maximum number of retransmissions, like in [WPAN11]. By analysing Equation (5.20), we reach the following conclusions:
If, after CCA, nodes determine that the channel is found to be idle and an ACK is correctly received following the transmission of a data packet, the minimum delay due to packet retransmissions, $D_{min\_Data\_Ret}$, is given by:

$$H_1 = T_{TA} + T_{DATA} + T_{TA} + T_{ACK} + T_{IFS} \tag{5.21}$$

The number of packet retransmissions for this case is given by $j = 0$. It is worthwhile to mention that, since we are considering the minimum delay, there is no need to consider the ACK wait duration period, T_{AW}, in the equation, which represents the longest time needed for receiving an ACK control packet;
If, after CCA, nodes determine that the channel is found to be idle and an ACK is not correctly received following the transmission of a data packet, in which the node only tries to retransmit a packet once (i.e., $j = 1$), the minimum delay due to packet retransmissions, $D_{min\_Data\_Ret}$, is given by $H_2 + H_3$, where:

$$H_2 = T_{TA} + T_{DATA} + T_{AW} \tag{5.22}$$

$$H_3 = \overline{CW_0} + ccaTime + H_1 \tag{5.23}$$

The term H_2 indicates that in the first transmission attempt no ACK has been received within T_{AW}. The term H_3 indicates that nodes only received an ACK control packet after retransmitting the packet one more time. The packets are retransmitted by considering the first contention window, CW_0, defined by the CSMA-CA algorithm [WPAN06];
If the number of retransmission attempts is more than one, it means that a node has failed to previously retransmit a packet and it will retry to transmit a packet until the number of maximum retransmissions, $MaxRet$, has been reached. The minimum delay due to packet retransmissions, $D_{min\_Data\_Ret}$, is given by:

$$H_2 + (j-1) \times H_4 + H_3 \tag{5.24}$$

where, $H_4 = \overline{CW_0} + ccaTime + H_2$. The term $(j-1) \times H_4$, indicates that the packet will be retransmitted by considering the first contention window in the range $j \in [2, MaxRet]$, and an ACK control packet will be correctly received in the last retransmission attempt given by H_3.
By combining Equations (5.19) and (5.20), the minimum average delay, D_{min}, due to the channel state (i.e., busy or idle) and packet retransmissions is given by:

$$D_{min} = \frac{D_{min\_CCA} + D_{min\_Data\_Ret}}{n} \tag{5.25}$$

In IEEE 802.15.4 basic access mode, if an erroneous channel is considered, the maximum average throughput, S_{max}, in bits per second, by considering packet retransmissions is given by:

$$S_{max} = \frac{8L_{DATA}}{D_{min}} \tag{5.26}$$

5.4 IEEE 802.15.4 with Packet Concatenation

The BACK mechanism was previously introduced in the IEEE 802.11e standard [WLAN05]. It improves channel efficiency by aggregating several ACK control packet responses into one special packet, the *BlockAck*. Hence, an ACK control packet will not be received in response to every data packet sent. The IEEE 802.11e standard defines two types of BACK mechanisms: immediate and delayed, depending on whether a *BlockAck* packet is transmitted, immediately after a *BlockAckReq* packet reception or not. Immediate BACK is suitable for high-bandwidth and low-latency traffic, while the delayed BACK is suitable for applications that tolerate moderate latency.

Since we intend to investigate the impact of the BACK mechanism in the context of IEEE 802.15.4 standard, defined for Low-Rate Wireless Personal Area Network (LR-WPAN), some modifications were made to accommodate the energy, throughput and end-to-end delay requirements for these networks. Therefore, the proposed solutions are totaly compliant with the standard.

Since WSN are composed by a large number of battery-operated nodes, one of the most important issues is energy conservation. In order to reduce the energy consumption due to the protocol overhead, the SBACK-MAC protocol is proposed, which combines contention-based, scheduling-based and BACK-based schemes to achieve energy efficiency. As explained before, the SBACK-MAC protocol considers the use of the RTS/CTS mechanism, in order to avoid the hidden terminal problem of nonbeacon-enabled multi-hop wireless networks, which may significantly degrade their performance [SuSu10]. Although, the RTS/CTS scheme is often employed to improve performance as it shortens packet collision duration and addresses the hidden station problem, until now, RTS/CTS is not proposed in any of the IEEE 802.15.4 standards. This reservation scheme actually involves the transmission of the short RTS and CTS control packets prior to the transmission of the actual data packet.

There is a number of studies in the literature on the performance of the RTS/CTS reservation mechanism in either IEEE 802.15.4 or 802.11 wireless networks [MiMu11, JiYi12, ChBV04a, ChBV04b]. The authors from [ChBV04a] study proposed a broadcasting method based on RTS/CTS for IEEE 802.15.4 networks, in which the sender node uses a RTS packet to select the receiver node from neighboring nodes. The work from [JiYi12] proposes an adaptive mechanism based on RTS/CTS in order to solve the hidden terminal problem in an IEEE 802.15.4 nonbeacon-enabled multi-hop network. Authors in [ChBV04a] studied the effectiveness of the RTS/CTS scheme in reducing the collision duration for IEEE 802.11 WLANs under certain scenarios. In a later work, authors in [ChBV04b] tried to optimally employ the RTS/CTS scheme by deriving an all-purpose expression for the RTS threshold, a manageable parameter that indicates the data length under which the data packets should be sent without RTS/CTS.

In the framework of this thesis, we also propose the use of RTS/CTS for IEEE 802.15.4 by considering the nonbeacon-enable mode combined with packet concatenation. The proposed solution shows that by considering the RTS/CTS mechanism combined with packet concatenation we improve the network performance in terms of maximum average throughput, minimum average delay and bandwidth efficiency.

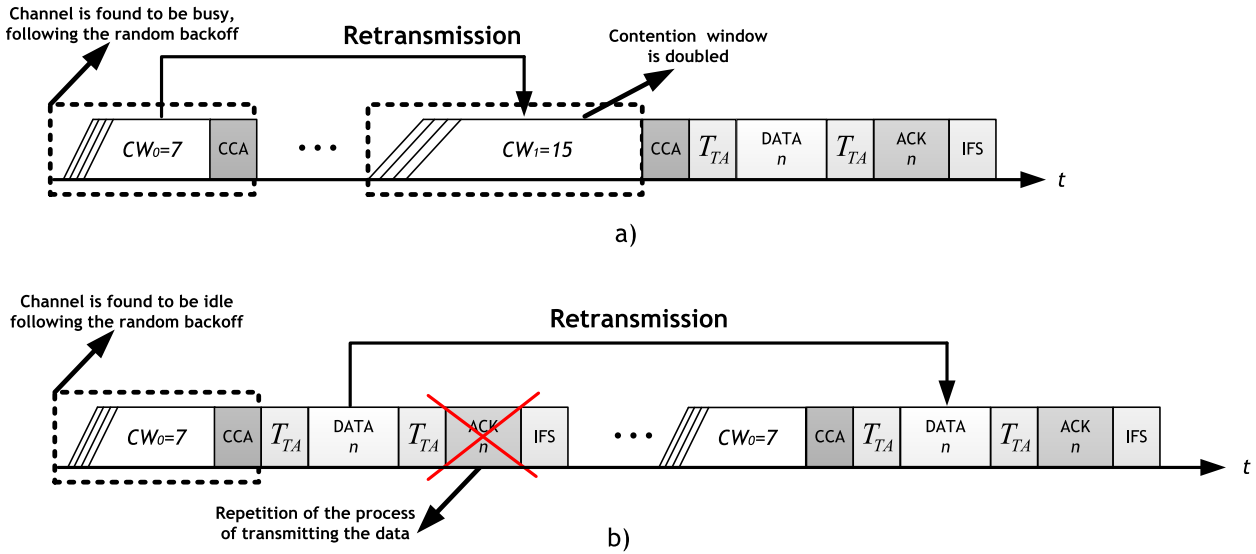

Figure 5.10: IEEE 802.15.4 basic access mode with retransmissions: a) channel is found to be busy and b) channel is found to be idle.

5.4.1 IEEE 802.15.4 with RTS/CTS combined with Packet Concatenation

The main reasons why IEEE 802.15.4 basic access mode does not consider the adoption of the RTS/CTS handshake mechanism are the following ones. (i) The introduction of RTS/CTS packets adds additional protocol overhead and, in a situation with low traffic load, short packet sizes could have the same order of magnitude of a RTS/CTS packet, (ii) The absence of a RTS/CTS handshake mechanism allows to reduce the system complexity.
Although these assumptions are true for some particular cases, we argue that in the presence of link layer errors the additional protocol overhead due to the use of RTS/CTS packets is mitigated by our concatenation mechanism. So, there is no need to repeat the backoff procedure for each data packet sent, but only once for each RTS/CTS set. Moreover, by using the proposed RTS/CTS mechanism packet collisions between the hidden nodes are avoided, allowing for decreasing the number of retransmitted packets and, thus, increasing the network performance.
In our proposal, we also assume that both the RTS and CTS packets have the structure of an ACK packet, which is assumed to have a limited size of 11 bytes, as shown in Table 5.1. The maximum data payload for IEEE 802.15.4 depends on the application (maximum payload could range between 102 and 118 bytes). Therefore, the length of the data packets could be approximately ten times greater than the control packets length.
IEEE 802.15.4 employing RTS/CTS with packet concatenation is composed by the following time periods:

- Backoff phase;
- CCA mechanism;
- Time needed for switching from receiving to transmitting;
- RTS transmission time;
- Time needed for switching from transmitting to receiving;
- CTS reception time.

Figure 5.11 presents the IEEE 802.15.4 RTS/CTS handshake mechanism.

Figure 5.11: IEEE 802.15.4 frame sequence with RTS/CTS.

As shown in Figure 5.11, in IEEE 802.15.4 employing RTS/CTS, nodes will use the same backoff procedure like IEEE 802.15.4 basic access mode. However, this process is not repeated for each data packet sent, but only for each RTS/CTS set. Therefore, the channel utilization is maximized by decreasing the deferral time period before transmitting a data packet, as shown in Figure 5.8. The proposed solution shows that, by considering the RTS/CTS mechanism combined with packet aggregation, the network performance is improved in terms of maximum throughput, minimum delay and bandwidth efficiency. This thesis also introduces an analytical model capable of accounting the retransmission delay and the maximum number of backoff stages. The successful validation of our analytical model will be carried out by comparison against simulation results by using the MiXiM framework of the OMNeT++ simulator [OMNe13].

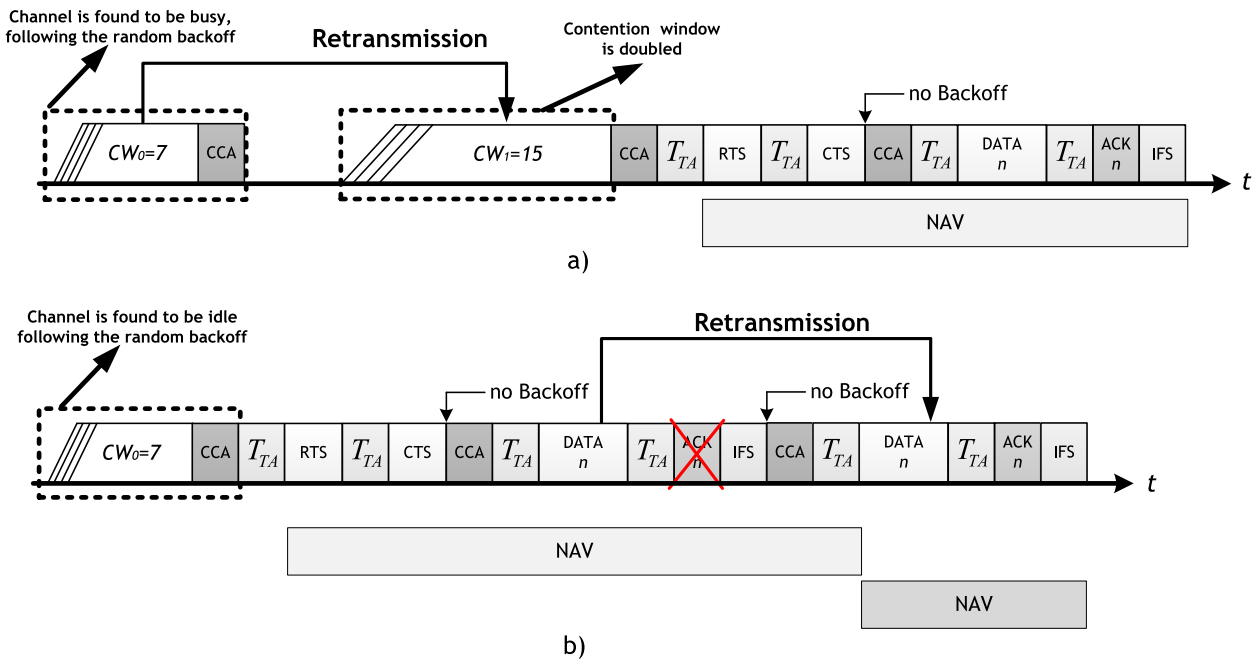

Figure 5.12: IEEE 802.15.4 with RTS/CTS with retransmissions: a) channel is found to be busy and b) channel is found to be idle.

The minimum delay due to CCA, $D_{min\_CCA\_RTS}$, to determine if the channel is found to be busy or idle, after the backoff phase, and before each RTS/CTS set, is given by:

$$D_{min\_CCA\_RTS} = \sum_{i=1}^{n/N_{agg}} \sum_{k=0}^{k \leqslant NB} \left(\overline{CW_k} + ccaTime\right) \quad , \quad NB \in [0, NB_{max}] \tag{5.27}$$

By analysing Equation (5.27), it can be concluded that nodes only determine the channel state once per RTS/CTS. Therefore, if a node has $n = 100$ data packets to send and the number of aggregated packets is equal to $N_{agg} = 10$, nodes only determine the channel state 10 times ($n/N_{agg} = 100/10 = 10$) plus the time need for transmitting the packets (until the maximum retry limit, $NB_{max} = 4,$ is reached).
If the channel is found to be idle during CCA and, after sending a data packet an ACK is not received within a duration of T_{AW}, the retransmission process will not consider the use of the backoff phase between two consecutive data packets, which allows to decrease the total overhead (as shown in Fig 5.12.b). Since any other stations can receive both the RTS, CTS, DATA or ACK packets, in the first transmission attempt they will set an internal timer called Network Allocation Vector (NAV) that is responsible for defining the time period a node will defer the channel access in order to avoid collisions.
In the IEEE 802.15.4 MAC protocol with RTS/CTS, the minimum delay due to packet retransmissions, $D_{min\_Data\_Ret\_RTS}$, when the channel is found to be idle during CCA (after the backoff phase), there is a data transmission, and an ACK is not received within a duration of T_{AW}, is given obtained follows:

$$D_{min\_Data\_Ret\_RTS} = \begin{cases} H_5 & , for\ j = 0 \\ H_6 & , for\ j \in [1, MaxRet] \end{cases} \tag{5.28}$$

where j is the number of packet retransmissions (RTX), and varies between 1 and $MaxRet$, as defined in [WPAN11].
The following lessons can be learned from the analysis of Equation (5.28):
If, after CCA, a node determines that the channel is found to be idle, and an ACK is correctly received for each packet sent, the minimum delay, $D_{min\_Data\_Ret\_RTS}$, is determined by:

$$\begin{aligned} H_5 = {} & T_{TA} + T_{RTS} + T_{TA} + T_{CTS} + \sum_{i=1}^{N_{agg}} (ccaTime + T_{TA} + T_{DATA} + T_{TA} + \\ & + ... + T_{ACK} + T_{IFS}) \end{aligned} \tag{5.29}$$

which means that there are no transmission errors. In this case, the number of retransmissions is given by $j = 0$.
If after CCA, a node founds the channel to be idle and an ACK has not been received within the duration of T_{AW}, for one or more packets sent (by considering aggregation), the minimum delay due to packet retransmissions, $D_{min\_Data\_Ret\_RTS}$, is determined by:

$$\begin{aligned} H_6 = {} & T_{TA} + T_{RTS} + T_{TA} + T_{CTS} \sum_{i=1}^{N_{agg}-m} (ccaTime + T_{TA} + T_{DATA} + T_{TA} + T_{ACK} + T_{IFS}) \\ & + ... + \sum_{i=1}^{m} (j_i) \times (ccaTime + T_{TA} + T_{DATA} + T_{AW}) \\ & + ... + \sum_{i=1}^{m} (ccaTime + T_{TA} + T_{DATA} + T_{TA} + T_{ACK} + T_{IFS}) \end{aligned} \tag{5.30}$$

The term $\sum_{i=1}^{N_{agg}-m}(ccaTime + T_{TA} + T_{DATA} + T_{TA} + T_{ACK} + T_{IFS})$ represents the $(n-m)$ transmitted packets that have successfully received an ACK response, where m denotes the number of transmitted packets that need retransmission. Since each individual packet can be retransmitted more than once, due to the fact that an ACK has not been received within a duration of T_{AW} duration. The term j_i, represents the number of times a packet has experienced retransmission until $MaxRet$ has been reached. We then assume that the ACK packet is received, which represents the last case given by: $\sum_{i=1}^{m}(ccaTime + T_{TA} + T_{DATA} + T_{TA} + T_{ACK} + T_{IFS})$. By combining Equations (5.27) and (5.28), the minimum average delay, $D_{min\_RTS\_CTS}$, due to the channel state (i.e., busy or idle) and packet retransmissions is given by:

$$D_{min\_RTS\_CTS} = \frac{D_{min\_CCA\_RTS} + D_{min\_Data\_Ret\_RTS}}{n} \tag{5.31}$$

In IEEE 802.15.4, by employing RTS/CTS combined with packet concatenation, if an erroneous channel is considered, the maximum average throughput, $S_{max\_RTS\_CTS}$, in bits per second, by considering packet retransmissions is given by:

$$S_{max\_RTS\_CTS} = \frac{8L_{DATA}}{D_{min\_RTS\_CTS}} \tag{5.32}$$

5.4.2 Proposed scheme design with *Block ACK Request*

In the previous Section we have presented the introduction of an RTS/CTS mechanism combined with packet concatenation to improve the IEEE 802.15.4 MAC layer performance. Next, SBACK-MAC protocol proposed, which combines contention-based, scheduling-based and BACK-based schemes to reduce the energy consumption due to the protocol overhead.
The version of the SBACK-MAC protocol without piggyback considers the exchange of of two special packets: *RTS ADDBA* and *CTS ADDBA*, *ADDBA* stands for "Add Block Acknowledgement". The structure of these packets is presented in Figure 5.13.a). After this successfully exchange, the data packets are transmitted from the transmitter to the receiver. Afterwards, by using the *BACK Request* primitive, the transmitter inquires the receiver about the total number of data packets that successfully reach the destination. In response, the receiver will send a special data packet called *BACK Response* identifying the packets that require retransmission, and the BACK mechanism finishes. The structure of these packets is shown in Figure 5.13.b) and c).

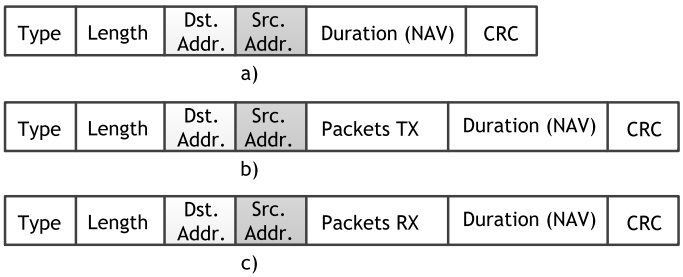

Figure 5.13: a) *RTS ADDBA Request* and *CTS ADDBA Response*, b) *BACK Request* and c) *BACK Response* packets format.

Figure 5.14 presents the message sequence chart for the BACK mechanism with *BACK Request*, based on [WLAN05]. The exchange of two special control packets, used in the beginning and at the end of the BACK mechanism, allows for mitigating the hidden-terminal and exposed-terminal problems like in IEEE 802.11e [WLAN05] (by using a RTS/CTS handshake).

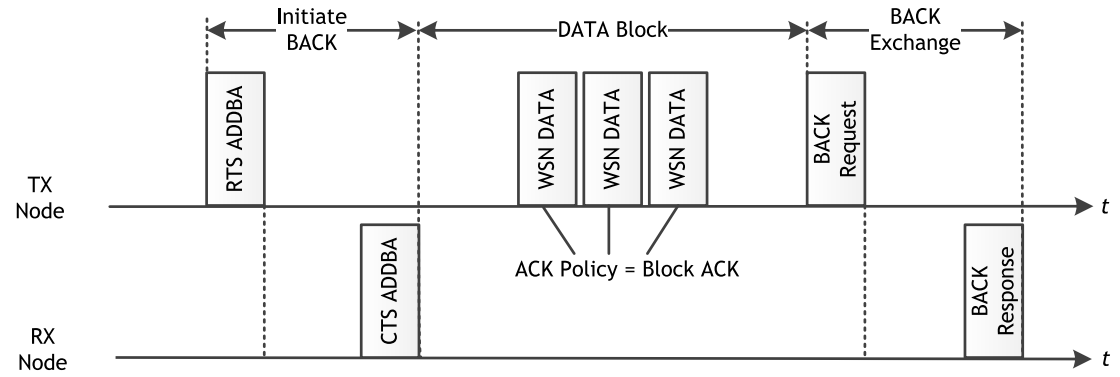

Figure 5.14: SBACK-MAC protocol - BACK mechanism with *BACK Request*.

The BACK mechanism aims at reducing the power consumption by transmitting less ACK control packets whilst decreasing the time periods the transceivers should switch between different states. By using the BACK, there is no need to receive an ACK for every DATA packet sent, as shown in Figure 5.15. However, during the data transmission there is no way to know how many packets have successfully reached the destination, except at the end of communication by using the *BACK Request*/*BACK Response*. Like in [WPAA08], we set BE equal to 0, as if there is no congestion. Therefore, the channel utilization is maximized by decreasing the deferral time before transmitting (i.e., the $Initialbackoff Period$ will be 0).

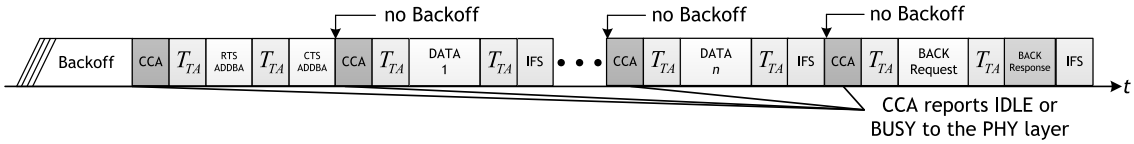

Figure 5.15: Timing relationship in the SBACK-MAC protocol with *BACK Request* (concatenation).

As presented in Figure 5.15, to overcome the overhead of the IEEE 802.15.4 MAC, several efficient MAC enhancements are proposed in which the frame concatenation concept is adopted. The idea is to transmit multiple MAC/PHY frames by using the BACK mechanism. In this thesis, a distributed scenario is considered, with single-destination and single-rate frame aggregation. In single-destination approaches, frames can be aggregated if they are available, and have the same source and destination address. Moreover, we also assume that the payload of the MAC frames cannot be modified.

In SBACK-MAC with *BACK Request*, every time a node as an *RTS ADDBA* to send, the transmission will follow the same backoff procedure like the one presented for IEEE 802.15.4 with RTS/CTS. Therefore, the minimum delay, $D_{min\_CCA\_BACK}$, in seconds, for determining if the channel state is found to be busy or idle during CCA, following the backoff phase is given as follows:

$$D_{min\_CCA\_BACK} = \sum_{i=1}^{n/N_{agg}} \sum_{k=0}^{k \leqslant NB} \left(\overline{CW_k} + ccaTime\right) \quad , \quad NB \in [0, NB_{max}] \tag{5.33}$$

In SBACK-MAC with *BACK Request* the *BACK Response* primitive is responsible to confirm the set of data packets successfully delivered to the destination by using an M bit bitmap. A bit value equal to one means that a data packet has successfully reached the destination, while a bit value equal to zero means that the corresponding data packet as failed to reach the destination. Therefore, when the transmitter node receives a *BACK Response*, it compares

the send/received M bit bitmap, and if needed it retransmits the frames that do not have reach the destination. Based on the received M bit bitmap two retransmissions mechanisms are envisaged. The first one considers retransmissions by using the DATA/ACK exchange, like in IEEE 802.15.4 basic access mode, whilst the second one considers a fixed extra time for retransmitting the packets like in [WPAN12].

A. Retransmissions by using DATA/ACK handshake

In SBACK-MAC with *BACK Request*, a group of data packets are transmitted (i.e., by using aggregation) with only one *RTS ADDBA*/*CTS ADDBA* set between the transmitter/receiver. Then, the receiver confirms the total amount of packets correctly received by using the BACK Response primitive. All the packets (*RTS ADDBA*, *CTS ADDBA*, DATA, *BACK Request* and *BACK Response)* have a NAV duration field and the neighbouring nodes are required to set its NAV field accordingly.
If packet retransmissions are needed, the basic DATA/ACK handshake is used. However, the retransmission process does not consider the use of the backoff phase between two consecutive data packets, which allows for decreasing the total overhead, as shown in Figures 5.16.a) and b). This way a "sort" of priority is being created for packet retransmissions.
The packets exchanged during the retransmission process (i.e., DATA and ACK) also have a NAV duration field in order to reserve the medium, accounting the extra time duration imposed by the retransmissions. This way, the problem of how non-participating nodes shall learn about the transaction elongation when they had only heard the initial *RTS ADDBA*/*CTS ADDBA* set is avoided.
It is worthwhile to mention that the NAV duration shall include the time period needed for retransmitting the packets and receiving the ACKs plus the $ccaTime$ and T_{TA} time periods, enabling to avoid packet collisions between neighbouring nodes. This is explained by the fact that when neighbouring nodes wake-up, they will try to access the channel by using the backoff phase defined by the first contention window. Therefore, the backoff timer counter plus the $ccaTime$ and T_{TA} time periods will avoid possible collisions with the ongoing retransmission process. In SBACK-MAC with *BACK Request*, the minimum delay due to packet retransmissions, $D_{min\_Data\_Ret\_BACK\_ACK}$, when the channel is found to be idle during CCA, there is a data transmission (by considering aggregation) and the retransmission process is ruled by the DATA/ACK handshake mechanism like in IEEE 802.15.4 basic access mode is given as follows:

$$D_{min\_Data\_Ret\_BACK\_ACK} = \begin{cases} H_7 & , \; for \; j = 0 \\ H_8 & , \; for \; j \in [1, MaxRet] \end{cases} \tag{5.34}$$

where j is the number of packet retransmissions, and could range between 1 and the maximum number of retransmissions, $MaxRet$, as defined in [WPAN06].
By analysing Equation (5.34), we conclude the following:
If, after CCA, a node determines that the channel is found to be idle, the aggregated packets are sent and a *BACK Response* is correctly received, confirming that all the transmitted packets

have successfully reach the destination, $D_{min\_Data\_Ret\_BACK\_ACK}$, is given by:

$$\begin{aligned} H_7 &= T_{TA} + T_{RTS\_ADDBA} + T_{TA} + T_{CTS\_ADDBA} \sum_{i=1}^{N_{agg}} (ccaTime + T_{TA} + T_{DATA} \\ &\quad + T_{TA} + T_{IFS}) + ccaTime + T_{TA} + T_{BRequest} + T_{TA} + T_{BResponse} + T_{IFS} \end{aligned} \tag{5.35}$$

which means that there are no transmission errors. For this case the number of retransmissions, is given by $j = 0$.

If after CCA, a node determines that the channel is found to be idle, the aggregated packets are sent and a ***BACK Response*** is correctly received, indicating that some packets need retransmission, $D_{min\_Data\_Ret\_BACK\_ACK}$, is given by:

$$\begin{aligned} H_8 &= H_7 + \sum_{i=1}^{m} [(j_i - 1) \times (ccaTime + T_{TA} + T_{DATA} + T_{AW})] + \\ &\quad \sum_{i=1}^{m} (ccaTime + T_{TA} + T_{DATA} + T_{TA} + T_{ACK} + T_{IFS}) \end{aligned} \tag{5.36}$$

The number of retransmitted packets, $MaxRet$, can only be retransmitted $(j_i - 1)$ times until $MaxRet$, has been reached, after we assume that the ACK packet must be received, which represents the last case given by $\sum_{i=1}^{m} (ccaTime + T_{TA} + T_{DATA} + T_{TA} + T_{ACK} + T_{IFS})$. It is worthwhile to mention that the term j_i represents the number of retransmissions, and could be different for each retransmitted packet, for $j \in [1, MaxRet]$.

By combining Equations (5.33) and (5.34), the minimum average delay, D_{min}, due to the channel state (i.e., busy or idle) and packet retransmissions is given by:

$$D_{min\_BACK} = \frac{D_{min\_CCA\_BACK} + D_{min\_Data\_Ret\_BACK\_ACK}}{n} \tag{5.37}$$

In SBACK-MAC with ***BACK Request***, by considering an erroneous channel, the maximum average throughput, S_{max_BACK}, in bits per second, by considering packet retransmissions is given by:

$$S_{max\_BACK} = \frac{8L_{DATA}}{D_{min\_BACK}} \tag{5.38}$$

B. Retransmissions by using an NAV extra time

The second proposed mechanism involves using a longer NAV period, accounting the retransmission of k lost packets, Figure 5.16.b). In this case there is no ACK to confirm that a given packet has successfully reached the destination, and nodes only try to retransmit a packet once.

In SBACK-MAC with ***BACK Request***, the minimum delay, $D_{min\_Data\_Ret\_BACK\_NAV}$, when the channel is found to be idle during CCA, there is a data transmission (by considering aggregation) and the retransmission process is ruled by a NAV extra time is given as follows:

$$D_{min\_Data\_Ret\_BACK\_NAV} = \begin{cases} H_9 & , for\ j = 0 \\ H_{10} & , for\ j = 1 \end{cases} \tag{5.39}$$

where j is the number of packet retransmissions, and could range between 1 and the maximum

number of retransmissions, $MaxRet$, as defined in [WPAN06]. By analysing Equation (5.39), the following conclusions can be reached:
If after CCA, a node determines that the channel is found to be idle, the aggregated packets are sent and a *BACK Response* is correctly received, confirming that all the transmitted packets have successfully reach the destination, then, the minimum delay due to packet retransmissions, $D_{min\_Data\_Ret\_BACK\_NAV}$, is given by:

$$\begin{aligned} H_9 &= T_{TA} + T_{RTS\_ADDBA} + T_{TA} + T_{CTS\_ADDBA} \sum_{i=1}^{N_{agg}} (ccaTime + T_{TA} + T_{DATA} \\ &\quad + T_{TA} + T_{IFS}) + ccaTime + T_{TA} + T_{BRequest} + T_{TA} + T_{BResponse} + T_{IFS} \end{aligned} \tag{5.40}$$

which means that there are no transmission errors. For this case the number of retransmissions, is given by $j = 0$.
If after CCA, a node determines that the channel is found to be idle, the aggregated packets are sent and a *BACK Response* is correctly received, indicating that some packets need retransmission, the minimum delay, due to packet retransmissions, $D_{min\_Data\_Ret\_BACK\_NAV}$, is given by:

$$H_{10} = H_9 + \sum_{i=1}^{k} (ccaTime + T_{TA} + T_{DATA} + T_{TA} + T_{IFS}) \tag{5.41}$$

where k represents the number of aggregated packets that are allowed to be retransmitted like in [WPAN12]. This means that this value must be carefully selected depending on the channel conditions, nodes may only need to retransmit a few data packets, or in an extreme case in which there is the need to retransmit all the aggregated packets.
By combining Equations (5.33) and (5.39), the minimum average delay, $D_{min\_BACK\_NAV}$, due to the channel state (i.e., busy or idle) and packet retransmissions is given by:

$$D_{min\_BACK\_NAV} = \frac{D_{min\_CCA\_BACK} + D_{min\_Data\_Ret\_BACK\_NAV}}{n} \tag{5.42}$$

In SBACK-MAC with *BACK Request*, by considering an erroneous channel, the maximum average throughput, S_{max}, in bits per second, by considering packet retransmissions is given by:

$$S_{max\_BACK\_NAV} = \frac{8L_{DATA}}{D_{min\_BACK\_NAV}} \tag{5.43}$$

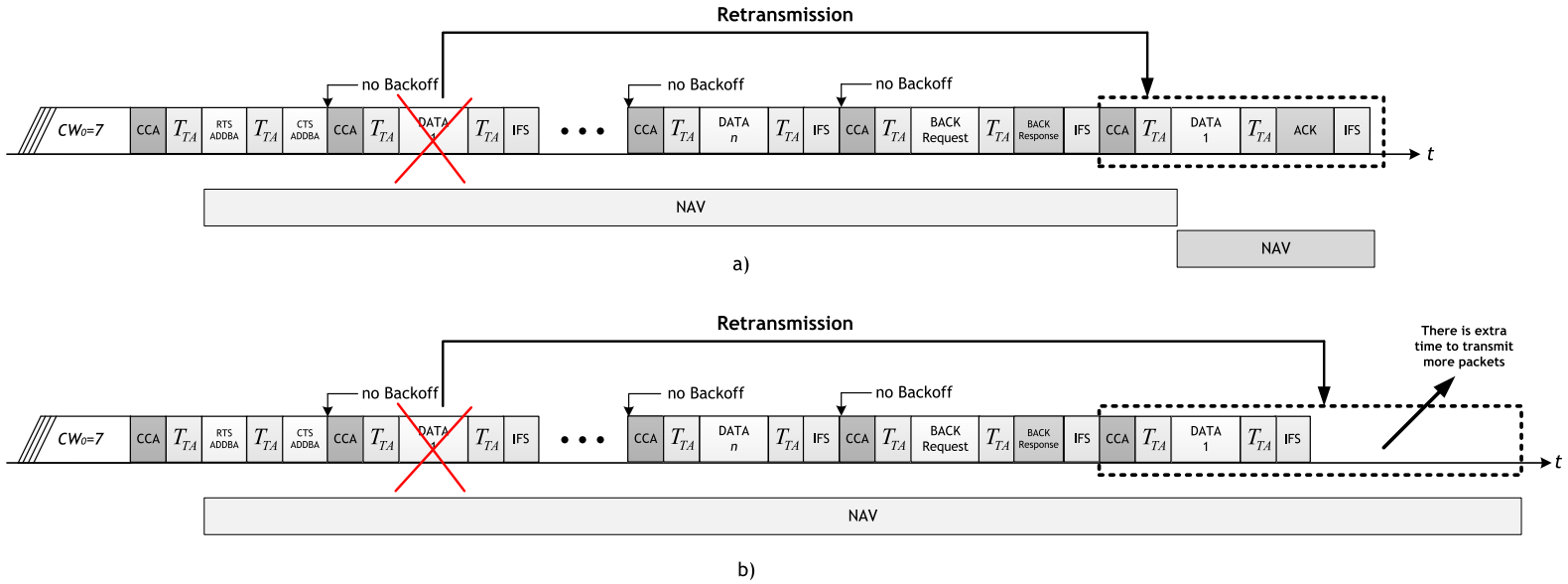

Figure 5.16: IEEE 802.15.4 with *BACK Request* (concatenation): a) Retransmissions by using DATA/ACK handshake and b) Retransmissions by using an NAV extra time.

5.4.3 Proposed scheme design with no *Block ACK Request*

The version of the SBACK-MAC protocol with no *BACK Request* ("piggyback mechanism") also considers the exchange of the *RTS ADDBA* and *CTS ADDBA* packets at the beginning of the communication. However, at the end of the communication the *BACK Request* primitive is not transmitted. Therefore, the last aggregated data frame, must include the information about the packets previously transmitted. However, with this scheme, the system becomes less robust. If the last aggregated data frame is lost, the destination does not know that an ACK needs to be sent back, Figure 5.17.

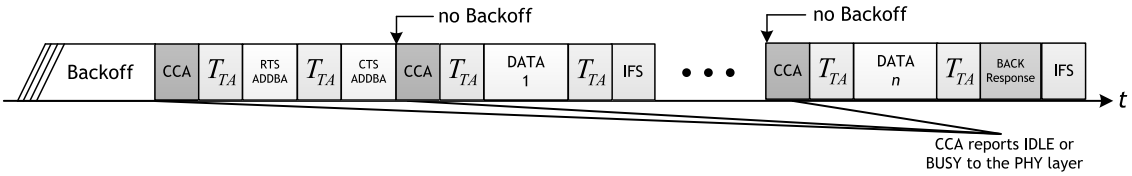

Figure 5.17: Timing relationship in the SBACK-MAC protocol with no *BACK Request* (piggyback).

As presented in Figure 5.17, the SBACK-MAC version with piggyback does not consider the use of the *BACK Request* primitive. Therefore, the control overhead and the delay is reduced whilst increasing the throughput. By "piggybacking" the BACK information into the last data fragment, however, with this scheme, the system becomes less robust. If the last aggregated frame (DATA frame n) is lost, the destination does not know that an ACK needs to be sent back.
The version of SBACK-MAC with no *BACK Request*, has the same retransmission scheme like in the SBACK-MAC with *BACK Request*, Figure 5.18.a) and b). As a consequence, the minimum delay, $D_{min\_CCA\_Piggy}$, in seconds, for determining if the channel state is found to be busy or idle during CCA, following the backoff phase is given as follows:

$$D_{min\_CCA\_Piggy} = \sum_{i=1}^{n/N_{agg}} \sum_{k=0}^{k \leqslant NB} \left(\overline{CW_k} + ccaTime\right) \quad , \quad NB \in [0, NB_{max}] \tag{5.44}$$

The SBACK-MAC with no *BACK Request* does not consider the use of *BACK Request* to inquire the receiver about the packets successfully received as shown in Figure 5.18. The information is piggybacked by using the last data packet transmitted within a burst. Based on the M bit bitmap for send/received two retransmissions mechanisms are envisaged. The first one considers retransmissions by using the DATA/ACK exchange like in IEEE 802.15.4 basic access mode as shown in Figure 5.18.a). The second one considers a fixed extra time for retransmitting the packets like in [WPAN06] as shown in Figure 5.18.b). If the last data packet if lost an *BACK Response* is not received within the *BACK Response* wait duration period, $T_{BRW} = T_{AW}$, nodes will try to retransmit the last data packet again once, as shown in Figure 5.18.c).

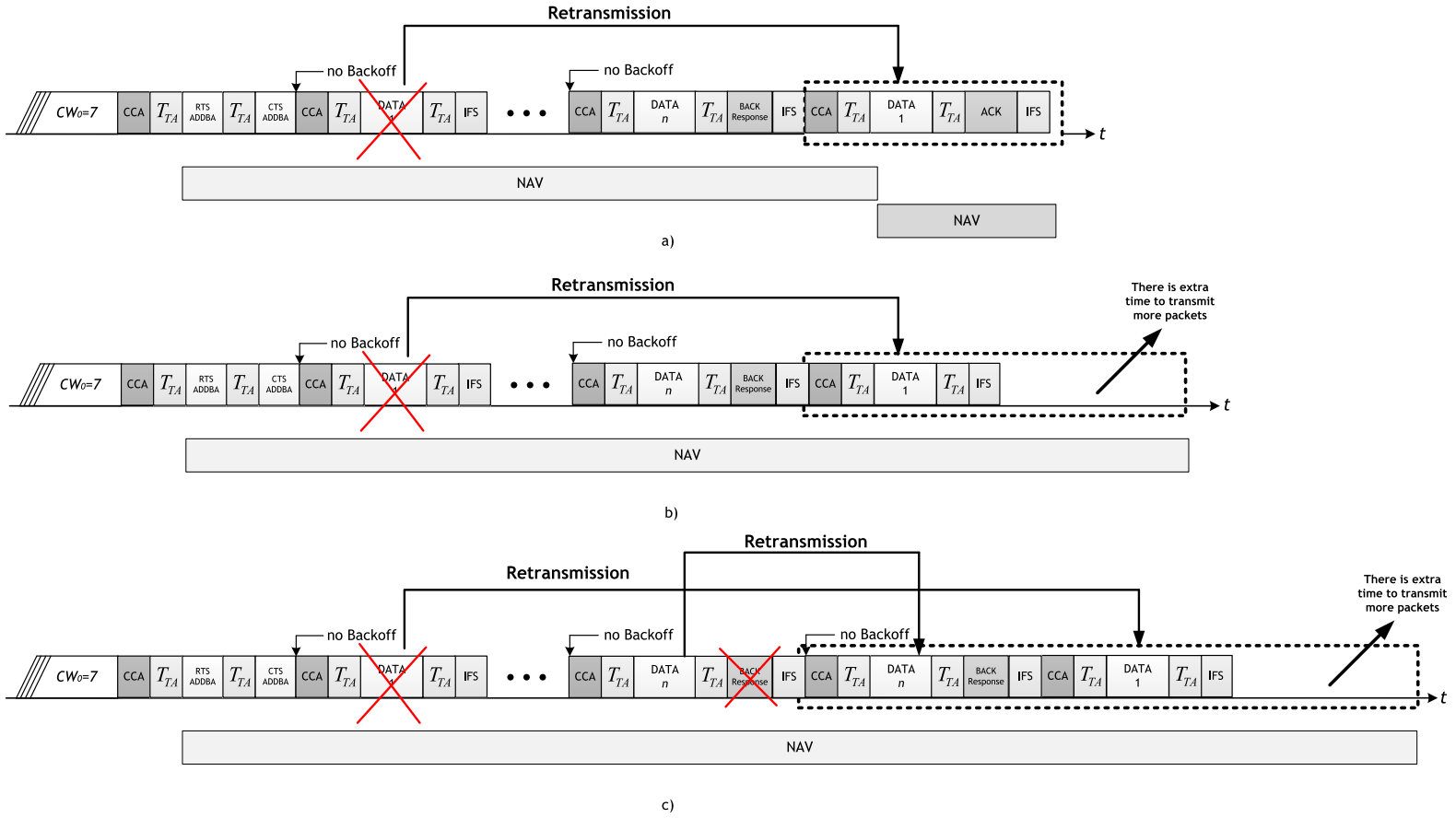

Figure 5.18: IEEE 802.15.4 with no *BACK Request* (piggyback): a) Retransmissions by using DATA/ACK handshake and b) Retransmissions by using an NAV extra time c) Retransmission of the last aggregated frame.

A. Retransmissions by using DATA/ACK handshake

In SBACK-MAC with no *BACK Request*, a group of data packets is transmitted (i.e., by using aggregation) with only one *RTS ADDBA*/*CTS ADDBA* set between the transmitter/receiver. Thus, the receiver confirms the total amount of packets correctly received by using the *BACK Response* primitive. All the packets (*RTS ADDBA*, *CTS ADDBA*, DATA and *BACK Response*) have a duration field, and the neighbouring nodes are required to set its NAV field accordingly. If packet retransmissions are needed, the basic DATA/ACK handshake is used. However, the retransmission process does not consider the use of the backoff phase between two consecutive data packets, which allows for decreasing the total overhead, as shown in Figures 5.18.a) and b). This way a "sort" of priority is being created for packet retransmissions.
The packets exchanged during the retransmission process (i.e., DATA and ACK) also have a NAV duration field in order to reserve the medium for the extra time duration imposed by retransmissions. This way, the problem of how a non-participating node shall learn about the elongation of the transaction when he has only heard the initial *RTS ADDBA*/*CTS ADDBA* exchange is avoided. The NAV duration shall also include the time period needed for retransmitting the packets and receiving the ACKs plus the $ccaTime$ and T_{TA} time periods enabling to avoid packet collisions between neighbouring nodes. This is explained by the fact that when neighbouring nodes wake-up they will try to access the channel by using backoff phase, defined by the first contention window. Therefore, the backoff timer counter plus the $ccaTime$ and T_{TA} time periods will avoid possible collisions with the ongoing retransmission process. In SBACK-MAC with no *BACK Request*, the minimum delay, $D_{min\_Data\_Ret\_Piggy\_ACK}$, when the channel is found to be idle during CCA, there is a data transmission (by considering aggregation) and the retransmission process is ruled by the DATA/ACK handshake mechanism like in IEEE 802.15.4 basic access mode is given as follows:

$$D_{min\_Data\_Ret\_Piggy\_ACK} = \begin{cases} H_{11} & , \; for \;\; j = 0 \\ H_{12} & , \; for \;\; j \in [1, MaxRet] \end{cases} \tag{5.45}$$

where j is the number of packet retransmissions, and could range between 1 and the maximum number of retransmissions, $MaxRet$, as defined in [WPAN06].
By analysing Equation (5.45), the following conclusions can be reached:
If after CCA, a node determines that the channel is found to be idle, the aggregated packets are sent and a *BACK Response* is correctly received, confirming that all the transmitted packets have successfully reach the destination, $D_{min\_Data\_Ret\_Piggy\_ACK}$, is given by:

$$\begin{aligned} H_{11} = \; & T_{TA} + T_{RTS\_ADDBA} + T_{TA} + T_{CTS\_ADDBA} \sum_{i=1}^{N_{agg}-1} (ccaTime + T_{TA} + T_{DATA} \\ & + T_{TA} + T_{IFS}) + ccaTime + T_{TA} + T_{DATA} + T_{TA} + T_{BResponse} + T_{IFS} \end{aligned} \tag{5.46}$$

which means that there are no transmission errors. For this case the number of retransmissions, is given by $j = 0$.
If after CCA, a node determines that the channel is found to be idle, the aggregated packets are sent and a *BACK Response* is correctly received, indicating that some packets need

retransmission, $D_{min\_Data\_Ret\_Piggy\_ACK}$, is given by:

$$H_{12} = H_{11} + \sum_{i=1}^{m} [(j_i - 1) \times (ccaTime + T_{TA} + T_{DATA} + T_{AW})] + \sum_{i=1}^{m} (ccaTime + T_{TA} + T_{DATA} + T_{TA} + T_{ACK} + T_{IFS}) \quad (5.47)$$

The number of retransmitted packets, $MaxRet$, can only be retransmitted $(j_i - 1)$ times until $MaxRet$, has been reached, we assume that the ACK packet has been received, which represents the last case given by $\sum_{i=1}^{m}(ccaTime + T_{TA} + T_{DATA} + T_{TA} + T_{ACK} + T_{IFS})$.

It is worthwhile to mention that the term j_i represents the number of retransmissions, and could be different for each retransmitted packet, for $j \in [1, MaxRet]$.

By combining Equations (5.44) and (5.45), the minimum average delay, D_{min_Piggy}, due to the channel state (i.e., busy or idle) and packet retransmissions is given by:

$$D_{min\_Piggy} = \frac{D_{min\_CCA\_BACK} + D_{min\_Data\_Ret\_BACK\_ACK}}{n} \quad (5.48)$$

In SBACK-MAC with no *BACK Request*, by considering an erroneous channel, the maximum average throughput, S_{max_Piggy}, in bits per second, by considering packet retransmissions is given by:

$$S_{max\_Piggy} = \frac{8L_{DATA}}{D_{min\_Piggy}} \quad (5.49)$$

B. Retransmissions by using an NAV extra time

The second proposed mechanism involves to use a longer NAV period, accounting the retransmission of k lost packets, Figure 5.18.b). In this case, there is no ACK to confirm that a given packet has successfully reached the destination, and nodes only try to retransmit a packet once.

In SBACK-MAC with no *BACK Request*, the minimum delay, $D_{min\_Data\_Ret\_Piggy\_NAV}$, when the channel is found to be idle during CCA, there is a data transmission (by considering aggregation) and the retransmission process is ruled by a NAV extra time is given as follows:

$$D_{min\_Data\_Ret\_Piggy\_NAV} = \begin{cases} H_{15} & , for\ j = 0 \\ H_{16} & , for\ j = 1 \end{cases} \quad (5.50)$$

where j is the number of packet retransmissions, and could range between 1 and the maximum number of retransmissions, $MaxRet$, as defined in [WPAN06].

By analysing Equation (5.50), the following conclusions can be reached:

If after CCA, a node determines that the channel is found to be idle, the aggregated packets are sent and a *BACK Response* is correctly received, confirming that all the transmitted packets have successfully reach the destination, $D_{min\_Data\_Ret\_Piggy\_NAV}$, is given by:

$$H_{15} = T_{TA} + T_{RTS\_ADDBA} + T_{TA} + T_{CTS\_ADDBA} \sum_{i=1}^{N_{agg}-1} (ccaTime + T_{TA} + T_{DATA} + T_{TA} + T_{IFS}) + ccaTime + T_{TA} + T_{DATA} + T_{TA} + T_{BResponse} + T_{IFS} \quad (5.51)$$

which means that there are no transmission errors. For this case the number of retransmissions, is given by $j = 0$.
If after CCA, a node determines that the channel is found to be idle, the aggregated packets are sent and a *BACK Response* is correctly received, indicating that some packets need retransmission, $D_{min\_Data\_Ret\_Piggy\_NAV}$, is given by:

$$H_{16} = H_{15} + \sum_{i=1}^{k}(ccaTime + T_{TA} + T_{DATA} + T_{TA} + T_{IFS}) \quad (5.52)$$

where k represents the number of aggregated packets that are allowed to be retransmitted like in [WPAN12]. This means that this value must be carefully selected depending on the application, since nodes may need to retransmit only a few data packets, or in an extreme case there is the need to retransmit all the aggregated packets.
By combining Equations (5.44) and (5.50), the minimum average delay, $D_{min\_Piggy\_NAV}$, due to the channel state (i.e., busy or idle) and packet retransmissions is given by:

$$D_{min\_Piggy\_NAV} = \frac{D_{min\_CCA\_Piggy} + D_{min\_Data\_Ret\_Piggy\_NAV}}{n} \quad (5.53)$$

In SBACK-MAC with *BACK Request*, by considering an erroneous channel, the maximum average throughput, S_{max_Piggy}, in bits per second, by considering packet retransmissions is given by:

$$S_{max\_Piggy\_NAV} = \frac{8L_{DATA}}{D_{min\_Piggy\_NAV}} \quad (5.54)$$

5.5 State Transition Diagram for IEEE 802.15.4 and SBACK-MAC

Figure 5.20 presents the state transition diagram for the SBACK-MAC and IEEE 802.15.4. There are 8 states been shared by both IEEE 802.15.4 and SBACK-MAC.The BACK mechanism is activated in the **TYPE ACK** state. The characterisation of possible states for the state machine is the following one:

States associated to transitions

- **IDLE_1**: The node is "ON", and there is no scheduled activity to take place;
- **BACKOFF_2**: The node will delay any activities for a random number of backoff periods;
- **CCA_3**: The node will use the PHY layer to determine the channel occupancy;
- **TRANSMIT_4**: The node transmit RTS, *RTS ADDBA*, DATA and *BACK Request* packets;
- **WAIT_ACK_5**: The node waits for an ACK packet;
- **WAIT_CTS_6**: The node waits for CTS or *CTS ADDBA* packets;
- **WAIT_BACK_RESPONSE_7**: The node waits for a *BACK Response* packet;
- **WAIT_SIFS_8**: The time between the reception of RTS, *RTS ADDBA, BACK Request* and DATA packets and the transmission of CTS, *CTS ADDBA*, *BACK Response* and ACK packets;
- **TRANSMIT_ACK_9**: The node transmits ACK packets;

- **TRANSMIT_CTS_10**: The node transmits CTS or *CTS ADDBA* packets;
- **TRANSMIT_*BACK Response*_11**: The node transmits *BACK Response* packets;
- **TRANSMIT_SYNCH_12**: the node transmits SYNCH packets;
- **ACK_POLICY_13**: The node will choose the use of normal ACK or BACK;
- **SLEEP_14**: The node will "turn OFF" the radio.

States of the packet

- **Type**: The type of the packet can be RTS, CTS, *RTS ADDBA*, *CTS ADDBA*, DATA, ACK, *BACK Request*, *BACK Response*, SYNCH;
- $N_{collisions}$: Number of collisions the packet as suffered;
- **Payload**;
- **Time of generation**;
- **Fragmentation**: If fragmentation is used;
- **Origin**;
- **Destination**;
- **First RTS**: Before sending packet put an RTS in first place on the queue to reserve the wireless medium;
- **Backoff value**.

Medium Access States

- **Free**: Medium is free, there is no ongoing transmission;
- **Busy**: Medium not free, there is a ongoing transmission.

Queue States

- **Not empty**: N packets are waiting for transmission;
- **Busy**: The buffer is empty.

Events that change the state of the machine

- **SLEEP_TIMEOUT**: Wake up from periodically sleep;
- **RETURN_TO_IDLE**: If the node has no packet to transmit, and have just choose the ACK Policy;
- **NAV_SLEEP_SCHEDULE**: Shutdown radio if a communication is sensed;
- **PERFORM BACKOFF**: Start the backoff procedure;
- **PERFORM CCA**: Start the CCA procedure;
- **CCA COMPLETE**: Channel is free, start transmission;
- **DATA/RTS/*RTS ADDBA*/*BACK Request* TRANSMISSION COMPLETE**: The node has successfully transmitted DATA, RTS, *RTS ADDBA and BACK Request* packets;

- **RETRANSMIT DATA/RTS/*RTS ADDBA/BACK Request* PACKET**: The node has successfully retransmitted DATA, RTS, RTS *ADDBA and BACK Request* packets;
- **ACK/CTS/*CTS ADDBA/BACK Response* RECEIVED**: The node has correctly received ACK, CTS, *CTS Response* and *BACK Response* packets;
- **PERFORM SIFS**: Start the SIFS procedure;
- **ACK/CTS/*CTS ADDBA/BACK Response* SIFS TIMEOUT**: Transmit ACK, CTS, *CTS Response* and *BACK Response* packets;
- **TYPE_OF_ACK_REQUEST**: ACK or BACK procedure;
- **TYPE_OF_ACK_REQUEST**: ACK or BACK procedure.

The state transition diagram for the SBACK-MAC and IEEE 802.15.4 was considered in the simulations by considering the WSN communication stack based on the MiXiM simulation framework [MiXi13] from the OMNeT++ [OMNe13] simulation engine. Figure 5.19 presents the main components that are responsible for simulating the channel access.

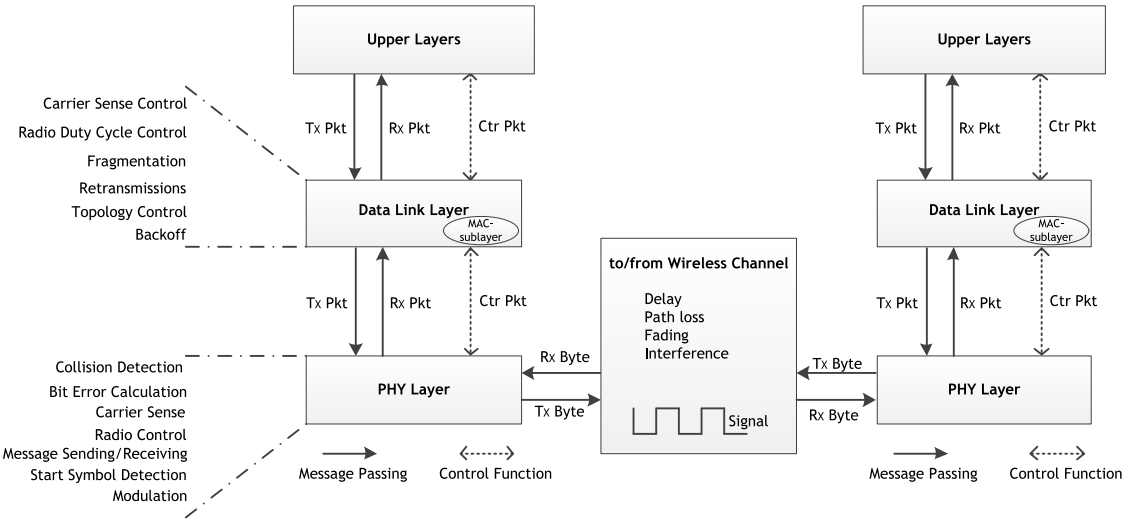

Figure 5.19: Layered model used by the IEEE 802.15.4 and SBACK-MAC

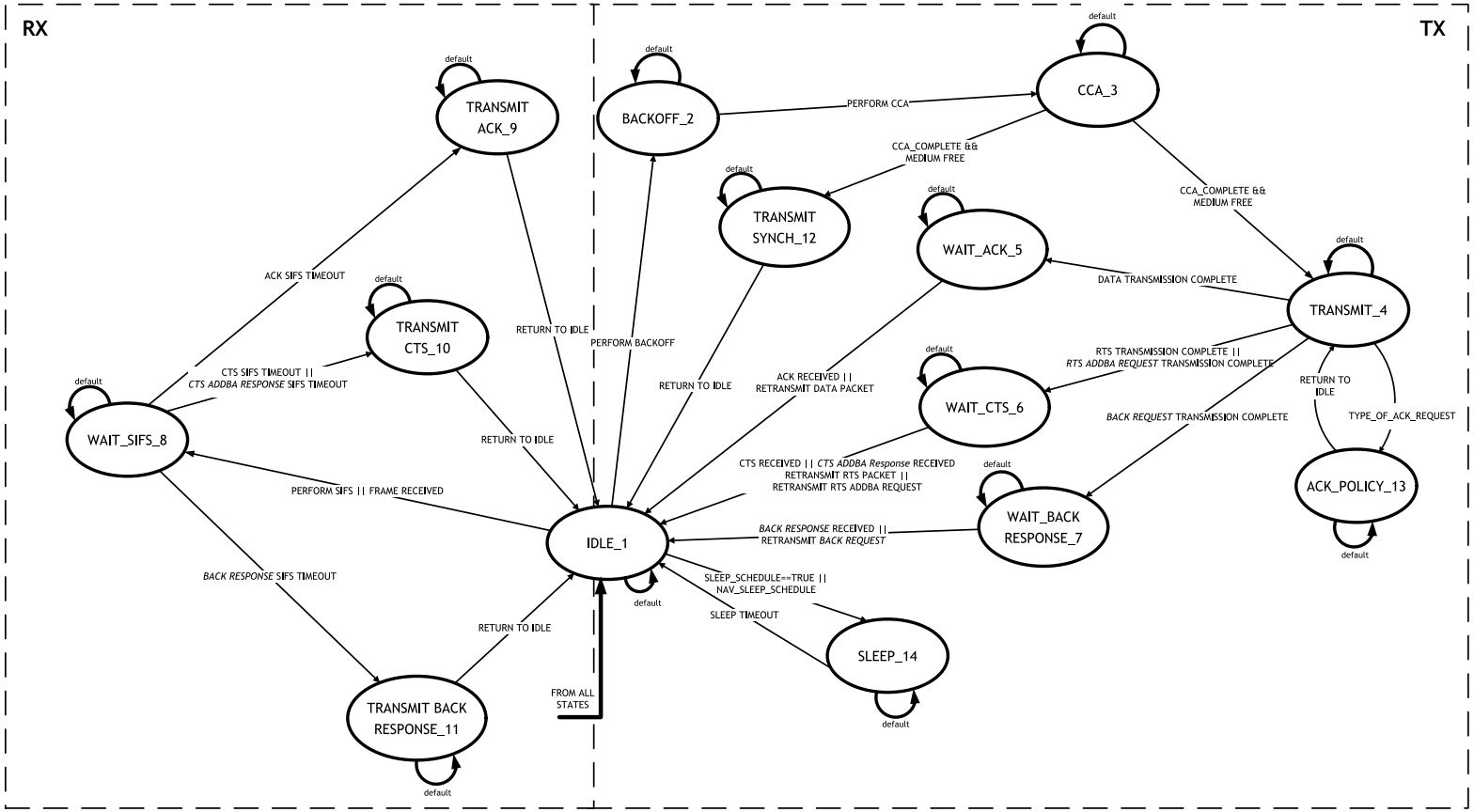

Figure 5.20: State transition diagram for IEEE 802.15.4 and SBACK-MAC.

5.6 Model for energy estimation

In order to know how much energy is spent by the SBACK-MAC protocol in each state an analytical model was conceived. A two-hop network, with two sources, one relay and two sinks, has been considered. Figure 5.21 shows the OMNeT++ [OMNe13] multi-hop star topology simulation setup. The packets from source node **A** flow, through node **C**, to sink node **D** while the packets originated by source node **B** flow, through node **C**, to reach sink node **E**.

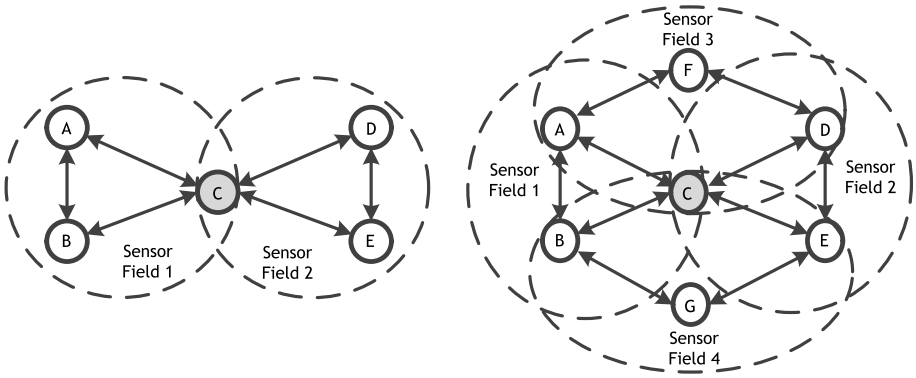

Figure 5.21: Multi-hop star topology simulation scenario: a) with no interferers and b) with two interferers.

The star network topology is challenging because there are abundant overhearing opportunities between neighbouring nodes. A node acting as coordinator may therefore take advantage of these opportunities to seek network optimisation. The star topology may also be viewed as a part of a larger network.Therefore, this type of network can be viewed as a building block for larger scale wireless networks. The performance metrics considered for a specific evaluation of the number of state transition of the SBACK-MAC protocol are the following ones:

- **Energy to Transmit**: is the amount of energy spent to transmit a packet;
- **Energy to Receive/Listen**: is the amount of energy spent to receive a packet or listen to the medium;
- **Energy to Sleep**: is the amount energy spent by a node during the time of inactivity (sleep state);
- **Energy Waste**: is the amount of energy spent by a node during the retransmission of a packet;
- **Total energy consumption**: is the total energy spent per node. The total energy consumption metric incorporates all previous metrics together into a single one. The intention is to have a joint perspective of all the factors that optimise the total energy in a global way.

The analysis of the sensor nodes performance is obtained through simulation by considering the CC2420, radio transceiver operating in the 2.4 GHz band. The reason for choosing the CC2420 radio transceiver from Chipcon is related to the fact that it currently the most popular radio chip on wireless sensor nodes [HeNL07].
Table 5.3 shows the specifications of the radio transceiver. Where P indicates the power spent by each state by considering a supply voltage of 3V.

Table 5.3: Specification of the CC2420 radio transceiver.

Parameter	CC2420
Frequency [GHz]	2.4
Modulation	O-QPSK
P_{Sleep} [μW]	0.06
$P_{Receive}$ [mW]	56.4
$P_{Transmit}$ [mW]	52.2
Data rate [kb/s]	250

The energy consumption of a given node over a period of time *t* is given as follows:

$$E(t) = (t_{tx} \times P_T) + (t_{rx} \times P_R) + (t_{sleep} \times P_S) + (t_{idle} \times P_I) \quad (5.55)$$

The mean of each variable is presented in Table 5.4.

Table 5.4: Notations for energy estimation.

Notation	Parameter
t_{tx}	Time on TX state
P_T	Power consumption in the transmitting state
t_{rx}	Time on RX state
P_R	Power consumption in the receiving state
t_{sleep}	Time on SLEEP state
P_S	Power consumption in the sleep state
t_{idle}	Time on IDLE state
P_I	Power consumption in the idle state

5.7 Performance Evaluation for IEEE 802.15.4 in the presence/ absence of RTS/CTS combined with packet concatenation

In this Section, we evaluate IEEE 802.15.4 with and with no RTS/CTS by using the MiXiM simulation framework [MiXi13] from the OMNeT++ [OMNe13] simulator. Figure 5.21.a) presents a two-hop network topology, with two sources, one relay, two sinks.

Figure 5.21.b) considers the same topology but two interferers are considered. Packets flow from source node **A**, through node **C**, to sink node **D**, while the packets originated by source node **B** flow, through node **C**, to reach sink node **E**. This topology is a simple star topology where node **C** acts as a central node.

The interferer nodes **F** and **G** are responsible for sending broadcast packets that will collide with the packets being sent by both the sources and the central node (i.e., in the case of interference). The level of interference of nodes nodes **F** and **G** imposes the retransmission on average of 20 % of the total number of packets being exchanged in the network.

The maximum average throughput, S_{max}, the minimum average delay, D_{min}, and the bandwidth efficiency, η, have been obtained through simulation by considering five different seeds, and a 95% confidence interval. Table 5.1 presents the MAC parameters considered for the network in our simulations. The performance analysis of the proposed schemes is conducted for both the best-case scenario (no errors) and by assuming an erroneous channel.

5.7.1 Minimum average delay in the presence and absence of RTS/CTS

A. Dependence on the number of TX packets for a fixed payload of 3 bytes

Figure 5.22 presents the analytical and simulation results for the minimum average delay, D_{min}, versus the number of transmitted packets with and with no retransmissions, by considering IEEE 802.15.4 with and with no RTS/CTS, as presented in Figures 5.10 and 5.12. A fixed payload size of 3 bytes (i.e., L_{DATA}= 3 bytes) is considered.
In [CUKK10], the authors have show that for shorter packet sizes IEEE 802.15.4 results in lower bandwidth efficiency, delay and throughput. Therefore, we will simulate the worst case scenario for wireless sensor networks, showing that our proposed mechanism can improve channel efficiency even under this circumstances.

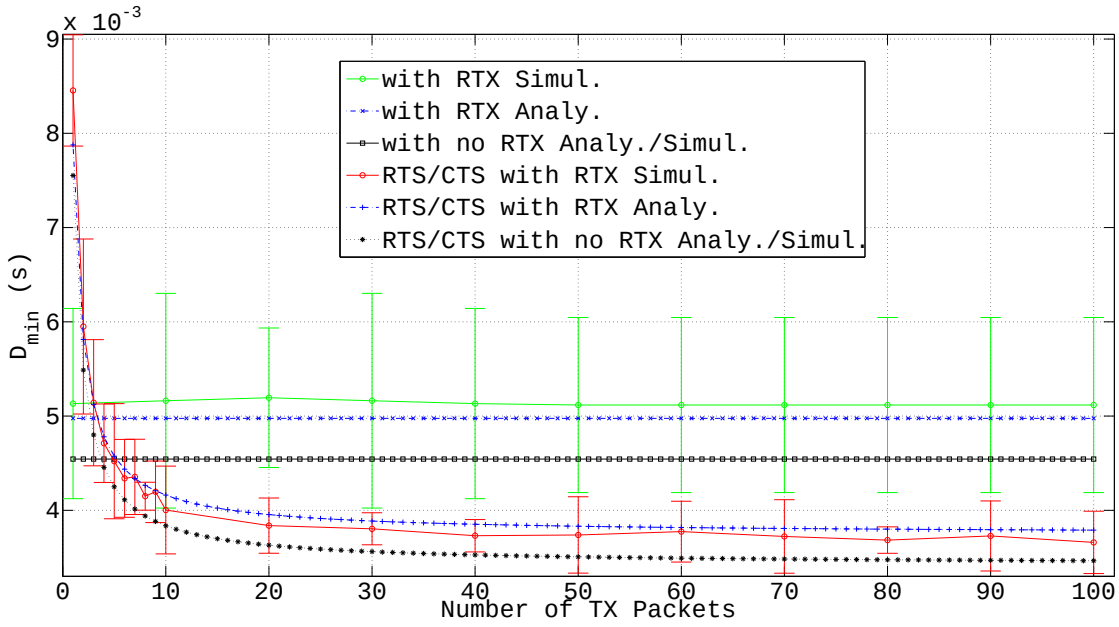

Figure 5.22: Minimum average delay as a function of the number of TX packets for a fixed payload size of 3 bytes for IEEE 802.15.4 with an with no RTS/CTS (no RTS/CTS is represented by the absence of the label RTS/CTS in the legend).

By analysing Figure 5.22 we conclude that by varying the number of TX packets, n, between 1 and 100, IEEE 802.15.4 basic access mode with no RTS/CTS globally presents the worst performance in terms of minimum average delay, D_{min}, for both the cases with and with no retransmissions. By comparing the case with no retransmissions with the one presented in [CUKK10], we conclude that the differences in terms of minimum average delay, D_{min}, are justified by the fact that the authors in [CUKK10] have not considered the time needed to switch the radio between the different states (i.e., $rxSetupTime$) [RoAO09].
The size of the 95 % confidence intervals shown in the simulations is explained by the fact that nodes will backoff for a random duration of time before attempting to access the channel later on, as presented in Equation (5.19). If the channel is found to be busy for each TX packet, nodes will double the backoff time counter during the backoff phase and the process is repeated until the maximum contention window is reached.
By considering IEEE 802.15.4 basic access mode with RTS/CTS combined with the packet concatenation feature, if the number of aggregated packets is higher than 5, IEEE 802.15.4 employing

RTS/CTS outperforms IEEE 802.15.4 with no RTS/CTS in terms of delay (and also throughput). This is explained by the fact that the backoff phase is not repeated for each transmitted data packet but only for each RTS/CTS set. Then, there is no backoff phase between two consecutive data packets, which allows for decreasing the total overhead, as shown in Figures 5.12.a) and b). Note that in Figure 5.22 the absence of RTS/CTS is represented by the absence of the label RTS/CTS in the legend.
For the case with retransmissions, since all the packets include the NAV duration, when nodes receive a packet that is not intended for them, they will avoid sending packets as long as this time has not expired. The retransmission process does not include the backoff phase like in the IEEE 802.15.4 basic access mode (i.e., $BE = 0$). By comparing the analytical and simulation results, we conclude that the theoretical results are similar and this actually verifies the accuracy of our proposed retransmission model. Performance results for D_{min} as a function of the number of TX packets show that, by using IEEE 802.15.4 with RTS/CTS with packet concatenation, for 5, 7 and 10 aggregated packets, D_{min} decreases 8 %, 14 % and 18 %, respectively. For more than 28 aggregated packets, D_{min} decreases approximately 30 %.

B. Dependence on the payload size for a number of transmitted packets equal to 10

Figure 5.23 presents the analytical results for the minimum average delay, D_{min}, as a function of the payload size by considering the four different scenarios presented on Figures 5.10 and 5.12. For this case the number of transmitted packets (aggregated) is equal to 10. The discontinuity around 18 bytes is due to the use of SIFS and LIFS (i.e., MPDU less of equal than 18 bytes must be followed by a SIFS, whilst MPDU longer than 18 bytes must be followed by a LIFS).
The results show that, IEEE 802.15.4 basic access mode with no RTS/CTS globally presents the worst performance in terms of minimum average delay, D_{min}, for both the cases with and with no retransmissions. By comparing IEEE 802.15.4 with no RTS/CTS with IEEE 802.15.4 with RTS/CTS and with retransmissions for small packets sizes (i.e., data payload less than 18 bytes), D_{min} is reduced by 25 %. For larger packet sizes, by considering the IEEE 802.15.4 standard with RTS/CTS, D_{min}, decreases 9 %. By comparing IEEE 802.15.4 with no RTS/CTS with IEEE 802.15.4 with RTS/CTS with no retransmissions for small packets sizes (i.e., data payload less than 18 bytes), D_{min} is reduced by 16 %. For larger packet sizes, by considering the IEEE 802.15.4 standard with RTS/CTS, D_{min}, decreases 9 % .

5.7.2 Maximum average throughput in the presence and absence of RTS/CTS

A. Dependence on the number of TX packets for a fixed payload of 3 bytes

Figure 5.24 compares the analytical and simulation results for the maximum average throughput, S_{max}, as a function of the number of TX packets, with and with no RTX between the cases of presence and absence of RTS/CTS.
By analysing Figure 5.24, we conclude that for the shortest payload sizes (i.e., $L_{DATA} = 3$), it is possible to improve the network performance by using the proposed RTS/CTS mechanism with packet concatenation. When the number of TX packets is higher than 5, IEEE 802.15.4 with RTS/CTS (with and with no retransmissions) achieves higher throughput in comparison to IEEE 802.15.4 with no RTS/CTS.

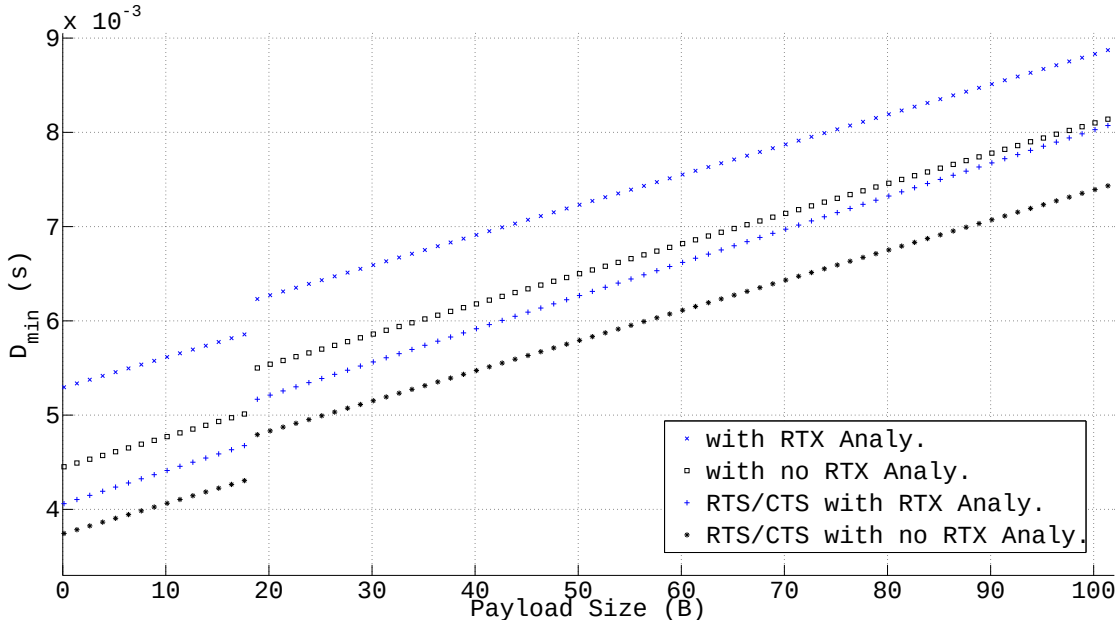

Figure 5.23: Minimum average delay as a function of the payload size for a number of TX packets equal to 10 for IEEE 802.15.4 with an with no RTS/CTS (no RTS/CTS is represented by the absence of the label RTS/CTS in the legend).

Moreover, we observe that by considering IEEE 802.15.4 in the basic access mode, S_{max} does not depend on the number of TX packets, and achieves the maximum value of 5.2 kb/s. For IEEE 802.15.4 with RTS/CTS combined with the packet concatenation feature, the maximum achievable throughput is 6.3 kb/s. Results for S_{max} as a function of the number of TX packets in IEEE 802.15.4 with RTS/CTS with packet concatenation show that, for 5, 7 and 10 aggregated packets, S_{max} increases 8 %, 14% and 18 %, respectively. For a number of aggregated packets higher than 28, S_{max} increases approximately 30 %.

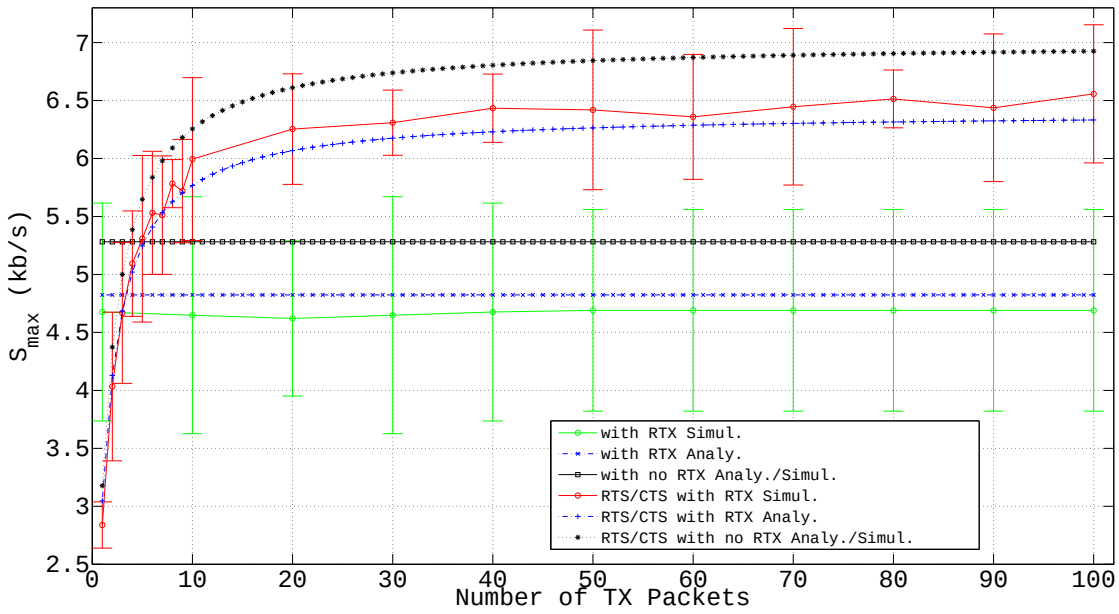

Figure 5.24: Maximum average throughput as a function of the number of TX packets for a fixed payload size of 3 bytes for IEEE 802.15.4 with an with no RTS/CTS (no RTS/CTS is represented by the absence of the label RTS/CTS in the legend).

B. Dependence on the payload size for a number of transmitted packets equal to 10

Figure 5.25 presents the analytical results for the maximum average throughput, S_{max}, as a function of the payload size by considering the four different scenarios presented on Figures 5.10 and 5.12.

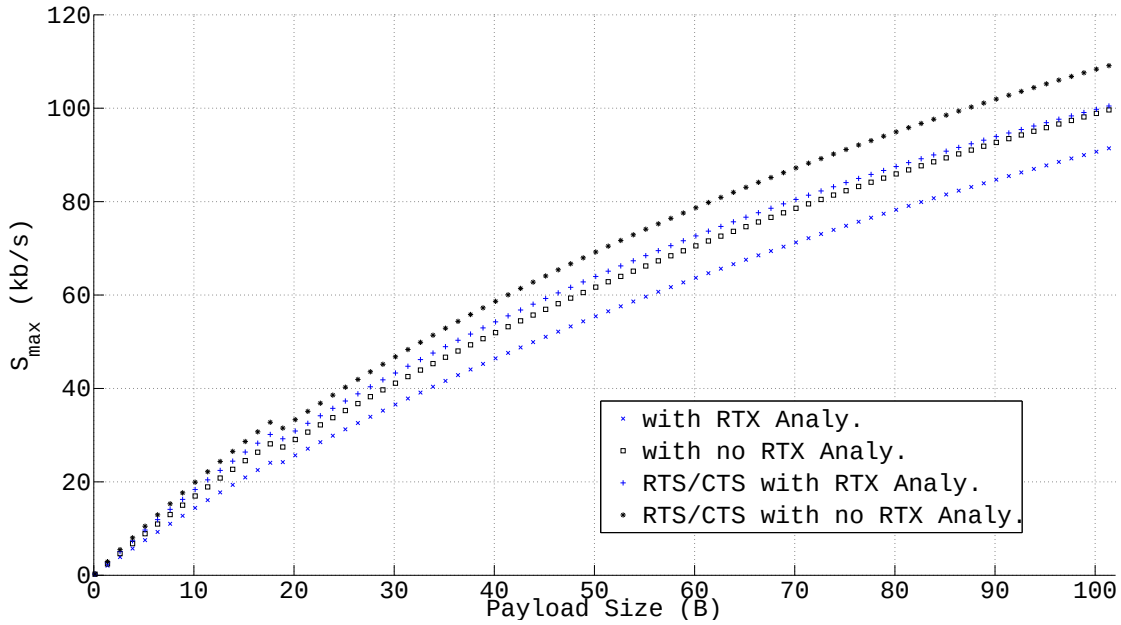

Figure 5.25: Maximum average throughput as a function of the of the payload size for a number of TX packets equal to 10 for IEEE 802.15.4 with an with no RTS/CTS (no RTS/CTS is represented by the absence of the label RTS/CTS in the legend).

The results show that IEEE 802.15.4 basic access mode with no RTS/CTS globally presents the worst performance in terms of maximum average throughput, S_{max}, for both the cases with and with no retransmissions. By comparing IEEE 802.15.4 not employing RTS/CTS with IEEE 802.15.4 employing RTS/CTS with retransmissions, for short packets sizes (i.e., data payload less than 18 bytes), S_{max}, increases 25 %. For longer packet sizes, by considering the IEEE 802.15.4 standard employing RTS/CTS, S_{max}, increases 9 %. By comparing IEEE 802.15.4 not employing RTS/CTS with IEEE 802.15.4 employing RTS/CTS with no retransmissions, for small packets sizes (i.e., data payload less than 18 bytes), S_{max} is increased 16 %. For longer packet sizes, by considering the IEEE 802.15.4 standard with RTS/CTS, S_{max}, increases 9 %.

5.7.3 Bandwidth efficiency in the presence and absence of RTS/CTS

The bandwidth efficiency, η, of IEEE 802.15.4 with and with no RTS/CTS, suggested by the authors from [LMMV05], is obtained by the following equation:

$$\eta = \frac{S_{max}}{R} \tag{5.56}$$

where R is the maximum data rate.

Figure 5.26 presents the bandwidth efficiency as a function of the number of TX packets, for a payload size of 3 bytes, again.

By analysing Figure 5.26 it is observable that, for IEEE 802.15.4 in the absence of RTS/CTS and with and with no retransmissions, the bandwidth efficiency is 1.9 % and 2.1 %, respectively. It

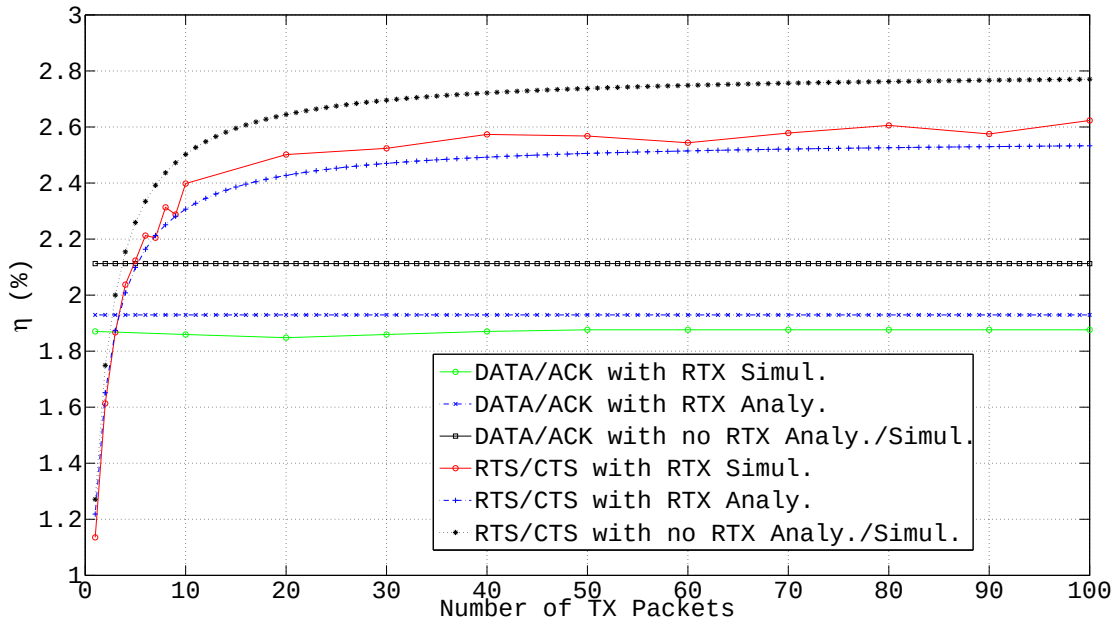

Figure 5.26: Bandwidth efficiency as a function of the number of TX packets for a fixed payload size of 3 bytes for IEEE 802.15.4 with an with no RTS/CTS (no RTS/CTS represents the absence of the label RTS/CTS in the legend).

can also be observed that, by varying the number of TX packets, the channel efficiency remains constant. The results show that, in the case of no retransmissions, the obtained results are very similar to the ones obtained in [CUKK10], [LMMV05], which again verifies the appropriateness of the proposed analytical formulation.

For IEEE 802.15.4 employing RTS/CTS and with and with no retransmissions, the bandwidth efficiency is dependent on the number of TX packet (by considering aggregation). The results show that by aggregating more than 5 packets IEEE 802.15.4 with RTS/CTS outperforms IEEE 802.15.4 with no RTS/CTS, in terms of bandwidth efficiency, η, where the maximum achievable value is 2.8% for payload size of 3 bytes.

Based on the results, we can conclude that even for short packet sizes (i.e., $L_{DATA} = 3$), by using the proposed RTS/CTS mechanism with packet concatenation, it is possible to improve channel efficiency.

5.8 Performance Evaluation for SBACK-MAC with and with no *BACK Request* by using a NAV extra time for retransmissions

In this Section we present the numerical results for the SBACK-MAC with and without *BACK Request* by considering an NAV extra time for retransmissions.

Figure 5.21.a) presents a two-hop network topology, with two sources, one relay, two sinks. Figure 5.21.b) considers the same topology but two interferers are considered. Packets flow from source node **A**, through node **C**, to sink node **D**, while the packets originated by source node **B** flow, through node **C**, to reach sink node **E**. This topology is a simple star topology where node **C** acts as a central node.

The interferer nodes **F** and **G** are responsible for sending broadcast packets that will collide with the packets being sent by both the sources and the central node (i.e., in the case of

interference). The level of interference of nodes nodes **F** and **G** imposes the retransmission on average of 20 % of the total number of packets being exchanged in the network.
The maximum average throughput, S_{max}, the minimum average delay, D_{min}, and the bandwidth efficiency, η, have been obtained through simulation by considering five different seeds, and a 95% confidence interval. Table 5.1 presents the MAC parameters considered for the network in our simulations. The performance analysis of the proposed schemes is conducted for both the best-case scenario (no errors) and by assuming an erroneous channel.
Appendix E presents extra results for the SBACK-MAC protocol with and without *BACK Request* by considering both the numerical and simulation results by using the MiXiM simulation framework [MiXi13] from the OMNeT++ [OMNe13], enabling to verify the validity of our analytical model presented in Section 5.4.3. The extra results include both the cases with retransmissions by using DATA/ACK handshake and the NAV extra time.

5.8.1 Minimum average delay in the presence and absence of *BACK Request*

A. Dependence on the number of TX packets for a fixed payload of 3 bytes

By analysing Figure 5.27, we conclude that for the shortest payload sizes (i.e., $L_{DATA} = 3$), it is possible to improve the network performance by using the SBACK-MAC with and with no *BACK Request* by using a NAV extra time. When the number of TX packets is higher than 7, SBACK-MAC with and with no *BACK Request* with and with no retransmissions, achieves lower delay in comparison to IEEE 802.15.4 in the basic access mode.
Performance results for D_{min} as a function of the number of TX packets show that, by using SBACK-MAC with and with no *BACK Request* with retransmissions, for 7 aggregated packets, D_{min} decreases 21 % and 35 %, respectively, when compared with the IEEE 802.15.4 basic access mode with retransmissions. For 10 aggregated packets, D_{min} decreases 31 % and 41 %, respectively, when compared with the IEEE 802.15.4 basic access mode with retransmissions. For more than 28 aggregated packets, by using SBACK-MAC with and with no *BACK Request* with retransmissions, D_{min} decreases 48 % and 53 %, respectively, when compared with the IEEE 802.15.4 basic access mode. By analysing Figure 5.27, we also conclude that by considering IEEE 802.15.4 employing RTS/CTS with no retransmissions (RTX) when the number of TX packet exceeds 40, it presents similar results when compared with SBACK-MAC with and with no *BACK Request* in which retransmissions are considered.

B. Dependence on the payload size for a number of transmitted packets equal to 10

Figure 5.28 presents the analytical results for the minimum average delay, D_{min}, as a function of the payload size by considering the four different scenarios presented on Figures 5.10, 5.12, 5.16 and 5.18. For this case the number of transmitted packets (aggregated) is equal to 10. The discontinuity around 18 bytes is due to the use of SIFS and LIFS (i.e., MPDU less of equal than 18 bytes must be followed by a SIFS, whilst MPDU greater than 18 bytes must be followed by a LIFS).
The results show that, IEEE 802.15.4 basic access mode globally presents the worst performance in terms of minimum average delay, D_{min}, for both the cases with and with no retransmissions. By considering SBACK-MAC with and with no *BACK Request* with retransmissions for small packets sizes (i.e., data payload less than 18 bytes), D_{min} is reduced by 50 % and 63%, respectively,

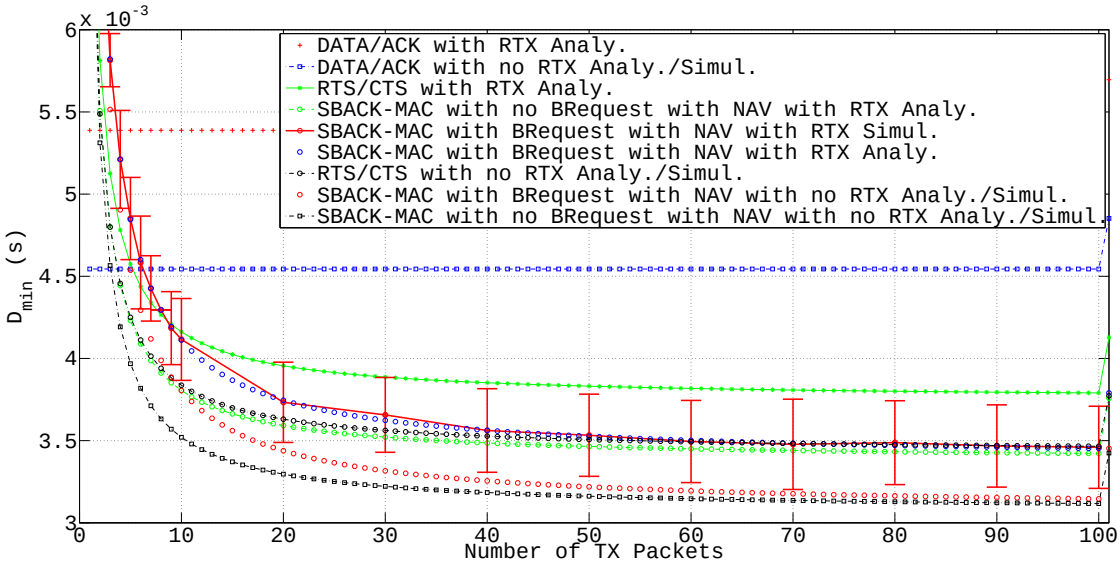

Figure 5.27: Minimum average delay as a function of the number of TX packets for a fixed payload size of 3 bytes for IEEE 802.15.4 with an with no RTS/CTS and SBACK-MAC with and with no *BACK Request*.

when compared with IEEE 802.15.4 basic access mode with retransmissions. For larger packet sizes, by considering the SBACK-MAC with and with no *BACK Request* with retransmissions, D_{min}, decreases 18 % and 30% when compared with IEEE 802.15.4 basic access mode with retransmissions. By comparing the analytical and simulation results, we conclude that the theoretical results are similar and this actually verifies the accuracy of our proposed retransmission model.

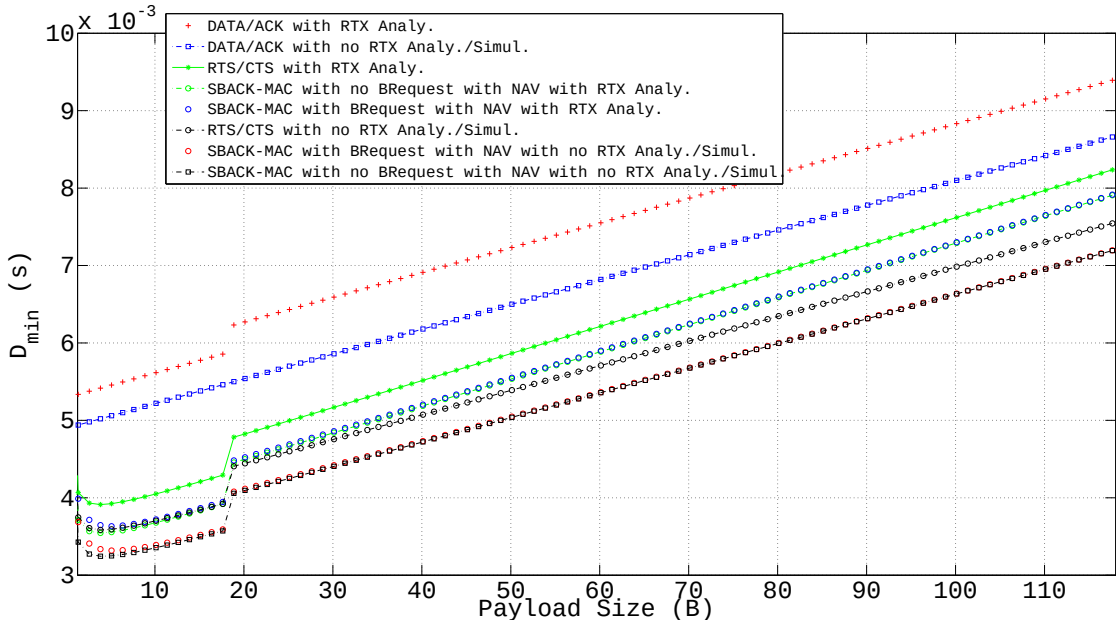

Figure 5.28: Minimum average delay as a function of the payload size for a number of TX packets equal to 10 for IEEE 802.15.4 with an with no RTS/CTS and SBACK-MAC with and with no *BACK Request*.

5.8.2 Maximum average throughput in the presence and absence of *BACK Request*

A. Dependence on the number of TX packets for a fixed payload of 3 bytes

By analysing Figure 5.29, we conclude that for the shortest payload sizes (i.e., $L_{DATA} = 3$), it is possible to improve the network performance by using the SBACK-MAC with and with no *BACK Request* by using a NAV extra time. When the number of TX packets is higher 7, SBACK-MAC with and with no *BACK Request* with and with no retransmissions, achieves shorter delay in comparison to IEEE 802.15.4 in the basic access mode. Performance results for S_{max} as a function of the number of TX packets show that, by using SBACK-MAC with and with no *BACK Request* with retransmissions, for 7 aggregated packets, S_{max} increases by 21 % and 35 %, respectively, when compared with the IEEE 802.15.4 basic access mode with retransmissions. For 10 aggregated packets, S_{max} increases by 31 % and 41 %, respectively, when compared with the IEEE 802.15.4 basic access mode with retransmissions. For more than 28 aggregated packets, by using SBACK-MAC with and with no *BACK Request* with retransmissions, S_{max} increases by 48 % and 53 %, respectively, when compared with the IEEE 802.15.4 basic access mode with retransmissions. By analysing Figure 5.29, we also conclude that by considering IEEE 802.15.4 with RTS/CTS with no retransmissions (RTX) when the number of TX packet is higher than 40, it presents similar results when compared with SBACK-MAC with and with no *BACK Request* with retransmissions.

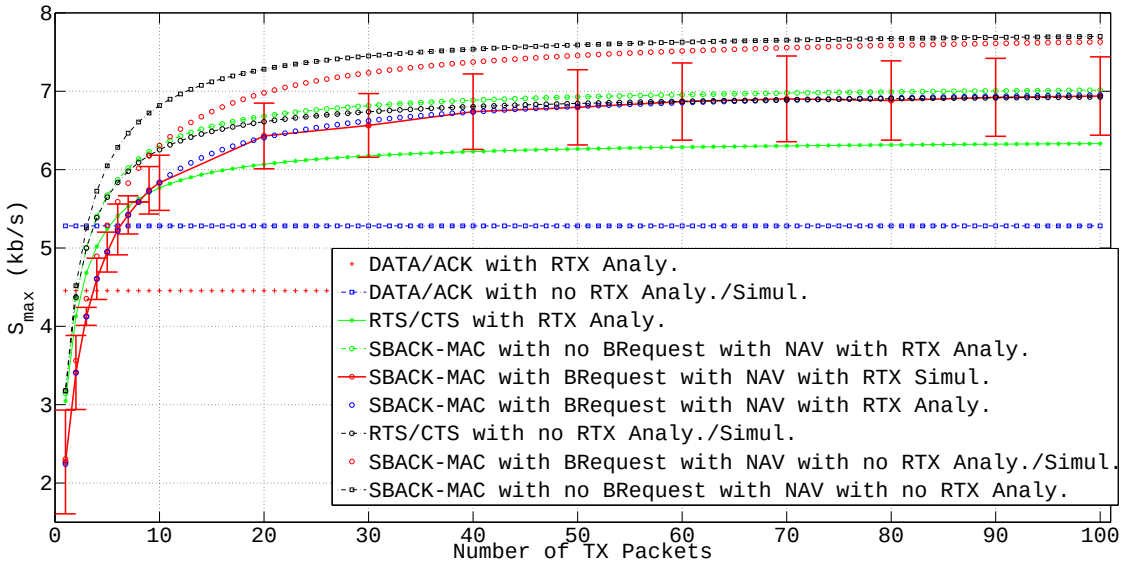

Figure 5.29: Maximum average throughput as a function of the number of TX packets for a fixed payload size of 3 bytes for IEEE 802.15.4 with an with no RTS/CTS and SBACK-MAC with and with no *BACK Request*.

B. Dependence on the payload size for a number of transmitted packets equal to 10

Figure 5.30 presents the analytical results for the maximum average throughput, S_{max}, as a function of the payload size by considering the four different scenarios presented on Figures 5.10 and 5.12.

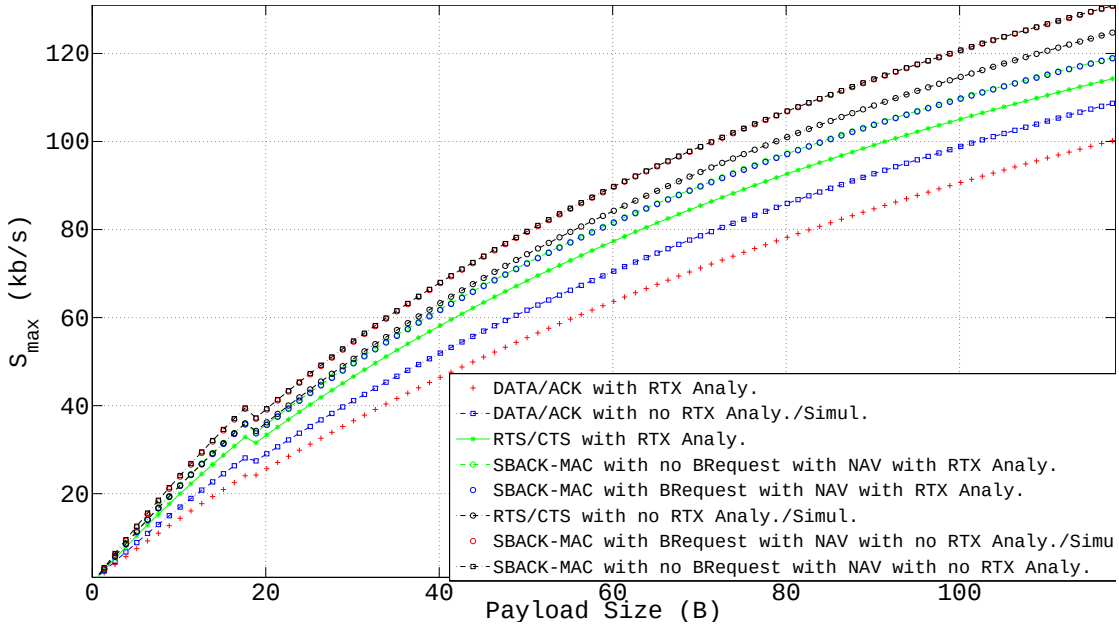

Figure 5.30: Maximum average throughput as a function of the payload size for a number of TX packets equal to 10 for IEEE 802.15.4 with an with no RTS/CTS and SBACK-MAC with and with no *BACK Request*.

The results show that, IEEE 802.15.4 basic access mode with no RTS/CTS globally presents the worst performance in terms of maximum average throughput, S_{max}, for both the cases with and with no retransmissions. By considering SBACK-MAC with and with no *BACK Request* with retransmissions for small packets sizes (i.e., data payload less than 18 bytes), S_{max}, increases by 41 % and 53% respectively, when compared with IEEE 802.15.4 basic access mode with retransmissions. For larger packet sizes, by considering SBACK-MAC with and with no *BACK Request* with retransmissions, S_{max}, increases by 18 % and 30% when compared with IEEE 802.15.4 basic access mode with retransmissions.

5.8.3 Bandwidth efficiency in the presence and absence of *BACK Request*

Figure 5.31 presents the bandwidth efficiency as a function of the number of TX packets, for a payload size of 3 bytes.

By analysing Figure 5.31 we can observe that for IEEE 802.15.4 in the absence of RTS/CTS and with and with no retransmissions, the bandwidth efficiency is 1.9 % and 2.1 %, respectively. It can also be observed that by varying the number of TX packets the channel efficiency remains constant. The results show that, in the case with no retransmissions, the obtained results are very similar to the ones obtained in [CUKK10] and [LMMV05], which again verifies the validity of the proposed analytical formulation.

For IEEE 802.15.4 with RTS/CTS and with and with no retransmissions, the bandwidth efficiency is dependent on the number of TX packet (by considering aggregation). The results show that by aggregating more than 5 packets IEEE 802.15.4 with RTS/CTS outperforms IEEE 802.15.4 with no RTS/CTS, in terms of bandwidth efficiency, η, where the maximum achievable value is 2.8 % for a payload size of 3 bytes. Based on the results, we can conclude that even for shortest packet sizes (i.e., $L_{DATA} = 3$), by using the proposed RTS/CTS mechanism with packet concatenation, it is possible to improve channel efficiency.

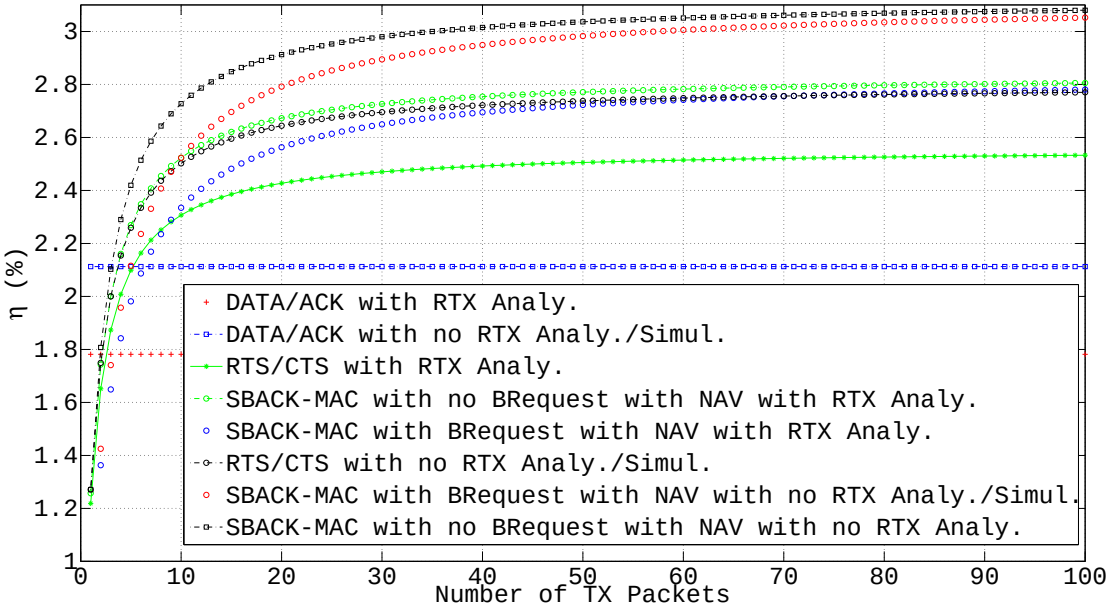

Figure 5.31: Bandwidth efficiency as a function of the number of TX packets for IEEE 802.15.4 with an with no RTS/CTS and SBACK-MAC with and with no *BACK Request*.

By using SBACK-MAC with and with no *BACK Request* with retransmissions, for 7 aggregated packets, η increases by 21 % and 35 %, respectively, when compared with the IEEE 802.15.4 basic access mode with retransmissions. For more than 30 aggregated packets, by using SBACK-MAC with and with no *BACK Request* with retransmissions, η increases by 48 % and 53 %, respectively, when compared with the IEEE 802.15.4 basic access mode with retransmissions.

5.9 Energy consumption for IEEE 802.15.4 in presence/absence of RTS/CTS and SBACK-MAC with and with no *BACK Request*

Figure 5.32 presents the average energy consumption as a function of the packet inter-arrival time for the CC2420 radio transceiver by considering the multi-hop star topology presented in Figure 5.21.a). Each source node (i.e., Node **A** and **B**) transmits 100 DATA packets with a data payload of 3 bytes (with a data generation interval between 1 and 10 s) to the coordinator node (effective data rate is 250 kb/s) that forwards the packet to the destination (i.e., Node **D** and **E**).

During one transmission cycle, there is only one active node that has always a frame to be sent whereas the other neighbouring nodes can only accept frames and provide ACKs or *BACK Responses*. Therefore, we are considering the best-case scenario (i.e., an ideal channel with no transmission errors). Table 5.5 presents the network parameters considered in the simulations. By analysing the results from Figure 5.32 one concludes that, when the packet inter-arrival time increases, the energy consumption of the radio transceiver also increases. This is explained by the fact that the radio transceiver needs to stays active for longer periods of time in order to deliver the packets being generated from the sources to the sink nodes. Therefore, the results for the energy consumption are lower in the case we have high traffic loads (the lowest packet inte-rarrival time), since the nodes are able to deliver packets faster and enter sooner in the sleep mode. In the case of a packet inter-arrival time of 1 s, source nodes are able to deliver all the data packets in the queue to the sink nodes in approximately 10 s, whereas for the

Table 5.5: Key simulation parameters.

Parameter	**Value**
Channel bitrate	250 kb/s
Operating frequency	2.4 GHz
Bandwidth	2 MHz
Modulation	O-QPSK
Transmitter power	0 dBm (1 mW)
Channel model	Free-space path loss
Path loss coefficient	2.5
Data Payload	3 bytes
Data packet size	18 bytes
Control packet sizes (ACK/RTS/CTS/*BACK Request*/*BACK Response)*	11 bytes
Duty cycle	12 %
Number of runs	5
Maximum simulation time	100 s
Packet inter-arrival time	from 1 to 10 s

case we have a packet inter-arrival time of 10 s, nodes need approximately 100 s to deliver the same amount of data. Moreover, the power spent in the RX/TX states is higher than in the SLEEP state. So, every time a node wakes-up and there is no task to perform, there will be an energy waste. This case is more frequent for longer packet inter-arrival times. Moreover, by using the SBACK-MAC protocol with and without *BACK Request* we decrease the total energy consumption of the network for all the inter-arrival periods. By comparing the obtained results for the energy consumption with the ones for the minimum average delay, D_{min}, presented in Figure 5.28, we conclude that there is a good match between the simulations and our analytical model. For the case with no retransmissions, SBACK-MAC with and with no *BACK Request* presents better performance when compared with IEEE 802.15.4 in the presence and absence of RTS/CTS. For all the cases the IEEE 802.15.4 standard in the basic access mode presents the worst performance in terms of energy.

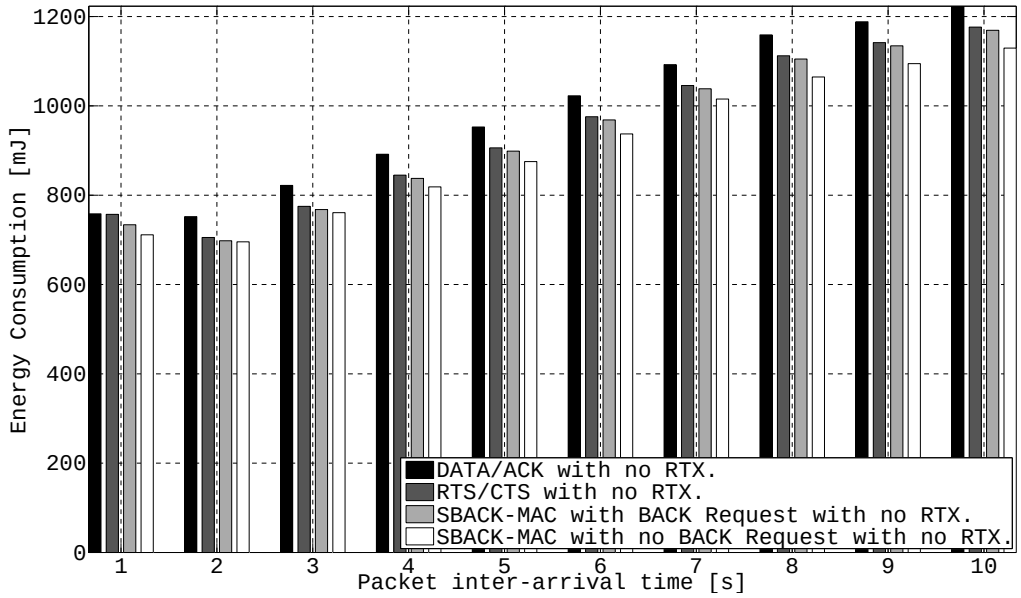

Figure 5.32: Energy consumption: a) IEEE 802.15.4 basic access, b) IEEE 802.15.4 with RTS/CTS, c) SBACK-MAC with *BACK Request* (concatenation) and d) SBACK-MAC with no *BACK Request* (piggyback).

5.10 Summary and conclusions

In this Chapter, we have proposed an IEEE 802.15.4 MAC layer enhancement by employing RTS/CTS combined with the packet concatenation feature for WSNs. The use of the RTS/CTS mechanism improves channel efficiency by decreasing the deferral time before transmitting a data packet. The proposed solution have shown that for the shortest payload sizes (i.e., $L_{DATA} = 3$) for the case with retransmissions, if the number of TX packets is lower than 5 (i.e., the number of aggregated packets), IEEE 802.15.4 with RTS/CTS and the application of packet concatenation achieves higher throughput values in comparison to IEEE 802.15.4 with no RTS/CTS even for shorter packet sizes. The advantage comes from not including the backoff phase into the retransmission process like IEEE 802.15.4 basic access mode (i.e., $BE = 0$). By comparing the analytical and simulation results, we conclude that the theoretical results are very similar and this actually verifies the accuracy of our proposed retransmission model. Performance results for, D_{min}, as a function of the number of TX packets show that, by using IEEE 802.15.4 with RTS/CTS with packet concatenation, for 5, 7 and 10 aggregated packets, D_{min}, decreases by 8 %, 14% and 18 %, respectively. For more than 28 aggregated packets, D_{min} decreases approximately 30 %.

This Chapter also presents the SBACK-MAC, a new innovative MAC protocol that uses a BACK mechanism to achieve channel efficiency for WSNs. The use of a BACK mechanism improves channel efficiency by aggregating several ACK into one special packet, the *BACK Response*. Two innovative solutions were proposed to improve the IEEE 802.15.4 performance. The first one considers the SBACK-MAC protocol in the presence of *BACK Request* (concatenation mechanism), while the second considers the SBACK-MAC in the absence of *BACK Request* (piggyback mechanism). The results have shown that for the shortest payload sizes (i.e., $L_{DATA} = 3$), it is possible to improve the network performance by considering the SBACK-MAC with and with no *BACK Request* by using a NAV extra time. When the number of TX packets is higher than 7, SBACK-MAC with and with no *BACK Request* with and with no retransmissions, achieves lower delay in comparison to IEEE 802.15.4 in the basic access mode as shows in Figure 5.33. Performance results for D_{min} as a function of the number of TX packets show that, by using SBACK-MAC with and with no *BACK Request* with retransmissions, for 7 aggregated packets, D_{min} decreases by 21 % and 35 %, respectively, when compared with the IEEE 802.15.4 basic access mode with retransmissions. For 10 aggregated packets, D_{min} decreases by 31 % and 41 %, respectively, when compared with the IEEE 802.15.4 basic access mode with retransmissions. For more than 28 aggregated packets, by using SBACK-MAC with and with no *BACK Request* with retransmissions, D_{min} decreases by 48 % and 53 %, respectively, when compared with the IEEE 802.15.4 basic access mode. Moreover, by considering IEEE 802.15.4 with RTS/CTS with no retransmissions (RTX) when the number of TX packet higher than 40, it presents similar results when compared with SBACK-MAC with and with no *BACK Request* with retransmissions. Figure 5.33 presents the decrease of the minimum average delay, D_{min}, for the proposed MAC sublayer protocols employing RTS/CTS with packet concatenation as a function of the number of TX packets, for the shortest payload sizes (i.e., $L_{DATA} = 3$).

Moreover, we observe that by considering IEEE 802.15.4 in the basic access mode, the maximum average throughput, S_{max}, does not depend on the number of TX packets, and achieves the maximum value of 5.2 kb/s. For IEEE 802.15.4 with RTS/CTS combined with the packet concatenation feature, the maximum achievable throughput is 6.3 kb/s. Results for S_{max} as a function of the number of TX packets in IEEE 802.15.4 with RTS/CTS with packet concatenation show that, for 5, 7 and 10 aggregated packets, S_{max} increases by 8 %, 14 % and 18 %,

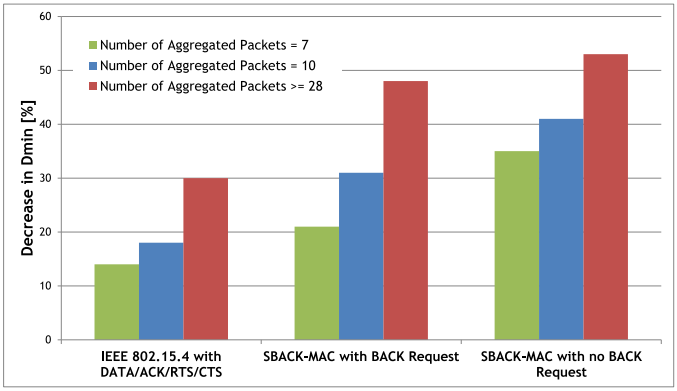

Figure 5.33: Decrease of the minimum average delay, as a function of the number of TX packets for the presented mechanisms employing RTS/CTS by considering a data payload of 3 bytes.

respectively, as shown in Figure 5.34. For a number of aggregated packets higher than 28, S_{max} increases approximately 30 %. Performance results for S_{max} as a function of the number of TX packets show that, by using SBACK-MAC with and with no *BACK Request* with retransmissions, for 7 aggregated packets, S_{max} increases by 21 % and 35 %, respectively, when compared with the IEEE 802.15.4 basic access mode with retransmissions. For 10 aggregated packets, S_{max} increases by 31 % and 41 %, respectively, when compared with the IEEE 802.15.4 basic access mode with retransmissions. For more than 28 aggregated packets, by using SBACK-MAC with and with no *BACK Request* with retransmissions, S_{max} increases by 48 % and 53 %, respectively, when compared with the IEEE 802.15.4 basic access mode with retransmissions. By analysing Figure 5.29, we also conclude that by considering IEEE 802.15.4 with RTS/CTS with no retransmissions (RTX) when the number of TX packet exceeds 40, it presents similar results when compared with SBACK-MAC with and with no *BACK Request* with retransmissions.
The proposed mechanisms also show that for more than 10 TX packets the bandwidth efficiency and energy consumption will be improved by do not considering the backoff phase between two consecutive data packets and by postpone ACKs via the use of the *BACK Response* control packet allowing for the aggregation of several ACK responses into one single packet. Figure 5.34 presents the decrease of the maximum average throughput, S_{max}, for the proposed MAC sub-layer protocols employing RTS/CTS with packet concatenation as a function of the number of TX packets, for the shortest payload sizes (i.e., $L_{DATA} = 3$).

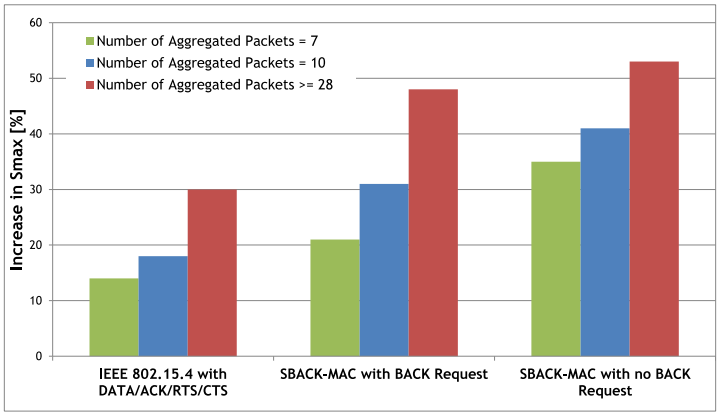

Figure 5.34: Increase of the maximum average throughput, as a function of the number of TX packets for the presented mechanisms employing RTS/CTS by considering a data payload of 3 bytes.

Chapter 6

Conclusions and Suggestions for Future Research

6.1 Conclusions

The interdisciplinary research on Wireless Sensor Networks (WSNs) is stimulating the development of totally new WSN services and applications to be supported by sensor nodes in the context of smart environments. In five years time, a massive scale deployment of WSNs applied to a wide range of applications and will certainly change the way people interact, live or even work within the surrounding ambient [BoVL13].

This thesis gives contributions on innovative energy-efficient WSN applications in Chapter 2, namely for medical environments and structure integrity health monitoring. Different prototype sensor belts have been conceived within the Smart-Clothing project, which aim at detecting the foetal movements in the last four weeks in a pregnant woman. The pregnant women can be either at home or in the hospital. An hierarchical wireless network with a Wi-Fi layer on top of the WSN was developed allowing for extra flexibility in data communication. An automatic measurement system based on the IEEE 802.15.4 standard for monitoring the temperature and humidity within civil engineering structures have also been conceived in the framework of the INSYSM project. This system can be very useful when carrying out large works in concrete, such as dams or bridges where the volume of concrete involved is massive. Since the curing process is the process that defines the concrete quality, if the values of humidity and temperature are known, the premature drying of the concrete surface can be avoided by hydrating it. This in turn, decreases cracking and increases concrete quality. Moreover, since the SHT15 and STH21 humidity and temperature sensors use a filter cap allowing for protecting the sensors from the alkaline environment they will not breakdown under hazardous conditions.

Chapter 3 gives contributions on the development of an energy self-sustainable WSN by considering RF energy harvesting as the primary energy source within the PROENERGY-WSN project.

The spectrum opportunities for RF energy harvesting to power supply the wireless sensor nodes in real indoor/outdoor scenarios have been identified. Moreover, a dual-band printed antenna has also been presented, with gains of the order of 1.8-2.06 dBi and 77.6-84 % efficiency respectively. The design of RF energy harvesting circuits have also been analysed, and the behaviour of a 5-stage Dickson voltage multiplier is obtained trough simulation and experimental results for power supplying an IRIS mote. Moreover, the PHY, MAC and network layers aspects of WBANs with electromagnetic energy harvesting and CR capabilities have also been addressed, showing that that CR offers a viable and future proof solution for addressing both scalability and coexistence issues.

In Chapter 4, different parameters related with WSN platforms have been evaluated. These parameters were addressed by taking into account three different groups of criteria: i) main characteristics, ii) power requirements and iii) expansibility, programming and community resources. By analysing the overall performance, we conclude that the Waspmote is the WSN platform that globally is ranked as the one that presents the best performance. It is worthwhile to mention that, since some criteria are more important than others, choosing the best

platform for WSNs depends on the criteria taken into account, as well as the application requirements.

In Chapter 5, the enhancement of the IEEE 802.15.4 MAC layer has been proposed by employing RTS/CTS combined with the packet concatenation feature for WSNs. The use of the RTS/CTS mechanism improves channel efficiency by decreasing the deferral time before transmitting a data packet. The proposed solution has shown that, even for the case with retransmissions, if the number of TX packets is lower than 5 (i.e., the number of aggregated packets), IEEE 802.15.4 employing RTS/CTS combined with concatenation achieves higher values for the throughput in comparison to IEEE 802.15.4 with no RTS/CTS even for shorter packet sizes. The advantage comes from not including the backoff phase into the retransmission process like the IEEE 802.15.4 basic access mode (i.e., $BE = 0$). By comparing the analytical and simulation results, we conclude that there is a perfect match. This actually verifies the accuracy of our proposed retransmission model. Performance results for the minimum average delay, D_{min}, as a function of the number of TX packets and by assuming a fixed payload size of 3 bytes (i.e., L_{DATA}=3 bytes) show that, by using IEEE 802.15.4 with RTS/CTS with packet concatenation, for 5, 7 and 10 aggregated packets, D_{min}, decreases by 8 % 14 % and 18 %, respectively. For more than 28 aggregated packets, D_{min} decreases approximately 30 %.

Moreover, we observe that by considering IEEE 802.15.4 in the basic access mode, the maximum average throughput, S_{max}, does not depend on the number of TX packets, and achieves the maximum value of 5.2 kb/s. For IEEE 802.15.4 with RTS/CTS combined with the packet concatenation feature, the maximum achievable throughput is 6.3 kb/s. In IEEE 802.15.4 employing RTS/CTS with packet concatenation, results for S_{max} as a function of the number of TX packets show that, for 5, 7 and 10 aggregated packets, S_{max} increases by 8 %, 14 % and 18 %, respectively. For a number of aggregated packets higher than 28, S_{max} increases approximately 30 %. Table 6.1 presents a summary of the performance results for maximum average throughput, S_{max}, and minimum average delay, D_{min}, as a function of the number of TX packets by considering a fixed payload size, of 3 bytes.

Table 6.1: Performance results for the maximum average throughput, S_{max} and minimum average delay, D_{min}, as a function of the number of transmitted packets relatively to IEEE 802.15.4 in the basic access mode by considering a fixed payload size of 3 bytes.

MAC protocol	**Number of Aggregated Pkts = 7**		**Number of Aggregated Pkts = 10**		**Number of Aggregated Pkts >= 28**	
	Increase S_{max} [%]	*Decrease D_{min} [%]*	*Increase S_{max} [%]*	*Decrease D_{min} [%]*	*Increase S_{max} [%]*	*Decrease D_{min} [%]*
IEEE 802.15.4 with RTS/CTS	14	14	18	18	30	30
SBACK-MAC with *BACK Request*	21	21	31	31	48	48
***SBACK-MAC with no* BACK Request**	35	35	41	41	53	53

Chapter 5 also presents the SBACK-MAC, a new innovative MAC protocol that uses a BACK mechanism to achieve channel efficiency for WSNs. The use of a BACK mechanism improves channel efficiency by aggregating several ACK into one special packet, the *BACK Response*. Two innovative solutions were proposed to improve the IEEE 802.15.4 performance. The first one considers the SBACK-MAC protocol in the presence of *BACK Request* (concatenation mechanism), while the second considers the SBACK-MAC in the absence of *BACK Request* (piggyback mechanism). The results showed that, for the shortest payload sizes (i.e., $L_{DATA} = 3$), it is possible to

improve the network performance by using the SBACK-MAC with and with no *BACK Request* by using a NAV extra time. When the number of TX packets is higher than 7, SBACK-MAC with and with no *BACK Request,* with and with no retransmissions, achieves lower delay in comparison to IEEE 802.15.4 in the basic access mode. By comparing the analytical and simulation results, we conclude that there is a perfect match, which enables to verify the accuracy of our model. Performance results for D_{min} as a function of the number of TX packets show that, by using SBACK-MAC with and with no *BACK Request* with retransmissions, for 7 aggregated packets, D_{min} decreases by 21 % and 35 %, respectively, when compared with the IEEE 802.15.4 basic access mode with retransmissions. For 10 aggregated packets, D_{min} decreases 31 % and 41 %, respectively, when compared with the IEEE 802.15.4 basic access mode with retransmissions. For more than 28 aggregated packets, by using SBACK-MAC in the presence and absence of *BACK Request* with retransmissions, D_{min} decreases by 48 % and 53 %, respectively, when compared with the IEEE 802.15.4 basic access mode. Moreover, by considering IEEE 802.15.4 with RTS/CTS with no retransmissions (RTX) when the number of TX packet higher than 40, it presents similar results when compared with SBACK-MAC with and with no *BACK Request* with retransmissions.
Performance results for S_{max} as a function of the number of TX packets show that, by using SBACK-MAC with and with no *BACK Request* with retransmissions, for 7 aggregated packets, S_{max} increases by 21 % and 35 %, respectively, when compared with the IEEE 802.15.4 basic access mode with retransmissions. For 7 aggregated packets, S_{max} increases by 31 % and 45 %, respectively, when compared with the IEEE 802.15.4 basic access mode with retransmissions. For more than 28 aggregated packets, by using SBACK-MAC with and with no *BACK Request* with retransmissions, S_{max} increases by 48 % and 53 %, respectively, when compared with the IEEE 802.15.4 basic access mode with retransmissions. We also conclude that by considering IEEE 802.15.4 with RTS/CTS with no retransmissions when the number of TX packet exceeds 40, S_{max}, presents similar results when compared with SBACK-MAC with and with no *BACK Request* with retransmissions.
The proposed mechanisms also show that for more than 10 TX packets the bandwidth efficiency and energy consumption will be improved by do not considering the backoff phase between two consecutive data packets and by postpone ACKs via the use of the *BACK Response* control packet allowing for the aggregation of several ACK responses into one single packet.
This thesis has given innovative contributions on the following main issues:

- Development and implementation of application-specific WSN solutions and strategies applied in real world applications such as: medical environments, civil engineering and utilities;
- Test of RF energy harvesting circuits for enabling energy self-sustainable WSN by considering electromagnetic energy harvesting as the primary energy source;
- Establishment of an evaluation criteria to obtain the overall performance of the hardware platforms, three different groups of criteria have been identified: i) main characteristics, ii) power requirements and iii) expansibility, programming and community resources.
- Evaluation of the IEEE 802.15.4 MAC layer performance by using the RTS/CTS combined with packet concatenation through numerical and simulation results;
- Proposal of an innovative MAC protocol that uses a BACK mechanism to achieve channel efficiency, the SBACK-MAC protocol. The SBACK-MAC allows the aggregation of several

ACK responses in one special packet. Two different solutions are addressed. The first one considers the SBACK-MAC protocol in the presence of *BACK Request* (concatenation) while the second one considers the SBACK-MAC in the absence of *BACK Request* (piggyback);

- Mathematical derivation of the maximum average throughput and the minimum average delay for the proposed mechanisms, either under ideal conditions (a channel environment with no transmission errors) or non ideal conditions (a channel environment with transmission errors), for IEEE 802.15.4 with and with no RTS/CTS and SBACK-MAC with and with no *BACK Request*.

6.2 Suggestions for Future Work

As future research, we propose the creation of a webpage enabling for access the data in real time in the cloud for the real time applications developed in the scope of this thesis.
Another suggestion for further research is to implement the SBACK-MAC with no *BACK Request* in the OMNeT++ simulator, since in the scope of this thesis we only derive the analytical model for the maximum average throughput and minimum average delay. In addition, we plan to compare the IEEE 802.15.4 with and with no RTS/CTS with SBACK-MAC with and with no *BACK Request* by considering the new optional Chirp Spread Spectrum (CSS) PHY layer at the 2.4 GHz frequency band, that enables to achieve a maximum data rate of 1 Mb/s against the results obtained in this thesis where the maximum data rate is 250 kb/s.
Finally, the performance of the innovative MAC sub-layer protocols proposed in this thesis will be verified through experimental measurements by using WSN hardware platforms (e.g., Waspmote platform), while varying the number of transmitted packets, the payload and the number of nodes.

Appendix A

IEEE 802.15.4 Standard

This Appendix presents the PHY and MAC layer specifications for the IEEE 802.15.4 standard and is organized into two parts: Section A.1 addresses the PHY aspects whilst Section A.2 discusses the MAC sub-layer aspects.

A.1 Physical Layer

The IEEE 802.15.4 PHY layer is responsible for providing the medium interface where the actual communication occurs. The PHY layer is the lowest component in the WSN protocol stack and is in responsible for providing control (activation and deactivation) of the radio transceiver, energy detection, link quality indication, CCA, channel selection, and data transmission/reception [GuCB03].

A.1.1 Channel Assignments

IEEE 802.15.4 networks can operate in several different frequency channels that are defined through a combination of channel numbers and pages allowing for identifying the frequency bands as well as the modulation employed. The channel pages where introduced in the IEEE 802.15.4-2006 standard allowing for distinguish between the different supported PHY layers as well as modulation schemes. In the previous release (i.e., the IEEE 802.15.4-2003 standard) there were no optional PHY layers with multiple frequency bands. One of the problems of the IEEE 802.15.4-2003 standard is that the modulation schemes were different for the 2.4 GHz, 868 MHz and 915 MHz frequency bands. Therefore, there was a need to change the local oscillator for each frequency as well as the modulator/demodulator block responsible for processing the signals. This in turn, imposes the use of separate processing blocks in order to support the different frequency bands. A larger portion of the radio was unused all the time. Since the popularity of the IEEE 802.15.4-2003 standard started to increase dominating the product offerings for low-rate wireless personal area networks (LR-WPANs), these PHY layers were not enough to respond to the markets demands. Moreover, there was also a need of better coexistence between IEEE 802.15.4 compliant devices and other RF technologies, such as IEEE 802.11 (i.e., WiFi) and Bluetooth.

The IEEE 802.15.4-2006 specification enables more flexibility to the radio transceivers, where different frequency bands can use the same modulation scheme (e.g., O-QPSK). The new modulation schemes were introduced for the radios operating in the 868 MHz and 915 MHz frequency bands, most likely because nobody was using them. This has the benefit of allowing the radio transceiver to span all three frequency bands.

In the IEEE 802.15.4-2006 standard, the PHY layer offers 20 kb/s of bit rate by using a single channel in the frequency range from 868 MHz to 868.6 MHz. This range of frequencies is used in Europe for applications, such as short-range wireless networking. The 915 MHz and 2.4 GHz are part of the ISM frequency bands. The 2.4 GHz band is used worldwide and the 915 MHz

band is used mainly in North America. The IEEE 802.15.4 standard requires simultaneous and joint support for the 868 MHz and 915 MHz frequency bands.
The 868/915 MHz Band Binary Phase-Shift Keying (BPSK) PHY, originally specified in 2003, offers a trade-off between complexity and data rate. The optional PHYs offers a much higher data rate than the one given by the 868/915 MHz BPSK PHY, which provides a data rate of 20 kb/s in the 868 MHz band and 40 kb/s in the 915 MHz band. The Amplitude Shift Keying (ASK) PHY offers data rates of 250 kb/s in both the 868 MHz and 915 MHz bands, the same data rate of the 2.4 GHz band PHY. In the 915 MHz band the O-QPSK PHY offers a signalling scheme identical to the one of the 2.4 GHz band PHY and a data rate equal to the one of the 2.4 GHz PHY band. In terms of data rate the O-QPSK PHY in the 868 MHz band supports a data rate of 100 kb/s.
Table A.1 presents an overview of the channels pages and numbers for the IEEE 802.15.4-2006 standard. For sake of simplicity from now on we will use the term IEEE 802.15.4 when referring to the IEEE 802.15.4-2006 standard.

Table A.1: Channel assignments for the IEEE 802.15.4 standard.

Channel Page	Channel Number	Frequency Band	Modulation	Data Rate (kb/s)	Symbol Rate (ksymbols/s)
0	0	868 MHz	BPSK	20	20
	1-10	915 MHz	BPSK	40	40
	11-26	2.4 GHz	O-QPSK	250	62.5
1	0	868 MHz	ASK	250	12.5
	1-10	915 MHz	ASK	250	50
	11-26	2.4 GHz	O-QPSK	250	62.5
2	0	868 MHz band	O-QPSK	100	25
	1-10	915 MHz band	O-QPSK	250	62.5
	11-26	Reserved	-	-	-
3	Reserved	Reserved	-	-	-

The frequencies for the IEEE 802.15.4 standard are divided by three different frequency bands with a total of 27 channels. The central frequencies are given by:

- $f_c = 868.3$, in MHz
- $f_c = 906 + (2 \times (k-1))$, in MHz, for $k = 1,\ 2, ...,\ 10$
- $f_c = 2405 + (5 \times (k-11))$, in MHz, for $k = 11,\ 12, ...,\ 26$

The 27 half-duplex channelization specified by the IEEE 802.15.4 standard shown in Figure A.1 is organized as follows:

- The 868 MHz band, ranging from 868.0 MHz to 868.6 MHz is used in Europe. It adopts a binary phase shift keying (BPSK) modulation format, with a DSSS at a chip-rate of 300 kchip/s. Only a single channel with data rate of 20 kb/s is available and devices shall be capable of achieving a sensitivity of -92 dBm or better. A pseudo-random sequence of 15 chips is transmitted within 50 μs symbol period.
- The 915 MHz band, ranging from 902 MHz to 928 MHz is used in the North American and Pacific area. It adopts a BPSK modulation format, with DSSS at a chip-rate of 600 kchip/s. Ten channels with data rate of 40 kb/s are available and the devices shall be capable of achieving a sensitivity of -92dBm or better. A pseudo-random sequence of 15 chips is transmitted in a 25 μs symbol period.

- The 2.4 GHz ISM band, ranging from 2400 MHz to 2483.5 MHz, adopts an O-QPSK modulation format, with a DSSS at 2 Mchip/s. Sixteen channels with data rate 250 kb/s are available and devices shall be capable of achieving a sensitivity of -85 dBm or better. A pseudo-random sequence of 15 chips is transmitted in a 16 μs symbol period.

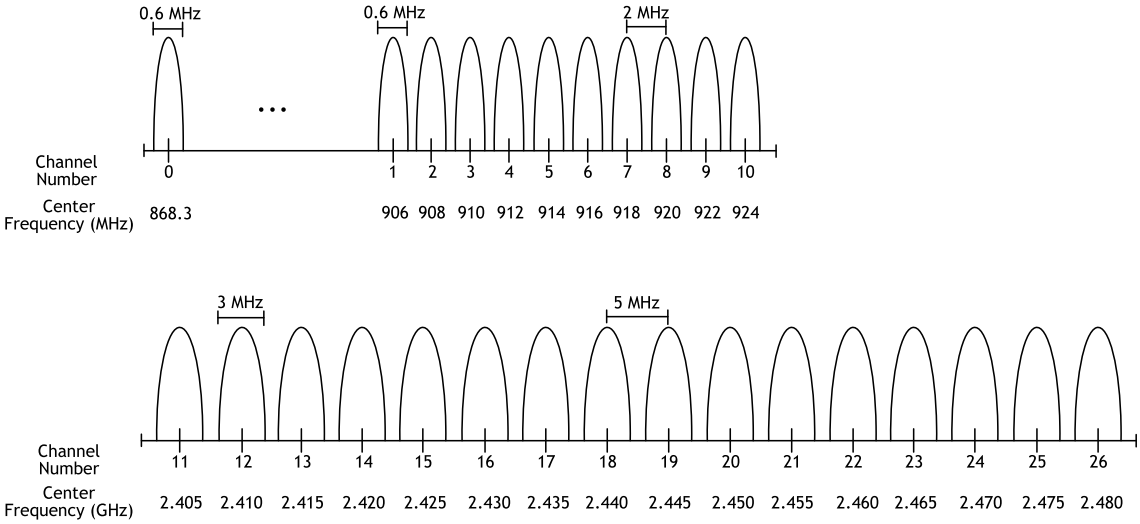

Figure A.1: IEEE 802.15.4 channelization at the 868/915 MHz and 2.4 GHz bands.

The IEEE 802.15.4a-2007 [WPAN07] was released, in order to support high-precision ranging capability (1m accuracy and better), high aggregate throughput, and ultra low power consumption (mainly due to low transmit power levels, typically under -10 dBm). It supports two additional PHY layers: 1) an UWB that operates in three different bands and 2) a CSS PHY in the 2.4 GHz ISM band. The choice of adopting UWB has many advantages when compared with narrowband systems as follows:

- **Improved channel capacity**: UWB technology enables the increase of channel capacity, since it offers a bandwidth of at least 500 MHz for high data rate communications. However, coverage range is limited up 10 m due to the low power levels mandated by Federal Communications Commission (FCC) and the Radio Spectrum Committee (RSC) of the European Commission (EC).

- **High-precision and ranging capabilities**: The very short pulses used in UWB enables precision ranging measurements whith high accuracy. Therefore, UWB can be applied in geolocation systems with an achievable ranging accuracy from 15 cm to 50 cm [A Non-Coherent 802.15.4a UWB Impulse Radio].

- **Low power consumption**: Since UWB radios have a simpe architecture, being the information transmitted by using low energy pulses with a duration of approximately 2 ns, this allows for energy and cost savings in addition to a reduction in the implementation complexity.

- **Resistance to multipath fading**: The UWB signals are very robust in terms of multipath fading due to its large bandwidth. The narrow pulses prevent multiple reflections, avoiding that multiple signals reach the receiving antenna by multiple paths, which can cause interference and phase shifting of the signals.

The UWB signals can operate in the following frequency bands:

- A sub-gigahertz band from 249.6 MHz to 749.6 MHz;
- A low band from 3.1 GHz to 4.8 GHz;
- A high band from 6.0 GHz to 10.6 GHz.

The UWB spectrum allowed by the Federal Communication Commission (FCC) is divided into 16 channels as shown in Table A.2. A compliant device shall support at least one of the mandatory channels (i.e., channels 0, 3 and 9). All the other channels are optional, where channels 4, 7, 11, and 15 are differentiated by having a larger bandwidth ($>$500 MHz).

Table A.2: UWB PHY band allocation.

Band Group	Channel Number	Center frequency (MHz)	Bandwidth (MHz)	Mandatory/ Optional
0	0	499.2	499.2	Mandatory bellow 1 GHz
1	1	3494.4	499.2	Optional
	2	3993.6	499.2	Optional
	3	4492.8	499.2	Mandatory in low band
	4	3993.6	1331.2	Optional
2	5	6489.6	499.2	Optional
	6	6988.8	499.2	Optional
	7	6489.6	1081.6	Optional
	8	7488.0	499.2	Optional
	9	7987.2	499.2	Mandatory in high band
	10	8486.4	499.2	Optional
	11	7987.2	1331.2	Optional
	12	8985.6	499.2	Optional
	13	9484.8	499.2	Optional
	14	9984.0	499.2	Optional
	15	9484.8	1354.97	Optional

A.1.2 Carrier Sense

The Carrier Sense (CS) mechanism is responsible for verifying the frequency channel availability, and report the sensing to the radio transceiver. Therefore, every time a node has a packet to transmit, it enters into the RX mode for detecting for any possible signal that might be present in the desired frequency channel. In contrast with the energy detection mechanism, where there is no attempt to identify or decode signals, during CS the signal is demodulated for verifying if the signal modulation and spreading characteristics belong to the PHY layer being currently utilized by the device. If the occupying signal is compliant with the IEEE 802.15.4 PHY layer, the device might choose to consider the channel busy regardless the signal energy level.

A.1.3 Received Signal Strength Indication

The quantized signal energy of each received packet allows for the creation of the RSSI. This signal strength indicator does not care about the "quality" or "correctness" of the signal. The RSSI availability indicates that a location-based system can be implemented without the need of any additional hardware for the individual nodes in the network. As presented in Table A.3, there are four parameters associated with the RSSI as follows [Fara08]:

- **Dynamic range**: The dynamic range specified in dB is responsible for indicate the minimum and maximum received signal energy. If the RSSI has a range of 100 dB (i.e., from -100 dBm to 0 dBm), the minimum signal energy that the receiver can measure is -100 dBm, whilst the maximum signal energy reported as RSSI is 0 dBm;
- **Accuracy**: The RSSI accuracy indicates the average error associated with the received signal strength. The CC2420 transceiver is capable of providing an accuracy of $\pm$6 dB;
- **Linearity**: The RSSI linearity indicates the relationship between maximum deviation of the RSSI versus the actual received signal power within the limits of $\pm$3 dB;
- **Average period**: The averaging period is required by IEEE 802.15.4 compliant transceivers to generate the Link Quality Indicator (LQI) being obtained by measuring the received signal strength over the first 8 symbol periods (128 μs).

Table A.3: RSSI Parameters [CC2420].

Parameter	Typical value	Unit
Dynamic range	100	dB
Accuracy	$\pm$6	dB
Linearity	$\pm$3	dB
Average period	128	μs

By considering a FIFO queue, like the one presented in Figure A.2, the RSSI value is obtained as follows:

- The time at which the packet was received (i.e., timestamp) and the RSSI are passed to the MAC and upper layers for analysis;
- When the packet is readed from the FIFO queue the second last byte contains the RSSI value (i.e., one byte value as a signed 2's complement value) that was measured after receiving 8 symbols of the actual packet;
- If the RSSI value was captured at the same time as the data packet being received, the RSSI value will reflect the intensity of received signal strength at that time, not necessarily the signal power belonging to the received data;
- When multiple nodes access to the medium at the same time, the RSSI value being captured could be erroneous (i.e., the value represents the overlay of several different signals).

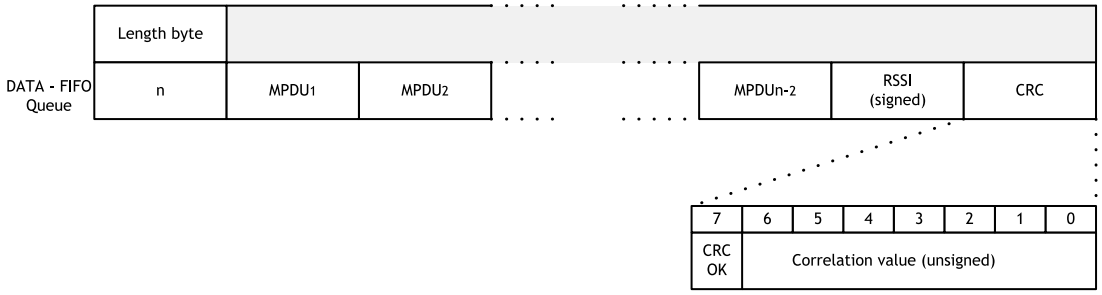

Figure A.2: Data buffering in a FIFO queue.

As described above the RSSI is represented as signed 2's complement value. However, the actual value can not be read and interpreted as the received signal strength. To convert the actual value to the received signal strength an offset must be added. The CC2420 radio transceiver offset taken by the data sheet is approximately -45 dB [CC2420]. However, this value is dependent on the actual antenna configuration.
WSN MAC protocols use RSSI measurements for localization, sensing, transmission power control and packet reception ratio modeling. To obtain the RSSI values two methods can be explored as stated in [VVLM11]. The first involves using the physical (theoretical) relationship between the RSSI and the distance. Therefore, free space and two ray ground models are used to obtain the theoretical RSSI. The second (experimental) method considers an empirical RSSI database filled with measurement records during an extensive calibration phase, and the location is estimated by fitting the measured RSSI to the database. However, since the RSSI provided by the redio transceivers has limited accuracy, which directly impacts on the estimated distance between the nodes, the path-loss determined experimentally can be a major source of errors [Fara08]. Empirical studies [NiHa93], have shown the log-normal shadowing model [Rapp02] provides more accurate multi-path channel models than Nakagami and Rayleigh for indoor environments. Therefore a good approximation for obtaining the RSSI in dBm is by considering the log-normal shadowing model as follows:

$$RSSI(d) = P_t - P_L(d) \tag{A.1}$$

where, P_t is the transmit power and $P_L(d)$ is the path loss at a given distance, d.
The $P_L(d)$ is given as follows:

$$P_L(d) = P_L(d_0) + 10\eta log10\left(\frac{d}{d_0}\right) + X_\sigma \tag{A.2}$$

where, $P_L(d_0)$ is known as the 1 m loss, or insertion loss that arises due to free-space path loss and antenna inefficiencies (i.e., reference value of path loss), η is the signal propagation constant (also named propagation exponent) and d is the distance between the transmitter and the receiver. The shadow effect is described by a zero mean gaussian random variable, X_σ, with standard deviation, σ^2, that models the random variation of the RSSI value.
The IEEE 802.15.4 standard suggests that a good approximation for obtaining the $P_L(d)$ at 2.4 GHz band is given by:

$$P_L(d) = \begin{cases} 40.2 + 20log_{10}d + X_\sigma & d \leq 8m \\ 58.5 + 33log_{10}d + X_\sigma & d > 8m \end{cases} \tag{A.3}$$

By analysing Equation (B.3) we conclude that the path loss model described in IEEE 802.15.4 has a two-segment function with a path loss exponent of 2.0 for a distance less or equal than 8 m and a path loss exponent of 3.3 for a distance longer than 8 m. Figure A.3 presents the RSSI as a function of the distance (we assume $P_t = 0\,dBm$ and $X_\sigma = 0$). By increase the distance we decrease the RSSI value.
The LQI is not a signal strength indicator like RSSI, instead is a metric of the current quality of the received signal. The LQI gives an estimate of how easily a received signal can be demodulated by accumulating the error magnitude between ideal constellations and the received signal over the 64 symbols immediately following the sync word. LQI is commonly used as a relative measurement of the link quality since the value is dependent on the modulation scheme. In

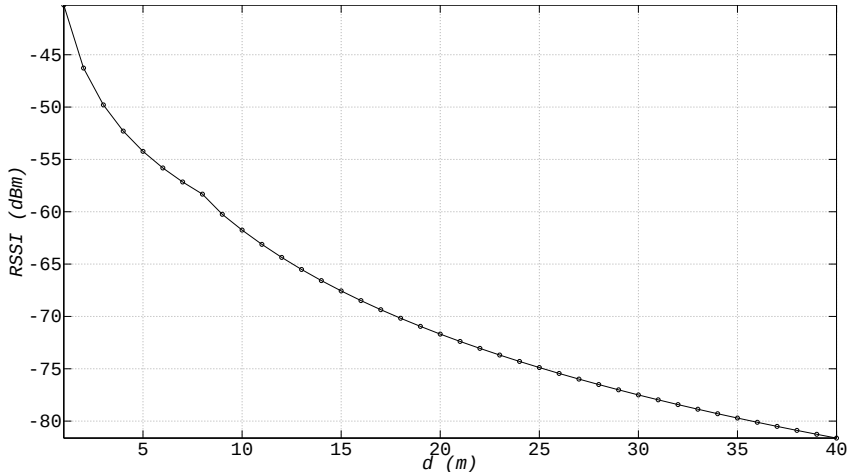

Figure A.3: RSSI as a function of the distance.

real deployment scenarios there are five "extreme situations" that can be used to describe the behaviour of the RSSI and LQI as follows:

- A weak signal with noise may give low RSSI and high LQI;
- A weak signal without noise may give low RSSI and low LQI;
- As strong noise coming from an interferer may give high RSSI and high LQI;
- A strong signal with low noise may give high RSSI and low LQI;
- A very strong signal that causes saturation at the receiver may give high RSSI and high LQI.

A.1.4 Clear Channel Assessment

When performing CSMA-CA, the MAC sub-layer request the PHY layer to perform CCA in order to detect if the medium is found to be busy or idle. The CCA period has a duration that is equal to $T_{CCA} = 8 \times T_{symbol}$ (i.e., 128 μs), where $T_{symbol} = 16\,\mu$s is the symbol time. The CCA operation has three operational modes as follows:

- **Energy Detection mode** - In this mode the CCA shall reports a busy medium if the received energy is above a given threshold, referred as energy detection threshold;
- **Carrier Sense mode** - The CCA reports a busy medium only if it detects a signal with the modulation and the spreading characteristics of IEEE 802.15.4 standard and which the signal may be higher or lower than the energy detection threshold;
- **Carrier Sense with Energy Detection mode** - The IEEE 802.15.4 defines 27 different wireless channels. A network can choose to operate within a given channel set. Hence, the PHY layer should be able to tune its transceiver into a specific channel upon the reception of a request from a higher layer.

A.2 Medium Access Control Layer

The IEEE 802.15.4 MAC layer is designed to support a large number of applications, such as industrial, medical and home applications for control and/or monitoring. The main function

performed by the MAC layer is the access control to the physical radio channel. It is responsible for the generation of ACK frames, support of PAN association and disassociation and the security control. The method used for random medium access is based on the IEEE 802.15.4 nonbeacon-enabled mode. It uses unslotted CSMA-CA to transmit frames. The core idea is the following: when one node needs to send data, it will compete for the wireless channel. If collisions occur nodes will backoff for a random period of time before attempting to access the channel. Depending on the application requirements, the IEEE 802.15.4 standard considers two topologies (i.e., star and peer-to-peer), as presented in Figure A.4.

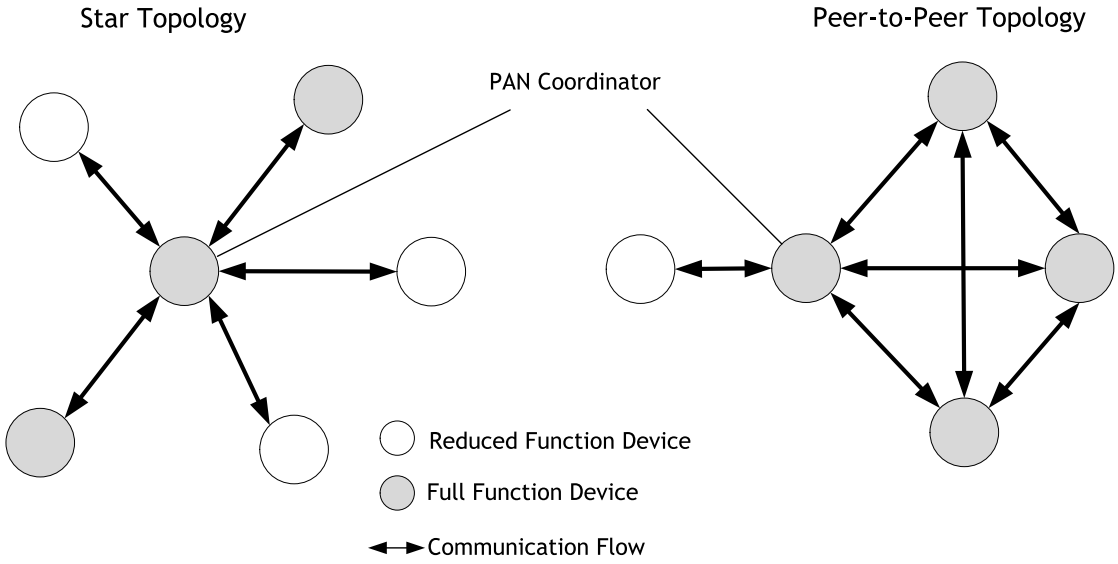

Figure A.4: Examples of star and peer-to-peer topologies.

The star topology is formed around a Full Function Device (FFD), so the communication is established between nodes and a single central controller, called the PAN coordinator which is the only node allowed to form links with multiple devices. The function of the PAN coordinator includes not only running a specific application but also be used to initiate, terminate or route the communications in the network. So the PAN coordinator acts like the primary controller of the personal area network. All devices operating on a network of any type of topology mentioned shall have a unique 64-bit address. This address may be used for direct communication within the PAN, or a short address may be allocated by the PAN coordinator when the device associates and used instead. The PAN coordinator often will be powered by a continuous power supply, while the devices will most likely be battery powered. Applications that benefit from a star topology include: home automation, personal computer (PC) peripherals, toys and games, and personal health care [WPAN06]. The IEEE 802.15.4 MAC protocol supports two operational modes: the nonbeacon-enabled mode and the beacon-enabled mode which can be selected by the PAN coordinator as presented in Figure A.5. In the nonbeacon-enabled mode the PAN coordinator do not transmit regular beacons, and so it transmits a data frame using a non-slotted CSMA-CA. In the beacon-enabled mode the beacons are periodically sent by the PAN coordinator, so when a device wishes to transfer the data to a coordinator it first listen the medium for a network beacon frame. The beacon frame is responsible by the boundaries establishment for the beginning of a superframe while defining a time interval to exchange packets between different nodes. The medium access is basically a slotted CSMA-CA. This mode is used in applications that require a certain amount of bandwidth and low latency so

that the PAN coordinator enables the allocation of some time slots in the superframe. These portions are called Guaranteed Time Slots (GTSs) and they are used in the situation when the node needs to have guaranteed services.
As described before the IEEE 802.15.4 has different types of topologies, so the data transfer model is always related with the network topology. In the peer-to-peer mode a device will communicate with other devices in its vicinity while in the star networks the communication exchange will occurs between a PAN coordinator and a network device. In the presence of a star network two types of data transfer mechanism could exist, depending on whether the PAN coordinator is beacon-enabled or nonbeacon-enabled.

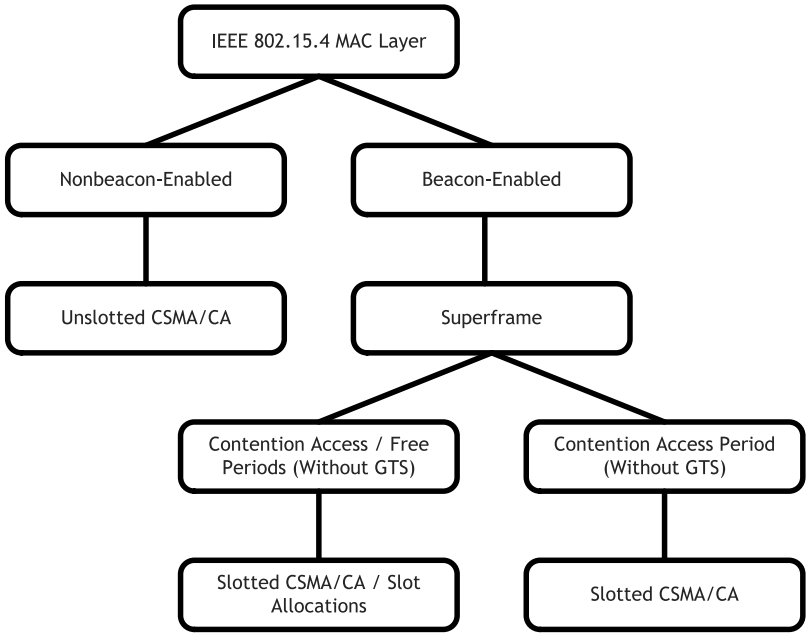

Figure A.5: IEEE 802.15.4 operational modes.

Beacon-enabled - Star Topology
In the presence of a beacon-enabled star topology, a network device that wants to send data to the PAN coordinator needs to listen for a beacon. In this case if a device does not have any Guaranteed Time Slot (GTS) assigned, it transmits the data frame in the contention access period in accordance with the CSMA-CA procedure. If the device has already a GTS assigned, it needs to wait for the appropriate time within the superframe structure in order to transmit its data frame. After receiving the data frame, the PAN coordinator sends an acknowledgement reply to the network device, as presented in Figure A.6.
In the cases when the PAN coordinator has data to send to a network device, it will set a special flag in its beacon. When the network device detects that the PAN coordinator has pending data for him, it will sends back a "data request" message and the PAN coordinator responds with an acknowledgment followed by the data frame, and finally an acknowledgement is sent from the network device in order to finish the transmission, as presented in Figure A.7.

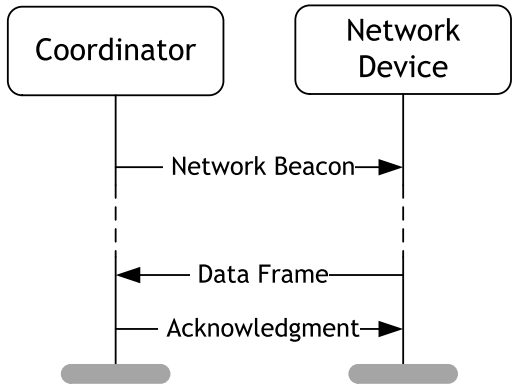

Figure A.6: Star topology - Communication to a coordinator in a beacon-enabled PAN.

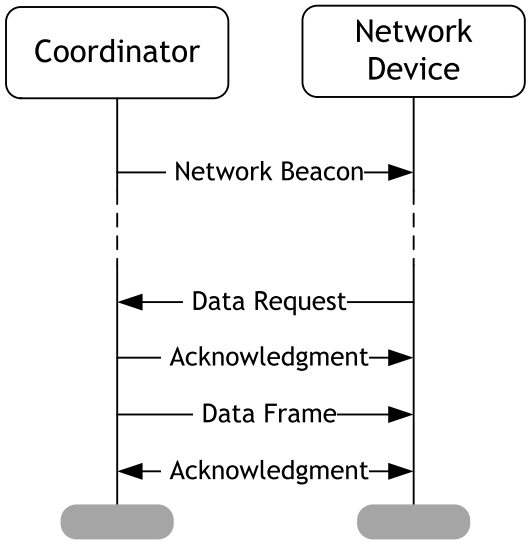

Figure A.7: Star topology - Communication from a coordinator in a beacon-enabled PAN.

Nonbeacon-enabled - Star Topology

In the case with a nonbeacon-enabled star network, a network device that wants to transfer data sends a data frame to the PAN coordinator by using the CSMA-CA procedure. After correctly receive the data frame the PAN coordinator will reply to the network device, sending back an acknowledgement message, as presented in Figure A.8.

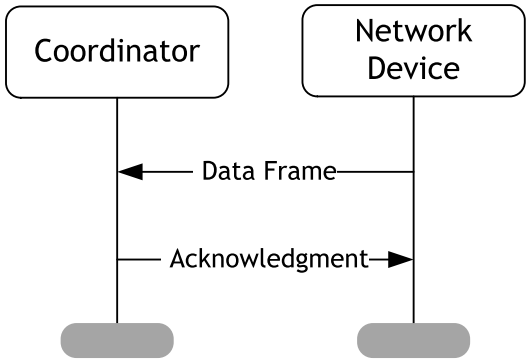

Figure A.8: Star network - Communication to a coordinator in a nonbeacon-enabled PAN.

In the cases the PAN coordinator requires a data transfer to a network device, it will keep

the data until the network device sends back a data request message. After that the PAN coordinator sends an acknowledgement followed by the data frame. Finally, the network device acknowledges the reception of the data frame, as presented in Figure A.9.

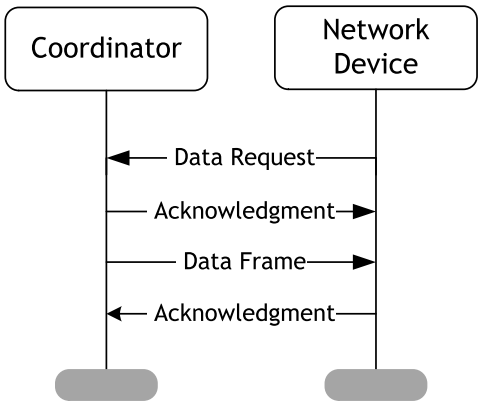

Figure A.9: Star network - Communication from a coordinator in a nonbeacon-enabled PAN.

Peer-to-Peer Data Transfer
As presented before there are different types of data transfer transactions. In the first type, the data is transferred to a coordinator and the network device transmits the data. In the second one the exchanging of the data is transmitted from a coordinator in which the device receives the data. Finally, in the third one, the exchanging of the data is between two peer devices. When a star topology is used, only two first types of these transactions are used because data may be exchanged only between the coordinator and a device. In a peer-to-peer topology, data may be exchanged between any two devices on the network and consequently all three transactions may be used in this topology. So in the peer-to-peer topology, the strategy is ruled by the specific network layer that is responsible for managing the WSN. A given network device may stay in reception mode, while scanning the radio channel for ongoing communications or it can send periodic "SYNCH" messages with other potential listening devices in order to achieve synchronisation.

A.2.1 MAC frames

The IEEE 802.15.4 standard defines four MAC frame structures:

- Beacon Frame;
- Data Frame;
- Acknowledgment Frame;
- MAC command frame.

The beacon frame is used by the coordinator in order to transmit beacons. This type of frame is used to identify the network and its structure, wake-up devices from the sleep mode to the listening mode and synchronise devices in the network, assuming an important role in the mesh and cluster-tree networks topology, especially because it can reduce energy consumption and extend battery lifetime due to synchronization. The entire MAC frame is used as a payload in a PHY packet. The MAC beacon frame structure is described in Figure A.10. The active part of the beacon frame is constituted by three parts: the MAC Header (MHR), the MAC payload

and the MAC Footer (MFR). The MHR contains information about the MAC frame control field, Beacon Sequence Number (BSN), addressing fields, and optionally the auxiliary security header. The MFR contains a field of a 16-bit Frame Check Sequence (FCS).

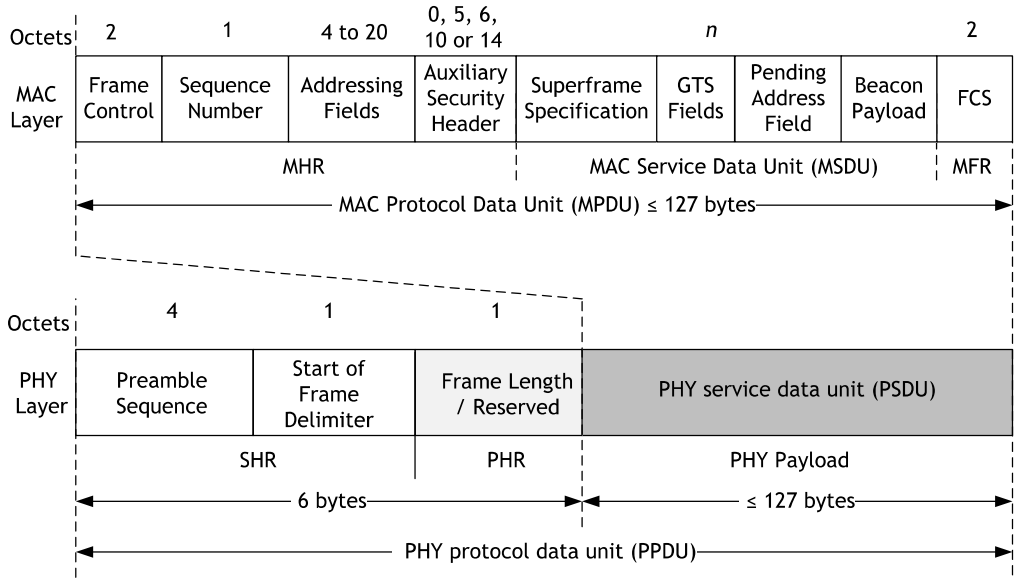

Figure A.10: Schematic view of the beacon frame and the PHY packet.

The data frame of the IEEE 802.15.4 standard is presented in Figure A.11. The data payload passed from the network to the MAC layer is referred as MAC Service Data Unit (MSDU). The MHR contains the frame control field, Data Sequence Number (DSN), addressing fields, and optionally the auxiliary security header. The MHR, MAC payload, and MFR together form the MAC data frame, (i.e., MAC Protocol Data Unit, MPDU). The MPDU is passed to the PHY as the PSDU, which becomes the PHY payload [WPAN06].

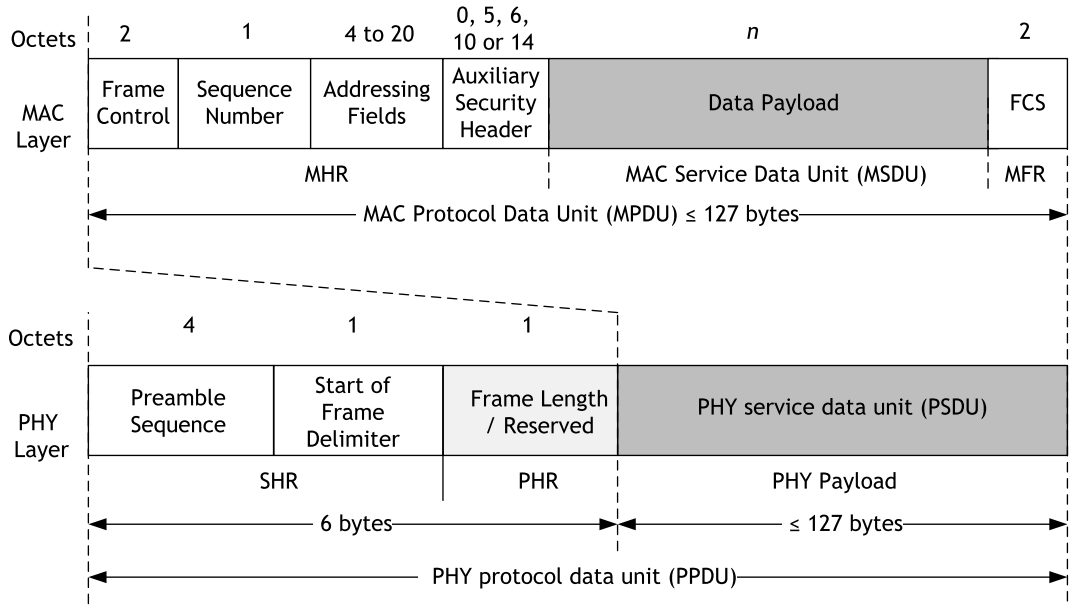

Figure A.11: Schematic view of the MAC data frame and the PHY packet.

The maximum allowed PPDU from the IEEE 802.15.4 standard is 133 bytes, Figure A.11. The PHY header is 6 bytes. Therefore, the MPDU is 127 bytes. The minimum and the maximum MHR

and MFR without security are 9 and 25 bytes respectively. Therefore, the maximum payload could range between 127-25=102 and 127-9=118 bytes. In order to ensure compliance with the IEEE 802.15.4-2003 release, the maximum data payload is assumed to be 102 bytes.

The acknowledgment frame, presented in Figure A.12, has a MHR and a MFR field, and does not have a MAC payload. The MHR contains the MAC Frame Control and DSN fields, and the MFR is composed by a 16-bit FCS. This type of frame has the simplest MAC frame format in the IEEE 802.15.4 standard. The acknowledgment frame is sent whenever the destination device successfully receives a packet that was previously sent to it.

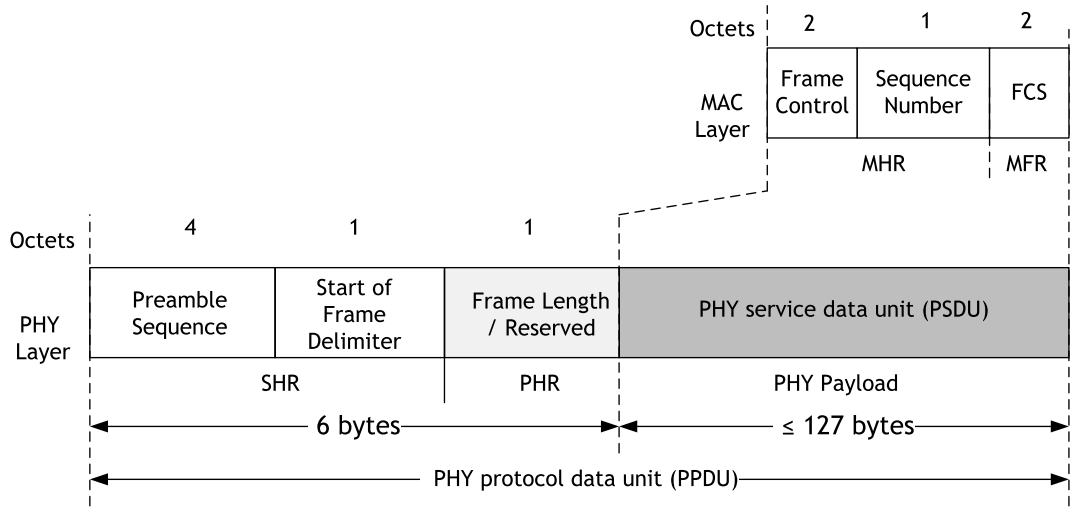

Figure A.12: Schematic view of the acknowledgment and the PHY packet.

The MAC command frame presented in Figure A.13 is used to request association or disassociation. The MAC payload contains the command type field that is responsible to determinate if the type of the command is an association request or a data request, while the command payload field contains the command itself.

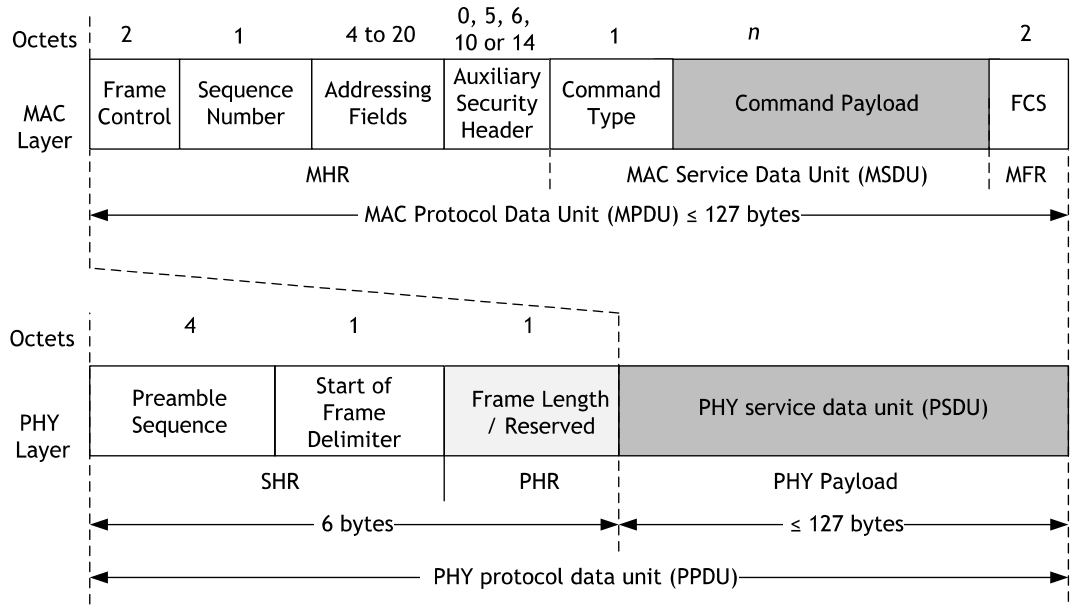

Figure A.13: Schematic view of the MAC command frame and the PHY packet.

All the command frames types defined by the MAC layer that a reduced function device may send or receive are described in Table A.4. The FFD device could transmit and receive all the command frame types shown in Table A.4, with the exception of the GTS request command.

Table A.4: Command Frame Types.

Command Frame Identifier	Command Name	Reduced Function Device (RFD)	
		TX	RX
0x01	Association Request	X	
0x02	Association Response		
0x03	Disassociation Notification	X	X
0x04	Data Request	X	X
0x05	PAN ID Conflict Notification	X	
0x06	Orphan Notification	X	
0x07	Beacon Request		
0x08	Coordinator Realignment		X
0x09	GTS Request		
0x0a - 0xff	Reserved		

In the IEEE 802.15.4 MAC layer between two successive frames transmitted an IFS period must be inserted. The IFS depends on whether the transmission transaction is acknowledged or unacknowledged. When the acknowledgement is received the IFS follows the acknowledgment frame and when the frame length do not exceeds the *aMaxSIFSFrameSize*, the acknowledgment must be followed by a short IFS (SIFS) period and the duration should be at least *aMinSIFSPeriod*. In the cases that the frame length exceeds *aMaxSIFSFrameSize*, the acknowledgment must be followed by a long IFS (LIFS) period as shown in Figure A.14.

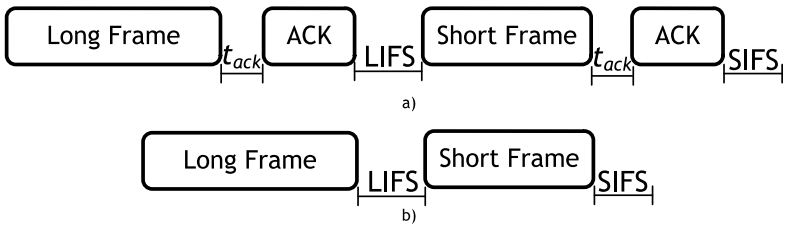

Figure A.14: Interframe Spacing (IFS) in a) Acknowledged Transmission and b) Unacknowledged Transmission.

The minimum LIFS and SIFS periods for the three different PHY layers specified by the IEEE 802.15.4 standard are presented in Table A.5.

Table A.5: Minimum LIFS and SIFS period.

PHY	*macMinLIFSPeriod*	*macMinSIFSPeriod*	Units
868-868.5 MHz BPSK	40	12	Symbols
902-928 MHz BPSK	40	12	Symbols
2400-2483.5 MHz O-QPSK	40	12	Symbols

A.2.2 Carrier Sense Multiple Access with Collision Avoidance

The IEEE 802.15.4 standard allows multiple devices to share the same frequency channel for data transmission whilst enabling reliable data delivery. The considered medium access mechanism, is the Carrier Sense Multiple Access with Collision Avoidance (CSMA-CA). The CSMA-CA, requires listening to the channel before transmitting in order to reduce the collision probability, being used before the transmission of data or MAC command frames within the CAP, unless the frame can be quickly transmitted due to an ACK of a data request command. The CSMA-CA algorithm shall not be used for the transmission of beacon frames in a beacon-enabled PAN, acknowledgment frames or data frames transmitted in the Contention-Free Period (CFP) [WPAN06]. Two versions of the CSMA-CA mechanism were created: (i) slotted CSMA-CA algorithm used in the beacon-enabled mode and (ii) non-slotted CSMA-CA algorithm used in the nonbeacon-enabled mode. Both approaches, use a basic time unit called Backoff Period (BP), which is equal to *aUnitBackoffPeriod* = 20 symbols (i.e., 0.32 ms).
When using slotted CSMA-CA, each operation (channel access, backoff counter and CCA) can only occur at the boundary of a BP. Additionally, the BP boundaries must be aligned with the slot boundaries of the superframe time [WPAN06]. In non-slotted CSMA-CA the backoff periods of one node are completely independent of the backoff periods of any other node in a PAN. The CSMA-CA algorithm, represented by the flowchart presented in Figure A.15, is invoked when a packet is ready to be transmitted. This algorithm, maintains three variables for each packet:

1. **Number of Backoffs (NB):** number of times the CSMA-CA algorithm was required to experience backoff due to unavailability. It is initialised to zero before each new transmission attempt.

2. **Backoff Exponent (BE):** enables the computation of the backoff delay, and represents the number of backoff periods that need to be clear of channel activity before a transmission can occur. The backoff delay is a random variable between $[0, 2^{BE} - 1]$.

3. **Contention Window (*CW*):** the number of backoff periods during which the channel must be sensed idle before accessing the channel. This type of variable is only used with slotted CSMA-CA. This value shall be initialized with the value *CW* = 2 before each transmission attempt and reset to two each time the channel is assessed to be busy (corresponding to 2 backoff periods). Each backoff period channel sensing, is performed during the 8 first symbols of the BP.

The unslotted CSMA-CA can be summarised in five steps as follows:

1. In the first step the *CW* variable is not used, since the non-slotted has no need to iterate the CCA procedure after detecting an idle channel. Hence, in Step 3, if the channel is found to be idle, the MAC protocol immediately starts the transmission of the current frame. Second, the non-slotted CSMA-CA does not support the battery life extension mode and *BE* is always initialised with the *macMinBE* value [WPAN06].

2. Steps 2, 3, and 4 are very similar to the slotted CSMA-CA algorithm. The only difference is that the CCA starts immediately after the expiration of the random backoff delay generated in Step 2.

3. In step 5 the MAC layer starts immediately transmitting its current frame after the channel is found to be idle during the CCA procedure.

For slotted CSMA-CA used in the beacon-enabled mode, nodes must perform two backoff periods (i.e., *CW* = 2) before trying transmitting the packet. This value shall be initialized to two before each transmission attempt and must be reset to two each time the channel is found to be busy. Then, if the channel is found to be idle, *CW* is decremented by 1 and compared with 0 [step (5)]. If *CW* is equal to 0 the CSMA-CA algorithm will finish by entering in the "Success" state, otherwise the algorithm will return to step (2) and the sensing phase (i.e., CCA) is repeated. Moreover in the beacon-enable mode the backoff period boundaries of a WPAN must be aligned with the superframe slot boundaries of the coordinator. Therefore, the beginning of the first backoff period of each node is aligned with the beginning of the beacon transmission, and the transmissions will start on the boundary of a backoff period [BMVF11].

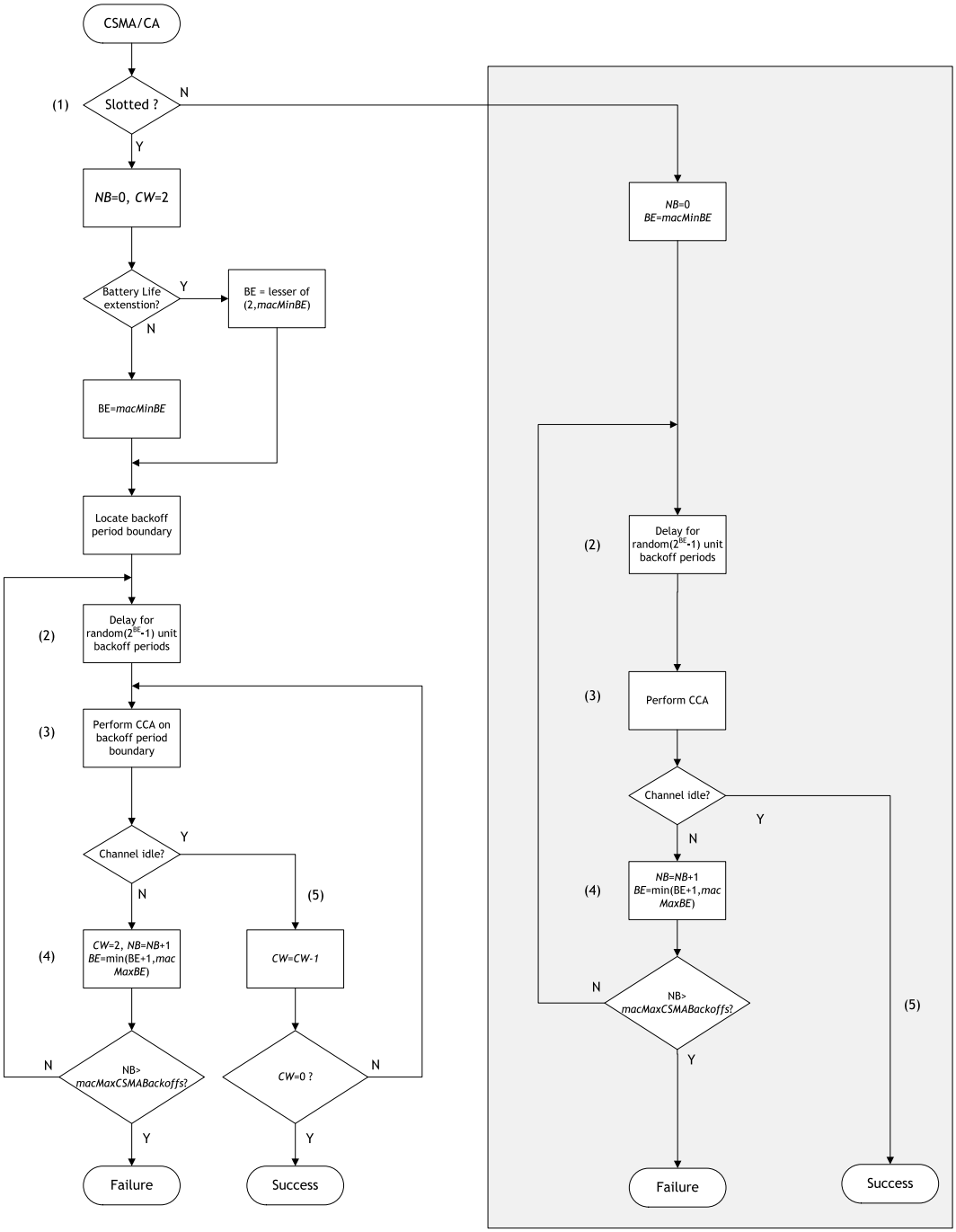

Figure A.15: CSMA-CA algorithm [WPAN06].

A.2.3 Nonbecon-enabled operation

A nonbeacon-enabled network allows every node participating in the network to transmit at any time the channel is found to be idle. Therefore, for such kind of networks, the nonbeacon-enabled mode seems to be more adapted to the scalability requirement than the beacon-enabled mode, in the former case all nodes are independent from the PAN coordinator and the communication is completely decentralised. In addition, the unslotted CSMA-CA in the nonbeacon-enabled mode will enable a better flexibility for large-scale IEEE 802.15.4-compliant peer-to-peer networks [Maha07]. Before, each transmission the MAC layer exchange messages with the PHY layer for packet transmission/reception. Figure A.16 presents the algorithms flowchart showing the interaction between the different packet types (e.g., DATA and ACK) and the control messages, being invoked when a packet is transmitted/received.

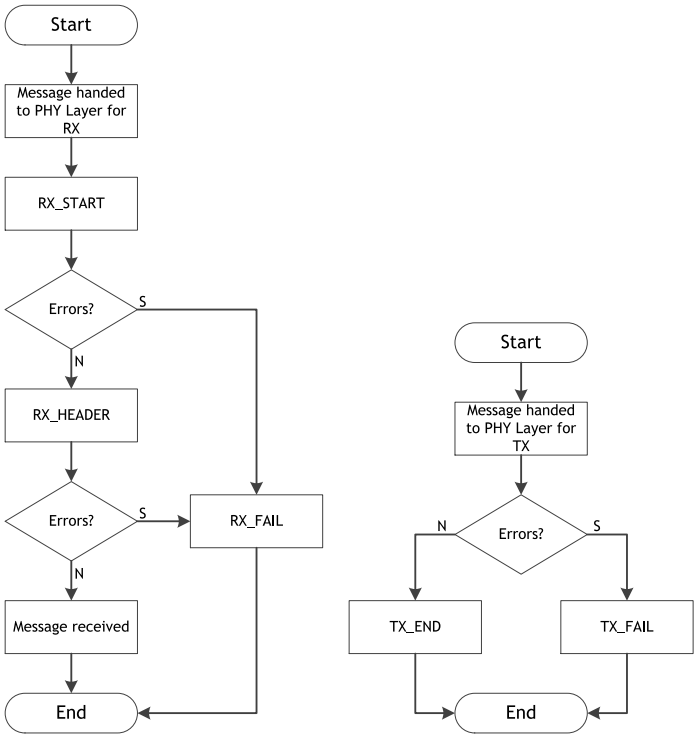

Figure A.16: Control messages flowchart.

The PHY and MAC layers exchange control messages every time an event occurs as follows:
PHY -> MAC

- **RX_START:** Start of message indicator;
- **RX_FAIL:** Failed to receive message after RX_START. The message can fail because Cyclic Redundancy Check (CRC) or collision;
- **TX_END:** Message being transmitted has completed;
- **TX_FAIL:** End of transmission (i.e., like TX_END) but the message has failed to be transmitted. For most radio transceivers, this should never happen (but there are valid cases for packet-based radios, e.g., CC2420).

After starting carrier sense, one of the following messages must be sent to the MAC layer as follows:

- **CHANNEL_IDLE:** If the specified "packet length" has been processed, and the carrier sense returns channel not "busy";
- **CHANNEL_BUSY:** If the carrier sense returns channel "busy".

MAC -> PHY

- **SET_TRANSMIT:** Switch the PHY layer to the transmit mode;
- **SET_LISTEN:** Switch the PHY layer to the listen mode;
- **SET_SLEEP:** Switch the PHY layer to the sleep mode;
- **START_CARRIER_SENSE:** Start carrier sense.

A.2.4 Becon-enabled operation

In the beacon-enabled mode the PAN coordinator periodically sends a beacon control frame to identify the PAN inside a given cluster and to synchronise all nodes that are associated to. The time period between two successive beacon frames is known as the superframe, also known as the Beacon Interval (BI) and it includes an active period and an inactive period as shown in Figure A.17.a).

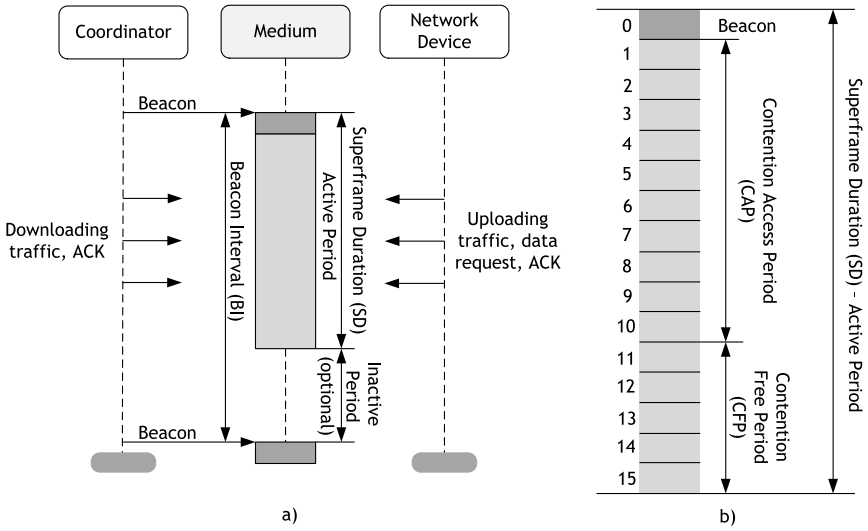

Figure A.17: a) Superframe Structure b) Active Period of the Superframe.

Within a give cluster all the communications occurs during the active portion of the superframe. Nodes can send/received data to the coordinator, being these two communication flows referred as uplink and downlink, respectively.
The active part, which represents the Superframe Duration (SD) is divided in 16 contiguous time slots. If the inactive period exists, nodes can enter in the sleep mode and save energy while they are inactive. The SD and the BI are calculated by using two parameters: the Superframe Order (SO) and the Beacon Order (BO). The Beacon Interval is given by:

$$BI = aBaseSuperframeDuration \times 2^{BO},\ 0 \leq BO \leq 14 \tag{A.4}$$

The Superframe Duration, which corresponds to the active period is given by:

$$SD = aBaseSuperframeDuration \times 2^{SO},\ 0 \leq SO \leq BO \leq 14 \tag{A.5}$$

The *aBaseSuperframeDuration* can be defined as follows:

$$aBaseSuperframeDuration = aBaseSlotDuration \times 16 = 960\ symbols \quad \text{(A.6)}$$

Where *aBaseSlotDuration* is the number of symbols forming a superframe slot when the superframe order is equal to 0 and has a value of 60 symbols. As shown before the *aBaseSuperframeDuration* is equal to 960 radio symbols (where a symbol has a time duration of 16μs), corresponding to 15.36 ms (assuming a bit rate of 250 kb/s in the 2.4GHz frequency band) and each time slot as a duration of 15.36/16=0.96 ms.
In Figure A.17.b) the active part of a superframe is divided into 16 contiguous time slots that are divided in to three parts: the beacon, the CAP and optionally the CFP. The beacons are used to synchronise the attached devices, to identify the PAN and to describe the structure of the superframes. The CAP is the period of time immediately following a beacon frame during which devices wish to transmit will compete for channel access using a slotted CSMA-CA mechanism, and the CFP is an optional feature in the IEEE 802.15.4 MAC and it follows immediately after the CAP, extending it to the end of the active portion of the superframe as shown in Figure A.17.b). If we want to allocate any GTS they must be located within the CFP and the primary objective is the use of these time slots in applications that require bandwidth for delay critical applications.

A.2.5 Hidden and Exposed node problems

One of the main factors that influence the received power (P_r) is the path loss. The Friis free-space equation relates the power received (P_r), at a distance, d, with the transmitted power (P_t), as follows:

$$P_r = P_t \cdot G_t \cdot G_r \cdot \left(\frac{\lambda}{4\Pi d}\right)^2 \quad \text{(A.7)}$$

where, G_t and G_r are the antenna gains of the transmitter and receiver, respectively. Based on Equation (A.7), we can observe that, the received power depends on the frequency (the higher the frequency is the lower the received power is), and decreases with the square of the distance (e.g., path-loss exponent equal to 2).
This path loss combined with the fact that any transceiver needs a minimum signal strength to demodulate signals successfully, leads to a maximum range that a sensor node can reach with a given transmit power [KaWi05]. If the nodes are out of the influential range, there is no way they can listen to each other. As a consequence, the hidden and exposed -terminal problems may occur, Figure A.18.
The hidden-terminal problem is one of the problems associated with the IEEE 802.15.4 CSMA-CA algorithm [WPAN06]. Consider the example presented in Figure A.18. In this case, both nodes D and A are located too far from each other. Therefore, the power detection mechanism does not detect the presence of another signal and assumes that the wireless medium is available. However, both nodes are able to communicate with node C. If both node D and A simultaneously transmit packets to node C at the same time, by performing CCA they will both find the wireless medium available and start transmitting the packets concurrently. However, this will create a collision of packets in node C. To overcome the hidden-terminal problem the authors from [Fara08] have proposed two solutions. The first solution considers changing the location of the

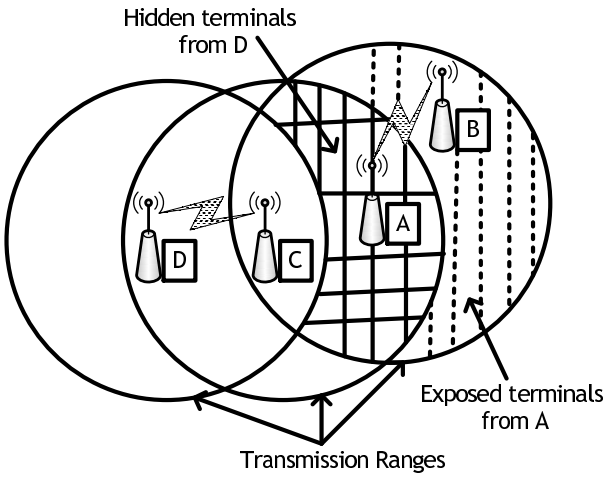

Figure A.18: Hidden and exposed terminals.

nodes or increasing the output power (of the hidden nodes) to ensure that both nodes D and A are able to hear each other. The second solution considers the use of the RTS/CTS handshake mechanism, which is not supported by IEEE 802.15.4.

The exposed-terminal problem occurs when node C transmits a packet to D, and some moment later A wants to transmit a packet to B. Although both nodes D and B would received their packets with no erros, the CSMA-CA performed by node A will prevent node A's transmission, since is in the radio influence range of node C. This suppression could lead to an needless waiting. Therefore, using the solutions presented for the hidden-terminal problem, are also suggested for the exposed-terminal problem.

A.2.6 Coexistence in the 2.4 GHz ISM band

With the appearance of more and more wireless devices operating in the 2.4 GHz ISM band portion of the radio spectrum, there was an increase of the signals from other interfering sources. Moreover, in most of the cases, there is no collaboration between these independent wireless networks, and the operation of one network may adversely affect the others. Therefore, there is a need for allowing a better coexistence between the different wireless devices operating in the same frequency band, whilst ensuring QoS. In order to cope with the design requirements and allow a better coexistence between the existing 2.4 GHz systems like Cordless Phones, Bluetooth, Wi-Fi (i.e., IEEE 802.11b/g/n) and IEEE 802.15.4, MAC management efficient techniques must be addressed allowing for mitigate the interference from other sources under hostile conditions. Figure A.19 presents the utilized channel bandwidth as well as the expect output power for each wireless system.

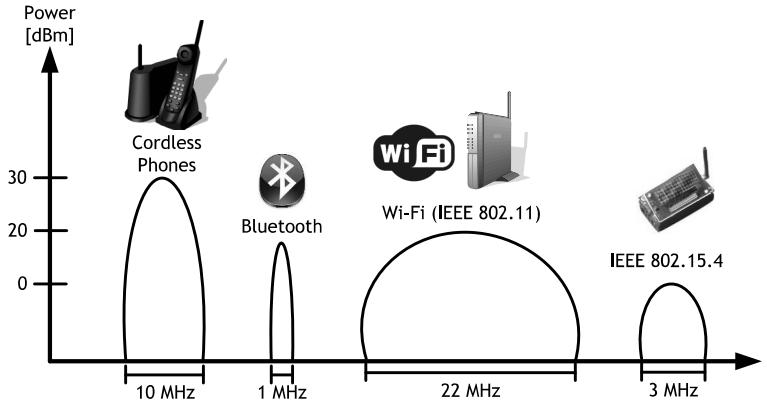

Figure A.19: Wireless systems operating in the 2.4 GHz ISM band.

Coexistence with Wi-Fi

The IEEE 802.15.4 standard was developed to address low data rate wireless communications. However, due to its low power, IEEE 802.15.4 is potentially vulnerable to interference by other wireless technologies having higher transmission powers and working in the same 2.4 GHz ISM band, such as IEEE 802.11b/g/n. The IEEE 802.11b/g/n wireless nodes have a typical output power ranging from 12 to 18 dBm [WPAN06], but can achieve values form the order of magnitude of 30 dBm. This is significantly higher than the typical 0 dBm output power of IEEE 802.15.4 nodes.

There are 14 channels defined for Wi-Fi in the 2.4 GHz ISM band. Not all of the channels are allowed in all countries: 11 are allowed by the FCC in the North American domain, 13 are allowed by the European Telecommunications Standards Institute (ETSI) in Europe and in Japan there is an extra channel (i.e., channel 14) for the IEEE 802.11b standard. The center frequency (f_c) channels are spaced 5 MHz apart (with the exception of a 12 MHz spacing between the last two channels), where each channel as a bandwidth of 22 MHz (after spreading using DSSS) as follows:

$$f_c\,[MHz]\begin{cases} 2412+5\times(k-1),\ 1\leqslant\ k\leqslant\ 11\ \ in\,North\ America \\ 2412+5\times(k-1),\ 1\leqslant\ k\leqslant\ 13\ \ in\,Europe \\ 2412+5\times(k-1),\ 1\leqslant\ k\leqslant\ 14\ \ in\,Japan \end{cases} \tag{A.8}$$

Table A.6 presents the fourteen IEEE 802.11 frequency channels available around the globe.

The IEEE 802.11 channels 1, 6 and 11 or 2, 7 and 12, or 3, 8 and 13 or 4, 9 and 14 (if allowed) can be used together as set of 3 non-overlapping channels. Since, by default Wi-Fi routers set channel 6 as the default channel, for this particular case the set of 3 non-overlapping channels are 1, 6 and 11. As presented in Figure A.1, the IEEE 802.15.4 standard defines 16 frequency channels working in the 2.4 GHz ISM band. Therefore, in order to avoid interference there is a need of choosing the non-overlapping ones in the proximity of an IEEE 802.11 network. This coexistence performance, can be accomplished by using a channel alignment scheme. Figure A.20 presents the IEEE 802.15.4 and IEEE 802.11b/g/n channel overlapping in detail for the 2.4 GHz ISM band.

The IEEE 802.15.4 frequency channels 15, 20, 25, and 26 are the ones that will suffer the least interference from IEEE 802.11b/g in North America compared to other IEEE 802.15.4 frequency channels. In Europe the IEEE 802.15.4 channels that will suffer the least interference from

Table A.6: Wi-Fi channel frequencies for the 2.4 GHz ISM Band.

Channel Number	Lower Frequency [MHz]	Center Frequency [MHz]	Upper Frequency [MHz]
1	2401	2412	2423
2	2406	2417	2428
3	2411	2422	2433
4	2416	2427	2438
5	2421	2432	2443
6	2426	2437	2448
7	2431	2442	2453
8	2436	2447	2458
9	2441	2452	2463
10	2446	2457	2468
11	2451	2462	2473
12	2456	2467	2478
13	2461	2472	2483
14	2473	2484	2495

IEEE 802.11 b/g are the channels 15, 16, 21 and 22.
By considering a scenario where both IEEE 802.11b/g and IEEE 802.11n wireless nodes exists simultaneously, Figure A.20. In this case, there is the possibility that IEEE 802.11n nodes consider the use of a channel bandwidth of 40 MHz in order to achieve higher data throughput. However, for this particular situation there will be a reduction of the total number of channels available. Thus, we can conclude that 2 channels (e.g., 3 an 11) of 40 MHz are used by IEEE 802.11n nodes, the 2.4 GHz ISM band will be heavily congested, being almost impossible the coexistence between the different wireless systems. Therefore, a good approach is to use only a single 40 MHz channel (if needed) when using 2.4 GHz ISM band by considering IEEE 802.11n.

Coexistence with Bluetooth

The Bluetooth (or IEEE 802.15.1) is a standard for short-range, low-cost and low-rate data communications. It operates in the 2.4 GHz ISM band, and uses the Frequency Hopping Spread Spectrum (FHSS) mechanism for spreading the signals. The Bluetooth devices use a channel bandwidth of 1 MHz, being the frequency channel selected by using a pseudorandom sequence. The maximum number of hops in Bluetooth is 1600 hops per second in the connection state [Fara08]. Therefore, the retransmission mechanism employed by IEEE 802.15.4 ensures the delivery of packets corrupted by the Bluetooth interference. Normally, if a Bluetooth device interferes with IEEE 802.15.4 during the first transmission attempt, and a collision occur, by using frequency hoping mechanism it goes to a different part of the radio spectrum for retransmission. There are 79 channels defined for Bluetooth as follows:

$$f_c\,[MHz] = 2402 + (k),\ 0 \leqslant\ k \leqslant\ 78 \tag{A.9}$$

where k in an integer that represents the channel number.
As presented in Equation (A.9) the Bluetooth channels are numbered from 0 to 78. Each channel has a bandwidth of 1 MHz and the f_c are spaced 1 MHz apart.
The Bluetooth devices generates an output power are generally less than 4 dBm for the most commonly class 2 devices (e.g., wireless headsets and keyboards), and the transmission range

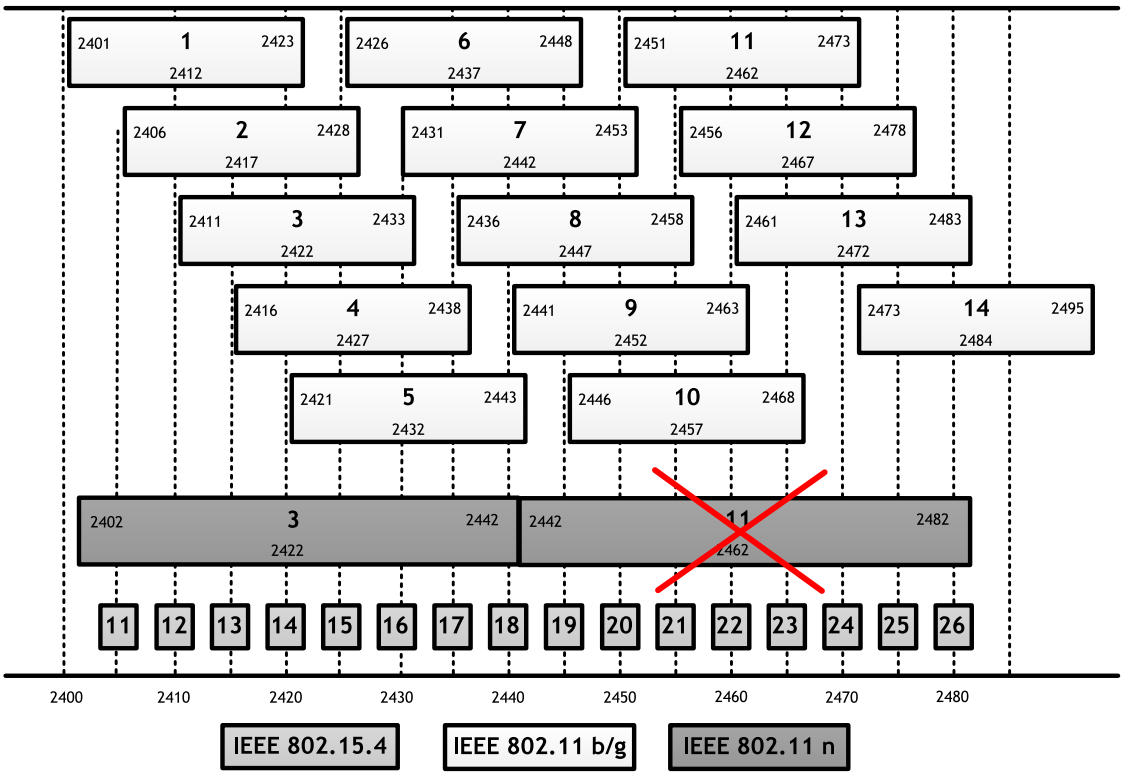

Figure A.20: IEEE 802.15.4 and IEEE 802.11b/g/n channel overlapping in the 2.4 GHz ISM band.

is about 10 m. The class 1 devices can achieve an output power up to 20 dBm and typically have a transmission range of 100 m. Although not mandatory for class 2 devices, almost all devices have embedded a power control unit in order to achieve energy efficiency. Therefore, the output power is often less than 4 dBm and can be as low as -30 dBm if the devices are close in proximity. The Bluetooth can achieve data rates of 1 Mb/s and 3 Mb/s for versions 1.2 and 2.0 respectively. To improve performance and mitigate the impact of interference caused by IEEE 802.11b/g/n networks an AFH mechanism has been introduced by the Bluetooth Special Interest Group (SIG).

The Bluetooth products before the creation of the AFH scheme employed a RFH scheme. Therefore, the first generation os Bluetooth devices was designed for using the 79 channels given by Equation (A.9). Therefore, when another wireless device tried to transmit this type of hopping results in occasional collisions. Figure A.21 presents an RFH example by considering Bluethooth, IEEE 802.15.4 and IEEE 802.11b/g/n devices working in the 2.4 GHz ISM band.

As presented before, although RFH helps avoiding collisions, some collisions still take place due to lack of adaptation to its environment. Therefore, the AFH was created in order to better adapt to the channel conditions by identifying the fixed sources of interference and excluding them from the list of available channels. This re-mapping process also involves reducing the number of channels to be used by the Bluetooth devices. Figure A.22 presents the same channel condition by considering the AFH mechanism.

Since the IEEE 802.15.4 standard employs an DATA/ACK handshake ACK mechanism for data retransmissions in case there are packet collisions with Bluetooth devices. This AFH is particular useful in dealing with frequency hopping interference problems. Since, the Bluetooth device by means of AFH, will hopped to another parth of the spectrum for retransmissions, which also enables IEEE 802.15.4 channel access with no errors. Moreover, the AFH mechanism not

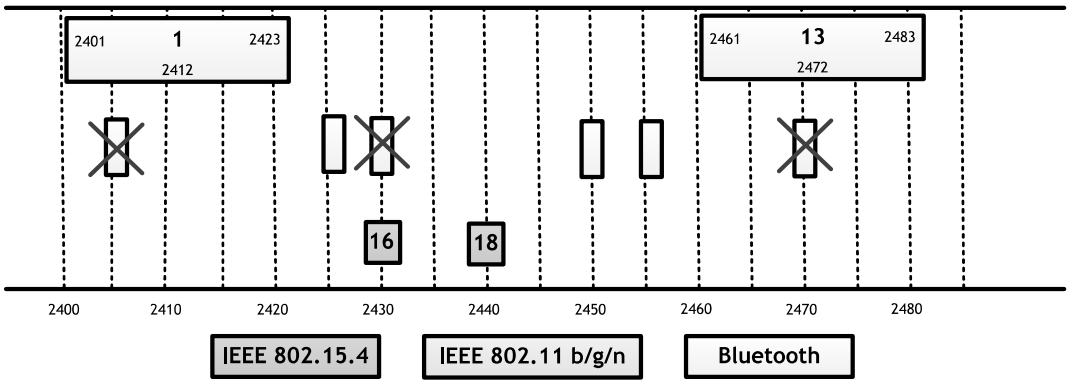

Figure A.21: Bluetooth RFH collisions.

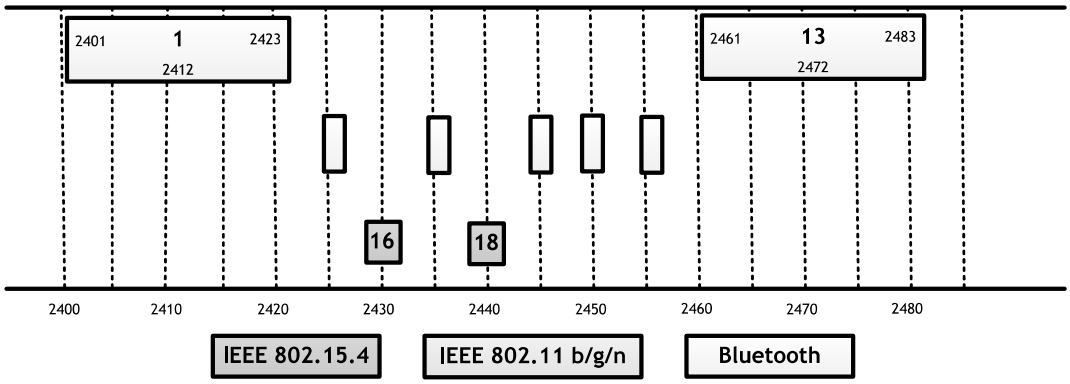

Figure A.22: Collisions avoided by the AFH mechanism.

only improves the performance of the Bluetooth devices, but it also reduces the effect of the Bluetooth network on other nearby networks that are not Bluetooth compliant [Fara08].

Other Sources of Interference

Since the cordless phones operating in the 2.4 GHz ISM band share channels frequencies with IEEE 802.11b/g/n networks, the interference from the 2.4 GHz ISM band cordless phones can completely stop a Wi-Fi network. Therefore, in order to improve the network performance mechanisms such as FHSS and DSSS are employed. For example if a cordless phone uses a DSSS, the channels used by the cordless phone and Wi-Fi network can be configured to avoid interference due to channel overleaping. The phones that use DSSS typically have a "channel" selection button allowing for manually change the frequency channel if need, whilst the phones with FHSS do not have such kind of button, since they are constantly changing from channel to channel. Another way to avoid the interference, is to use some cordless phones that already work in the 5 GHz band.

Appendix B

O-QPSK modulation for the IEEE 802.15.4 PHY layer at 2.4 GHz

This Appendix presents the O-QPSK modulation applied in the context of the IEEE 802.15.4 PHY layer. The signal spreading and despreading is also addressed, allowing to improve the SNR and reduce the effects of interferers.

B.1 QPSK modulation

The Quadrature Phase-Shift Keying (QPSK) is a digital modulation used to transmit two different messages over the same frequency band. From a bit stream two bits are taken at a time and mapped into signals as shown in Table B.1. Since each bit occupies one bit interval (T_b), the signals corresponding to the "digits" (or symbols) 00, 01, 11, 10 last a symbol duration of $T_s = 2T_b$. The QPSK modulation exploits the fact that $Vcos(2\pi f_c t)$ and $Vsin(2\pi f_c t)$ are orthogonal over the interval $(0, T_b)$ when $f_c = k/T_b$, where k is an integer. Figure B.1 presents the block diagram for the QPSK modulator.

Table B.1: QPSK signal mapping.

Bit pattern	Message	Signal transmitted	
00	m_1	$s_1(t) = Vcos(2\pi f_c t)$	$0 \leqslant t \leqslant T_s = 2T_b$
01	m_2	$s_2(t) = Vsin(2\pi f_c t)$	$0 \leqslant t \leqslant T_s = 2T_b$
10	m_3	$s_2(t) = -Vsin(2\pi f_c t)$	$0 \leqslant t \leqslant T_s = 2T_b$
11	m_4	$s_2(t) = -Vcos(2\pi f_c t)$	$0 \leqslant t \leqslant T_s = 2T_b$

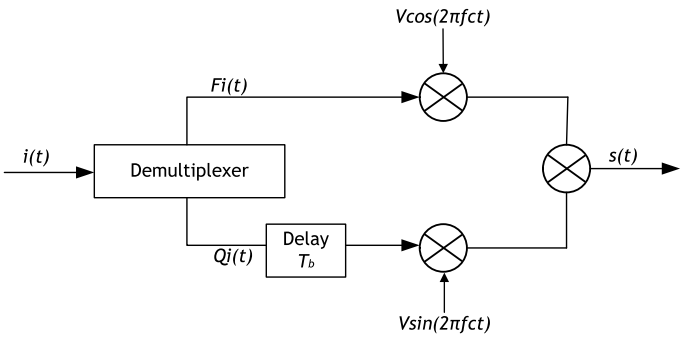

Figure B.1: Block diagram of a QPSK modulator.

The bit stream is first converted to an Non-Return-to-Zero Level (NRZ-L) waveform $i(t)$ with ± 1 levels. The waveform $i(t)$ is then demultiplexed into even, F_i, and odd, $Q(i)$, bit streams (waveforms) where and are mnemonics for the in-phase and quadrature, respectively. The individual bits in each stream modulates the in-phase carrier, $Vcos(2\pi f_c t)$, and quadrature carrier, $Vsin(2\pi f_c t)$, respectively. The bit sequences for the different branches of a QPSK modulator are presented in Figure B.2.

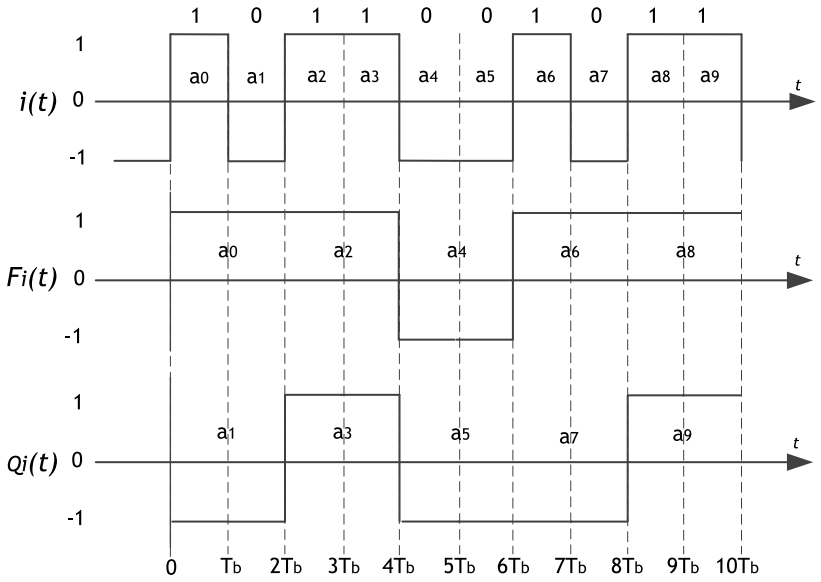

Figure B.2: QPSK modulator bit streams.

The transmitted signal is given by:

$$s(t) = F_i(t)Vcos(2\pi f_c t) + Q_i(t)Vsin(2\pi f_c t) \tag{B.1}$$

Rewritten the expression, the transmitted signal is given by:

$$\begin{aligned} s(t) &= \sqrt{F_i^2(t) + Q_i^2(t)}Vcos\left(2\pi f_c t - tan^{-1}\left(\frac{Q_i(t)}{F_i(t)}\right)\right) \\ &= \sqrt{2}Vcos[2\pi f_c t - \Theta(t)] \end{aligned} \tag{B.2}$$

The phase is $\Theta(t)$ is determined as follows:

$$\Theta(t) = \begin{cases} -3\Pi/4 & if\ F_i = -1,\ Q_i = -1\ (bits\ are\ 00) \\ 3\Pi/4 & if\ F_i = -1,\ Q_i = +1\ (bits\ are\ 01) \\ -\Pi/4 & if\ F_i = +1,\ Q_i = -1\ (bits\ are\ 10) \\ \Pi/4 & if\ F_i = +1,\ Q_i = +1\ (bits\ are\ 11) \end{cases} \tag{B.3}$$

Figures B.3 and B.4 presents the in-phase and quadrature components by considering the bit sequence presented in Figure B.2.

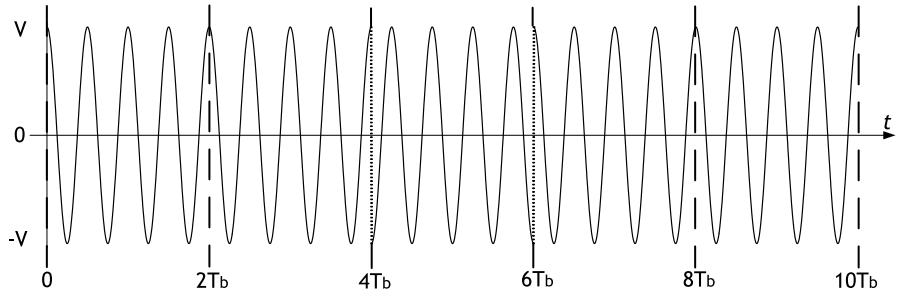

Figure B.3: In-phase component of the QPSK modulator.

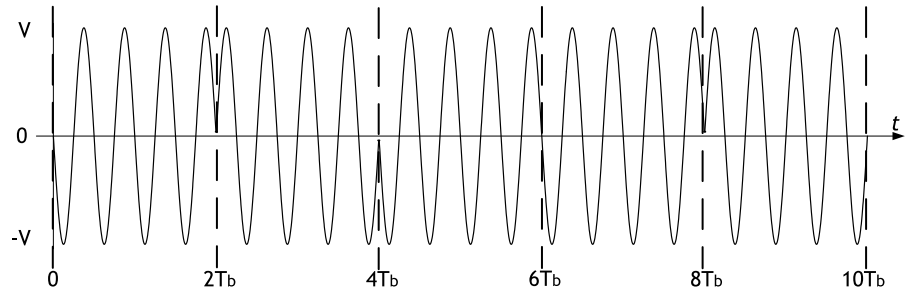

Figure B.4: Quadrature component of the QPSK modulator.

Figure B.5 presents the QPSK transmitted waveform.

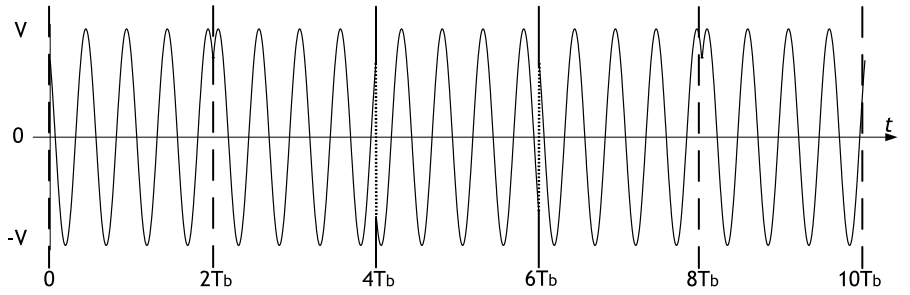

Figure B.5: QPSK waveform.

The idea of using a QPSK signal is to have an envelope that is ideally constant. However, this modulation can be used by different communication standards so as the signals must be band-limited by a band-pass filter, in order to fulfil the channel bandwidth requirements. Hence, the filter function will degrade the envelope properties. Moreover, every time a phase shift of Π occurs, the envelope will pass through zero momentary. Therefore, before transmitting, the QPSK signal is typically amplified by using a nonlinear power amplifier, the filter side lobes of the signal spectrum are also recreated. In order to avoiding such situations the of use linear amplifiers is advised. However, as explained in [NgSh09], these amplifiers have less efficiency when compared with the nonlinear amplifiers. The solution to deal with the Π phase shift problem is to consider an O-QPSK signal. This way, the possible changes are 0 or $\pm\Pi/2$ whilst the phase changes occur more frequently.

B.2 O-QPSK modulation

The difference between O-QPSK and QPSK consists in offsetting the F_i and Q_i bit streams by T_b. For the sake of simplicity, we assume that $T_b = T_c$, where T_c is the inverse of the chip rate [WPAN06]. Therefore, the phase changes occur more frequently, namely every T_b, and not every $T_s = 2T_b$ like in the QPSK modulation. Figure B.6 presents the block diagram for an O-QPSK modulator. The bit sequences for the different branches of an O-QPSK modulator are presented in Figure B.7.
The O-QPSK modulated signal is given by:

$$s(t) = F_i(t)Vcos(2\pi f_c t) + Q_i(t)Vsin(2\pi f_c t) \tag{B.4}$$

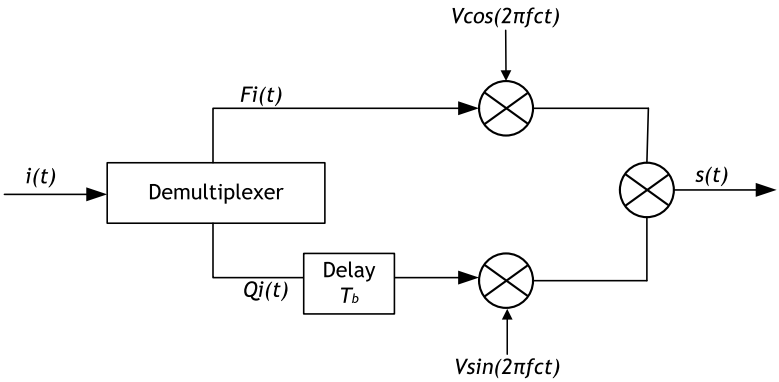

Figure B.6: Block diagram of an O-QPSK modulator.

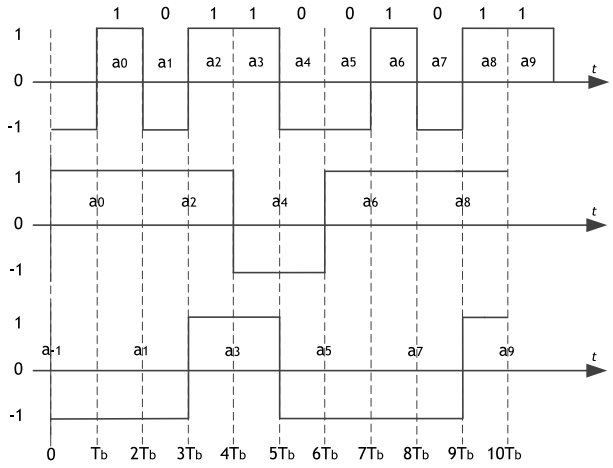

Figure B.7: O-QPSK modulator bit streams.

The O-QPSK odd and even chips (i.e., 32-streams) are generated in the same way as they would be generated for QPSK, with the exception that for the O-QPSK modulation the $F_i(t)$ and $Q_i(t)$ bit streams are offseted by T_b. By using the offset, the phase changes that occur in the combined signal never exceed $\pm\Pi/2$. As shown in Figure A.7, the O-QPSK signal cannot undergo a change of Π like in QPSK since the F_i bit stream has a transition in the middle of the Q_i bit stream. Hence, we conclude that the O-QPSK modulation limits the maximum abrupt phase shift in $s(t)$ whilst having better performance when compared with QPSK by avoiding having $F_i(t)$ and $Q_i(t)$ simultaneously crossing the 0 value, which could cause large amplitude variations in the envelope. Since in linear amplifiers zero crossing needs high power consumption, the use of O-QPSK also decreases the energy spent by the radio transceiver.

Figures B.8 and B.9 present, the in-phase and quadrature components for the bit sequence presented in Figure B.7. Figure B.10 shows the O-QPSK transmitted waveform itself.

The IEEE 802.15.4 radio transceivers operating in the 2.4 GHz band may employ a DSSS spreading technique. As a consequence the transmitter signal takes-up more bandwidth than the required to transmit the information signal being modulated. The name "spread spectrum" derives from the fact that the carrier signals occur over the full bandwidth (spectrum) of the sensor nodes transmitting frequency. The DSSS technique employs an O-QPSK modulation offering data rates up to 250 kb/s. The modulation and spreading technique uses a 16-ary quasi-orthogonal modulation, where four information bits are used to select one of 16 nearly orthogonal Pseudo-random Noise (PN) sequences to be transmitted.

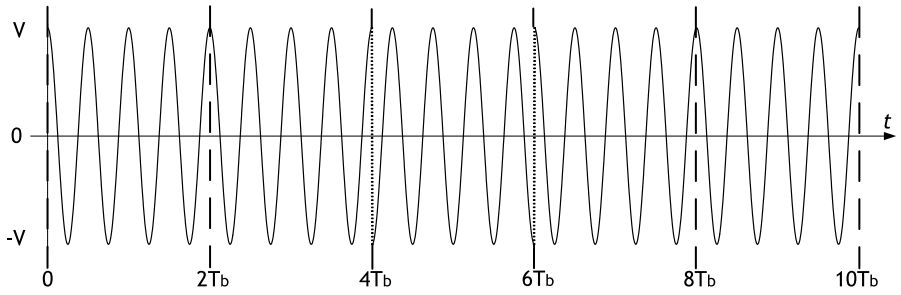

Figure B.8: In-phase component of the O-QPSK modulator.

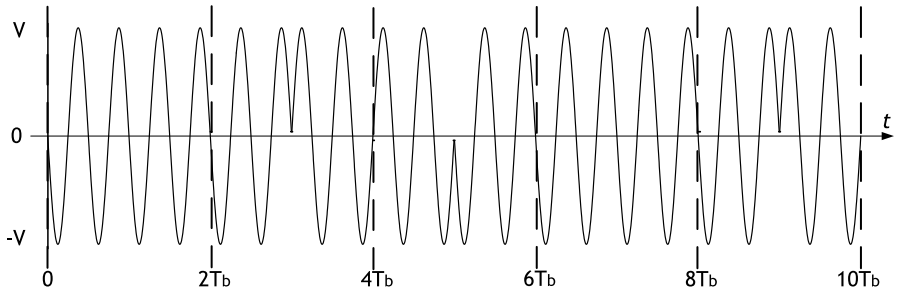

Figure B.9: Quadrature component of the O-QPSK modulator.

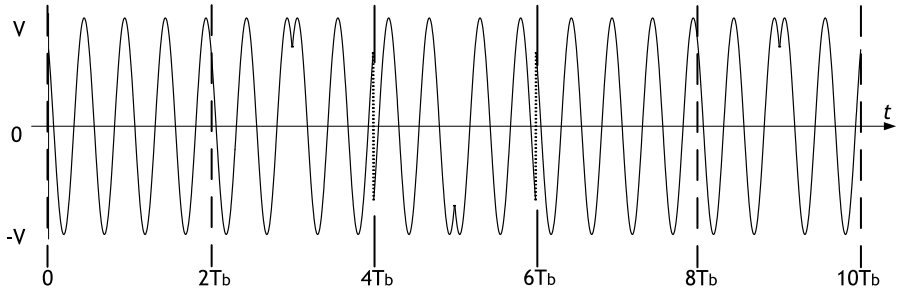

Figure B.10: O-QPSK waveform.

Next, the PN sequences for the successive data symbols are concatenated and the aggregated chips are modulated onto the carrier by using the O-QPSK modulator with half-sine pulse shaping, as shown in Figure B.11.

Figure B.11: Block diagram for the spreading and modulation functions.

Table B.2 presents the mapping between the data symbols and the 32-chip PN sequences. The data symbol bits are read from left to the right instead of right to left in this table. The bit-to-symbol module is responsible for mapping each octet (i.e., a group of eight bits) of the binary data by using the 4 least significant bits (LSBs) (b0, b1, b3, b4) to map one data symbol, and the 4 most significant bits (MSBs) (b4, b5, b6, b7) to map the next data symbol. Each symbol will be responsible for specifying one of the 16 nearly orthogonal 32-bit chip PN sequences for the transmission [WPAN06].

Table B.2: Symbol-to-chip mapping in the 2.4 GHz band.

Data symbol (decimal)	Data symbol (binary) (b0 b1 b2 b3)	Chip values (c0 c1 ... c30 c31)
0	0 0 0 0	1 1 0 1 1 0 0 1 1 1 0 0 0 0 1 1 0 1 0 1 0 0 1 0 0 0 1 0 1 1 1 0
1	1 0 0 0	1 1 1 0 1 1 0 1 1 0 0 1 1 1 0 0 0 0 1 1 0 1 0 1 0 0 1 0 0 0 1 0
2	0 1 0 0	0 0 1 0 1 1 1 0 1 1 0 1 1 0 0 1 1 1 0 0 0 0 1 1 0 1 0 1 0 0 1 0
3	1 1 0 0	0 0 1 0 0 0 1 0 1 1 1 0 1 1 0 1 1 0 0 1 1 1 0 0 0 0 1 1 0 1 0 1
4	0 0 1 0	0 1 0 1 0 0 1 0 0 0 1 0 1 1 1 0 1 1 0 1 1 0 0 1 1 1 0 0 0 0 1 1
5	1 0 1 0	0 0 1 1 0 1 0 1 0 0 1 0 0 0 1 0 1 1 1 0 1 1 0 1 1 0 0 1 1 1 0 0
6	0 1 1 0	1 1 0 0 0 0 1 1 0 1 0 1 0 0 1 0 0 0 1 0 1 1 1 0 1 1 0 1 1 0 0 1
7	1 1 1 0	1 0 0 1 1 1 0 0 0 0 1 1 0 1 0 1 0 0 1 0 0 0 1 0 1 1 1 0 1 1 0 1
8	0 0 0 1	1 0 0 0 1 1 0 0 1 0 0 1 0 1 1 0 0 0 0 0 0 1 1 1 0 1 1 1 1 0 1 1
9	1 0 0 1	1 0 1 1 1 0 0 0 1 1 0 0 1 0 0 1 0 1 1 0 0 0 0 0 0 1 1 1 0 1 1 1
10	0 1 0 1	0 1 1 1 1 0 1 1 1 0 0 0 1 1 0 0 1 0 0 1 0 1 1 0 0 0 0 0 0 1 1 1
11	1 1 0 1	0 1 1 1 0 1 1 1 1 0 1 1 1 0 0 0 1 1 0 0 1 0 0 1 0 1 1 0 0 0 0 0
12	0 0 1 1	0 0 0 0 0 1 1 1 0 1 1 1 1 0 1 1 1 0 0 0 1 1 0 0 1 0 0 1 0 1 1 0
13	1 0 1 1	0 1 1 0 0 0 0 0 0 1 1 1 0 1 1 1 1 0 1 1 1 0 0 0 1 1 0 0 1 0 0 1
14	0 1 1 1	1 0 0 1 0 1 1 0 0 0 0 0 0 1 1 1 0 1 1 1 1 0 1 1 1 0 0 0 1 1 0 0
15	1 1 1 1	1 1 0 0 1 0 0 1 0 1 1 0 0 0 0 0 0 1 1 1 0 1 1 1 1 0 1 1 1 0 0 0

Moreover, for the IEEE 802.15.4 standard the O-QPSK even-indexed chips are represented by the bit stream (F_i) onto the in-phase and the odd-indexed chips are represented by the bit stream (Q_i) onto the quadrature phase offset by T_c, as shown in Figure B.12.The data symbol is represented by a 32-chip sequence, as shown in Table B.2. The chip rate is 2.0 Mchip/s since it is 32 times the symbol rate (i.e, 62.5 ksymbol/s).

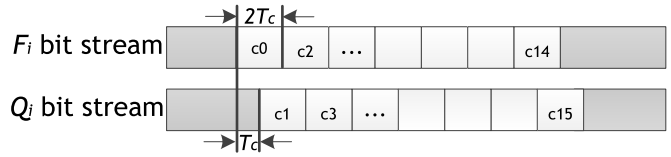

Figure B.12: O-QPSK chip offsets.

B.3 Minimum Shift Keying

If the rectangular pulse shapes used in O-QPSK are replaced by the following sinusoidal pulse shapes using $cos(\pi t/2T_c)$ and $sin(\pi t/2T_c)$ in the I and Q components respectively, the resulting modulation is known as Minimum Shift Keying (MSK). In [Fara08], the authors present a typical half-sin pulse shape filter in order to modify the shape of the binary pulses, as shown in Figure B.13.

Figure B.13: Half-sin pulse shaping filter.

Equations (B.5) and (B.6) present the half-sin pulse shape filter functions responsible to replace each bit stream with one half of sinusoidal signal in the in-phase and in quadrature respectively.

$$Filter_F(t) \begin{cases} cos(\pi t/2T_c),\ 0 \leqslant\ t \leqslant\ 2T_c \\ 0, \quad otherwise \end{cases} \tag{B.5}$$

$$Filter_Q(t) \begin{cases} sin(\pi t/2T_c),\ 0 \leqslant\ t \leqslant\ 2T_c \\ 0, \quad otherwise \end{cases} \tag{B.6}$$

where, T_c, represents the width of the bit.
Figure B.14 presents the block diagram for the MSK modulator.

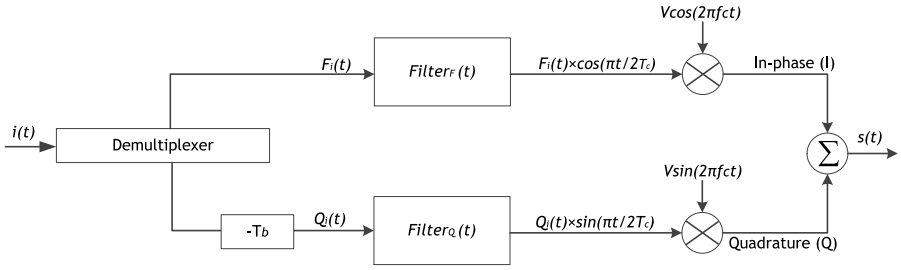

Figure B.14: MSK Modulator.

After applying the half-sine pulse shaping filter, the MSK modulated signal is given by:

$$s(t) = F_i(t)cos\left(\frac{\pi t}{2T_c}\right) Vcos(2\pi f_c t) - Q_i(t)sin\left(\frac{\pi t}{2T_c}\right) Vsin(2\pi f_c t) \tag{B.7}$$

To represent the MSK signal a chip rate of 2.0 Mchip/s (T_c = 500 ns) was considered. Figures B.15 and B.16 present the in-phase and quadrature components for the MSK modulator. Figure B.17 shows the resulting MSK transmitted waveform.

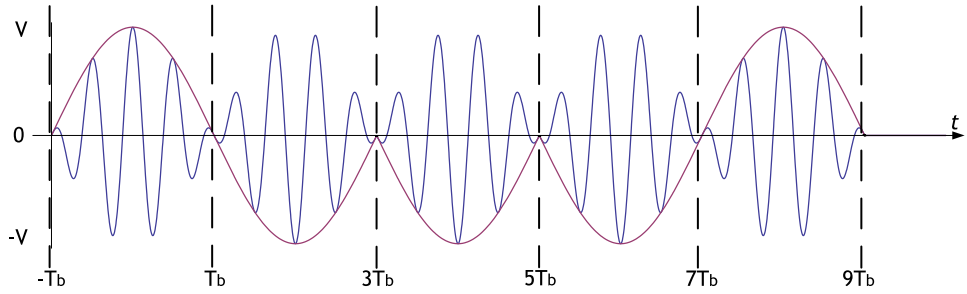

Figure B.15: In-phase component of the MSK modulator.

As it was already mentioned, the IEEE 802.15.4 defines that, for a radio transceiver operating in the 2.4 GHz band the PHY symbol rate shall be 62.5 ksymbol/s. Since the 32 chips are transmitted in the same time periods for transmitting 4 bits (one symbol), 32 times the symbol rate (i.e., 32×62.500), gives us a 2 Mchip/s rate.

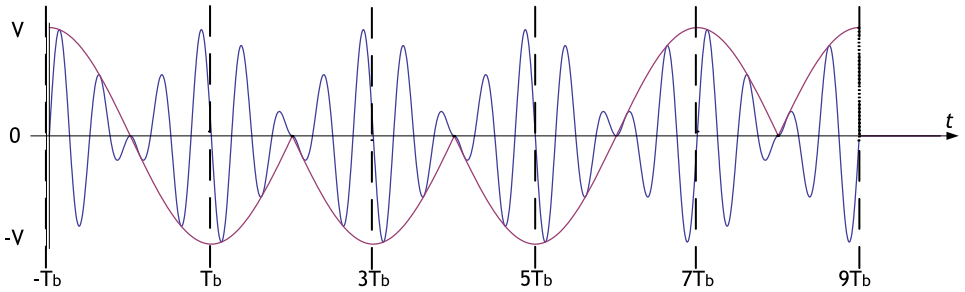

Figure B.16: Quadrature component of the MSK modulator.

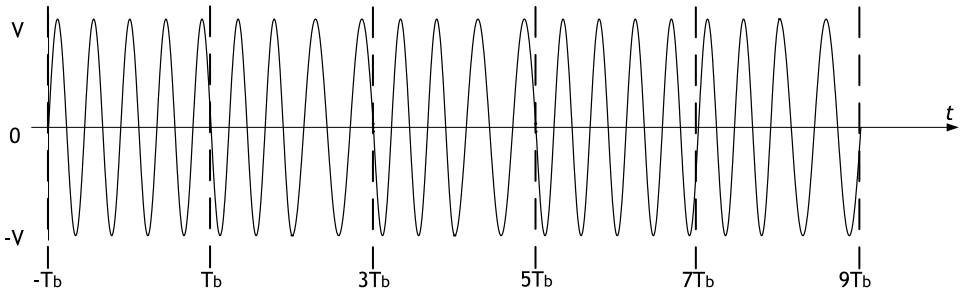

Figure B.17: MSK waveform.

A summary of all the calculations performed in order to obtain the value for T_c (as explained before, T_c is the inverse of the chip rate) are presented as follows:

$$\begin{cases} maximum\ data\ rate = 250\ kbps \\ maximum\ symbol\ data\ rate = 62.5\ ksymbols/s \\ bits\ per\ symbol = 4 \\ symbol\ period = 1/symbol\ frequency \\ bits\ per\ symbol = 250\ kbps/62.5\ ksymbols/s = 4 \\ symbol\ period = 1/62.5\ ksymbols/s = 16\mu s \\ T_c = 1/2\ Mchip/s = 500ns \end{cases} \tag{B.8}$$

B.4 Signal spreading

As explained before in the context of the O-QPSK modulation, every 4 bits are mapped in a 32-chip PN sequence. As so, there will be an increase of the over-the-air bit rate by a factor of eight. The total bandwidth will also increases by a factor of eight. Since the bit rate is proportional to the signal bandwidth, the signal bandwidth also increases by a factor of eight. The basic concept of signal spreading and despreading is shown in Figure B.18.

After spreading the bandwidth will be 2 MHz, and the magnitude of the power spectral density will decrease since the signal energy is "spread" over a larger bandwidth. In the despreading side, the signal energy will be concentrated back to the original bandwidth. The 32-chip PN sequence received is then compared with one of the 16 possible chip sequences presented in Table B.2. The most similar will be selected as the receiver chip sequence, being converted in the original data bit sent. Notice that the despreading technique does not affect the noise level in the 250 kHz bandwidth of interest. By increasing the desired band without increasing the noise level, the effective SNR is increased by the signal despreading. This increase in the

signal SNR will directly improve the receiver sensitivity.

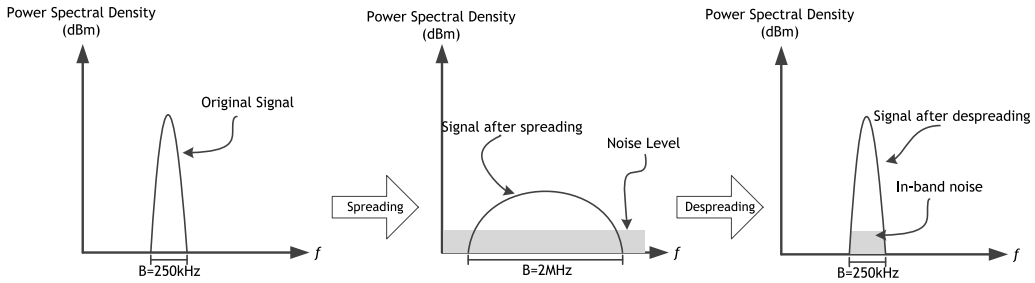

Figure B.18: Signal spreading and despreading.

This improvement in the SNR is referred in the IEEE 802.15.4 as the Spreading Gain (SG). The value of the SG is equal to the ratio of the signal bit rate after spreading to the signal bit rate before spreading. For the 2.4 GHz band the SG is given by:

$$SG = 10 \times log_{10}\left(\frac{2 \times 10^6}{250 \times 10^3}\right) \simeq 9\ dB \tag{B.9}$$

By considering the presence of an interfering signal, when the signal arrives at the destination, the despreading technique will concatenate the signal energy back to the 250 kHz bandwidth. And the interfering signal will be "spread" over a large bandwidth, Figure B.19. Moreover, in the receiver a filter will be applied to remove the spectral contents outside the 250 kHz bandwidth. The remaining portion of the interferer signal in the frequency band of interest has much lower power compared to the original interferer signal.

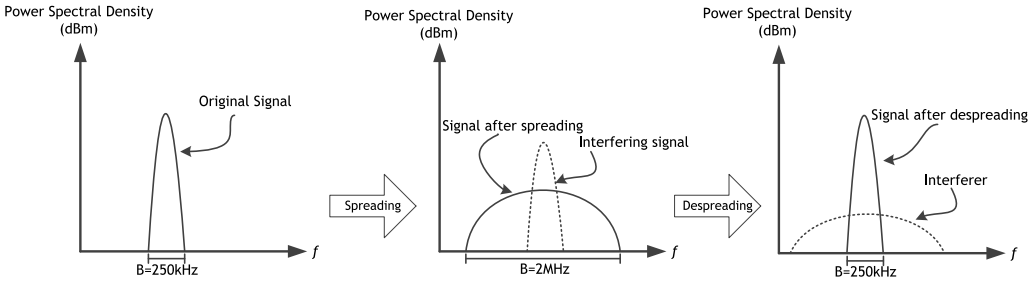

Figure B.19: Signal spreading and despreading by considering the effect of an interferer.

The signal-to-interference ratio (SIR) can be defined as the ratio of desired signal power to the total interference power:

$$SIR = \frac{Desired\ Signal\ Power}{Total\ Interference\ Power} \tag{B.10}$$

Appendix C

Energy consumption model for lifetime evaluation

The simplest model for determine the battery lifetime (T) is the Peukert's Law [RaVr01] enabling to define the non-linear relationship between the battery lifetime and the discharge rate without modelling the recovery effect. According to Peukert's law, T, can be obtained by dividing the capacity (Q) by a constant discharge current (I) as follows:

$$T = \frac{Q}{I^k} \tag{C.1}$$

where k represents the Peukert constant obtained experimentally for each battery. Ideally, Q is equal to the battery capacity and k is equal to 1. However, in practice Q has a value close to the battery's capacity, and k is a number greater than one (representing the non-linear characteristics of a battery). Depending on the battery type we are considering, k can have different values depending on the battery type. In this work we assume k equal to 1.05.
The majority of the WSN platforms use two AA batteries, where the node's capacity ranges from 2500 mAh to 3000 mAh. By assuming a battery capacity of $Q = 2500$ mAh and an average current consumption of $I = 0.3$ mAh the total battery lifetime is given as follows:

$$T_t = \frac{2500 \times 10^{-3}}{(0.3 \times 10^{-3})^{1.05}} = 12501.5\, hours \tag{C.2}$$

This result shows that by considering a current consumption of 0.3 mA and a capacity of 2500 mAh a node can last at least 12501.5 hours (approximately 520 days) before running out of battery. By analysing Equation (C.1), one may concludes, that Q can be considered as the total battery capacity, Q_t, or the drained capacity Q_d after an operation duration time (t_d). By considering the same assumptions of the model presented in [PaSS01] we can model the remaining capacity (Q_r) as follows:

$$Q_r = Q_t^{'} - Q_d \tag{C.3}$$

where, $Q_t^{'}$ represents the previous stored capacity over the interval $T_d < T_c$ and $Q_d \leq Q_t^{'} \leq Q_t$. The drained capacity ($Q_d$) over the time duration interval ranging from T_0 to T_d is given as follows:

$$Q_d = \int_{t=T_0}^{T_0+T_d} I(t)\, dt \tag{C.4}$$

By combining Equations (C.3) and (C.4) the remaining capacity, Q_r, is given as follows:

$$Q_r = Q_t^{'} - \int_{t=T_0}^{T_0+T_d} I(t)\, dt \tag{C.5}$$

where $I(t) = I^k$ is the drained capacity over the time duration T_d expressed as follows:

$$Q_d = \int_{t=T_0}^{T_0+T_d} I(t)\, dt = I^k t|_{t=T_0}^{T_0+T_d} = I^k \times (T_0 + T_d) - I^k \times (T_0) = I^k \times T_d \quad \text{(C.6)}$$

The remaining capacity, Q_r,can be simplified as follows:

$$Q_r = Q_t^{'} - I^k \times T_d \quad \text{(C.7)}$$

In order to evaluate the lifetime of the WSN platforms, we will estimate the overall energy consumption by the number of neighbouring nodes. During one transmission cycle, there is only one active node that has always a frame to be sent whereas the other neighbouring nodes can only accept frames and provide ACKs. Figure C.1 presents the IEEE 802.15.4 basic access mode by assuming a fixed-length duty cycle of 1%, being composed by the following time periods:

- Sleep Period;
- Time needed for switching from sleep to receiving;
- Backoff phase;
- CCA mechanism;
- Time needed for switching from receiving to transmitting;
- DATA transmission time;
- Time needed for switching from transmitting to receiving;
- ACK reception time;
- Time needed for switching from receiving to sleep;
- Sleep Period.

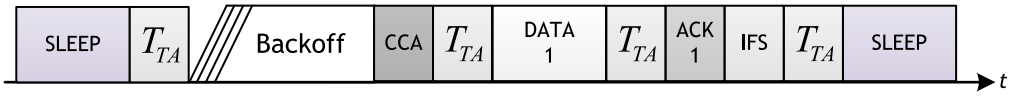

Figure C.1: IEEE 802.15.4 basic access mode.

The definition of the time periods presented in Figure C.1, have already been defined in the previous Chapters. Table C.1 summarizes the key parameters for the IEEE 802.15.4 standard that will be used to evaluate the lifetime of the WSN platforms.

Table C.1: IEEE 802.15.4 typical parameters and values.

Description	Symbol	Value
Backoff period duration	T_{BO}	320 μs
CCA detection time	T_{CCA}	128 μs
Setup radio to RX or TX states [RoAO09]	$rxSetupTime$	1720 μs
Time delay due to CCA	$ccaTime$	1920 μs
LIFS time	T_{LIFS}	640 μs
TX/RX or RX/TX switching time	T_{TA}	192 μs
PHY length overhead	L_{H_PHY}	6 bytes
MAC overhead	L_{H_MAC}	9 bytes
DATA payload	L_{DATA}	118 bytes
ACK frame length	L_{ACK}	11 bytes
DATA transmission time	T_{DATA}	4256 μs
ACK transmission time	T_{ACK}	352 μs
Data Rate	R	250 kb/s

The maximum backoff contention window, CW_{max}, is given as follows:

$$CW_{max} = \left(2^{BE} - 1\right) \times T_{BO} = (2^3 - 1) \times 320\,\mu s = 2.24\,ms \tag{C.8}$$

The average backoff contention window, $\overline{CW}$, is given by:

$$\overline{CW} = \left(\frac{CW_{max}}{2}\right) = 1.12\,ms \tag{C.9}$$

The time delay, due to CCA is given by:

$$ccaTime = rxSetupTime + T_{CCA} \tag{C.10}$$

The transmission times for the DATA and ACK frames are given as follows:

$$T_{DATA} = 8 \times \frac{L_{H\_PHY} + L_{H\_MAC} + L_{DATA}}{R} \tag{C.11}$$

$$T_{ACK} = 8 \times \frac{L_{H\_PHY} + L_{ACK}}{R} \tag{C.12}$$

By assuming, we are in the presence of an ideal channel with no errors. During one active period, there is only one node that has always a frame to be sent, whereas the other neighbouring nodes can only accept frames and provide acknowledgments.
The minimum delay, D_{min}, on average, for transmitting a packet and the successful reception of the ACK is given as follows:

$$D_{min} = \overline{CW} + ccaTime + T_{TA} + T_{DATA} + T_{TA} + T_{ACK} + T_{IFS} \tag{C.13}$$

By using the Peukert's Law, we have calculated the lifetime of a wireless sensor node by considering a capacity between 2500 mAh and 3000 mAh. The average current consumption accounts the current state of the radio transceiver (i.e., TX/RX/IDLE) and the microcontroller states (ACTIVE/SLEEP). Therefore, the energy consumption for transmitting/receiving a packet is given by:

$$\overline{I} = [i_{tx} \cdot t_{tx} + i_{rx} \cdot t_{rx} + i_{sleep} \cdot t_{sleep} + i_{\mu Pact} \cdot t_{\mu Pact} + i_{\mu Psleep} \cdot t_{\mu Psleep}] \cdot N \qquad \text{(C.14)}$$

The meaning of each variable is presented in Table C.2.

Table C.2: Notations for the average current estimation.

Notation	Parameter
$i_{\mu Pact}$	Microcontroller current on active state
$i_{\mu Psleep}$	Microcontroller current on sleep state
i_{tx}	Transceiver current on TX state
i_{rx}	Transceiver current on RX state
i_{sleep}	Transceiver current on SLEEP state
t_{tx}	Time on TX state
t_{rx}	Time on RX state
t_{sleep}	Time on SLEEP state
$t_{\mu Pact}$	Active time microcontroller
$t_{\mu Psleep}$	Sleep time microcontroller
$\overline{I}$	Average current consumption
N	Number of neighbours

Figure C.2 presents the lifetime results in years for each WSN platform, by assuming a fixed-length duty cycle of 1%.

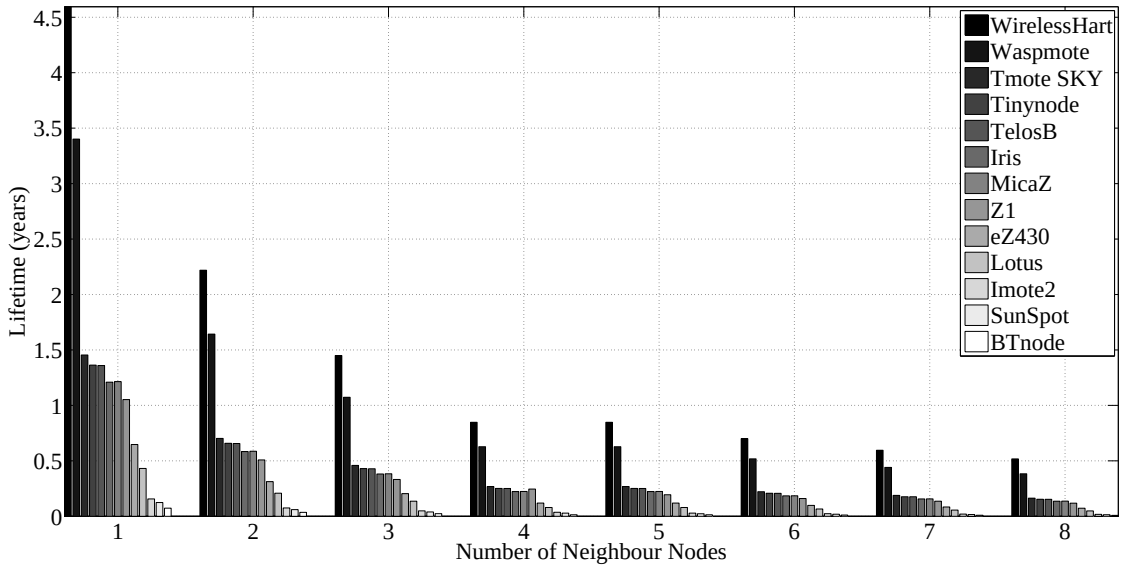

Figure C.2: Lifetime of the WSN platforms..

Appendix D

Detailed characterization of Wireless Sensor Network platforms

This Appendix presents some of the "well known" wireless sensor network platforms as well as the main features and technical characteristics. The platforms operate in the Industrial, Scientific and Medical (ISM) 2.4 GHz band and are compliant with the IEEE 802.15.4 standard. Specific information related with these platforms has been extracted from their datasheets, and are presented bellow. The information related with the MICAz and Imote2 platforms has already been presented in Section 4.

D.1 TelosB

The TelosB was inspired by the MICAx platform [Telo13], belonging to a newer generation of motes when compared with the MICA family, as they have a USB interface for data collection and programming [IPPB11]. This platform is an open source project, which includes: IEEE 802.15.4 compliant radio transceiver, integrated antenna, low-power MCU with extended memory and an optional sensor board. Figure D.1 presents the TelosB platform, while Table D.1 presents the characterisation parameters from the datasheet.

Figure D.1: TelosB platform.

D.2 Sun SPOT

The Sun SPOT platform was developed to enable the development of new applications and wireless sensor devices [SUNS13]. This WSN platform allows the easy development of applications even for programmers who have never worked before with embedded devices. Figure D.2 presents the Sun SPOT platform, while Table D.2 presents the characterisation parameters from the datasheet.

Figure D.2: Sun SPOT platform.

Table D.1: TelosB characterisation parameters.

Computational and storage subsystem		**Interfaces**	
Microcontroller	TI MSP430	Analog Inputs, Digital I/O, I2C, SPI, UART,	
RAM	10 kB	USB, 8 ADC (12 bit)	
Program Flash Memory	48 kB FLASH		
Speed	8 MHz		
Operating System	TinyOS		
Communication subsystem		**Miscellaneous**	
Transceiver	CC2420	**Power Source**	2 AA type batteries (3V)
Operating Frequency	2.4 GHz	P_{Sleep}	3 μW
Data Rate	250 kb/s	$P_{Receive}$	69 mW
Modulation Scheme	O-QPSK	$P_{Transmit}$	52.2 mW
Protocol	IEEE 802.15.4 compliant		
Range	$\simeq$ 75-100 m outdoor $\simeq$ 20-30 m indoor		

Table D.2: Sun SPOT characterisation parameters.

Computational and storage subsystem		**Interfaces**	
Microcontroller	ARM 920T	Analog Inputs, I2C, GPIOs, 4 ADC (12 bit)	
RAM	1 MB		
Program Flash Memory	8 MB FLASH		
Speed	400 MHz		
Operating System	TinyOS		
Communication subsystem		**Miscellaneous**	
Transceiver	CC2420	**Power Source**	3.7V rechargeable, 750 mAh lithium-ion battery
Operating Frequency	2.4 GHz	P_{Sleep}	3.7 μW
Data Rate	250 kb/s	$P_{Receive}$	74 mW
Modulation Scheme	O-QPSK	$P_{Transmit}$	66.6 mW
Protocol	IEEE 802.15.4 compliant		
Range	$\simeq$ 75-100 m outdoor $\simeq$ 20-30 m indoor		

D.3 IRIS

The IRIS platform presented in Figure D.3, is a mote operating at the 2.4 GHz frequency band used for enabling low-power wireless sensor networks. It provides high-level functional integration and was designed to optimize the addition of wireless mesh networking technology to a wide variety of custom sensing applications [IRIS13]. The main features are the increased radio range and twice the program memory when compared with the previous generations of MICA motes. The IRIS platform can be programmed by using the Mote Runner [RUNN13] software cre-

ated by IBM. The advanced hardware and software combination offers a user friendly platform for testing, debugging and maintaining applications. Table D.3 summarizes the characterisation parameters related with the functional and physical characteristics of the platform.

Figure D.3: IRIS platform.

Table D.3: IRIS characterisation parameters.

Computational and storage subsystem		**Interfaces**	
Microcontroller	ATmega1281	Analog Inputs, Digital I/O, I2C, SPI, UART,	
RAM	8 kB	8 ADC (10 bit)	
Program Flash Memory	128 kB FLASH		
Speed	400 MHz		
Operating System	TinyOS		
Communication subsystem		**Miscellaneous**	
Transceiver	AT86RF230	**Power Source**	2 AA type batteries (3V)
Operating Frequency	2.4 GHz	P_{Sleep}	3 μW
Data Rate	250 kb/s	$P_{Receive}$	48 mW
Modulation Scheme	O-QPSK	$P_{Transmit}$	51 mW
Protocol	IEEE 802.15.4 compliant		
Range	> 300 m outdoor > 50 m indoor		

D.4 Lotus

The LOTUS platform presented in Figure D.4, was developed around the low power ARM7 Cortex M3 CPU and incorporates the best of IRIS, TelosB and Imote2 into a single board [LOTU13]. LOTUS was built on a modular and stackable design, incorporating connectors for expansion boards, and features several new capabilities that enhance the overall functionality of MEMSIC's wireless sensor networking products and solutions. LOTUS is backward compatible with MEMSIC's MDA and MTS sensor data acquisition boards. Table D.4 summarizes the characterisation parameters from the datasheet.

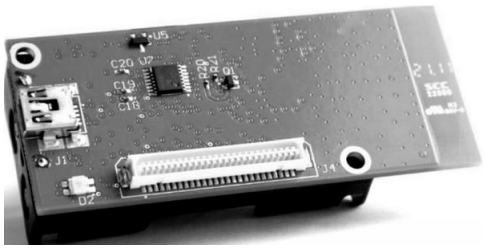

Figure D.4: Lotus platform.

Table D.4: Lotus characterisation parameters.

Computational and storage subsystem		**Interfaces**	
Microcontroller	Cortex® M3 32-bit	Analog Inputs, Digital I/O, I2C, SPI, UART,	
RAM	64 kB SRAM	8 ADC (10 bit)	
Program Flash Memory	512 kB FLASH		
Speed	100 MHz		
Operating System	TinyOS		
Communication subsystem		**Miscellaneous**	
Transceiver	LPR2400	**Power Source**	2 AA type batteries (3V)
Operating Frequency	2.4 GHz	P_{Sleep}	0.06 μW
Data Rate	250 kb/s	$P_{Receive}$	48 mW
Modulation Scheme	O-QPSK	$P_{Transmit}$	51 mW
Protocol	IEEE 802.15.4 compliant		
Range	> 300 m outdoor > 50 m indoor		

D.5 Waspmote

The Waspmote platforms is a developer's oriented platform [WASP13], enabling to work with different communication protocols (i.e., IEEE 802.15.4, Bluetooth and GPRS) and different ISM frequency bands (i.e., 2.4 GHz, 868 MHz and 900 MHz) enabling the creation of wireless links up to 12 Km. By using the low power sleep state it can save battery energy when there is no sensing task assigned to it, enabling the batteries to work for several years. The Waspmote is compatible with more than 100 sensors and its open source IDE makes really easy to start working with it. Figure D.5 presents the Waspmote platform, whilst Table D.5 presents the characterisation parameters from the datasheet.

Figure D.5: Waspmote platform.

Table D.5: Waspmote characterisation parameters.

Computational and storage subsystem		**Interfaces**	
Microcontroller	ATmega1281	Analog Inputs, Digital I/O, I2C,	
RAM	8 kB	SPI, UART, USB, 7 ADC (10 bit)	
Program Flash Memory	128 kB FLASH ROM 2 GB SD card		
Speed	100 MHz		
Operating System	Linux operating system		
Communication subsystem		**Miscellaneous**	
Transceiver	XBee-802.15.4	**Power Source**	2300/6600 mAh rechargeable battery
Operating Frequency	2.4 GHz	P_{Sleep}	0.18 μW
Data Rate	250 kb/s	$P_{Receive}$	45 mW
Modulation Scheme	O-QPSK	$P_{Transmit}$	45 mW
Protocol	IEEE 802.15.4 compliant ZigBee®		
Range	$\simeq$ 500 m outdoor $\simeq$ 100 m indoor		

D.6 WirelessHART

The WirelessHART™ LTP5902 platform from Linear Technology® is tailored for battery-powered energy harvesting wireless devices and for applications that require high performance and scalability features [WIHA13]. The WirelessHART LTP5902 enables a decade of battery lifetime by using innovative IEEE 802.15.4-compliant design and an integrated long-range power amplification. Additionally, motes can work both as routers and nodes, enabling a full mesh topology that provides more redundant routes and higher network performance. The radio circuitry includes a MMCX-type antenna connector that reduces the RF design complexity. Figure D.6 presents the LTP5902 platform, while Table D.6 presents thecharacterisation parameters from the datasheet.

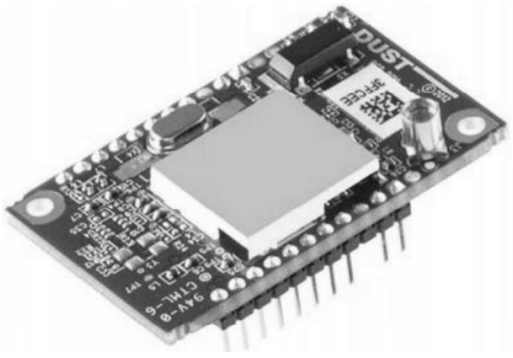

Figure D.6: WirelessHART platform.

Table D.6: WirelessHART characterisation parameters.

Computational and storage subsystem		**Interfaces**	
Microcontroller	ARM® Cortex-M3	Analog Inputs, Digital I/O, UART,	
RAM	72 kB	4 ADC (10 bit)	
Program Flash Memory	512 kB		
Speed	50 MHz		
Operating System	-		
Communication subsystem		**Miscellaneous**	
Transceiver	LTP5902 FR	**Power Source**	2 AA type batteries (3V)
Operating Frequency	2.4 GHz	P_{Sleep}	3.6 μW
Data Rate	250 kb/s	$P_{Receive}$	13.5 mW
Modulation Scheme	O-QPSK	$P_{Transmit}$	16.2 mW
Protocol	IEEE 802.15.4 compliant		
Range	$\simeq$ 300 m outdoor $\simeq$ 100 m indoor		

D.7 Tmote SKY

The Tmote SKY is a hardware platform for ultra-low power wireless sensor applications. It has humidity, temperature and light sensors incorporated [TMOT13]. It also includes circuitry for monitoring the battery voltage in real time. The platform was design to enable mesh network applications, with an IEEE 802.15.4 compliant radio transceiver. Figure D.7 presents the Tmote SKY platform, while Table D.7 presents the characterisation parameters from the datasheet.

Figure D.7: Tmote Sky platform.

Table D.7: Tmote Sky characterisation parameters.

Computational and storage subsystem		**Interfaces**	
Microcontroller	TI MSP430	Analog Inputs, Digital I/O, I2C, SPI,	
RAM	10 kB	UART, USB, 8 ADC (10 bit)	
Program Flash Memory	48 kB FLASH		
Speed	8 MHz		
Operating System	TinyOS, Contiki and MantisOS		
Communication subsystem		**Miscellaneous**	
Transceiver	CC2420	**Power Source**	2 AA type batteries (3V)
Operating Frequency	2.4 GHz	P_{Sleep}	3 μW
Data Rate	250 kb/s	$P_{Receive}$	60 mW
Modulation Scheme	O-QPSK	$P_{Transmit}$	53.1 mW
Protocol	IEEE 802.15.4 compliant		
Range	> 125 m outdoor $\simeq$ 50 m indoor		

D.8 Tinynode

Tinynode is an ultra-low power platform that can be supplied by using using 2 or 3 lithium batteries [Tiny13]. In the sleep state batteries can last more than 5 years. It sustains 19 configurable I/O pins, 6 analog inputs and 2 analog outputs, and has an 8 MHz TI MSP430 microcontroller, an on-board temperature sensor and a 30 pin Molex 52465-3071 board-to-board connector. It can be configured for long-range applications with low-bandwidth or for short-range applications with high-bandwidth. The Semtech XE 1205 transceiver can operate in 868 MHz or 915 MHz ISM frequency bands having the capability of using multichannel. Figure D.8 shows the Tinynode platform, while Table D.8 presents the characterisation parameters from the datasheet.

Figure D.8: Tinynode platform.

Table D.8: Tinynode characterisation parameters.

Computational and storage subsystem		**Interfaces**	
Microcontroller	TI MSP430	Analog Inputs, Digital I/O, SPI,	
RAM	10 kB	LVTTL (3V), UART, 6 ADC (12 bit)	
Program Flash Memory	48 kB FLASH		
Speed	8 MHz		
Operating System	TinyOS		
Communication subsystem		**Miscellaneous**	
Transceiver	Semtech XE 1205	**Power Source**	2 or 3 AA type batteries (3/4.5V)
Operating Frequency	868/915 MHz	P_{Sleep}	3 μW
Data Rate	20/40 kb/s	$P_{Receive}$	44.7 mW
Modulation Scheme	BPSK	$P_{Transmit}$	74.7 mW
Protocol	IEEE 802.15.4 compliant		
Range	> 200 m outdoor $\simeq$ 40 m indoor		

D.9 Z1

The Z1 platform was created by Zolertia for WSN applications [ZNOD13]. It includes a digital accelerometer, temperature sensors, a CC2420 radio transceiver and the 2^{nd} generation of MSP430f2617 microcontrollers for ultra-low-power consumption enabling to increase the lifetime of the sensor nodes. It supports the TinyOS and ContikiOS operating systems, and allows both the 6LoWPAN and ZigBee® stacks. The platform is compatible with other hardware platforms like the T-Mote family. Figure D.9 presents the Z1 platform, while Table D.9 provides more information about the functional and physical characterisation parameters from the datasheet.

Figure D.9: Z1 platform.

Table D.9: Z1 characterisation parameters.

Computational and storage subsystem		**Interfaces**	
Microcontroller	TI MSP430f2617	Analog Inputs, I2C, SPI, USB, UART, GPIO	
RAM	8 kB		
Program Flash Memory	92 kB FLASH		
Speed	16 MHz		
Operating System	TinyOS, Contiki		
Communication subsystem		**Miscellaneous**	
Transceiver	Semtech XE 1205	**Power Source**	2 AA or 2 AAA type batteries (3V)
Operating Frequency	2.4GHz	P_{Sleep}	3 μW
Data Rate	250 kb/s	$P_{Receive}$	56.4 mW
Modulation Scheme	O-QPSK	$P_{Transmit}$	52.2 mW
Protocol	IEEE 802.15.4 compliant		
Range	$\simeq$ 75-100 m outdoor $\simeq$ 20-30 m indoor		

D.10 BTnode

The BTnode platform presented in Figure D.10 has two radio transceivers, the CC1000 and the Zeevo ZV4002 Bluetooth [BTNO13]. It operates in the 433 MHz and 915 MHz ISM frequency bands. The software is open-source and includes demo examples in C programming. It can also be programmed by using the TinyOS operating system. Table D.10 presents the characterisation parameters from the datasheet.

Figure D.10: BTnode platform.

Table D.10: BTnode characterisation parameters.

Computational and storage subsystem		**Interfaces**	
Microcontroller	ATmega 128L	Analog Inputs, Digital I/O, SPI, ISP, I2C,	
RAM	64 kB	UART, ADC	
Program Flash Memory	128 kB FLASH		
Speed	8 MHz		
Operating System	TinyOS, BTnut		
Communication subsystem		**Miscellaneous**	
Transceiver	CC1000	**Power Source**	2 AA type batteries(3V)
Operating Frequency	433/915 MHz	P_{Sleep}	9.9 mW
Data Rate	9.6 kb/s	$P_{Receive}$	102.3 mW
Modulation Scheme	FSK	$P_{Transmit}$	102.3 mW
Protocol	Freq. Hopping		
Range	$\simeq$ 75-100 m outdoor $\simeq$ 20-30 m indoor		

D.11 EZ430-RF2500

The EZ430-RF2500 platform [EZTI13], is a low-power hardware tool developed by Texas Instruments (TI) that incorporates a MSP430F2274 microcontroller and a CC2500 radio transceiver working in the ISM 2.4 GHz frequency band. Although CC2500 has reduced power consumption, the protocol stack is not IEEE 802.15.4 compliant, although it also has the 16 frequency channels ranging from 2405 MHz to 2480 MHz as in IEEE 802.15.4. Figure D.11 presents the EZ430-RF2500 platform, while Table D.11 provides more information about the functional and physical characterisation parameters from the datasheet.

Figure D.11: EZ430-RF2500 platform.

Table D.11: EZ430-RF2500 characterisation parameters.

Computational and storage subsystem		**Interfaces**	
Microcontroller	TI MSP430	Analog Inputs, Digital I/O, SPI,	
RAM	1 kB	LVTTL (3V), UART, ADC	
Program Flash Memory	32 kB FLASH		
Speed	8 MHz		
Operating System	-		
Communication subsystem		**Miscellaneous**	
Transceiver	CC2500	**Power Source**	2 AAA type batteries(3V)
Operating Frequency	2.4 GHz	P_{Sleep}	1.2 μW
Data Rate	250/500 kb/s	$P_{Receive}$	49.8 mW
Modulation Scheme	2-FSK, MSK	$P_{Transmit}$	63.6 mW
Protocol	-		
Range	> 50 m outdoor > 50 m indoor		

Previously it has been shown that a vast diversity of WSN platforms can be found on the market, where the majority employs the IEEE 802.15.4 compliant radio transceivers and a few employ their own standards and protocols. Based on that a comparison will be made in Section 4 enabling choose the most appropriate hardware platform for WSNs based on three different groups of criteria: i) main characteristics, ii) power requirements and iii) expansibility, programming and community resources.

Appendix E

Additional results for the MAC Sub-layer Protocols Employing RTS/CTS with Packet Concatenation

Additional results for the SBACK-MAC protocol are presented in the following section of this Appendix. Therefore, we provide performance evaluation for IEEE 802.15.4 with and with no RTS/CTS and SBACK-MAC with and with no *BACK Request* with no retransmissions

E.1 Minimum average delay

A. Dependence on the number of TX packets for a fixed payload of 3 bytes

Figure E.1 presents the analytical and simulation results for the minimum average delay, D_{min}, as a function of the number of TX packets with no retransmissions (RTX).

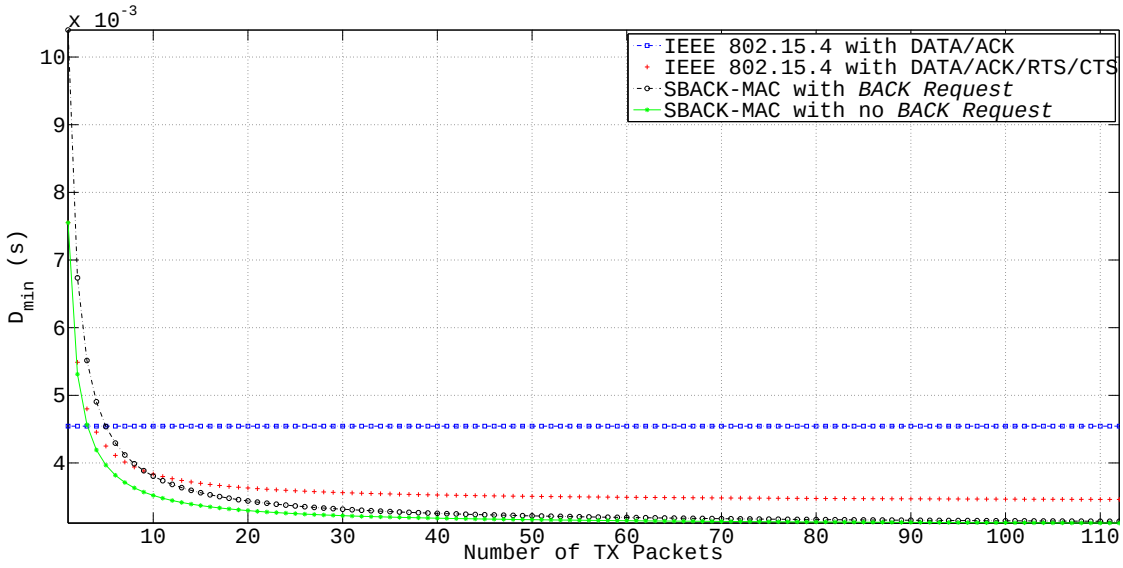

Figure E.1: Minimum average delay as a function of the number of TX packets with no RTX.

By considering a number of aggregated packets equal to 10 we have the following observations:

- For the IEEE 802.15.4 standard with RTS/CTS, D_{min}, is decreased approximately 18 % when compared with IEEE 802.15.4 in the basic access mode;
- For the SBACK-MAC protocol with and with no *BACK Request*, D_{min}, is decreased by 18 % and 30 %, respectively when compared with IEEE 802.15.4 in the basic access mode;
- The minimum average delay, D_{min}, for the IEEE 802.15.4 with and with no RTS/CTS is 0.0045 s and 0.0038 s, respectively;
- The minimum average delay, D_{min}, for the SBACK-MAC with and with no *BACK Request* is 0.0038 s and 0.0034 s, respectively.

By using a number of aggregated packets equal to 80 we observe the following::

- For the IEEE 802.15.4 standard with RTS/CTS, D_{min}, is decreased approximately 28 % when compared with IEEE 802.15.4 in the basic access mode;
- For the SBACK-MAC protocol with and with no *BACK Request*, D_{min}, is decreased by 40 % and 45 %, respectively when compared with IEEE 802.15.4 in the basic access mode;
- The minimum average delay, D_{min}, for the IEEE 802.15.4 with and with no RTS/CTS is 0.0045 s and 0.0035 s, respectively;
- The minimum average delay, D_{min}, for the SBACK-MAC with and with no *BACK Request* is 0.0032 s and 0.0031 s, respectively.

B. Dependence on the payload size for a number of transmitted packets equal to 10

Figure E.2 presents the analytical and simulation results for the minimum average delay, D_{min}, as a function of the payload size with no retransmissions (RTX).

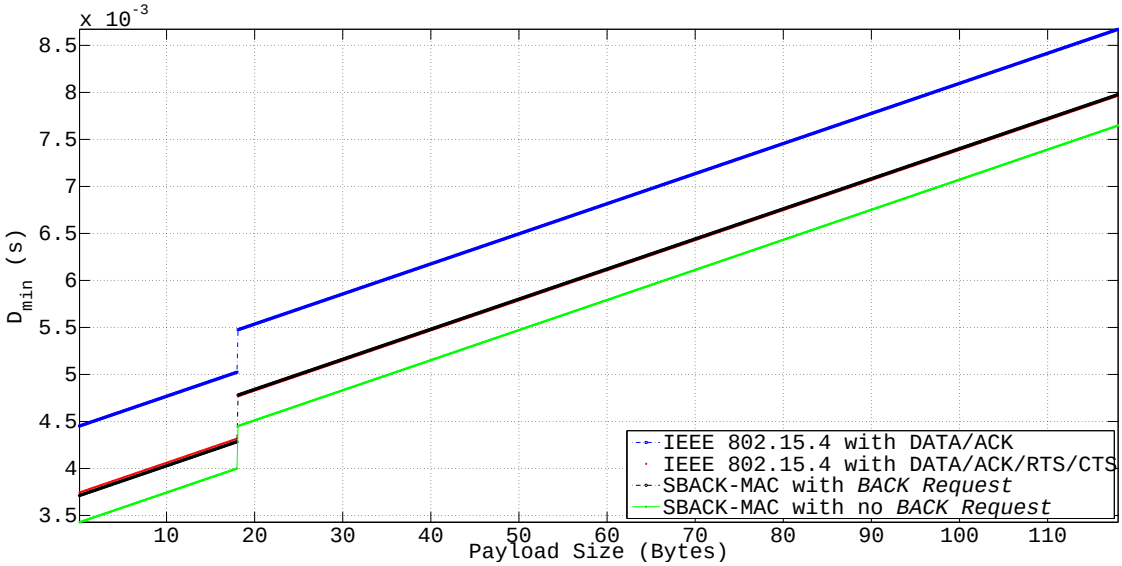

Figure E.2: Minimum average delay as a function of the payload size with no RTX.

By considering small packet sizes (i.e., data payload less than 18 bytes), for a payload of 17 bytes we notice that:

- By considering the IEEE 802.15.4 standard with RTS/CTS, D_{min}, is decreased approximately 17 % when compared with IEEE 802.15.4 in the basic access mode;
- For the SBACK-MAC protocol with and with no *BACK Request*, D_{min}, is decreased by 17 % and 25 %, respectively, when compared with IEEE 802.15.4 in the basic access mode;
- The minimum average delay, D_{min}, for IEEE 802.15.4 with and with no RTS/CTS is 0.005 s and 0.0043 s, respectively;
- The minimum average delay, D_{min}, for SBACK-MAC with and with no *BACK Request* is 0.0043 s and 0.004 s, respectively.

For longer packet sizes (i.e., data payload longer than 18 bytes), and for a data payload equal to 118 bytes we observe that:

- By considering the IEEE 802.15.4 standard with RTS/CTS, D_{min}, is decreased approximately 8.8 % when compared with IEEE 802.15.4 in the basic access mode;
- For the SBACK-MAC protocol with and with no *BACK Request*, D_{min} is decreased by 8.6 % and 13%, respectively when compared with IEEE 802.15.4 in the basic access mode;
- The minimum average delay, D_{min} , for IEEE 802.15.4 with and with no RTS/CTS is 0.0087 s and 0.0079 s, respectively;
- The minimum average delay, D_{min} , for the SBACK-MAC with and with no *BACK Request* is 0.008 s and 0.0076 s, respectively.

E.2 Maximum average throughput

A. Dependence on the number of TX packets for a fixed payload of 3 bytes

Figure E.3 presents the analytical and simulation results for the maximum average throughput, S_{max}, as a function of the number of TX packets by considering a fixed payload size, of $L_{DATA} =$ 3 bytes. When the number of TX packets (formed by the physical and MAC header plus the data payload, with a total number of bytes given by: $L_{PHY} + L_{MAC} + L_{DATA}$) is less than 3 the IEEE 802.15.4 standard in the basic access achieves higher throughput than SBACK-MAC with and with no *BACK Request*. Moreover, by using the IEEE 802.15.4 standard in the basic access mode S_{max}, does not depend on the number of TX packets, attaining a value equal to 5.2 kb/s, whereas for SBACK-MAC with and with no *BACK Request* (i.e., concatenation and piggyback) S_{max} increases by increasing the number of TX packets (i.e., the number of aggregated packets).

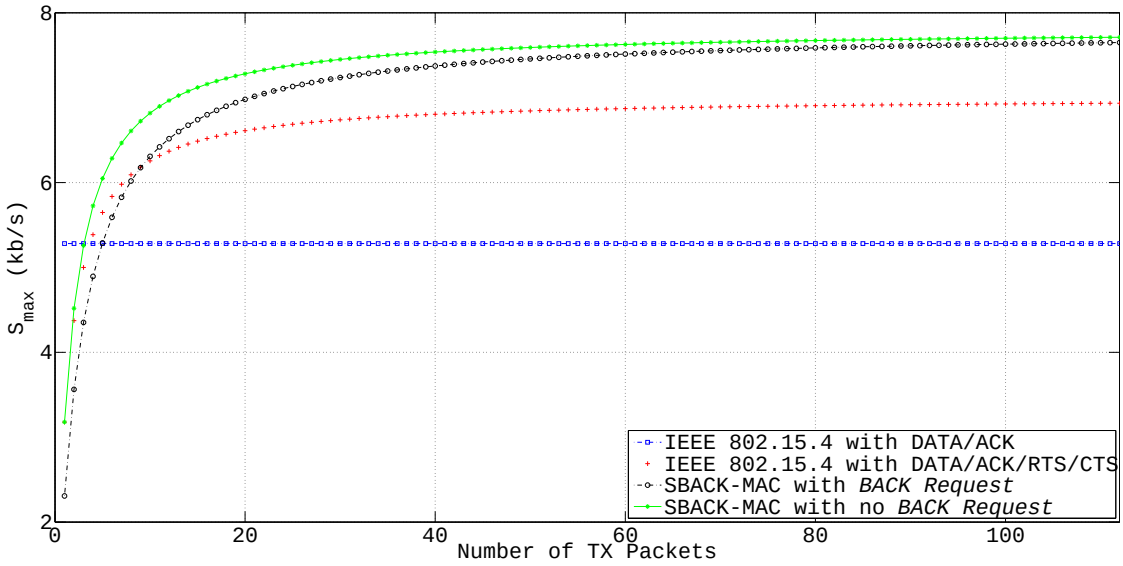

Figure E.3: Maximum average throughput as a function of the number of TX packets with no RTX.

For a number of aggregated packets equal to 10:

- By using the IEEE 802.15.4 standard with RTS/CTS, S_{max}, is increased approximately 20 % when compared with IEEE 802.15.4 in the basic access mode;
- For the SBACK-MAC protocol with and with no *BACK Request*, S_{max}, is increased by 21 % and 30 %, respectively when compared with IEEE 802.15.4 in the basic access mode;
- The maximum average throughput, S_{max}, for IEEE 802.15.4 with and with no RTS/CTS is 5.2 kb/s and 6.25 kb/s, respectively;
- The maximum average throughput, S_{max}, for SBACK-MAC with and with no *BACK Request* is 6.3 kb/s and 6.8 kb/s, respectively.

For a number of aggregated packets equal to 80:

- By considering the IEEE 802.15.4 standard with RTS/CTS, S_{max}, is increased approximately 30 % when compared with IEEE 802.15.4 in the basic access mode;
- For the SBACK-MAC protocol with and with no *BACK Request*, S_{max}, is increased by 43 % and 45 %, respectively when compared with IEEE 802.15.4 in the basic access mode;
- The maximum average throughput, S_{max}, for IEEE 802.15.4 with and with no RTS/CTS is 5.2 kb/s and 6.9 kb/s, respectively;
- The maximum average throughput, S_{max}, for SBACK-MAC with and with no *BACK Request* is 7.58 kb/s and 7.67 kb/s, respectively.

B. Dependence on the payload size for a number of transmitted packets equal to 10

Figure E.4 illustrates the analytical and simulation results for maximum average throughput, S_{max}, as a function of the payload size with no retransmissions (RTX).

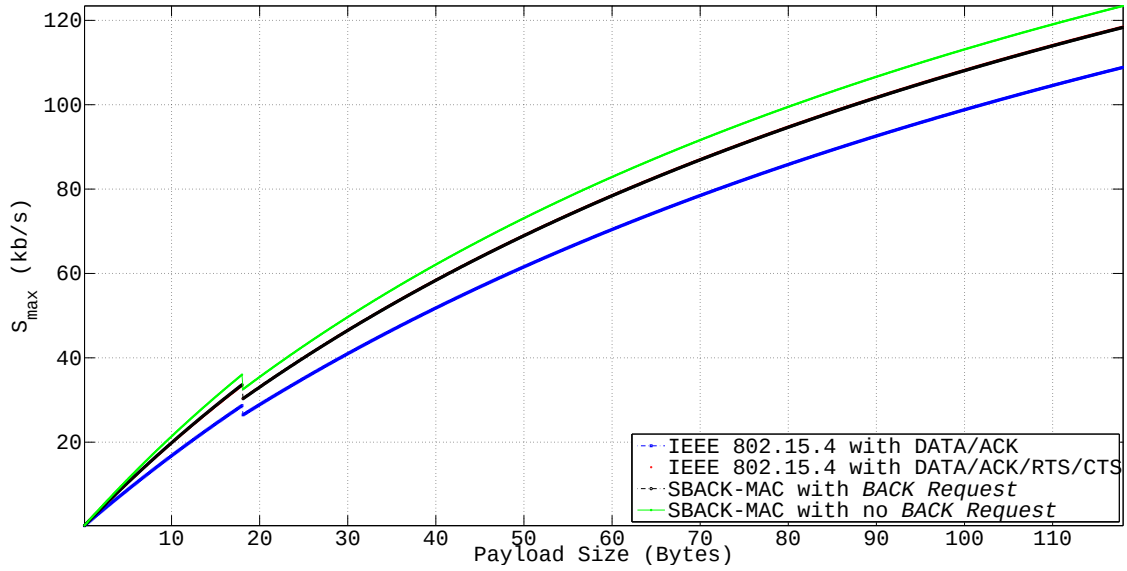

Figure E.4: Maximum average throughput as a function of the payload size with no RTX.

By considering small packet sizes (i.e., data payload less than 18 bytes), for a payload of 17 bytes:

- By considering the IEEE 802.15.4 standard with RTS/CTS, S_{max}, is increased approximately 17 % when compared with IEEE 802.15.4 in the basic access mode;
- For the SBACK-MAC protocol with and with no *BACK Request*, S_{max}, is increased by 17 % and 25 %, respectively when compared with IEEE 802.15.4 in the basic access mode;
- The maximum average throughput, S_{max}, for IEEE 802.15.4 with and with no RTS/CTS is 28.66 kb/s and 33.53 kb/s, respectively;
- The maximum average throughput, S_{max}, for SBACK-MAC with and with no *BACK Request* is 33.6 kb/s and 36 kb/s, respectively.

By using longer packet sizes (i.e., data payload longer than 18 bytes), for a data payload equal to 118 bytes:

- By considering the IEEE 802.15.4 standard with RTS/CTS, S_{max}, is increased approximately 8.8 % when compared with IEEE 802.15.4 in the basic access mode;
- For the SBACK-MAC protocol with and with no *BACK Request*, S_{max}, is increased by 8.6 % and 13 %, respectively when compared with IEEE 802.15.4 in the basic access mode;
- The maximum average throughput, S_{max}, for IEEE 802.15.4 with and with no RTS/CTS is 108.9 kb/s and 118.5 kb/s, respectively;
- The maximum average throughput, S_{max}, for SBACK-MAC with and with no *BACK Request* is 118.3 kb/s and 123.4 kb/s, respectively.

E.3 Final remarks

In this Appendix we have shown a new innovative MAC sub-layer employing RTS/CTS with packet concatenation. The SBACK-MAC with and with no *BACK Request* was compared against IEEE 802.15.4 with and with no RTS/CTS. Figure E.5 presents the increase of the maximum average throughput, S_{max}, as a function of the payload size. For small packet sizes, S_{max}, is increased by 17 % for IEEE 802.15.4 with RTS/CTS and SBACK-MAC with *BACK Request* and 25 % for the SBACK-MAC with no *BACK Request*. By considering longer packet sizes, S_{max}, is increased by 8.8 % for IEEE 802.15.4 with RTS/CTS, 8.6 % for SBACK-MAC with *BACK Request* and 25 % for SBACK-MAC with no *BACK Request*.
Figure E.6 presents the decrease of the minimum average delay, D_{min}, as a function of the payload size. For small packet sizes, D_{min}, is decreased by 17 % for IEEE 802.15.4 employing RTS/CTS and SBACK-MAC with *BACK Request* and 25 % for the SBACK-MAC with no *BACK Request*. By considering longer packet sizes, D_{min}, is decreased by 8.8 % for the IEEE 802.15.4 employing RTS/CTS, 8.6 % for SBACK-MAC with *BACK Request* and 25 % for SBACK-MAC with no *BACK Request*.

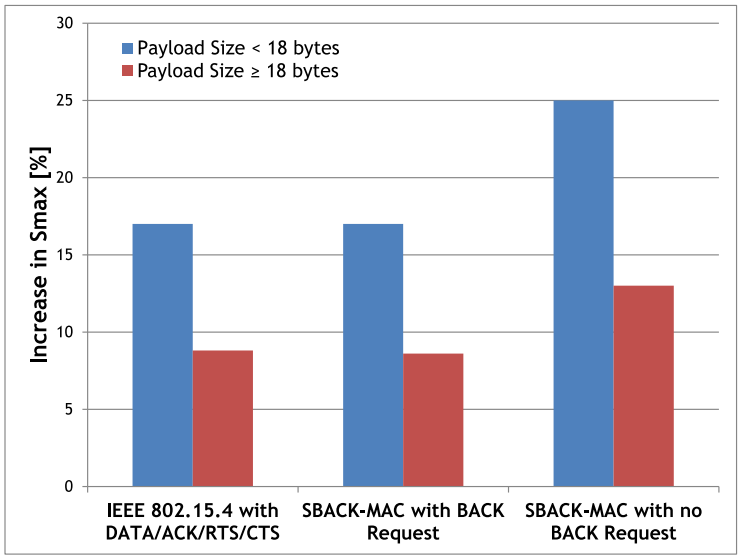

Figure E.5: Increase of the maximum average throughput, S_{max}, as a function of the payload size for the presented MAC sub-layer mechanisms.

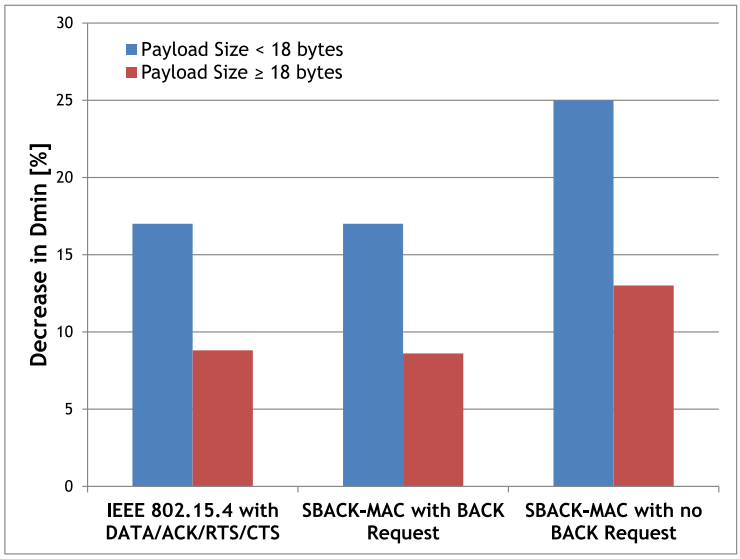

Figure E.6: Decrease of the minimum delay, D_{min}, as a function of the payload size for the presented MAC sub-layer mechanisms.

Figure E.7 presents the increase of the maximum average throughput, S_{max}, as a function of the number of TX packets (aggregated). For 10 aggregated packets, S_{max}, is increased by 20 % for IEEE 802.15.4 employing RTS/CTS, 21 % for SBACK-MAC with *BACK Request* and 30 % for the SBACK-MAC with no *BACK Request*. By considering 80 aggregated packets, S_{max} is increased by 30 % for IEEE 802.15.4 with RTS/CTS, 43 % for SBACK-MAC with *BACK Request* and 45 % for the SBACK-MAC with no *BACK Request*.

Figure E.8 presents the decrease of the minimum average delay, D_{min}, as a function of the number of TX packets. For 10 aggregated packets, D_{min}, is decreased by 18 % for the IEEE 802.15.4 with RTS/CTS and SBACK-MAC with *BACK Request* and 30 % for the case we consider the SBACK-MAC with no *BACK Request*. By considering 80 aggregated packets, D_{min}, is decreased by 28 % for the IEEE 802.15.4 with RTS/CTS, 40 % for SBACK-MAC with *BACK Request* and 45 % for SBACK-MAC with no *BACK Request*.

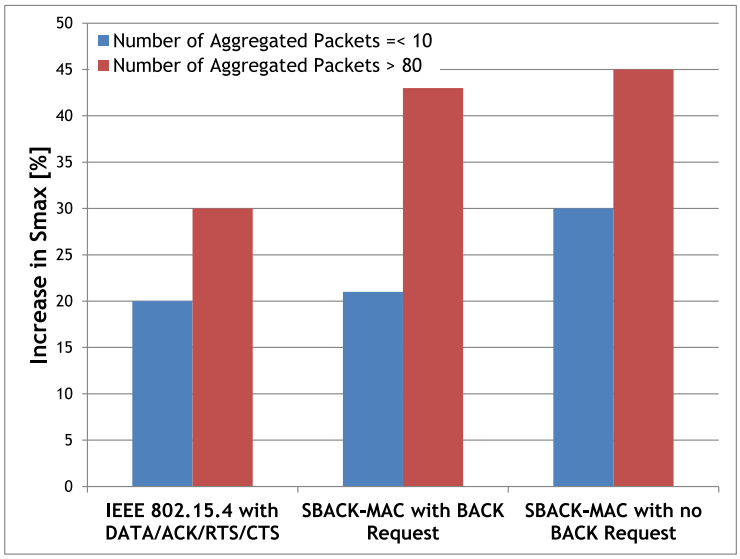

Figure E.7: Increase of the maximum throughput, S_{max}, as a function of the number of TX packets for the presented MAC mechanisms.

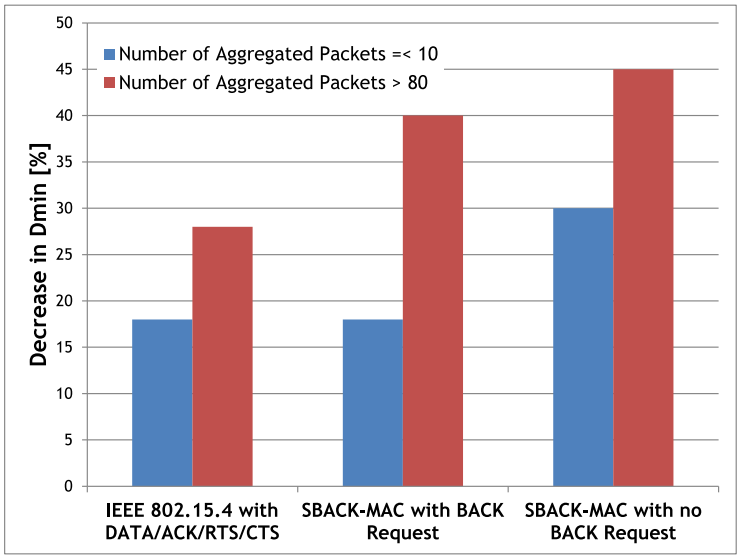

Figure E.8: Decrease of the minimum average delay, D_{min}, as a function of the payload size for the presented MAC sub-layer mechanisms.

References

[ADSS13] Advanced Design System (ADS) software, Aug 2013. [Online]. Available: http://www.home.agilent.com/en/pc-1297113/advanced-design-system-ads?&cc=PT&lc=eng.

[AkKE09] O. B. Akan, O. B. Karli and O. Ergul, "Cognitive Radio Sensor Networks," *IEEE Network*, vol. 23, no. 4, pp. 30-40, Aug. 2009.

[ASSC02] I. F. Akyildiz, W. Su, Y. Sankarasubramaniam, and E. Cayirci, "A survey on sensor networks," *IEEE Communications Magazine*, vol. 40, no. 8, pp. 102-114, Aug. 2002.

[BaVC13a] N. Barroca, F. J. Velez and P. Chatzimisios, "Block Acknowledgment Mechanisms for the optimization of channel use in Wireless Sensor Networks", in *Proc. of The 24th Annual IEEE International Symposium on Personal, Indoor and Mobile Radio Communications (PIMRC 2013)*, London, UK, Sep. 2013, pp. 1570-1575.

[BaVC13b] N. Barroca, F. J. Velez and P. Chatzimisios, "ACK aggregation mechanisms for the optimization of channel use in WSN with CR capabilities", Short Term Scientific Mission Report, COST-STSM-ECOST-STSM-IC0905-170513-030636, Thessaloniki, Greece, May 2013.

[BaGV13] N. Barroca, Paulo T. Gouveia and F. J. Velez, "Impact of Switching Latency Times in Energy Consumption of IEEE 802.15.4 Radio Transceivers," in *Proc. of The 9th Conference on Telecommunications - Conftele 2013*, Castelo Branco, Portugal, May 2013.

[BALR10] L. M. Borges, P. Araújo, A. S. Lebres, A. Rente, L. R. Salvado, F. J. Velez, J. M. de Oliveira, N. Barroca and J. M. Ferro, "Wearable sensors for foetal movement monitoring in low risk pregnancies" - Chapter in *Wearable and Autonomous Biomedical Devices and Systems for Smart Environment: Issues and Characterization*, Aimé Lay-Ekuakille; Subhas Chandra Mukhopadhyay, Springer, Norwell, MA, USA, 2010.

[BBTV13] N. Barroca, L. M. Borges, J. Tavares, F. J. Velez, R. C.-Santiago and I. Balasingham "Identification of the Opportunistic Radio Frequency Bands for Energy Harvesting in Wireless Body Area Networks," in *Proc. of the 9th Conference on Telecommunications Conftele 2013*, Castelo Branco, Portugal, May 2013.

[BBVC13] N. Barroca, L. M. Borges, F. J. Velez and P. Chatzimisios, "Performance Analysis of IEEE 802.15.4 by Using CSS PHY and RTS/CTS Combined with Packet Concatenation", *submitted IEEE Communications Letters, Dec. 2013*.

[BBVC14] N. Barroca, L. M. Borges, F. J. Velez and P. Chatzimisios, "IEEE 802.15.4 MAC Layer Performance Enhancement by employing RTS/CTS combined with Packet Concatenation", *in Proc. of The IEEE International Conference on Communications (ICC)*, Sydney, Australia, Jun. 2014.

[BBVL08] L. M. Borges, N. Barroca, F. J. Velez, and A. S. Lebres. Flex Sensor Belt. Technical Report TR-3-2008, Universidade da Beira Interior, Covilhã, Portugal, Mar. 2008.

[BBVL09a] L. M. Borges, N. Barroca, F. J. Velez and A. S. Lebres, "Wireless Flex Sensor Belt Networks for Foetal Movement Monitoring in Low Risk Pregnancies," in *Proc. of XIX*

IMEKO World Congress Fundamental and Applied Metrology, Lisbon, Portugal, Sep. 2009, pp. 1750-1754.

[BBVL09b] L. M. Borges, N. Barroca, F. J. Velez, and A. S. Lebres, "Smart-Clothing Wireless Flex Sensor Belt Network for Foetal Health Monitoring," in *Proc. of WiPH 2009 - International Workshop on Wireless Pervasive Healthcare (held in conjunction with 3rd International Conference on Pervasive Computing Technologies for Healthcare 2009)*, London, UK, Mar. 2009, pp. 1-4.

[BBVM11] N. Barroca, L. M. Borges, F. J. Velez, Filipe M., Ma. Górski, and J. C. Gomes. "Wireless Sensor Networks applied to Engineering Structures". Technical Report TR-1-2011, Universidade da Beira Interior, Covilhã, Portugal, Nov. 2011.

[BBVM13] N. Barroca, L. M. Borges, F. J. Velez, Filipe M., Ma. Górski, and J. C. Gomes. "Cognitive Radio for Medical Body Area Networks Using Ultra Wideband,"*IEEE Wireless Communications, Special Issue on Cognitive Radio Networks - A Practical Perspective*, vol. 40, no.1, pp. 1156-1166, Mar. 2013.

[BDKG08] N. Buenfeld, R. Davis, A. Karmini and A. Gilbertson, "Intelligent monitoring of concrete structures," 666th ed., CIRIA, London, UK, 2008.

[BeWi10] S. Beeby and N. White, *Energy Harvesting for Autonomous Systems (Smart Materials, Structures, and Systems)*, *Artech House*, Norwood, USA, Jun. 2010.

[BFBT12] N. Barroca, J. M. Ferro, L. M. Borges, J. Tavares and F. J. Velez, "Electromagnetic Energy Harvesting for Wireless Body Area Networks with Cognitive Radio Capabilities," in *Proc. of URSI Seminar of the Portuguese Committee*, Lisbon, Portugal, Nov. 2012.

[BMVF11] C. Buratti, M. Martalò, R. Verdone and G. Ferrari, *Sensor Networks with IEEE 802.15.4 Systems*, Springer, New York, USA, 2011.

[BoVL13] L. M. Borges, F. J. Velez and A. S. Lebres, "Survey on the Characterization and Classification of Wireless Sensor Networks Applications," *submitted to IEEE Communications Surveys and Tutorials*, Dec. 2013 (to be revised and resubmitted).

[BQ2513] BQ25504, Ultra Low Power Boost Converter with Battery Management for Energy Harvester Applications, Aug 2013. [Online]. Available: http://www.ti.com/product/bq25504.

[BRVS08] L. M. Borges, A. Rente, F. J. Velez, L. R. Salvado, A. S. Lebres, J. M. de Oliveira, P. Araújo and J. M. Ferro, "Overview of Progress in Smart-Clothing Project for Health Monitoring and Sport Applications," in *Proc. of the First International Symposium on Applied Sciences in Biomedical and Communication Technologies (ISABEL 2008)*, Aalborg, Denmark, Oct. 2008, pp. 1-6.

[BSGT13] N. Barroca, H. M. Saraiva, P. T. Gouveia, J. Tavares, L. M. Borges, F. J. Velez, C. Loss, R. Salvado, P. Pinho, R. Gonçalves, N. B. Carvalho, R. C.-Santiago, I. Balasingham, "Antennas and Circuits for Ambient RF Energy Harvesting in Wireless Body Area Networks", in *Proc. of the 24th Annual IEEE International Symposium on Personal, Indoor and Mobile Radio Communications (PIMRC 2013)*, London, UK, Sep. 2013, pp. 527-532.

[BTNO13] BTnode, Jan 2013. [Online]. Available: http://www.btnode.ethz.ch/pub/uploads/Main/btnode_rev3.24_productbrief.pdf.

[Buen11] N. Buenfeld, "Editorial: Automated monitoring of concrete structures: research opportunities," *Magazine of Concrete Research*, vol. 63, no. 2, pp. 79-80, Feb. 2011.

[BuVe09] C. Buratti and R. Verdone, "Performance Analysis of IEEE 802.15.4 Non Beacon-Enabled Mode," *IEEE Transactions on Vehicular Technology*, vol. 58, no. 7, pp. 3480-3493, Sep. 2009.

[BVFB09] N. Barroca, F. J. Velez, J. M. Ferro, L. M. Borges, A. S. Lebres, "Desenho de Protocolos de Controlo de Acesso ao Meio Eficientes do Ponto de Vista Energético em Redes de Sensores Sem Fios," in *Proc. of Engenharia' 2009 - Inovação e Desenvolvimento*, Covilhã, Portugal, Nov. 2009.

[BVFB10] N. Barroca, F. J. Velez, J. M. Ferro, L. M. Borges, A. S. Lebres, "Energy-Aware Wireless Sensor Networks MAC Modelling and Simulation with Efficient Transceivers," (invited paper for the Special Session on "Internet of Things") *in Proc. of the 13th International Symposium on Wireless Personal Multimedia Communications*, Recife, Brazil, Oct. 2010.

[BVLN14] L. M. Borges, F. J. Velez, A. S. Lebres and N. Barroca, "Frame Capture Effect and Reliability Based Decider Implementation in the MiXiM IEEE 802.15.4 Simulator Framework," in *Prof. of The 7th International ICST Conference on Simulation Tools and Techniques (SIMUtools 2014)*, Lisbon, Portugal, Mar. 2014.

[CaSV09] O. Cabral, A. Segarra, and F. J. Velez, "Implementation of IEEE 802.11e Block Acknowledgement Policies," *IAENG International Journal of Computer Science (IJCS)*, vol. 36, no. 1, pp. 85-93, Feb. 2009.

[CC2420] Texas Instruments, "2.4 GHz IEEE 802.15.4/ZigBee-Ready RF Transceiver (Rev. B)", CC2420 datasheet [Revised, Feb. 2012].

[ChBV04a] P. Chatzimisios, A. C. Boucouvalas and V. Vitsas,"Effectiveness of RTS/CTS handshake in IEEE 802.11a wireless LANs", *IET Electronics Letters*, vol. 40, no 14, pp. 915-916, Jul. 2004.

[ChBV04b] P. Chatzimisios, A. C. Boucouvalas and V. Vitsas, "Optimisation of RTS/CTS handshake in IEEE 802.11 Wireless LANs for maximum performance", in *Proc. of the IEEE Global Telecommunications Conference Workshops,* Dallas Texas, USA, 29 Nov.- 3 Dec. 2004, pp. 270-275.

[ChHu12] C.-Y. Chang and S.-S. Hung, "Implementing RFIC and sensor technology to measure temperature and humidity inside concrete structures," *Construction and Building Materials*, vol. 26, no. 1, pp. 628-637, Jan. 2012.

[CLNL06] P. Cruz, D. De Léon, J. Nunes, and C. K. Y. Leung, "Design and mechanical characterization of fibre optic plate sensor for cracking monitoring," *Sensors and Materials*, vol. 18, no. 6, pp. 283-299, Jan. 2006.

[COOL12] COOLNESS, Nov. 2012. [Online]. Available: http://www.ctt.upc.edu/arxius/ca/.

[CoSa07] S. L. Cotton and W. G. Scanlon, "Characterization and Modeling of the Indoor Radio Channel at 868 MHz for a Mobile Bodyworn Wireless Personal Area Network," *IEEE Antennas and Wireless Propagation Letters*, vol. 6, no. 1, pp. 51-55, Jan. 2007.

[COST13a] COST 2100. EU COST Action 2100: Pervasive Mobile Ambient Wireless Communications, Jan. 2013. [Online]. Available: http://www.cost2100.org/.

[COST13b] COST IC1004. EU COST Action IC1004: Cooperative Radio Communications for Green Smart Environments, Jan. 2013. [Online]. Available: http://www.ic1004.org/.

[COST13c] COST IC0905 TERRA. EU COST Action IC0905 TERRA: Techno-Economic Regulatory Framework for Radio Spectrum Access for Cognitive Radio/Software Defined Radio, Jan. 2013. [Online]. Available: http://www.cost-terra.org/.

[CUKK10] M. S. Chowdhury, N. Ullah, M. H. Kabir, P. Khan and K. S. Kwak, "Throughput, Delay and Bandwidth Efficiency of IEEE 802.15.4a Using CSS PHY", in *Proc. of International Conference on Information and Communication Technology Convergence (ICTC)*, Jeju Island, Korea, Nov. 2010, pp. 158-163.

[CYTA10] D. Cavdar, H. B. Yilmaz, T. Tugcu and F. Alagoz, "Analytical modeling and resource planning for cognitive radio systems," *Wireless Communications and Mobile Computing*, vol. 12, no. 3, pp. 277-292, Feb. 2010.

[Czap06] P. P. Czapski, "A Survey: MAC Protocols For Applications of Wireless Sensor Networks," in *Proc. of TENCON 2006: 2006 IEEE Region 10 Conference*, Hong Kong, China, Nov. 2006.

[DeEA06] I. Demirkol, C. Ersoy and F. Alagöz, "MAC Protocols for Wireless Sensor Networks: A Survey," *IEEE Communications Magazine*, vol. 44, no. 4, pp. 115-121, Apr. 2006.

[DuFa09] G. S. Duffó and S. B. Farina, "Development of an embeddable sensor to monitor the corrosion process of new and existing reinforced concrete structures," *Construction and Building Materials*, vol. 23, no. 8, pp. 2746-2751, Aug. 2009.

[EZTI13] eZ430-RF2500 wireless development tool, Jan. 2013. [Online]. Available:http://www.ti.com/lit/ug/slau227e/slau227e.pdf.

[FaKu11] M. O. Farooq and T. Kunz, "*Operating Systems for Wireless Sensor Networks: A Survey*, vol. 11, no. 6, pp. 5900-5930, May 2011.

[Fara08] S. Farahani, *ZigBee Wireless Networks and Transceivers, Newnes*, Newton, MA, USA, 2008.

[Filt12] Filter Cap SF2 for Humidity and Temperature Sensor SHT2x, Dec. 2012. [Online]. Available: http://www.sensirioncom/en/pdf/product_information/Datasheet_filter-cap_sf2.pdf.

[FRDD06] A. Fort, J. Ryckaert, C. Desset, and P. D. Doncker, "Ultra-Wideband Channel Model for Communication Around the Human Body," *IEEE Journal on Selected Areas in Communications*, vol. 24, no. 4, pp. 927-933, Apr. 2006.

[Fried09] M. Friedrich, "Miniature Mobile Sensor Platforms for Condition Monitoring of Structures," *IEEE Sensors Journal*, vol. 9, no. 11, pp. 1439-1448, Nov. 2009.

[GaLi05] G. Ganesan and Y. G. Li, "Cooperative Spectrum Sensing in Cognitive Radio Networks," in *Proc. of First IEEE International Symposium on New Frontiers in Dynamic Spectrum Access Networks*, 2005, pp. 137-143.

[GrJa05] C. Gribbin and D. James, "Assessing fetal health," *Current Obstetrics & Gynaecology*, vol. 15, no. 4, pp. 221-227, Aug. 2005.

[GuCB03] J. A. Gutiérrez, E. H. Callaway, and R. L. Barrett, *Low-Rate Wireless Personal Area Net-works: Enabling Wireless Sensors with IEEE 802.15.4*, 1st ed. Standards Information Network - IEEE Press, USA, 2003.

[Harb11] A. Harb, "Energy harvesting: State-of-the-art," *Renewable Energy*, vol. 36, no. 10, pp. 2641-2654, Oct. 2011.

[HeNL07] M. Healy, T. Newe and E. Lewis, "Efficiently securing data on a wireless sensor network," *Journal of Physics: Conference Series*, Sensors and their Applications XIV, vol. 76, no. 1, pp. 1-6, Sep. 2007.

[HXSM12] P. Huang, L. Xiao, S. Soltani and M. Mutka, "The evolution of MAC protocols in wireless sensor networks: A survey," *IEEE Communications Surveys Tutorials*, vol. 15, no. 1, pp. 101-120, Apr. 2012.

[Hygr12] Hygroclip, Nov. 2012. [Online]. Available:http://www.rotronic-usa.com/ds/Hygroclip.pdf.

[Imot13] Imote2 - advanced sensor network node platform, Jan. 2013. [Online]. Available: http://web.univ-pau.fr/~cpham/ENSEIGNEMENT/PAU-UPPA/RESA-M2/DOC/Imote2_Hardware_Reference_Manual.pdf.

[IMSR09] IMS Research, Dec. 2009. [Online]. Available:http://www.imsresearch.com/press-release/Over_20_million_802154_Chips_Sold_in_2009.

[InMa09] D. Inaudi and L. Manetti, "Reinforced Concrete Corrosion Wireless Monitoring System," in *Proc of 4th International Conference on Structural Health Monitoring on Intelligent Infrastructure*, Zurich, Switzerland, Jul. 2009.

[INSY13] INSYSM. EU FP7 INSYSM Project: Intelligent Systems for Structures Strengthening and Monitoring, Jan. 2013. [Online]. Available:http://insysm.polsl.pl/.

[IPPB11] S. S. Iyengar, N. Parameshwaran, V. V. Phoha, N. Balakrishnan and C. D. Okoye, *Fundamentals of Sensor Network Programming - Applications and Technology*, Wiley, New Jersey, USA, 2011.

[IRIS13] IRIS motes, Jan. 2013. [Online]. Available: http://www.memsic.com/support/documentation/wireless-sensor-networks/category/7-datasheets.html?download=135%3Airis.

[JiYi12] D. Jingshan, Z. Yiqun and M. Lixiang, "An adaptive RTS/CTS mechanism in IEEE 802.15.4 for multi-hop networks", in *Proc. of the International Conference on Computational Problem-Solving*, Leshan, ROC, Oct. 2012, pp. 155-159.

[JRPC01] E. Jovanov, D. Raskovic, J. Price, J. Chapman, A. Moore, and A. Krishnamurthy, "Patient Monitoring Using Personal Area Networks of Wireless Intelligent Sensors," *Biomedical Sciences Instrumentation*, vol. 37,no. 1, pp. 373-378, Mar. 2001.

[Jurd07] R. Jurdak, *Wireless Ad Hoc and Sensor Networks: A Cross-Layer Design Perspective*, Springer, New York, USA, 2007.

[KaFi03] U. Karthaus and M. Fischer, "Fully integrated passive UHF RFID transponder IC with 16.7-μW minimum RF input power," *IEEE J. Solid State Circuits*, vol. 38, no. 10, pp. 1602-1608, Oct. 2003.

[KaWi05] H. Karl and A. Willig, *Protocols and Architectures for Wireless Sensor Networks*, Wiley, Chichester, UK, 2005.

[KhAli11] B. M. Khan and F. H. Ali, "Collision Free Mobility Adaptive (CFMA) MAC for wireless sensor networks," *Telecommunication Systems*, vol. 52, no. 4, pp. 2459-2474, Apr. 2011.

[KPTB06] E. C. Karvounis, C. Papaloukas, M. Tsipouras and P. Bougia, "Remote maternal and fetal health monitoring during pregnancy," in *Proc. of The International Special Topic Conference on Information Technology Applications in Biomedicine* (ITAB2006), Loannina, Greece, Oct. 2006.

[LeMF08] T. Le, K. Mayaram, and T. Fiez, "Efficient far-field radio frequency energy harvesting for passively powered sensor networks," *IEEE Journal of Solid-State Circuits*, vol. 43, no. 5, pp. 1287-1302, May 2008.

[LMMV05] B. Latre, P.D. Mil, I. Moerman, N. V. Dierdonck, B. Dhoedt and P. Demeester, "Maximum Throughput and Minimum Delay in IEEE 802.15.4," in *Mobile Ad-hoc and Sensor Networks*, Springer-Verlag Berlin Heidelberg, pp. 866-876, 2005.

[LOTU13] LOTUS , Jan. 2013. [Online]. Available:http://www.memsic.com.php5-12.dfw1-1.websitetestlink.com/support/documentation/wireless-sensor-networks/category/7-datasheets.html?download=186%3Alotus.

[MaAn09] I. Martínez and C. Andrade, "Examples of reinforcement corrosion monitoring by embedded sensors in concrete structures," *Cement and Concrete Composites*, vol. 31, no. 8, pp. 545-554, May 2009.

[Maha07] N. P. Mahalik, *Sensor Networks and Configuration: Fundamentals, Standards, Platforms, and Applications*, Springer, New York, USA, 2007.

[MCSH10] W. J. McCarter, T. M. Chrisp, G. Starrs, Niall Holmes and L. Basheer, "Developments in Monitoring Techniques for Durability Assessment of Cover-zone Concrete," in *Proc of 2nd International Conference on Durability of Concrete Structures*, Sapporo, Japan, Nov. 2010.

[McVe04] W. Mccarter and O. Vennesland, "Sensor systems for use in reinforced concrete structures," *Construction and Building Materials*, vol. 18, no. 6, pp. 351-358, Jul. 2004.

[MICz13] MICAz - Wireless Measurement System, Jan. 2013. [Online]. Available: http://www.memsic.com.php5-12.dfw1-1.websitetestlink.com/support/documentation/wireless-sensor-networks/category/7-datasheets.html?download=148%3Amicaz.

[MiMu11] J. Mizuguchi, M. Murata and W. Uemura, "A broadcasting method based on RTS/CTS for an ad-hoc network", in *Proc. of the 15th IEEE International Symposium on Consumer Electronics*, Singapore, Singapore, Jun. 2011, pp. 104-106.

[MiXi13] MiXiM - Modeling framework for mobile and fixed wireless networks, Oct. 2013. [Online]. Available: http://mixim.sourceforge.net/.

[MLT109] MLT1010 Datasheet, Jan. 2009. [Online]. Available:http://www.adinstruments.com\ /products/mlt1010d#overview.

[Nard13] NARDA-SMR spectrum analyser, Jul. 2013. [Online]. Available: http://www.narda-sts.com.

[NgSh09] H.H. Nguyen and E. Shwedyk, *A First Course in Digital Communications*, Cambridge University Press, New York, US, 2009.

[NiHa93] H. Nikookar and H. Hashemi, "Statistical modeling of signal amplitude fading of indoor radio propagation channels," in *Proc of 2nd International Conference on Universal Personal Communications*, New Jersey, USA 1993, pp. 84-88.

[NMLC12] P. Nintanavongsa, U. Muncuk, D. R. Lewis and K. R. Chowdhury, "Design optimization and implementation for RF energy harvesting circuits," *IEEE Journal on Emerging and Selected Topics in Circuits and Systems*, vol. 2, no. 1, pp. 24-33, Mar. 2012.

[NoSR08] A. Norris, M. Saafi, and P. Romine, "Temperature and moisture monitoring in concrete structures using embedded nanotechnology/microelectromechanical systems (MEMS) sensors," *Construction and Building Materials*, vol. 22, no. 2, pp. 111-120, Feb. 2008.

[OMNe13] OMNeT++ Network Simulation Framework, Sep. 2013. [Online]. Available: http://www.omnetpp.org/.

[PaSS01] S. Park, A. Savvides and M. B. Srivastava , "Battery Capacity Measurement and Analysis using Lithium Coin Cell Battery," in *Proc. of International Symposium on* Low Power Electronics and Design, 2001, pp. 382-387.

[PLAN13] Planning and Optimization for the Coexistence of Mobile and Wireless Networks Towards Long Term Evolution (PLANOPTI), Out. 2013. [Online]. Available: http://www.e-projects.ubi.pt/planopti/index.html.

[Powe13] Powercast, Jul. 2013. [Online]. Available: http://www.powercastco.com.

[PrLi11] C. Providakis and E. Liarakos, "T-WiEYE: An early-age concrete strength development monitoring and miniaturized wireless impedance sensing system," *Procedia Engineering*, vol. 10, no. 0, pp. 484-489, Jan. 2011.

[PROE13] PROENERGY-WSN, Sep. 2013. [Online]. Available: http://www.e-projects.ubi.pt/proenergy-wsn/index.html.

[QuKe10] B. Quinn and G. Kelly, "Feasibility of embedded wireless sensors for monitoring of concrete curing and structural health," in *Proc. of Sensors and Smart Structures Technologies for Civil, Mechanical, and Aerospace Systems*, San Diego, USA, Mar. 2010.

[Rapp02] T. S. Rappaport, *Wireless Communications: Principles and Practice*, Prentice Hall, New Jersey, USA, 2002.

[RaVr01] D. Rakhmatov and S. Vrudhula, "An analytical high-level battery model for use in energy management of portable electronic systems," in *Proc. of International Conference on Computer Aided Design (ICCAD'01)*, 2001, pp. 488-493.

[RESP12] Respisense, Nov. 2012. [Online]. Available: http://www.respisense.com/en/index.php.

[RJSL08] D. Raychaudhuria, X. Jinga, I. Seskara, K. Lea and J. B. Evansb, "Cognitive radio technology: From distributed spectrum coordination," *Pervasive and Mobile Computing*, vol. 4, no. 3, pp. 278-302, Feb. 2008.

[RoAO09] J. Rousselot, M. Aoun and R. S. Oliver, "Accurate Timeliness Simulations for Real-TimeWireless Sensor Networks," in *Proc. of The Third UKSim European Symposium on Computer Modeling and Simulation*, Neuchatel, Switzerland, Nov. 2009, pp. 476-481.

[RoWR04] S. Roundy, P. K. Wright, and J. M. Rabaey, *Energy Scavenging for Wireless Sensor Networks:With Special Focus on Vibrations*, Kluwer Academic Publishers, Massachusetts, USA, 2004.

[RUNN13] Mote Runner, Jan. 2013. [Online]. Available: http://www.zurich.ibm.com/moterunner/.

[SAWS11] SA-WSN, Nov. 2012. [Online]. Available: http://cordis.europa.eu/projects/rcn/93930/_en.html.

[SBVS14] R. C. Santiago, N. Barroca, F. J. Velez, H. M. Saraiva, P. T. Gouveia, J. Tavares and L. M. Borges, "Case Study: Cognitive Radio in Medical Environments," 2014.

[Skla98] B. Sklar, *Digital Communications: Fundamentals and Applications*, Pentice Hall, New Jersey, 1988.

[SMAR12] Smart-Clothing. Smart-Clothing Project: Smart Clothing for Health Monitoring and Sport Applications, Dec. 2012. [Online]. Available: http://www.e-projects.ubi.pt/smart-clothing/.

[SNHN12] R. C. Santiago, K. E. Nolan, O. Holland, L.de Nardis, J. M. Ferro, N. Barroca, L. M. Borges, F. J. Velez, V. Gonçalves and I. Balasingham, "Cognitive Radio for Medical Body Area Networks Using Ultra Wideband," *IEEE Wireless Communications Magazine, Special Issue on Cognitive Radio Networks - A Practical Perspective*, vol. 19, no.4, pp. 74-81, Aug. 2012.

[SoMZ07] Kazem Sohraby, Daniel Minoli and Taieb Znati, *Wireless Sensor Networks: Technology, Protocols, and Applications*, 1st ed. Wiley-Interscience, New Jersey, USA, 2007.

[SuKu11] S. Sudevalayam and P. Kulkarni, "Energy Harvesting Sensor Nodes: Survey and Implications," *IEEE Communications Surveys & Tutorials*, vol. 13, no. 3, pp. 443-461, Sep. 2011.

[SUNS13] Sun SPOT, Jan. 2013. [Online]. Available: http://www.sunspotworld.com/docs/Yellow/SunSPOT-Programmers-Manual.pdf.

[SuSu10] M. Sun, K. Sun and Y. Zou, "Analysis and improvement for 802.15.4 multi-hop network," in *Proc. of International Conference on Communications and Mobile Computing*, Kunming, Yunnan, China, Nov. 2009, pp. 52-56.

[TBSB13] J. Tavares, N. Barroca, H. M. Saraiva, L. M. Borges, F. J. Velez, C. Loss, R. Salvado, P. Pinho, R. Gonçalves and N. B. C., "Spectrum Opportunities for Electromagnetic Energy Harvesting from 350 MHz to 3 GHz," in *Proc. of The 7th International Symposium on Medical Information and Communication Technology (ISMICT 2013) - Special Session on Antennas and Propagation for Body Area Network*, Tokyo, Japan, Mar. 2013.

[Telo13] TelosB - Wireless Measurement System, Jan. 2013. [Online]. Available: http://www.memsic.com.php5-12.dfw1-1.websitetestlink.com/support/documentation/wireless-sensor-networks/category/7-datasheets.html?download=152%3Atelosb.

[Tiny13] Tinynode 584, Jan. 2013. [Online]. Available: http://www.tinynode.com/?q=system/files/TN584_Users_Manual_v_1_3.pdf.

[TMOT13] Tmote Sky - Ultra low power IEEE 802.15.4 compliant wireless sensor module, Jan. 2013. [Online]. Available: http://www.snm.ethz.ch/snmwiki/pub/uploads/Projects/tmote_sky_datasheet.pdf.

[VDMC08] R. Verdone, D. Dardari, G. Mazzini, and A. Conti, *Wireless Sensor and Actuator Networks: Technologies, Analysis and Design*, Academic Press, London, UK, 2008.

[VeMu12] H. Venkataraman and G.-M Munteam, *Green Mobile Devices and Networks - Energy Optimization and Scavenging Techniques*, CRC Press, Boca Raton, Florida, 2012.

[VPMS07] R. Vullings, C. Peters, M. Mischi, R. Sluijter, G. Oei and J. Bergmans, "Artifact reduction in maternal abdominal ECG recordings for fetal ECG estimation," in *Proc. of the Annual International Conference of the IEEE Engineering in Medicine and Biology Society*, Lyon, France, Aug. 2007, pp. 43-46.

[VVLM11] F. Vanheel, J. Verhaevert, E. Laermans, I. Moerman and P. Demeester, "Automated linear regression tools improve RSSI WSN localization in multipath indoor environment," *EURASIP Journal on Wireless Communications and Networking*, vol. 2011, no. 1, pp. 1-27, Jul. 2011.

[WaQZ08] H. Wang, H. Qin, and L. Zhu, "A Survey on MAC Protocols for Opportunistic Spectrum Access in Cognitive Radio Networks," in *Proc. of International Conference on Computer Science and Software Engineering*, 2008, pp. 214-218.

[WASP13] Waspmote project, Jan. 2013. [Online]. Available: http://www.libelium.com/downloads/documentation/waspmote_datasheet.pdf.

[WIHA13] SmartMesh® WirelessHART, Jan. 2013. [Online]. Available: http://cds.linear.com/docs/en/datasheet/5900-WHMf.pdf.

[WISE12] WISEBED project, Nov. 2012. [Online]. Available: http://www.wisebed.eu/.

[WLAN05] *Part 11: Wireless LAN Medium Access Control (MAC) and Physical Layer (PHY) specifications*, IEEE Std. 802.11e™, Nov. 2005.

[WPAA08] S. Woo, W. Park, S. Ahn, S. An, and D. Kim, "Knowledge-Based Exponential Backoff Scheme in IEEE 802.15.4 MAC," *Lecture Notes in Computer Science*, vol. 5200, pp. 435-444, Nov.2008.

[WPAN05] *Part 15.1: Wireless Medium Access Control and Physical Layer Specifications for Low-Rate Wireless Personal Area Networks*, IEEE Std. 802.15.1™, Jun. 2005.

[WPAN06] *Part 15.4: Wireless Medium Access Control and Physical Layer Specifications for Low-Rate Wireless Personal Area Networks*, IEEE Std. 802.15.4™, Sep. 2006.

[WPAN07] *Part 15.4: Wireless Medium Access Control and Physical Layer Specifications for Low-Rate Wireless Personal Area Networks - Amendment 1: Add Alternate PHYs*, IEEE Std. 802.15.4™, Aug. 2007.

[WPAN09] *Part 15.5: Mesh Topology Capability in Wireless Personal Area Networks (WPANs)*, IEEE Std 802.15.5™, Jun. 2009.

[WPAN11] *Part 15.4: Low-Rate Wireless Personal Area Networks - Revision of IEEE Std 802.15.4-2006*, IEEE Std. 802.15.4™, Sep. 2011.

[WPAN12] *Wireless Medium Access Control and Physical Layer Specifications for Low-Rate Wireless Personal Area Networks, IEEE Std. 802.15.4e (Amendment to IEEE Std 802.15.4 -2011)*, Apr. 2012.

[Xiao05] Y. Xiao, "IEEE 802.11 performance enhancement via concatenation and piggyback mechanisms," *IEEE Transactions on Wireless Communications*, vol. 4, no. 5, pp. 2182-2192, Sep. 2005.

[XiZW10] M. Xie, W. Zhang and K.-K. Wong, "A Geometric Approach to Improve Spectrum Efficiency for Cognitive Relay Networks," *IEEE Transactions on Wireless Communications*, vol. 9, no. 1, pp. 268-281, Jan. 2010.

[YeHD04] W. Ye, J. Heidemann and D. Estrin, "Medium Access Control with coordinated Adaptive Sleeping for Wireless Sensor Networks," *IEEE/ACM Transactions on Networking*, vol. 12, no. 3, pp. 493-506, Jun. 2004.

[YiFC10] F. Yildiz, D. Fazarro and K. Coogler, "The Green Approach: Self-Power House Design Concept for Undergraduate Research," *Journal of Industrial Technology*, vol. 26, no. 2, pp. 1-10, Apr. 2010.

[YMAV05] H. Yan, J. G. M. Montero, A. Akhnoukh, L. C. N. de Vreede, and J. N. Burghart, "An integration scheme for RF power harvesting," in *Proc. of The 8th Annual Workshop on Semiconductor Advances for Future Electronics and Sensors*, Veldhoven, Netherlands, Nov. 2005, pp. 64-66.

[ZhFR12] Y. Zhou, B. Froppier and T. Razban, "Schottky Diode Rectifier for Power Harvesting Application," in *Proc. of The IEEE International Conference on RFID-Technologies and Applications (RFID-TA)*, Nice, France, Oct. 2012, pp. 429-432.

[ZLWZ09] X. Zhou, L. Lin, J. Wang and X. Zhang, "Cross-layer Routing Design in Cognitive Radio Networks," *Wireless Personal Communications*, vol. 49, no. 1, pp. 123-131, Apr. 2009.

[ZNOD13] Z1 low-power wireless module, Jan. 2013. [Online]. Available: http://zolertia.com/sites/default/files/Zolertia-Z1-Datasheet.pdf.